komunikácie

COMMUNICATIONS

SCIENTIFIC LETTERS OF THE UNIVERSITY OF ŽILINA

Volume 28

MULTIDISCIPLINARY JOURNAL FOR SCIENCES IN TRANSPORT

UNIVERSITY
OF ŽILINA

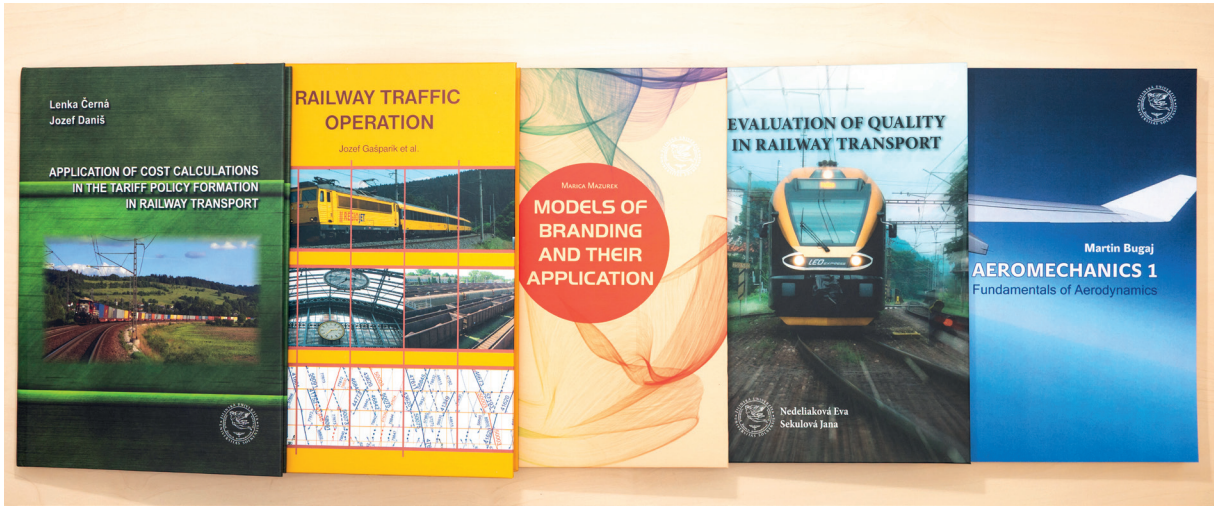


ISSN 1335-4205

4/2026

UNIVERSITY OF ŽILINA
EDIS-Publishing House
UNIZA

EDIS-Publishing House of the University of Žilina (UZ) is one of the University of Žilina's consituents. The beginning of its existence dates back to 1990. In the course of its work, the publishing house has published more than 5 100 titles of book publications, especially university textbooks, scientific monographs, scripts, prose, but also enriched the book market with titles of regional, children's and popular literature.
Students and professional public have the opportunity to purchase published titles in the „Selling Study Literature" directly on the premises of the University of Žilina, in the EDIS shop or upon order on a „cash on delivery" basis. All published titles are available at: www.edis.uniza.sk.



EDIS-Publishing House of the University of Žilina offers book titles in English

Eva Nedeliaková, Jana Sekulová
EVALUATION OF QUALITY IN RAILWAY TRANSPORT
ISBN 978-554-1272-6 Price 8.00 €

Martin Bugaj
AEROMECHANICS 1
ISBN 978-80-554-1675-5 Price 14.50 €

Marica Mazurek
MODELS OF BRANDING AND THEIR APPLICATION
ISBN 978-80-554-1705-9 Price 9.00 €

Jozef Melcer
DYNAMICS OF STRUCTURES
ISBN 978-80-554-1698-4 Price 19.00 €

Jozef Gašparík et al.
RAILWAY TRAFFIC OPERATION
ISBN 978-80-554-1281-8 Price 15.80 €

Lenka Černá, Jozef Daniš
APPLICATION OF COST ALCULATIONS IN THE TARIFF POLICY FORMATION IN RAILWAY TRANSPORT
ISBN 978-80-554-1391-4 Price 7.61 €

Tetiana Hovorushchenko et.al.
CD - INTELLIGENT INFORMATION-ANALYTICAL TECHNOLOGIES...
ISBN 978-80-554-1729-5 Price 3.50 €

Karol Matiaško, Michal Kvet, Marek Kvet
CD - PRACTICES FOR DATABASE SYSTEMS
ISBN 978-80-554-1397-6 Price 2.20 €

Veronika Valašková, Daniela Kucharová
USB - STATICS OF STRUCTURES 3
ISBN 978-80-554-1826-1 Price: 8,90 €

Michal Kvet, Karol Matiaško, Štefan Toth
USB - PRACTICAL SQL FOR ORACLE CLOUD
ISBN 978-80-554-1880-3 Price: 11,30 €

Michal Kvet, Karol Matiaško, Marek Kvet
USB - BECOME EXPERT IN MYSQL PRACTICES FOR DATABASE SYSTEMS IN MYSQL
ISBN 978-80-554-1786-8 Price 13.50 €

Michal Kvet, Alenka Baggia, Monika Borkovcová, Diana Mudrinić, Frane Urem
E-book - Environmental Data Analysis
ISBN 978-80-554-2145-2 Price 0,00 €

Michal Kvet
E-book – Become master in SQL
ISBN 978-80-554-2132-2 Price 0,00 €

EDIS-Publishing House UNIZA
Univerzitná 8215/1,
010 26 Žilina,
Slovakia

e-mail: edis_objednavky@uniza.sk, edis@uniza.sk
www.edis.uniza.sk

KOMUNIKÁCIE
COMMUNICATIONS

VEDECKÉ LISTY ŽILINSKEJ UNIVERZITY
SCIENTIFIC LETTERS OF THE UNIVERSITY OF ZILINA
multidisciplinary journal for sciences in transport

A - OPERATION AND ECONOMICS IN TRANSPORT

COMPARATIVE ANALYSIS OF THE T1 TRANSIT PROCEDURE AND TIR SYSTEM: INSTITUTIONAL AND COST EFFICIENCY PERSPECTIVES FROM AZERBAIJAN A83
N. Karimov, E. Alirzaev

OPERATIONAL FACTORS AND THEIR IMPACT ON SELECTION OF APPROACH SYSTEMS AT REGIONAL PUBLIC INTERNATIONAL AIRPORTS A95
R. Stryk, L. Kontriková, D. Mičulka

GENDER DIFFERENCES IN VISUAL ATTENTION AND STATED PREFERENCES DURING EVALUATION OF BATTERY ELECTRIC VEHICLES: AN EXPLORATORY EYE-TRACKING STUDY A113
V. Cvacho, R, Madleňák, A. Pagano, E. Kozłowski

SYNCHRONIZING PUBLIC TRANSPORT SCHEDULES WITH GENETIC ALGORITHMS: CHOOSING THE HEURISTIC PARAMETERS A126
V. Naumov, A. Tazhmuratova, I. Taran, Y. Melnikova, D. Kapica

THE ESG-ORIENTED APPROACHES TO DEVELOPING A SUSTAINABLE RAIL FREIGHT MARKET: METHODOLOGY AND EFFECTIVENESS ASSESSMENT A137
B. Aimagambetova, O. Kisselyova, R. Mussaliyeva, Y. Karsybayev, M. Chazhabayeva

B - MECHANICAL ENGINEERING IN TRANSPORT

MODELLING AND OPTIMIZATION OF HYDROGEN FUEL SYSTEMS IN RAILWAY VEHICLES USING DATA ANALYSIS AND MACHINE LEARNING B137
O. Shepel, J. Dižo, M. Blatnický, M. Bučko

ADAPTING D-FMEA TO INCREASING PRODUCT COMPLEXITY: A STUDY OF CONVENTIONAL AND MECHATRONIC SHOCK ABSORBERS B149
Ł. Rudolf, M. Roszak, L. Kuchariková

TOWARDS THE DIGITAL TWIN-ENABLED V2I MONITORING OF SHIP POWER PLANTS UNDER REAL OPERATING CONDITIONS B158
A. Holovan, I. Gritsuk, I. Honcharuk , O. Volska, A. L. Simanenkov, A. A. Ivanov

C - ELECTRICAL ENGINEERING IN TRANSPORT

EVALUATION AND EXPERIMENTAL VALIDATION OF POWER CONVERTER TOPOLOGIES FOR A BIDIRECTIONAL GRID-CONNECTED BATTERY ENERGY STORAGE SYSTEM C67
M. Praženica, P. Resutík, S. Kaščák, M. Prídala, M. Kuchař

NUMERICAL ASSESSMENT OF ELECTROMAGNETIC EXPOSURE FROM MOTORCYCLE HELMET COMMUNICATION SYSTEMS C84
Z. Pšenáková, M. Smetana, G. Lo Sciuto, D. Dvončová

D - CIVIL ENGINEERING IN TRANSPORT

OPTIMISING URBAN TRAFFIC FLOW THROUGH GREEN-WAVE SIGNAL COORDINATION: EFFECTS ON DELAYS, FUEL CONSUMPTION AND EMISSIONS IN BAKU **D70**
M. Baghirov, H. Ahmedov

STOPPED FRACTION AND CLOSURE FAILURE IN CONGESTED MACROSCOPIC FUNDAMENTAL DIAGRAMS: A SUMO-BASED SIMULATION STUDY **D86**
T. Noguchi

This is an open access article distributed under the terms of the Creative Commons Attribution 4.0 International License (CC BY 4.0), which permits use, distribution, and reproduction in any medium, provided the original publication is properly cited. No use, distribution or reproduction is permitted which does not comply with these terms.

COMPARATIVE ANALYSIS OF THE T1 TRANSIT PROCEDURE AND TIR SYSTEM: INSTITUTIONAL AND COST EFFICIENCY PERSPECTIVES FROM AZERBAIJAN

Elvin Alirzayev[1], Nijat Karimov[2,*]

[1]Academy of the State Customs Committee, Department of Customs and Management, Baku, Azerbaijan
[2]Azerbaijan University of Architecture and Construction, Department of Transport and Logistics, Baku, Azerbaijan

*E-mail of corresponding author: nijat.karimov1987@gmail.com

Elvin Alirzayev 0000-0002-1244-1263, Nijat Karimov 0000-0002-5057-9677

Resume
The role and effectiveness of the T1 customs procedure in international transit transportation were examined in this study. It analyzes the legal framework, operational mechanism, and impact of the T1 procedure on logistics processes, while comparing its characteristics with the TIR system within the Common Transit (CT) framework. The findings demonstrate that the T1 procedure enhances customs control, reduces transit time and logistics costs, and strengthens risk management. Furthermore, the implementation of the New Computerised Transit System (NCTS) improves the transparency, traceability, and operational efficiency of transit operations, thereby facilitating regional trade integration. However, the geographical scope of the T1 procedure remains limited to the European Union (EU) and European Free Trade Association (EFTA) countries, restricting its wider application in global transit transport.

Article info
Received 13 May 2026
Accepted 27 July 2026
Online 26 August 2026

Keywords:
T1 procedure
international transit
Common Transit (CT)
TIR system
transit efficiency
customs clearance

Available online: https://doi.org/10.26552/com.C.2026.049

ISSN 1335-4205 (print version)
ISSN 2585-7878 (online version)

1 Introduction

International trade constitutes a fundamental pillar of the modern global economy, playing a crucial role in strengthening economic interdependence among countries. In this context, the efficiency of freight transportation largely depends on the proper design and effective implementation of customs procedures. Transit transportation, defined as the movement of goods under customs supervision across national borders, ensures the continuity, predictability, and stability of international trade flows [1-2]. The ongoing standardization and digitalization of transit procedures further enhance logistics performance by reducing operational costs and shortening delivery times [3-5]. Within this framework, the T1 document represents a key customs instrument. Operating under the Common Transit (CT) system, it facilitates the secure and controlled movement of goods across the European Union and EFTA territories [4, 6]. The T1 procedure ensures that goods remain under continuous customs supervision throughout the entire transit process, while also providing customs authorities with essential data for monitoring and control purposes [1-2]. Beyond its regulatory function, the system significantly contributes to improving logistical efficiency, reducing administrative and transportation costs, and increasing operational flexibility for transport operators [7-8]. When compared to the TIR system, the T1 procedure is generally regarded as a more regionally efficient and administratively flexible alternative for transit operations.

Comparative studies indicate that the Common Transit system provides advantages in customs integration, electronic data exchange, and risk management mechanisms [6, 8]. In this research was investigated the role of the T1 document in international transit, focusing on its operational mechanisms and its impact on logistics performance, cost reduction, and trade facilitation [9-10].

2 Historical development and legal basis of the T1 procedure

The TIR system is not considered as a fully universal mechanism for all the transit operations; therefore, many carriers and logistics operators have increasingly searched for alternative transit solutions [8, 11]. The need for an alternative transit regime within Europe emerged in 1968 following the adoption of the Common Customs Tariff in the European Economic Community (EEC) and the progressive harmonization of customs legislation among Member States [1, 6]. The establishment of a unified customs framework and the enlargement of the European integration area contributed to the signing of the Common Transit Convention and the Single Administrative Document Convention in 1987. On this legal basis, the Common Transit (CT) procedure was officially developed and later implemented across the European Union and EFTA (European Free Trade Association) countries, including Switzerland, Liechtenstein, Norway, and Iceland [1, 6].

In subsequent years, the Common Transit system expanded significantly and was joined by several European and neighboring countries, including the Czech Republic, Slovakia, Hungary, Poland, Bulgaria, Romania, Turkey, Ukraine, Slovenia, Lithuania, Latvia, and Estonia [6]. As of 2025, the geographical scope of the CT system has continued to broaden due to increasing regional economic integration and trade facilitation initiatives [4, 6].

The CT procedure is divided into two principal regimes: external transit and internal transit. External transit applies to goods entering the European Union from the third countries and governs their transportation within or through EU/EFTA territories under customs supervision. In such cases, the T1 document is issued for international transit operations [1, 6]. Internal transit, referred to as the T2 procedure, applies to goods originating within the EU that are transported between Member States or through EFTA territories while maintaining their customs status [1].

Transit operations under the CT procedure are permitted only when an appropriate financial guarantee is submitted to the customs office of departure. This guarantee is provided by the principal responsible for the transport operation and may take the form of a cash deposit or a bank guarantee [1]. In the case of non-compliance with customs regulations, the principal bears full responsibility for customs duties, taxes, and other financial liabilities. If goods transported under the T1 procedure fail to arrive at the designated customs office, the principal remains liable for all customs obligations associated with the shipment [1-2].

The main customs document used within the CT system is the Single Administrative Document (SAD), which serves as the standard customs declaration form for import, export, and transit operations across EU/EFTA territories [1, 6]. The principal or an authorized customs representative is responsible for declaring the goods and ensuring their proper delivery to the customs office of destination. The SAD contains multiple copies intended for export control, import clearance, transit monitoring, and statistical purposes [6].

In practical application, the T1 transit declaration is completed by the principal or customs agent using specific copies of the SAD form at the customs office of departure. Separate copies are used for the office of departure, the office of destination, return confirmation procedures, and customs statistics [4, 6].

The T1 procedure is widely regarded as an effective alternative to the TIR Convention guarantee mechanism. Although both systems pursue similar objectives in facilitating international transit operations, the primary distinction lies in their guarantee structures. Under the TIR system, the guarantee is provided through an international guaranteeing association coordinated by the IRU, whereas under the T1 procedure, transport operators may directly cooperate with customs representatives or use national guarantee systems operating within EU/EFTA territories [2, 8].

Compared to the TIR system, the T1 procedure offers several operational advantages. It does not require separate international guarantee fees or association membership contributions, which may reduce transportation costs and administrative burdens for carriers [7-8, 12]. In addition, the absence of strict limitations on the number of unloading or delivery points per vehicle increases operational flexibility, particularly for consolidated cargo transportation and multimodal logistics operations [8].

Overall, the CT/T1 procedure is considered as more advantageous than the TIR system in several operational and administrative aspects, particularly within the European transit environment [8]. Nevertheless, certain limitations remain. The geographical scope of the T1 procedure is restricted primarily to EU and EFTA territories, while the transit through third countries may still require additional guarantees under alternative systems, such as TIR [1-2]. Furthermore, unlike the globally recognized TIR mechanism, the CT system remains predominantly regional in nature and is mainly limited to the European customs area [6, 11].

3 Literature review

International trade facilitation and customs transit systems have been extensively analyzed in the academic literature as key determinants of global logistics performance and international trade efficiency. Empirical studies demonstrate that improvements in customs procedures, logistics infrastructure, and regulatory harmonization significantly enhance trade flows while reducing transaction and transportation costs between countries [9, 13-14].

A substantial body of research highlights the

important role of international organizations such as the World Trade Organization (WTO) and the World Customs Organization (WCO) in establishing global standards for trade facilitation and customs modernization. In particular, the WTO Trade Facilitation Agreement (TFA) and the WCO Revised Kyoto Convention are widely recognized as foundational legal instruments for simplifying customs procedures, improving transparency, and harmonizing border control mechanisms [2, 15]. These international frameworks provide the institutional basis for development of modern transit systems and digital customs environments [2].

Within this context, the Logistics Performance Index (LPI) and related World Bank studies indicate that countries possessing more efficient customs systems and advanced logistics infrastructure achieve higher levels of international competitiveness and trade integration [10, 16-17]. Reports published by the OECD further confirm that trade facilitation measures contribute directly to reducing border delays, increasing supply chain reliability, and improving the efficiency of international logistics corridors [5, 18].

The Common Transit (CT) system and the T1 procedure represent important regional customs instruments within the European transit environment. According to European Commission reports, the implementation of the New Computerised Transit System (NCTS) has significantly improved the transparency, efficiency, and risk management capacity of transit operations within EU and EFTA territories [4]. Furthermore, the Union Customs Code established a harmonized legal framework that strengthened customs cooperation and standardized transit procedures across Member States [1].

Comparative studies examining the T1 (CT) and TIR systems indicate that, while the TIR system provides a globally recognized guarantee mechanism suitable for long-distance international transport, the T1 procedure demonstrates greater operational efficiency within integrated regional markets such as the European Union due to its digital infrastructure and harmonized customs regime [2, 8]. Reports issued by UNECE confirm that the TIR system remains particularly important for international transit operations extending beyond the EU customs territory and involving multiple third countries [6, 19].

Digitalization has emerged as one of the main drivers of efficiency in customs transit systems. Research demonstrates that electronic declarations, automated customs procedures, real-time data exchange, and risk-based control mechanisms substantially improve customs performance while reducing administrative burdens and transit delays [2, 4, 20]. In this regard, the implementation of the NCTS is considered a major institutional innovation within the broader process of European customs modernization [4].

Regional integration initiatives, such as the Middle Corridor and Eurasian transport networks, have further increased the strategic importance of efficient transit systems. Studies published by the OECD emphasize that improvements in corridor performance, logistics infrastructure, and customs coordination are essential for strengthening trade connectivity between Europe and Asia [5, 21].

From a theoretical perspective, transport geography and logistics management studies underline the importance of inland connectivity, port regionalization, and supply chain coordination in improving the international trade efficiency [22-23]. In parallel, customs modernization has become increasingly associated with supply chain security, institutional reforms, and integrated logistics governance [2, 8].

Finally, comparative analyses of international transit systems suggest that the effectiveness of customs procedures depends primarily on three interrelated factors: legal harmonization, digital infrastructure, and geographical coverage [4, 8, 24]. While the T1/CT system demonstrates the high operational efficiency within the EU/EFTA region, the TIR system remains more appropriate for global-scale transit operations extending beyond the European customs area [2, 6]. This dual structure reflects the coexistence of regional and global transit governance models in the contemporary international trade and logistics system.

4 Research methodology

In this study was employed a qualitative research design based on document analysis, comparative policy analysis, and descriptive statistical analysis to evaluate the role of the T1 transit procedure in facilitating international trade and export operations. Qualitative document analysis is widely recognized as an appropriate methodological approach for examining customs regulations, institutional frameworks, and trade facilitation policies because it enables the systematic interpretation of official documents, legal instruments, and policy reports [1, 10]. In logistics and customs research, this approach is frequently used to evaluate institutional mechanisms where direct experimental or survey-based data are unavailable [8].

The study relied exclusively on the secondary data obtained from internationally recognized organizations and official government institutions. The principal sources include publications of the European Commission, UNECE, OECD, World Bank, the State Customs Committee of the Republic of Azerbaijan, and the State Statistical Committee of Azerbaijan. These sources provide verified information on the legal framework of the Common Transit (CT) system, operational characteristics of the T1 procedure, customs modernization, trade facilitation measures, logistics performance, and Azerbaijan's export and transport statistics [4, 16].

To examine the institutional characteristics of

the T1 procedure, in this research was applied the comparative policy analysis. Comparative analysis is widely used in transport and logistics studies to identify similarities and differences between customs transit systems operating under different legal and organizational frameworks [8]. In this study, the T1 procedure operating within the Common Transit system was compared to the TIR system in terms of customs guarantees, administrative requirements, geographical coverage, operational flexibility, digitalization, and logistics efficiency. This comparison allows for the identification of the operational advantages and limitations of both transit mechanisms under different transport conditions.

The empirical component of the study is based on descriptive statistical analysis. Official statistical data covering the period 2020-2025 were collected to analyze the dynamics of Azerbaijan's exports, the geographical distribution of exports, the development of non-oil exports, and the role of road transport in export logistics [16]. Descriptive statistical techniques, including trend analysis, percentage analysis, and comparative assessment, were employed to identify changes in export structure and transport performance over time.

Furthermore, in the study was conducteds a comparative cost analysis of the T1 procedure and the TIR Carnet using official tariff and guarantee information available through the Common Transit System and related customs authorities [4, 6]. The analysis examined how guarantee requirements, insurance premiums, and administrative costs vary according to the invoice value of transported goods. Based on these comparisons, in the study was evaluated the economic suitability of the T1 procedure for different cargo value categories and identifies the approximate threshold at which the TIR system becomes a more cost-efficient alternative.

It should be noted that the primary data collection methods, such as surveys, interviews, or field experiments, were not employed in this research. Therefore, the findings should be interpreted as an institutional and comparative assessment based on verified secondary sources rather than as evidence of direct causal relationships between the implementation of the T1 procedure and export growth. Instead, the analysis' aim was to explain how the institutional characteristics of the T1 procedure-including customs harmonization, electronic transit management, and flexible guarantee mechanisms-may contribute to improving logistics efficiency and facilitating international trade within the Common Transit area [1, 4].

The combination of document analysis, comparative policy analysis, descriptive statistical analysis, and comparative cost assessment provides a comprehensive methodological framework for evaluating the effectiveness of the T1 transit procedure from legal, institutional, operational, and economic perspectives. This mixed qualitative-descriptive approach has been widely adopted in previous studies examining customs modernization, trade facilitation, and international logistics performance [1, 8].

4.1 Analysis of the role and effectiveness of the T1 document in ınternational transit

The efficiency of customs procedures in international transit transportation is widely recognized as one of the principal determinants of overall logistics chain performance and trade competitiveness [9, 13]. Within this context, the T1 procedure, operating under the framework of the Common Transit (CT) system, serves as an important institutional mechanism ensuring the secure, rapid, and cost-efficient movement of goods under customs supervision across EU and EFTA territories [1, 6]. The effectiveness of the T1 document may be evaluated through several criteria, including optimization of customs control procedures, reduction of transit time, management of financial risks, lowering of administrative costs, and enhancement of operational flexibility [2, 8]. Empirical and institutional studies indicate that the T1 procedure demonstrates the high efficiency among regional transit systems across most of these dimensions [2, 8].

One of the primary advantages of the T1 procedure is the standardization and legal harmonization of customs processes. The unified customs framework implemented within the European Union and EFTA countries, strengthens cooperation and mutual trust among customs authorities while minimizing redundant inspections during transit operations [1, 6]. This harmonized system facilitates the uninterrupted movement of goods, reduces delays at border crossing points, and contributes to the continuity and reliability of international logistics chains. Furthermore, the implementation of electronic customs systems and digital transit declarations significantly increases procedural transparency and reduces dependence on manual administrative processes [4, 6].

The positive impact of the T1 procedure is also evident in terms of transit time reduction and logistics cost optimization. Electronic data exchange systems, automated customs processing, and pre-declaration mechanisms substantially reduce waiting times at border crossings, thereby decreasing vehicle idle time and fuel consumption [2, 4]. As a result, transportation operators benefit from the lower operational expenses and improved delivery time predictability, which contributes to higher logistics efficiency and customer reliability [9, 13].

An additional advantage of the T1 procedure is its flexible guarantee mechanism, which enables customs duties and taxes to remain suspended throughout the transit operation until the goods reach the customs office of destination [1-2]. The financial responsibility assigned to the principal enhances the efficiency of customs

administration while reducing administrative burdens for transport operators participating in the Common Transit system [1, 8].

From a risk management perspective, the T1 procedure is closely aligned with modern customs control principles and risk-based supervision mechanisms. The assignment of financial responsibility to the principal reduces fiscal risks for customs administrations and ensures more effective enforcement in cases of transit irregularities or customs violations [1-2, 25]. In addition, differentiated risk assessment procedures enable customs authorities to accelerate the clearance of low-risk consignments while concentrating inspections on high-risk shipments [1-2].

Operational flexibility constitutes another important advantage of the T1 procedure. The absence of strict limitations regarding the number of unloading or delivery points per vehicle increases efficiency in consolidated cargo transportation, multimodal operations, and partial shipment logistics [8]. Consequently, the T1 system functions not only as a customs control instrument but as an effective logistics optimization mechanism, as well, supporting modern supply chain management [7-8].

Nevertheless, the T1 procedure also possesses certain limitations. The most significant constraint relates to its geographical scope, which remains primarily limited to EU and EFTA territories [1, 6]. When the transit operations involve third countries outside the Common Transit framework, additional guarantee systems and customs procedures may be required, potentially increasing administrative complexity and affecting operational continuity [6, 11].

The analysis demonstrates that the T1 procedure represents a highly efficient institutional mechanism for international transit operations within the EU/EFTA region [1, 6]. Through the acceleration of customs procedures, reduction of logistics costs, improvement of risk management mechanisms, and enhancement of operational flexibility, the T1 system provides an effective regional solution for modern international transit transportation and trade facilitation [5, 8].

4.2 Selection of the optimal transit document based on invoice value of goods

In international road transport operations, selecting the appropriate customs transit document depends on several economic and operational factors, including the invoice value of the goods, customs territory coverage, guarantee requirements, and the geographical scope of the transport operation [2, 6, 8].

The TIR Carnet remains one of the most widely used international customs transit documents under the framework of the TIR Convention [2, 6]. The cost of the TIR Carnet generally depends on the number of sheets included in the carnet. For example, a 6-sheet TIR Carnet costs approximately 100 $, while a 16-sheet carnet costs around 185 $. These values may vary according to the daily exchange rate between the Swiss franc and the Azerbaijani manat determined by the Central Bank of the Republic of Azerbaijan. The TIR system also operates through an international guarantee chain that secures customs duties and taxes throughout the transit operation [2, 6].

By contrast, the T1 transit procedure, which is applied within the Common Transit system, follows a different guarantee structure. Under this procedure, customs duties and taxes applicable to goods originating from non-EU countries remain suspended throughout transit and become payable only after the goods arrive at the customs office of destination [1]. The T1 declaration simultaneously serves as both a transit declaration and a financial guarantee instrument covering the potential customs liabilities [1, 6].

Unlike the TIR system, the T1 procedure does not require participation in the international TIR guarantee chain. Instead, financial responsibility is assumed by the principal under the Common Transit framework, providing greater flexibility in guarantee management and reducing certain administrative costs associated with regional transit operations [1-2, 8]. In addition, electronic declaration processing and harmonized customs procedures improve the administrative efficiency, shorten border-crossing times, and enhance transparency throughout the transit process [2, 4].

The choice between the TIR Carnet and the T1 procedure therefore depends primarily on the characteristics of the transport operation. For transit movements extending beyond the geographical scope of the Common Transit area, particularly those involving multiple non-member countries, the TIR system generally offers broader international applicability under a globally recognized legal framework [2, 6]. Conversely, for transport operations conducted entirely within the Common Transit territory, the T1 procedure provides greater administrative flexibility, simplified customs formalities, and potentially lower overall operational costs [1, 8].

The invoice value of the goods also plays an important role in selecting the most appropriate transit document. Since the financial guarantee under the T1 procedure is directly related to the customs duties and taxes potentially payable on the transported goods, higher-value consignments may require correspondingly larger guarantees. In contrast, the cost of the TIR Carnet depends primarily on the type and number of carnet sheets rather than on the commercial value of the cargo. Consequently, the economic efficiency of each procedure varies according to shipment value, customs liability, transport route, and guarantee requirements.

The selection of the optimal transit document should be based on a comprehensive assessment of shipment characteristics, customs obligations, geographical coverage, and operational requirements, rather than on a single cost criterion. Such an approach enables

transport operators to optimize customs compliance, minimize logistics costs, and improve the efficiency of international transit operations.

4.3 Comparative analysis of T1 transit document costs based on cargo invoice value

Analysis of T1 transit document tariffs shows that for every additional USD 5,000 of cargo value, a guarantee of approximately USD 932 is required. Specifically, when the invoice value of goods ranges from USD 29,500 to USD 100,000, an additional USD 932 guarantee is applied for each incremental USD 5,000 of cargo value, while insurance premiums increase by approximately USD 2-5 at each step.

For the cargo valued between USD 100,000 and USD 200,000, the guarantee amount increases to approximately USD 1,863 for each additional USD 10,000 of cargo value. Similarly, for goods valued between USD 200,000 and USD 300,000, the guarantee increases to approximately USD 2,795 per additional USD 15,000, while for shipments valued between USD 300,000 and USD 490,000, the guarantee reaches approximately USD 3,726 per additional USD 20,000. Insurance premiums also increase progressively, generally rising by USD 5-10 for each additional USD 5,000-10,000 of cargo value and by approximately USD 10-15 for higher value intervals.

Based on the comparative analysis of the presented data, it can be observed that the applicability of the T1 transit document and the TIR Carnet is directly linked to the invoice value of goods.

The T1 transit procedure is based on a variable economic model in which the guarantee obligations and service fees increase progressively with the invoice value of cargo [1, 8]. As shown in the data, for low-value shipments, both the guarantee requirement and overall cost of the T1 procedure remain relatively low. However, as cargo value increases, the required guarantee rises significantly, resulting in a higher financial burden and reduced cost efficiency. In particular, for goods approaching or exceeding USD 100,000, the T1 mechanism becomes less economically efficient due to the immobilization of working capital and additional financial costs.

In international road transport, the TIR system is based on a unified customs guarantee principle with a maximum coverage of EUR 100,000 [2, 6]. This feature is considered one of the main advantages of the TIR Carnet. Regardless of the cargo value, the guarantee remains fixed, and carriers can transit through multiple countries without requiring additional national guarantee mechanisms. As a result, administrative procedures are simplified, border crossing times are reduced, and overall logistics efficiency is improved [2].

In practical logistics, the EUR 100,000 threshold (approximately USD 119,000) is considered as a critical break-even point. Below this level, the T1 procedure may be more cost-effective due to lower service fees and flexible guarantee structures. However, above this threshold, the TIR system becomes more economically and operationally efficient, as it eliminates additional financial burdens and ensures faster transit execution [8].

For example, under the TIR system, a shipment valued at EUR 100,000 is covered by an equivalent guarantee without additional increases. In contrast, under the T1 system, the same shipment may require significantly lower effective guarantee coverage (approximately USD 22,165 in comparative estimates). At the same time, the TIR system does not impose additional guarantees for cargo exceeding EUR 100,000, whereas in the T1 system, guarantees continue to increase with cargo value.

It can be concluded that while the T1 procedure may still provide adequate coverage for high-value shipments, it is associated with higher service-related costs (approximately USD 425 in total estimates). In contrast, the TIR Carnet requires an average fee of approximately USD 103 (or USD 187 for a 16-page carnet), while providing full-value guarantee coverage. Therefore, the TIR system becomes more advantageous when the scale of transport operations and associated risk justify the fixed cost structure [2, 8].

In general, the attractiveness of the T1 system increases for the low-value cargo and low-risk transport routes. Considering that transit risks in European-bound exports are relatively lower, service fees may constitute a significant share of total logistics costs, making the T1 procedure more attractive for certain carriers [8].

On the other hand, access to the TIR system requires formal membership in an international guarantee chain, involving several administrative procedures. In some cases, incomplete documentation or non-compliance with requirements may delay access to the system. In this context, the T1 procedure can be considered a more accessible alternative [2, 6].

4.4 Export and transport structure in the Republic of Azerbaijan

In recent years, the foreign trade turnover of the Republic of Azerbaijan has demonstrated a significant upward trend. Total foreign trade increased from USD 24.472 billion in 2020 to USD 49.423 billion in 2025, representing more than a twofold growth. During the same period, export volumes rose from USD 13.741 billion to USD 25.043 billion, reflecting an increase of approximately 1.82 times.

Moreover, since Georgia joined the Common Transit (CT) system as of 1 February 2025, local carriers can now access this system electronically through authorized customs brokers and digital platforms, further enhancing

its accessibility and operational efficiency [4, 6].

Export performance reached its peak in 2022, when the total exports amounted to USD 38.147 billion. This increase was largely driven by a substantial rise in exports to the European Union, which nearly doubled and reached approximately USD 25 billion in the same period. When exports are classified by destination regions-European Union (EU), Commonwealth of Independent States (CIS), and other countries-it is observed that the EU accounts for the dominant share of approximately 67.7%, indicating its strategic importance in Azerbaijan's foreign trade structure.

Table 1 *Illustrates the estimated cost structure of the T1 procedure and the related guarantee obligations depending on the invoice value of transported goods, [26]*

Value of goods, $	Guarantee amount, $	Insurance premium, $
29,500	5,305	105
35,000	6,329	110
40,000	7,261	112
45,000	8,192	115
50,000	9,124	120
55,000	10,055	125
60,000	10,987	130
65,000	11,918	132
70,000	12,850	135
75,000	13,781	137
80,000	14,713	140
85,000	15,644	145
90,000	16,576	148
95,000	17,507	152
100,000	18,439	155
110,000	20,302	160
120,000	22,165	170
130,000	24,028	175
140,000	25,891	185
150,000	27,754	190
160,000	29,617	195
170,000	31,480	205
180,000	33,343	210
190,000	35,206	215
200,000	37,069	225
215,000	39,863	235
230,000	42,658	245
245,000	45,452	255
260,000	48,247	265
275,000	51,041	275
290,000	53,836	285
310,000	57,562	300
330,000	61,288	320
350,000	65,014	330
370,000	68,740	350
390,000	72,466	360
410,000	76,192	370
430,000	79,918	385
450,000	83,644	400
470,000	87,370	415
490,000	91,096	425

In parallel, non-oil exports have also shown strong growth dynamics. Compared to 2020, non-oil exports have nearly doubled, reaching USD 3.6 billion and accounting for 14.5% of total exports, which represents the highest recorded share in the analyzed period. This trend reflects ongoing diversification efforts in the national export structure and a gradual reduction in dependence on the oil and gas sector.

The data for 2020-2025 indicate that Azerbaijan's export structure is increasingly oriented toward the European market, while non-oil sector development is gradually strengthening its role in the national economy. These structural changes also have direct implications for transport and logistics systems, particularly in relation to transit efficiency and integration into international supply chains.

Table 1 presents the estimated cost structure of the T1 transit procedure according to the invoice value of the transported goods. The results indicate a direct relationship between the value of the goods and both the required guarantee amount and the insurance premium. As the invoice value increases, the guarantee obligations and insurance costs also rise proportionally, reflecting the higher financial risk associated with higher-value shipments.

4.5 Analysis of export growth and transport structure

The increase in export volumes in Azerbaijan has been accompanied by a corresponding growth in transportation activities. Total freight transportation increased from 42.407 million tons in 2000 to 51.283 million tons in 2023, reaching 47.595 million tons in 2025. More than 88% of these transport operations are attributed to pipeline (stationary) transportation, indicating its dominant role in the country's logistics system.

The road transport of export goods has also shown a steady upward trend. In 2000, road freight exports amounted to 1.395 million tons, while by 2025 this figure had increased to 2.7084 million tons, representing a growth of approximately 94%.

Over the same period, pipeline transportation increased by around 10%, reflecting its relatively stable but less dynamic structure compared to road transport.

The share of the road transport in total exports (excluding pipeline transport) has increased significantly from 34.6% to 47.4%, demonstrating a gradual shift toward more flexible and responsive logistics modes. In value terms, the road transportation accounts for approximately 62.6% of total export operations (excluding pipeline transport), highlighting its strategic importance in Azerbaijan's foreign trade logistics.

Overall, the data indicate that the road transport plays a crucial role in export logistics by enhancing efficiency, flexibility, and international market accessibility.

In Figure 1 shows a bar chart of Azerbaijan's exports by three country groups-CIS, EU, and Others-as percentage shares for the years 2020–2025. The EU's share increased from 49.5% in 2020 to 65.6% in 2022. It then decreased slightly to 64.4% in 2023 and 63.3% in 2024 before increasing again to 67.7% in 2025. In contrast, the share of the Others group decreased steadily from 41.0% in 2020 to 25.3% in 2025.

The CIS had the smallest share during the whole period, decreasing from 9.5% in 2020 to 4.3% in 2022 and then increasing gradually to 7.1% in 2025. Overall, the figure shows that the EU's share of Azerbaijan's exports increased, the share of the Others group decreased, and the CIS maintained a small share throughout the period.

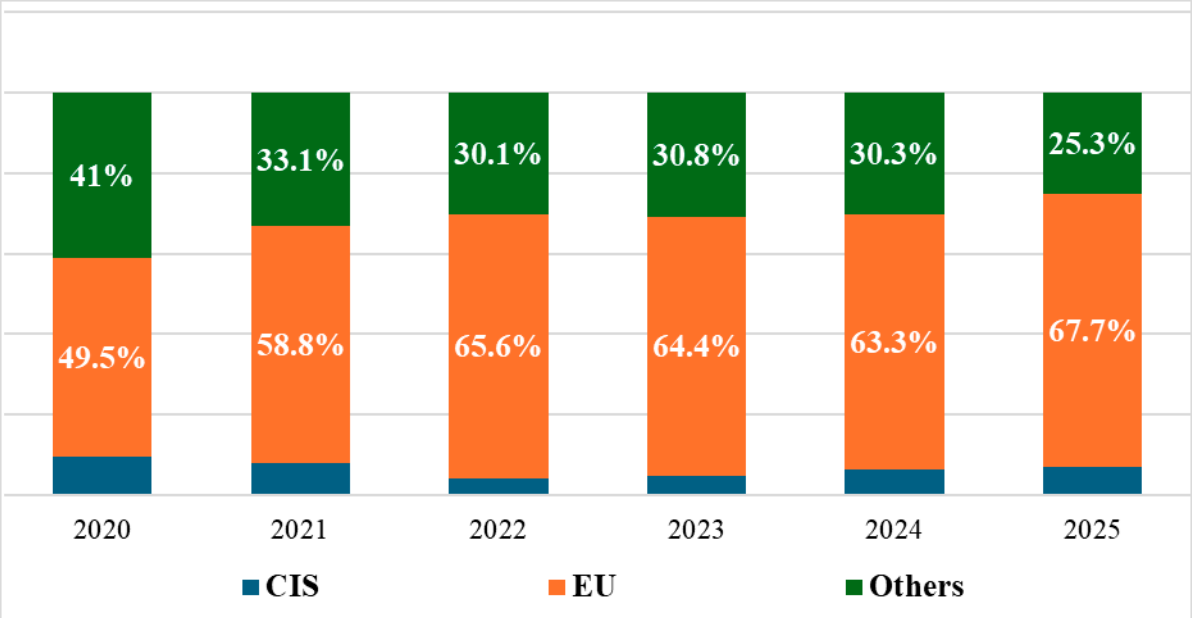


Figure 1. *Export of the Republic of Azerbaijan by Country Groups, share (%)*

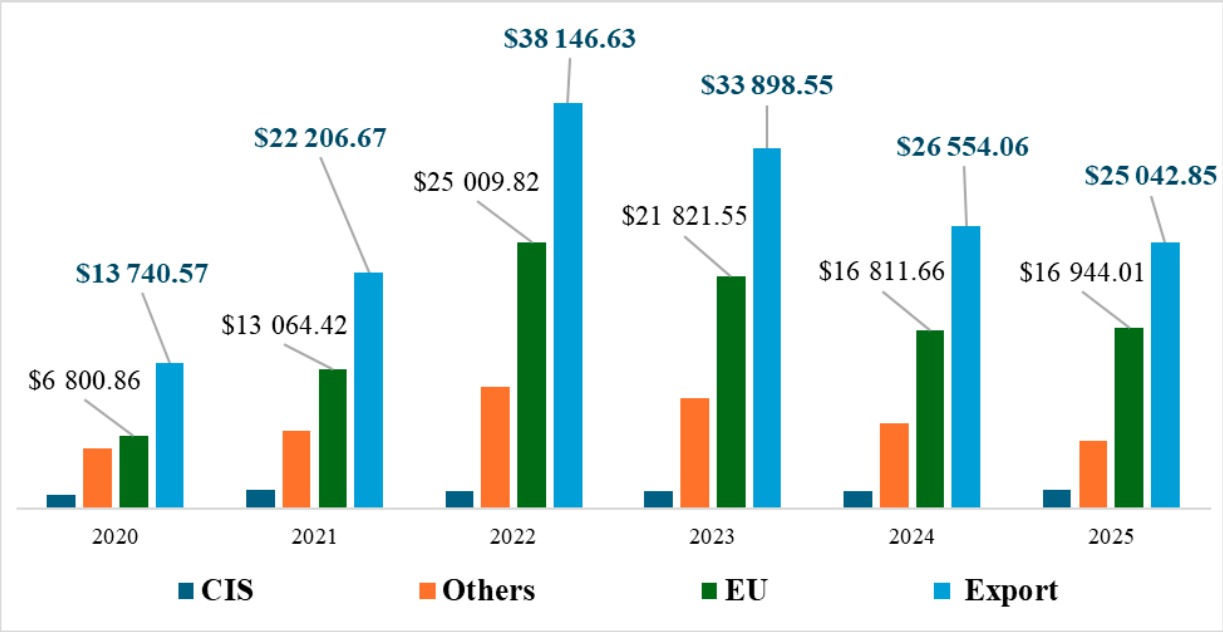


Figure 2 *Export of the Republic of Azerbaijan, by Country Groups, billion USD, [27]*

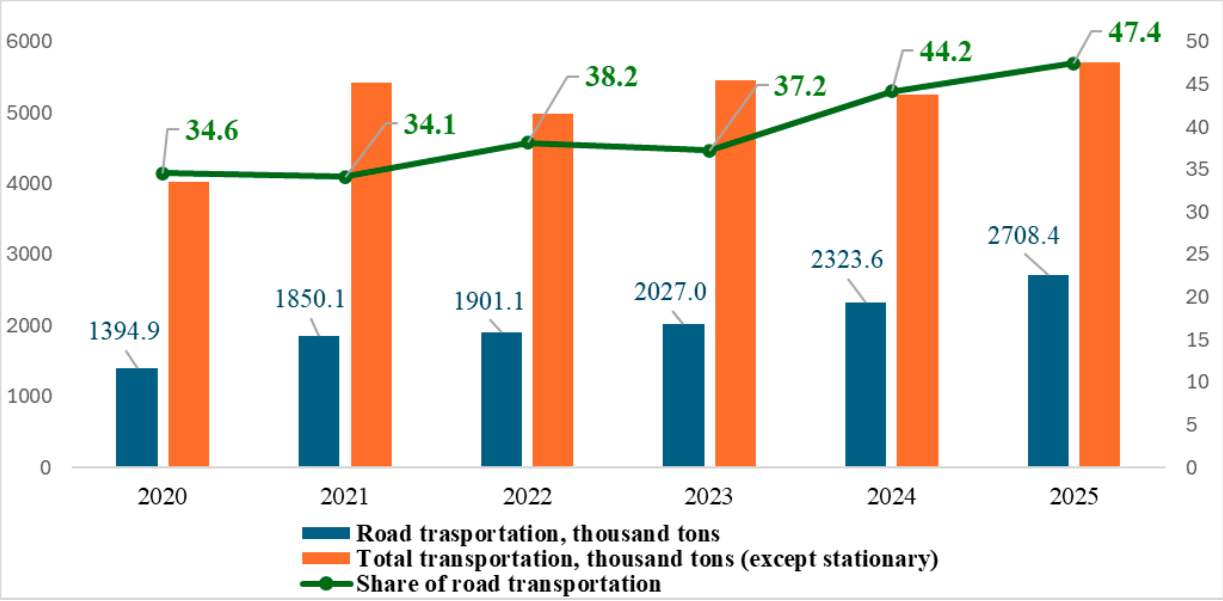


Figure 3 *Volume and share of export transportation by road transport, in thousand tons and percentage, [28]*

In Figure 2, the export volumes of the same three country groups are presented in absolute value terms, together with total exports. The total exports were at their lowest in 2020, rose steadily to a peak of around $38.1 billion in 2022, and then gradually declined over 2023–2025 to about $25 billion by 2025. The EU group showed the most notable growth over this period, rising from $6.8 billion in 2020 to $25 billion in 2022, before declining to $16.9 billion by 2025. The "Others" group grew between 2020 and 2022 and then declined between 2022 and 2025, while the CIS group stayed relatively stable throughout, ranging between $1.3–1.8 billion. This indicates that 2022 was a peak year across all groups, followed by a decline in total exports, while the EU's relative weight continued to grow.

In Figure 3, combining bar and line charts, three indicators are presented: the volume of goods transported by road, the total transportation volume (excluding stationary/pipeline transport), and the share of road transport in total transportation. The road-transported freight rose steadily from 1,394.9 thousand tons in 2020 to 2,708.4 thousand tons in 2025 - an increase of roughly 94%. Total transportation volume also grew overall, albeit unevenly, from 4,032.6 thousand tons in 2020 to 5,708.6 thousand tons in 2025. The share of the road

transport rose almost continuously, from 34.6% in 2020 to 47.4% in 2025. These figures clearly demonstrate the growing role of road transport, both in absolute volume and in its share of total transportation, confirming the paper's central point about the "strengthening role of road transport".

5 Conclusion and recommendations

In 2025, Azerbaijan's non-oil exports reached their highest level over the last six years, both in terms of value (USD 3.6 billion) and share in total exports (14.5%). The share of the road transport in total exports (excluding stationary transport) reached 47.4% in 2025. In value terms, road transportation (excluding stationary transport) accounted for 62.6% of total exports. These figures indicate the need for further optimization of the regulatory and procedural framework governing transport operations to improve logistics efficiency and facilitate international trade.

The conducted research indicates that the efficiency of international transit transportation is closely associated with the organization of customs procedures, legal harmonization, the level of digitalization, and the effectiveness of financial guarantee mechanisms. In this context, the T1 procedure serves as an important institutional instrument that may facilitate regional transit transport and reduce logistics costs within the framework of the Common Transit (CT) system. The analysis suggests that the T1 document performs effectively in key operational areas, including optimization of customs control, reduction of transit time, improvement of risk management, and enhancement of operational flexibility for carriers.

It is also evident that the legal and technological integration among EU and EFTA countries is a key factor supporting the effective implementation of the T1 procedure. The introduction of electronic transit systems, particularly the New Computerised Transit System (NCTS), has improved information exchange, increased transparency in customs control, and reduced delays at border-crossing points. These developments may improve the predictability of logistics operations and facilitate regional trade flows.

A comparative analysis of the T1 procedure and the TIR system shows that, although both mechanisms aim to ensure secure international transit and effective customs control, their scope of application and functional advantages differ. The TIR system, as a global transit mechanism, is more suitable for long-distance and multi-country transport operations. In contrast, the T1 procedure appears to offer advantages under conditions of regional integration due to lower administrative costs, faster customs clearance, and more flexible logistics arrangements. Accordingly, the T1 and TIR systems should be considered complementary rather than competing mechanisms.

At the same time, the main limitation of the T1 procedure is its geographical scope, which is restricted to EU and EFTA countries. When the transit routes involve third countries, additional guarantee mechanisms are required, increasing operational complexity and reducing procedural continuity. Nevertheless, in the context of the growing importance of regional economic blocs in global trade, the relevance of regional transit systems such as T1 is likely to continue increasing.

Thus, the analysis suggests that the T1 transit document may be more suitable for the international transit of the low- and medium-value goods from a cost-efficiency perspective. For the high-value goods, however, the TIR Carnet appears to be a more appropriate solution due to its fixed and internationally recognized guarantee mechanism. This highlights the importance for carriers and logistics operators of considering cargo value as a key economic criterion when selecting a transit regime.

Due to the complexity of procedures for joining the TIR system, the need to reduce financial risks in cargo transportation, and Georgia's recent accession to the Common Transit (CT) system as of 1 February 2025, carriers exporting goods to Europe have increasingly shown a preference for the T1 procedure as an accessible alternative.

Based on the research findings, several recommendations can be proposed. First, further digitalization of transit procedures and deeper integration of information systems are essential for increasing the efficiency of the T1 mechanism. Expanding electronic document circulation and enabling real-time data exchange may further reduce border-crossing times and administrative burdens.

Second, expanding the geographical scope of the T1 procedure, particularly through the integration of countries involved in the Middle Corridor and East-West transport routes into the CT framework, could facilitate regional trade and support more efficient transit operations. In this regard, strengthening legal harmonization and mutual recognition mechanisms remains essential.

Third, introducing more flexible financial guarantee mechanisms for the small and medium-sized transport operators could increase competition in the transit market and improve the overall quality of logistics services.

Fourth, the development of risk-based customs control systems and the application of advanced analytical technologies may enhance procedural efficiency while maintaining transport security.

In conclusion, the T1 procedure may be regarded as a modern customs instrument that demonstrates considerable potential for improving the efficiency of regional transit operations within the international transit system. Its further development through digital transformation, legal integration, and logistics

optimization may improve the efficiency, security, and predictability of international transit operations and facilitate international trade.

Acknowledgment

The authors would like to express their sincere gratitude to the institutions and organizations whose publicly available statistical data, legal documents, and policy reports were used in this research. No external funding was received for the preparation of this study.

Conflicts of Interest

The authors declare that they have no known competing financial interests or personal relationships that could have appeared to influence the work reported in this paper.

References

[1] Regulation (EU) No. 952/2013 of the European Parliament and of the Council laying down the Union Customs Code - European Union [online]. 2013. Available from: https://eur-lex.europa.eu/eli/reg/2013/952/oj/eng

[2] World Trade Organization. Trade Facilitation Agreement. Geneva, Switzerland, 2017.

[3] DU, Y., MENG, Q., WANG, S. Mathematically calculating the transit time of cargo through a liner shipping network with various trans-shipment policies. *Maritime Policy and Management* [online]. 2017, **44**(2), p. 248-270. ISSN 0308-8839, eISSN 1464-5254. Available from: https://doi.org/10.1080/03088839.2016.1274831

[4] New Computerised Transit System (NCTS) - European Commission [online]. (2024). Available from: https://taxation-customs.ec.europa.eu/online-services/online-services-and-databases-customs/new-computerised-transit-system-ncts_en

[5] Trade Facilitation and the Global Economy - Organisation for Economic Co-operation and Development [online]. 2023. Available from: https://www.oecd.org/en/publications/trade-facilitation-and-the-global-economy_9789264277571-en.html

[6] World Customs Organization. Transit Guidelines. 2022.

[7] BATISTA, L. Translating trade and transport facilitation into strategic operations performance objectives. *Supply Chain Management* [online]. 2012, **17**(2), p. 124-137. ISSN 1359-8546, eISSN 1758-6852. Available from: https://doi.org/10.1108/13598541211212870

[8] ANDERSON, J. E., VAN WINCOOP, E. Trade costs. *Journal of Economic Literature* [online]. 2004, **42**(3), p. 691-751. ISSN 0022-0515, eISSN 2328-8175. Available from: https://doi.org/10.1257/0022051042177649

[9] CARBALLO, J., GRAZIANO, A. G., SCHAUR, G., AND VOLPE MARTINCUS, C. The effects of transit systems on international trade. *Review of Economics and Statistics* [online]. 2024, **106**(4), p. 1083-1098. ISSN 0034-6535, eISSN 1530-9142. Available from: https://doi.org/10.1162/rest_a_01189

[10] AL-Shboul, M. A. Facilitating trade and improving supply chain security through transit trade mobility: An empirical investigation from developing country. *Cogent Social Sciences* [online]. 2023, **9**(2), 2263942. eISSN 2331-1886. Available from: https://doi.org/10.1080/23311886.2023.2263942

[11] GRAINGER, A., RUNDLE, J. M., AHSEN, S. R. Customs and humanitarian logistics. *Global Trade and Customs Journal* [online]. 2019, **14**(4), p. 154-168. ISSN 1569-755X, eISSN 1875-6468. Available from: https://doi.org/10.54648/GTCJ2019015

[12] HUMMELS, D. Transportation costs and international trade in the second era of globalization. *Journal of Economic Perspectives* [online]. 2007, **21**(3), p. 131-154. ISSN 0895-3309, eISSN 1944-7965. Available from: https://doi.org/10.1257/jep.21.3.131

[13] DENNIS, A., SHEPHERD, B. Trade facilitation and export diversification. *The World Economy* [online]. 2011, **34**(1), p. 101-122. ISSN 0378-5920, eISSN 1467-9701. Available from: https://doi.org/10.1111/j.1467-9701.2010.01303.x

[14] PORTUGAL-PEREZ, A., WILSON, J. S. Export performance and trade facilitation reform: hard and soft infrastructure. *World Development* [online]. 2012, **40**(7), p. 1295-1307. ISSN 0305-750X, eISSN 1873-5991. Available from: https://doi.org/10.1016/j.worlddev.2011.12.002

[15] WILSON, J. S., MANN, C. L., OTSUKI, T. Assessing the benefits of trade facilitation: a global perspective. *The World Economy* [online]. 2005, **28**(6), p. 841-871. ISSN 0378-5920, eISSN 1467-9701. Available from: https://doi.org/10.1111/j.1467-9701.2005.00709.x

[16] ARVIS, J.-F., OJALA, L., SHEPHERD, B., ULYBINA, D., WIEDERER, C. Connecting to compete 2023: trade logistics in an uncertain global economy - the logistics performance ındex and ıts ındicators [online]. Washington DC: World Bank, 2023. Available from: https://doi.org/10.1596/39760

[17] WILSON, J. S., MANN, C. L., OTSUKI, T. Trade facilitation and economic development: a new approach to quantifying the impact. *World Bank Economic Review* [online]. 2003. ISSN 0258-6770, eISSN 1564-698X. Available from: https://doi.org/10.1596/17183

[18] HOEKMAN, B, NICITA, A. Trade policy, trade costs, and developing country trade. *World Development* [online]. 2011, **39**(12), p. 2069-2079. ISSN 0305-750X, eISSN 1873-5991. Available from: Available from: https://doi.org/10.1016/j.worlddev.2011.05.013

[19] United Nations Economic Commission for Europe. Convention on a Common Transit Procedure. 2023.

[20] DJANKOV, S., FREUND, C., PHAM, C. S. Trading on time. *Review of Economics and Statistics* [online]. 2010, **92**(1), p. 166-173. ISSN 0034-6535, eISSN 1530-9142. Available from: https://doi.org/10.1162/rest.2009.11498

[21] CHENG, M. C. B., WANG, D., WANG, J. J. A port-based evaluation framework of trade facilitation policies: case of Shenzhen and Hong Kong. *Case Studies on Transport Policy* [online]. 2018, **6**(2), p. 297-307. ISSN 2213-624X, eISSN 2213-6258. Available from: https://doi.org/10.1016/j.cstp.2018.04.007

[22] MARTINEZ-ZARZOSO, I., GARCIA-MENENDEZ, L., SUAREZ-BURGUET, C. Impact of transport costs on international trade: the case of Spanish ceramic exports. *Maritime Economics and Logistics* [online]. 2003, **5**, p. 179-198. ISSN 1479-2931, eISSN 1479-294X. Available from: https://doi.org/10.1057/palgrave.mel.9100069

[23] BENSASSI, S., MARQUEZ-RAMOS, L., MARTINEZ-ZARZOSO, I., SUAREZ-BURGUET, C. Relationship between logistics infrastructure and trade: Evidence from Spanish regional exports. *Transportation Research Part A: Policy and Practice* [online]. 2015, **72**, p. 47-61. ISSN 0965-8564, eISSN 1879-2375. Available from: https://doi.org/10.1016/j.tra.2014.11.007

[24] SHEPHERD, B., WILSON, J. S. Trade facilitation in ASEAN member countries: Measuring progress and assessing priorities. *Journal of Asian Economics* [online]. 2009, **20**(4), p. 367-383. ISSN 1049-0078, eISSN 1873-7927. Available from: https://doi.org/10.1016/j.asieco.2009.03.001

[25] BEVERELLI, C., TICKU, R. Reducing tariff evasion: the role of trade facilitation. *Journal of Comparative Economics* [online]. 2022, **50**(2), p. 534-554. ISSN 0147-5967, eISSN 1095-7227. Available from: https://doi.org/10.1016/j.jce.2021.12.004

[26] Worldwide Solution GEO https://www.rs.ge/NCTSInfo-en?cat=5&tab=1

[27] https://customs.gov.az/en/faydali/gomruk-statistikasi/statistics-bulletin

[28] https://www.stat.gov.az/source/trade/?lang=en

This is an open access article distributed under the terms of the Creative Commons Attribution 4.0 International License (CC BY 4.0), which permits use, distribution, and reproduction in any medium, provided the original publication is properly cited. No use, distribution or reproduction is permitted which does not comply with these terms.

OPERATIONAL FACTORS AND THEIR IMPACT ON SELECTION OF APPROACH SYSTEMS AT REGIONAL PUBLIC INTERNATIONAL AIRPORTS

Rostislav Stryk*, Lenka Kontriková, David Mičulka

VSB-TUO, Faculty of Mechanical Engineering, Institute of Transport, Ostrava-Poruba, Czech Republic

*E-mail of corresponding author: rostislav.stryk@vsb.cz

Rostislav Stryk 0000-0002-9949-9213, Lenka Kontriková 0000-0002-0726-9307, David Mičulka 0000-0002-3938-7957

Resume

Regional public international airports undergo periodic modernization, including the modernization of air navigation and approach systems. In this paper is proposed a transferable decision-making framework based on the Analytic Hierarchy Process (AHP) for selecting approach systems at airports with potential mixed civil-military traffic. Its main contribution is an AHP-based procedure adapted to the operational and technical conditions of approach-system modernization. The procedure is demonstrated through a case study of Ostrava/Mosnov International Airport, assessing selected alternatives and their operational impacts on long-term airport development in the context of possible future mixed civil–military operations and national security interests.

Article info

Received 19 May 2026
Accepted 27 July 2026
Online 14 September 2026

Keywords:

approach systems
AHP method
VORTAC
GBAS
regional airport
mixed civil-military operations
LKMT airport

Available online: https://doi.org/10.26552/com.C.2026.052

ISSN 1335-4205 (print version)
ISSN 2585-7878 (online version)

1 Introduction

The current push to develop the infrastructure of regional international airports (hereinafter "regional airports") stems, on one hand, from the efforts of their operators (owners) to connect regional airports to the European and global aviation network through a portfolio of scheduled passenger and cargo routes, and, on the other hand, from the growing importance of regional airports for air carriers, for whom these airports are increasingly becoming a suitable alternative to large and overloaded airport hubs.

The issue of defining the very concept of a regional airport is not uniform in professional literature. In [1], the authors state that there is still no generally accepted definition of a regional airport in Europe. The definitions used vary according to traffic volume, the airport's function within the transport network, the nature of the routes served, or geographical location.

Regional airports are currently used primarily on a seasonal basis. To mitigate this seasonal effect, it is essential for regional airports to develop and ensure year-round operations of scheduled air routes, whether passenger or cargo. Another area of focus is the possibility of military branches of the state utilizing and sharing civil airport infrastructure.

One of the most important requirements for ensuring the regularity of air transport is a high level of reliability in flight safety and the ability to operate flights at the scheduled time and to the planned destination. For this reason, as a part of the development of scheduled air transport at regional airports, increasing emphasis is being placed on equipping them with modern air navigation infrastructure that ensures this regularity to the greatest extent possible. An important component of an airport's air navigation infrastructure is formed by approach systems, which enable airport operations even under adverse weather conditions. From an economic perspective, the modernization of approach systems must be viewed as an investment. The acquisition, installation, and operation of new approach systems at an airport fulfil all the typical characteristics of an investment-it is a long-term asset whose use generates revenue over an extended period. However, its acquisition

is often associated with significant initial cash outlays.

An example of such an investment is the purchase and installation of an ILS approach system. Based on the authors' internal sources and knowledge, published articles [2] and [3], and contracts published in the register of contracts of state institutions [4] and [5], it appears that the acquisition cost of a Category I ILS system currently amounts to approximately $800,000, while the installation of a Category II/III ILS system, including the corresponding precision approach lighting system, reaches up to $1,600,000. Annual maintenance costs for Category I are approximately $75,000, while annual maintenance costs for Category II/III reach approximately $165,000. The difference is therefore twofold, and clear arguments must be presented for the purchase and installation of the more expensive Category II/III ILS system.

Investment projects, related to the selection of an appropriate type of approach system, may also be influenced by the type of operations currently taking place at the airport or being considered for the future. One such example is the so-called mixed civil-military operations (the joint operation of civil and military aircraft). The positive synergies of mixed civil-military operations may be accompanied by complications caused by the differing requirements of civil and military aircraft regarding approach systems, particularly due to differences in aircraft avionics. Airports with mixed civil-military operations can be divided into two groups. The first group consists of military airports with civil air traffic, where the primary function of the airport is military; an example is Pardubice Airport (LKPD), which is explicitly designated in the AIP of the Czech Republic as a military airport with civil air traffic [6]. The second group consists of civil public international airports with a current military presence or where part of the airport infrastructure is shared with a military unit; an example is Kraków-Balice Airport (EPKK) [7], where the operator specifies a separate civil section of the airport and the existence of a military section with the 8th Air Transport Base [8].

Selecting the appropriate type of approach system as a part of a regional airport's modernization thus becomes a significant challenge that can fundamentally affect the airport's attractiveness and its long-term viability. Since manufacturers provide precise cost estimates for installing specific types of approach systems only after assessing the individual needs and configuration of each airport, and since this information is not generally available even at a basic level, it is not possible to evaluate the economic aspects of this issue in general terms. However, it is possible to at least perform an operational analysis and evaluation of the individual options for modernizing approach systems using the AHP method.

The AHP method finds the wide application in air transport, particularly where it is necessary to evaluate options based on multiple criteria that are difficult to compare to one another. For example, in [9], the authors used the AHP method to assess the "target windows" concept as part of the modernization of European ATM; in [10], the AHP method was applied in combination with the PROMETHEE and VIKOR methods when selecting a suitable location for a military airport, and in [11], the method was used to determine the optimal service level of an airport terminal for low-cost carriers.

In summary, the aforementioned studies confirm the broad applicability of the AHP method in air transport and demonstrate its suitability for complex aviation decision-making problems involving multiple criteria and stakeholders. However, previous applications of AHP in aviation were primarily focused on airport location selection, airport service quality, airline or ATM operational concepts, or other airport-related decision-making problems. To the authors' knowledge, in no published study has been proposed a structured AHP-based methodological framework for selecting an airport approach system in the specific context of regional public international airports with expected mixed civil-military traffic. This context is important since the mixed traffic may involve different requirements related to aircraft equipage, operational minima, interoperability, resistance to interference, continuity of service and the strategic usability of airport infrastructure. The originality of this paper therefore does not lie in the AHP method itself, but in the formulation of a domain-specific decision-making framework that combines the approach-system alternatives with operational usability, aircraft equipage, installation complexity, resistance to interference and future flexibility. The proposed framework is demonstrated on the case of Ostrava/Mosnov Airport, but its structure is transferable to other regional airports facing similar modernization decisions.

2 Approach systems at regional airports

Using information from the aeronautical information publications of selected Eurocontrol member states [12], a survey was conducted of the current state of equipment at regional civil airports, including civil airports with mixed civil-military operations, designated for IFR operations in the Czech Republic, Slovakia, Poland, and Hungary. Each of the 24 analyzed regional airports certified as public international airports has a runway capable of two-way use. Of the total 48 runways, 15 are equipped with ILS CAT I, 7 have ILS CAT II, and only 2 runways at regional airports in Central European countries have ILS CAT III. The VOR approaches are available on 32 runways, and 16 runways have published NDB approaches. The most widespread type of approach is RNP, which uses GNSS satellite navigation and is published for 45 runways. If the modernization of radio navigation equipment for approach and landing at regional airports is being considered, then, considering the assumption of mixed civil-military operational use,

ILS, GBAS, TACAN, and VORTAC approach systems can be considered.

2.1 The ILS system

The ILS (Instrument Landing System) is a precision approach system that provides an aircraft with vertical and horizontal guidance information during approach and landing at an airport in adverse weather conditions. By its very nature, the ILS system can only be used for a specific runway direction. It allows for a precise approach and landing only in a direct line that follows the runway's centerline and, together with the approach descent path, intersects the runway plane at a single specific point, known as the touchdown point. At some airports, procedures are published and applied that utilize the back-course beam of the localizer for the opposite runway direction, known as the "back-course," which is a signal directed towards the opposite side of the localizer. However, this method of use has limiting characteristics. In the direction of use, it is not optimized for precise aircraft guidance, is less stable, and may have greater deviations. A significant disadvantage is that it provides only directional guidance during the approach and landing, without ensuring vertical guidance. The ILS system is divided into several categories based on accuracy, minimum required runway visibility, and minimum decision height.

2.1.1 ILS - category I (CAT I)

ILS CAT I is a standard approach system that enables precise approaches and landings for aircraft down to a decision height (DH) of 200 feet (approx. 60 m) and a minimum runway visual range of 550 metres. Where runway visibility data is not available, the minimum visibility value at which the ILS CAT I system can be used for approach and landing is replaced by an observed prevailing visibility value of 800 metres.

In terms of the usability of ILS CAT I equipment by civil and military aircraft, it is one of the most widely used approach methods. For the civil aircraft intended for IFR operations, avionics enabling approach and landing using ILS CAT I are nearly standard and rank among the basic instrumentation of most civil aircraft. Military transport aircraft in Western countries are also standardly equipped with avionics enabling approach and landing using ILS CAT I. For combat aircraft, precision approach and landing are primarily based on precision approach radar, which does not require any special onboard equipment; however, some military combat aircraft are equipped with this system.

Benefits of ILS CAT I:

- relatively low installation and maintenance costs compared to higher ILS categories (CAT II/III),
- sufficient coverage for most common operational and meteorological conditions,
- compatibility with the instrumentation of most aircraft and the qualifications of flight crews, who do not need to be additionally certified or specially trained for this procedure,
- lower demands on additional airport infrastructure compared to higher ILS categories (CAT II/III).

Risks of ILS CAT I:

- limited use in extremely poor weather conditions with reduced visibility (fog, heavy snowfall, heavy rain, etc.),
- possible signal interference (e.g., from terrain or ground obstacles),
- the need to establish protective sensitivity zones near individual system antennas.

2.1.2 ILS - category II/III (CAT II/III)

The installation of a Category II/III ILS system enables Category II and III approaches and landings, as well as controlled takeoffs. The decision height for ILS CAT II is lower than 200 ft (60 m), but not lower than 100 ft (30 m); for ILS CAT III, the approach may be conducted with a decision height lower than 100 ft (30 m) or without a specified decision height.

ILS CAT II/III systems significantly increase the likelihood of completing an approach and landing at an airport, thereby enhancing the attractiveness and usability of airports even under adverse meteorological conditions. Especially in the case of scheduled commercial air transport, where significant costs may arise from a potential forced diversion to an alternate airport and the associated additional costs not only for the flight itself but also for the subsequent ground transportation of passengers or cargo, the successful completion of the landing process at the original destination is essential.

A disadvantage of ILS CAT II/III systems is that they require independent backup power sources for the key components to ensure operational continuity even in the event of a main power failure. Airports equipped with an ILS CAT II/III system must also have high-intensity runway lighting systems (e.g., centerline and touchdown zone lights) that supplement radio navigation with visual guidance during approach and landing.

Aircraft are not universally equipped for ILS CAT II/III approach and landing operations. For a civil aircraft, it is common among modern airliners designed for long-haul passenger transport. For older aircraft, it is up to the airline to decide whether investing in the necessary equipment is necessary for the commercial and operational use of the aircraft. For example, in the case of cargo aircraft intended for scheduled air cargo transport, this equipment is desirable for the successful conduct of business operations. In addition to aircraft certification, special flight crew training is required to perform ILS CAT II/III approaches and landings. The situation is similar for military aircraft.

Benefits of ILS CAT II/III:

- the ability to operate even under very adverse weather conditions, which reduces the likelihood of flights having to divert to alternate airports,
- minimization of delays and disruptions to air traffic, increasing the airport's appeal to airlines seeking alternate airports in case of deteriorating weather conditions and the inability to complete the flight to the original destination airport,

Risks of ILS CAT II/III:

- high acquisition and operating costs,
- the need for special aircraft equipment and crew certification for approaches and landings in low visibility can significantly limit the number of suitable flights,
- more demanding maintenance and greater demands on adjacent infrastructure (e.g., runway lighting system),
- the need to modify the existing procedures and introduce special procedures for low-visibility operations, including regular training for all personnel (airport and air traffic control staff),
- the need to establish CAT II/III holding areas, including the installation of stop bars and ensuring their remote control,
- expansion of the sensitive area of the GP and LOC equipment and the need to prevent signal interference from aircraft, mobile devices, or airport obstacles.

2.2 GBAS (Ground-Based Augmentation System)

The GBAS is a ground-based system designed to improve the accuracy of GNSS navigation; compared to the ILS system, it enables precision approaches with significantly lower requirements for airport infrastructure. Honeywell developed a GBAS system called SmartPath SLS-4000 (for CAT I minima), which received operational certification from the FAA in 2009. This was followed in 2011 by European certification from the German Federal Aviation Authority (BAF). GBAS approach systems are designated according to the operational minimum for which they are certified. A distinction is made between GAST C (GBAS Approach Service Type C) systems, which correspond to CAT I approach minima, and GAST D systems with minima corresponding to CAT II/III [13]. The implementation of GNSS approaches must always undergo a risk assessment process related to the introduction of the selected approach type, as detailed in [14].

Compared to the ILS system, the GBAS system offers more advantages at both the technical and operational levels, and even at smaller airports with lower traffic volumes, it may be technically and operationally more feasible to implement this system. An example of the implementation procedure is included in the pre-project research report [15], and a summary of operational experience with the use of the CAT I GBAS system in actual airport operations is the subject of article [16]. The installation and operation of the GBAS system does not require the designation of critical sensitive zones to the extent required by the ILS system (e.g., relocation of holding points). The GBAS system allows for the projection of the final approach path along a curved trajectory, which is particularly advantageous when it is necessary to avoid noise-sensitive areas or to direct traffic away from densely populated areas. The system is suitable for precision instrument approaches in complex geographical areas where a direct ILS approach cannot be implemented, e.g., due to high surrounding terrain. Unlike an ILS approach, which is calibrated for only one glide path angle (typically 3°), the use of a single airport GBAS system allows for the operational application of various approach glide paths, including different touchdown points on the runway. This can also be advantageously utilized to reduce minimum separation distances between aircraft due to wake turbulence, thereby achieving an overall increase in runway capacity utilization.

Currently, the GBAS system is implemented, for example, at European airports in Bremen, Frankfurt am Main (Germany), Zurich (Switzerland), and Malaga (Spain), and in the U.S. at airports such as Newark and Houston [17]. The implementation of the GBAS system was the subject of [18]; author conducted a feasibility analysis of installing the GBAS system at Václav Havel Airport Prague, Czech Republic. In [19] was analyzed the development of Viseu Airport in Portugal over time and predicted traffic over a 10-year horizon. Study [20] was focused on assessing the feasibility of implementing a GBAS system at LinZhi Airport in Tibet, China. The study evaluated the availability of GBAS Type C (GAST C) and Type D (GAST D) approach services.

A significant disadvantage of installing a GBAS system for precision approach and landing is currently its very low penetration in the user sector, namely, in aircraft avionics. At present, very few types of civil transport aircraft are equipped with the necessary avionics. Another significant obstacle to the wider use of the GBAS system in air traffic is its certification only for operations under CAT I conditions (GAST C). This is a lower approach category than that currently offered by airports equipped with the ILS CAT II/III system.

In the case of military aircraft, the GBAS system can be used if the military aircraft in question are equipped with the appropriate onboard avionics. However, in the context of using the GNSS in a military environment, the JPALS (Joint Precision Approach and Landing System) is typically preferred for these purposes due to safety and resistance to interference. The JPALS system was developed specifically for the needs of military aviation and compared to the GBAS system, offers additional advantages such as mobility and the ability to operate in environments with limited navigation infrastructure.

The system consists of components similar to those of the civilian GBAS. The system achieves guidance accuracy of up to 200 mm [21] and is primarily used for precision approaches on aircraft carriers [22]. The system's mobility is ensured by "eJPALS," which is capable of providing precise guidance to up to 50 designated targets within a 20-nautical-mile radius [23]. The system can be activated at any location as needed within 60 to 90 minutes after deployment. The use of the GBAS system by military aircraft can be expected primarily at airports with mixed civil-military traffic, or during peacekeeping or coalition missions, when military aircraft equipped with the necessary avionics can safely use civilian airport infrastructure.

Benefits of GBAS:

- the ability to use a single installation for approaches to multiple runways, thereby significantly reducing costs, compared to using an ILS system, where each runway requires its own ILS installation,
- greater flexibility - it allows for various approach trajectories, which can reduce noise pollution or enable approaches in mountainous terrain,
- increased runway capacity - various descent trajectories and, where applicable, different touch-down points allow for reduced spacing between aircraft, considering wake turbulence,
- lower operating and maintenance costs compared to the ILS system,
- resistance to signal interference from fixed obstacles (terrain or airport-related),
- minimal extent of protective sensitivity zones.

Risks of GBAS:

- requires aircraft equipped with GBAS-compatible receivers, which is currently a very limited group of aircraft,
- aircraft operators' reluctance to upgrade avionics may limit its wider adoption,
- initial investment may be high depending on the need for additional airport equipment,
- current certification limitations to only GBAS Type C (GAST C) approaches and landings,
- dependence on the GNSS signal and all risks associated with potential GNSS signal interference.

2.3 TACAN (Tactical Air Navigation System)

TACAN is a military radio navigation system that provides data on the direction and slant range to a TACAN ground radio navigation station [24]. Its operating principle is similar to that of VOR/DME. The TACAN operates in the UHF band (962-1213 MHz) and combines both functions-azimuth navigation (determining the direction to the transmitter) and distance measurement, which provides data on the distance from the transmitter.

The TACAN is not commonly installed at civil airports. If implemented, it is typically in a hybrid version, known as a VORTAC station. The advantages of the TACAN system include, above all, greater accuracy than that of a VOR/DME combination (TACAN has smaller directional deviations than a classic VOR and a higher update frequency and accuracy than a classic DME), better performance in challenging conditions (it operates even in difficult terrain and in environments with high interference), and the ability to encrypt it or operate it in a secure mode, which makes it ideal for military use. A major disadvantage is the incompatibility of civilian aircraft with its use.

2.4 VORTAC (TACAN + VOR)

VORTAC is a combined navigation system that integrates the military TACAN system with standard VOR (VHF Omnidirectional Range) navigation equipment. It therefore provides both directional guidance (VOR for civil aviation and TACAN for military purposes) and distance measurement (DME, available to both sectors). The VORTAC system is primarily used at airports with mixed civil-military traffic. It can be used, for example, as a backup system for approach systems

Table 1 *Comparison of selected approach systems in terms of their basic technical and operational characteristics*

Features	ILS	GBAS (Ground-Based Augmentation System)	VORTAC
Function	It provides precise guidance during approach and landing in both the horizontal and vertical planes.	By correcting the GNSS signal, it enables the precise guidance during approach and landing in both the horizontal and vertical planes.	It provides bearing (course (*)) and distance (DME) information.
Usage	Precision approach and landing (3D) under CAT I, CAT II, or CAT III conditions	Precision 3D approach and landing (currently CAT I certification only)	En-route navigation and non-precision instrument approach (2D) without vertical guidance (*)
Accuracy	Extremely precise horizontal and vertical guidance	High-precision positioning with GNSS error correction (to within centimetres)	High accuracy for directional guidance (*) and distance
Frequency range	VHF (LOC: 108-112 MHz) + UHF (GS: 329-335 MHz)	GPS L1 (1575.42 MHz) + VHF Data Broadcast (VDB), 108–117.975 MHz	VOR: VHF (108-117.95MHz) TACAN (*) and DME: UHF (962-1213 MHz)

(*) Note: The TACAN component is usable only for military or government aircraft

Table 2 *Comparison of selected approach systems in terms of their operational resilience, implementation requirements, benefits, limitations, and compatibility*

Features	ILS	GBAS (Ground-Based Augmentation System)	VORTAC
Interference resistance	Susceptible to interference and signal reflections from obstacles	Dependent on availability and quality of the GNSS signal - susceptible to interference and spoofing	Interference-resistant TACAN (*) component, encryption capability
Signal availability	Limited range (approx. 25-30 km) for a single runway only	Wide coverage - can serve multiple runways at a single airport	Limited range; line of sight required
Difficulty of installation	High (each runway requires its own ILS); CAT II and CAT III installations require additional equipment	Lower than ILS - a single, strategically located station that can serve the entire airport	A central, suitable location allows for approaches to two-way runways (two runways, one VORTAC)
Advantages	Reliable and proven, CAT II/III suitable for use in extremely low visibility conditions	Versatile, more affordable than ILS, compatible with modern avionics	Suitable for both civilian and military use; TACAN section resistant to interference; option for shielded mode; option for military use
Disadvantages	Costly maintenance, each runway direction requires its own system and a wide, sensitive area to protect the signal	Dependence on availability and quality of the GNSS signal requires equipment on board aircraft (currently a small percentage of aircraft)	It does not provide vertical guidance during approach, which is only 2D
Compatibility	Universal, standard-issue avionics for all aircraft in commercial service	So far, only modern aircraft equipped with GNSS and SBAS/GBAS receivers; a small percentage	Most military and civil aircraft are equipped with the necessary avionics as standard (*)

(*) Note: The TACAN component is usable only for military or government aircraft

based on GNSS signal reception. In the event of GNSS signal interference, VORTAC can provide alternative navigation [25]. For a civil aircraft operated under IFR, navigation equipment must correspond to the planned route, airspace requirements, and procedures used. In its Acceptable Means of Compliance for commercial air transport, EASA lists, among other things, a VOR receiver as part of such equipment [26]. For a military and government aircraft, TACAN equipment is widely used, with EUROCONTROL noting that most government aircraft are equipped with DME and TACAN systems for conventional navigation [27]. The use of VORTAC equipment is negatively affected by the fact that it allows only for imprecise, so-called 2D, approaches due to the lack of vertical guidance.

Benefits of VORTAC:

- wide compatibility - allows for use by both civil and military aircraft,
- provision of navigation data for mixed civil-military traffic - VOR provides civil directional guidance, while TACAN ensures higher accuracy and the option of encryption for military use,
- DME availability for both sectors - both civil and military aircraft can use the same distance information,
- navigation redundancy - VORTAC provides a backup navigation system in the event of a failure of other GNSS systems.

Risks of VORTAC:

- higher maintenance costs - the combination of two systems requires more complex servicing and is more technically and organizationally demanding than a purely civil VOR/DME (interconnection of civil and military technology),
- lower accuracy than GBAS or ILS - although it provides reliable data, it is not as accurate as modern landing systems and does not allow for approaches and landings in low visibility,
- does not provide vertical guidance like GBAS and ILS,
- risk of premature decommissioning before the end of its planned service life due to the transition to modern satellite navigation - if the technical and security issues associated with GNSS (vulnerability to jamming and outages) are resolved, as has already been done with the military JPALS system, and the use of GNSS-based technologies subsequently expands, some VOR equipment at VORTACs may be used less frequently and their operation could become uneconomical.

2.5 Summary - comparison of different types of approach systems

Tables 1 and 2 present a comparison of the selected approach systems-ILS, GBAS, and VORTAC-in terms of their different characteristics. The standalone TACAN

Table 3 *Price comparison of systems in 2015 (based on [28] and supplemented by the authors from public sources)*

Approach Technology Comparison				
Feature	ILS	GBAS	SBAS	VORTAC
Coverage	One runway end	All runways at the installed airport	Continental (based on number of installed reference stations)	Both ends of a bidirectional runway (depending on ground station location)
Equipment and installation Cost (capital)	$1,500K per runway end	~$3,300K per airport	TBC - $1,000M+ per country	~$500K-$1M per station (includes both VOR and TACAN subsystems)
O&M Annual cost	>$140K per ILS Flight test/ calibrate once per year	$85K - $135K per station, parts, and labour; annual flight inspection not req.	$50M-$100M per country	~$50K-$100K (maintenance, calibration, power, testing)
Users per approach	1 (plus other in sequence)	Unlimited	Unlimited	Unlimited
Number of approaches	1	26 (48 w/Cat III) approaches from one ground station (approaches broadcast from ground station)	Unlimited non-precision approaches (airborne database contains approaches)	Limited non-precision approaches, usually 1 (based on radials DME arcs and position of MAPt)
Aircraft equipage	ILS receiver	GLS avionics	SBAS capable GPS receiver, approach data base	VOR/DME or TACAN receiver (military); VOR receiver (civil)
Capabilities	One approach per ILS; Cat I, II, and III	Flexible approaches: multiple glide slopes, thresholds, offsets; No ILS critical area; Cat I, growth to Cat II/III	Flexible non-precision approaches including LPV	Non-precision approach; lateral guidance only (no vertical guidance)

system is not included in the tables. Given its very limited use in civil aviation, it makes sense to consider installing it only in combination with a VOR system, i.e., as a VORTAC system. From the civil aviation perspective, the ILS CAT II/III system remains the key system for approach and landing in low-visibility conditions. However, the system is expensive and requires a separate installation for each runway. The GBAS system is a modern alternative that uses GNSS signals with corrections. Additionally, the system is not yet widely adopted, due to the higher cost of receivers, the potential for GNSS signal interference, and insufficient certification (only CAT I). VORTAC is a system particularly suitable for airports with a military presence, where the VOR component and distance measurements using the TACAN component are utilized by civil aircraft as a supplementary navigation system or for VOR/DME approach purposes.

A price comparison of the systems is presented in Table 3; it was conducted by Honeywell in June 2015 and supplemented with information obtained by the authors from public sources [28].

When deciding on selection of a suitable approach system, one cannot evaluate only the purchase costs of the equipment and its installation. The economic suitability of individual options must be assessed within a broader life-cycle framework, which includes not only initial investment costs but also operating costs, routine and non-routine maintenance, flight verification, replacement of technical components, ensuring operational readiness, and costs associated with potential system unavailability or an inadequate category of operating minima [29-30]. Furthermore, it is necessary to consider the broader economic impacts on carriers, passengers, cargo shippers, air traffic service providers, or other entities involved in the air transport system [31-32].

The lower acquisition costs for an approach system may, without a broader assessment, represent a more economically advantageous solution; however, if such a system does not provide sufficient operational usability under degraded meteorological conditions, it may lead to frequent diversions to alternate airports, delays, flight cancellations, or a reduction in the ability to attract new carriers and business opportunities. In its standard inputs for economic analyses, EUROCONTROL provides separate values for the costs of delays, flight cancellations, and diversions, and specifies recommended cost values per diverted flight [31].

3 AHP-based methodological framework for approach-system selection

The proposed framework consists of a structured sequence of decision-making steps that adapt the general AHP procedure to the operational and technical specifics of approach-system modernization at regional public international airports. It is intended for cases in which several technically feasible approach-system

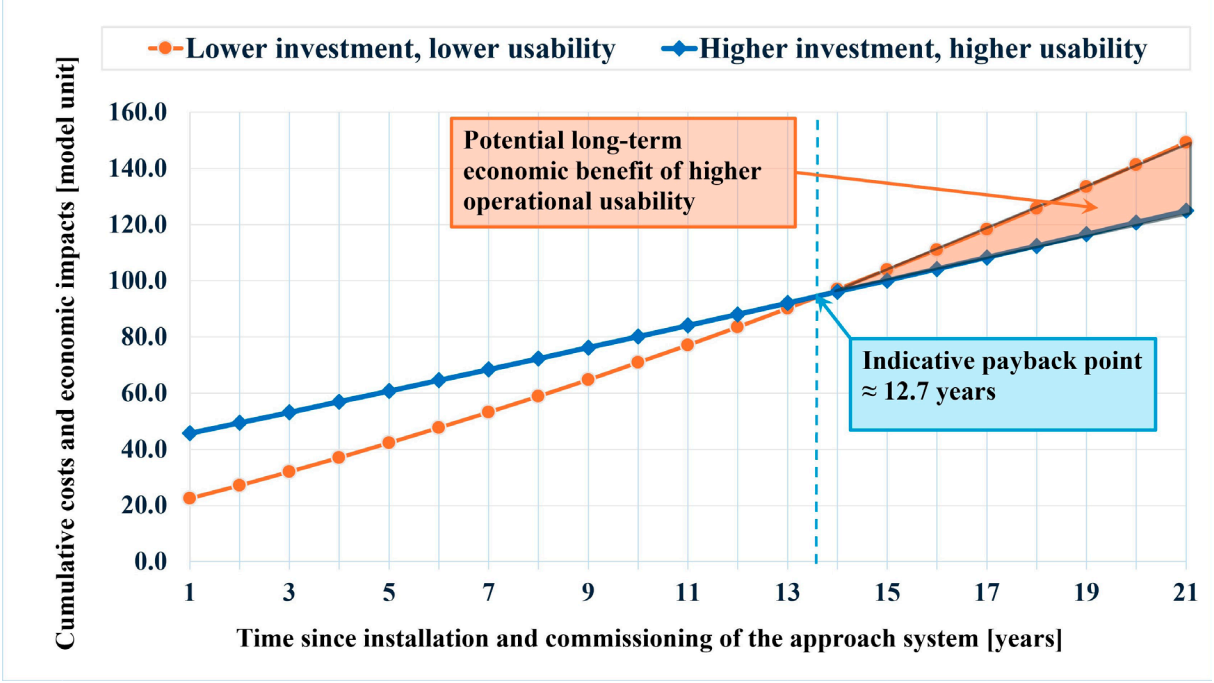


Figure 1 *Illustrative trend of cumulative costs for the approach system over time*

alternatives must be assessed with respect to expected traffic structure, including potential mixed civil-military operations, aircraft equipage, operational usability, installation constraints, resistance to interference and future flexibility.

The selection of an appropriate approach system for airport modernization is influenced by a range of operational, technical and strategic factors that must be assessed simultaneously. Given the complexity of the issue, the AHP method, which enables multi-criteria decision-making, was selected for the purpose of evaluating the suitable approach-system alternatives [33]. This method allows for structuring a complex decision-making problem into a hierarchy of simpler elements, including the objective, criteria, and alternatives, and subsequently determining their relative importance through pairwise comparisons [34].

Figure 1 provides an illustrative chart showing that an option requiring a higher initial investment may be more cost-effective in the long run due to lower losses resulting from diversions, cancelled flights, and missed business opportunities.

3.1 Proposed decision-making procedure for selecting an approach system

The proposed decision-making procedure is divided into consecutive steps that guide the airport operator or decision-maker from the initial operational assessment to the final ranking of approach-system alternatives:

1. An evaluation of existing approach systems, including the preparation of an overview of current approach systems, taking into account their expected service life, ranking the equipment based on actual operational use and minimum OCH/OCA altitudes, which determine the probability of completing the approach and landing, and the preparation of a list of the advantages and disadvantages of the individual installed approach systems.
2. Establishment of a uniform time horizon for which the decision is implemented. This depends, for example, on the design life of the runway, or on the time that has elapsed in the past between the introduction of the two previous consecutive and technologically significantly different approach systems. For example, the average interval between technologically significant implementations in the field of approach systems-from NDB, VOR, ILS, and MLS to GBAS-is 19 years [35].
3. Determining the scope and type of anticipated operations within a defined time horizon. This depends on the planned operational and commercial focus and use of the airport. If mixed civil-military operations were expected, it is necessary to specify the intensity and composition of military operations and coordinate further steps with the military.
4. The expected fleet structure should be assessed according to the anticipated composition of aircraft types most likely to use the airport under the expected business model within the assessed time horizon. Particular attention should be paid to the anticipated avionics and navigation equipment of the aircraft and their compatibility with existing and proposed approach systems. The approach systems and equipment considered for modernization should then be defined, including an assessment

of currently available systems that could improve the airport's usability in the context of the expected type and mix of traffic over the planned time horizon (v_1 to v_p).

5. Establishment of evaluation criteria. Their definition should take into account the information obtained in the previous steps (1-4). Before defining the final evaluation criteria, it was also necessary to consider whether economic aspects should be included directly in the AHP model. Although the acquisition and operating costs are undoubtedly important for the final investment decision, they were not included as a separate AHP criterion in this study. Reliable and comparable life-cycle cost data for all evaluated alternatives were not available, since the costs of installation, certification, maintenance, flight inspection, protection zones, power supply backup and integration into existing airport systems strongly depend on the specific configuration of each airport, procurement conditions and national regulatory requirements. Including only approximate or incomplete cost estimates could therefore distort the operational and technical comparison of the alternatives. The proposed AHP model is therefore intentionally limited to operational and technical suitability, while economic feasibility is considered a necessary subsequent step before final investment approval. On this basis, within the framework of the presented methodology, five criteria were defined (K_1 up to K_5), which can be applied to other airports or modified as needed. These criteria are as follows:
   a. Aircraft equipped with this technology (K_1) - an assessment of the extent to which aircraft are equipped with specific equipment (e.g., how many of the aircraft expected to operate at the airport have the necessary onboard equipment compatible with the systems proposed in the alternatives) and how significant it is for the selected alternative to take into account the avionics of the expected aircraft types that will use the airport most frequently;
   b. The complexity of the placement and installation of technology at the airport (K_2) - an assessment of the scope of the establishment of protection and sensitive zones for the proposed system or facility, and the associated procedural and operational restrictions; how significant these restrictions are for the selected option; and how significant their impact is on airport operations;
   c. Equipment immunity to interference (K_3) - an assessment of how significant the criterion of the ability of the sought-after guidance system or device to withstand external influences and perform its function reliably is, and to what extent this criterion is relevant and important for the expected operation, so that the device can perform this function;
   d. The applicability of the technology (K_4) - an assessment of the importance placed on usable operational minima expressed in terms of approach precision, minimum visibility, and minimum decision height, taking into account the operational use and the expected operational and business model of the airport, and the significance of ensuring the ability to approach and land even under very low visibility conditions;
   e. Flexibility in the use of technology within the airport (K_5) - determining the level of importance of the flexibility of the target system, for example, for approaching and landing on multiple runways, the flexibility of the approach trajectory in both the horizontal and vertical planes, the possibility of multiple touchdown points, or its applicability for area or terminal navigation.
6. Application of the AHP Method. Selected experts (ideally representatives of the airport operator, commercial entities expected to significantly contribute to airport operations, representatives of the air traffic services provider, etc.) should assess, using pairwise comparisons, the relative importance of individual criteria and alternatives. The assessment will reflect previously defined operational, commercial, geographical, environmental, and other relevant requirements and expectations. Based on these assessments, the following steps will be carried out:
   a. Saaty pairwise comparison matrix for the established criteria will be created;
   b. Saaty pairwise comparison matrices for individual alternatives with respect to each evaluation criterion will be created;
   c. Geometric means will be calculated and the weights of individual criteria and the local weights of alternatives with respect to each criterion will be determined through normalization;
   d. The consistency of the pairwise comparison matrices will be verified by calculating the Consistency Index (CI) and the Consistency Ratio (CR);
   e. Global priorities and the overall ranking of the alternatives will be calculated.
7. Decision on the selection of an appropriate approach system. The alternative that received the highest global score when the AHP method was applied S_i, represents an approach system that has been evaluated as the most suitable approach system for the purposes of the airport's modernization, considering the planned and expected operational development of the regional airport in question.

The flowchart in Figure 2 illustrates the proposed methodology algorithmically.

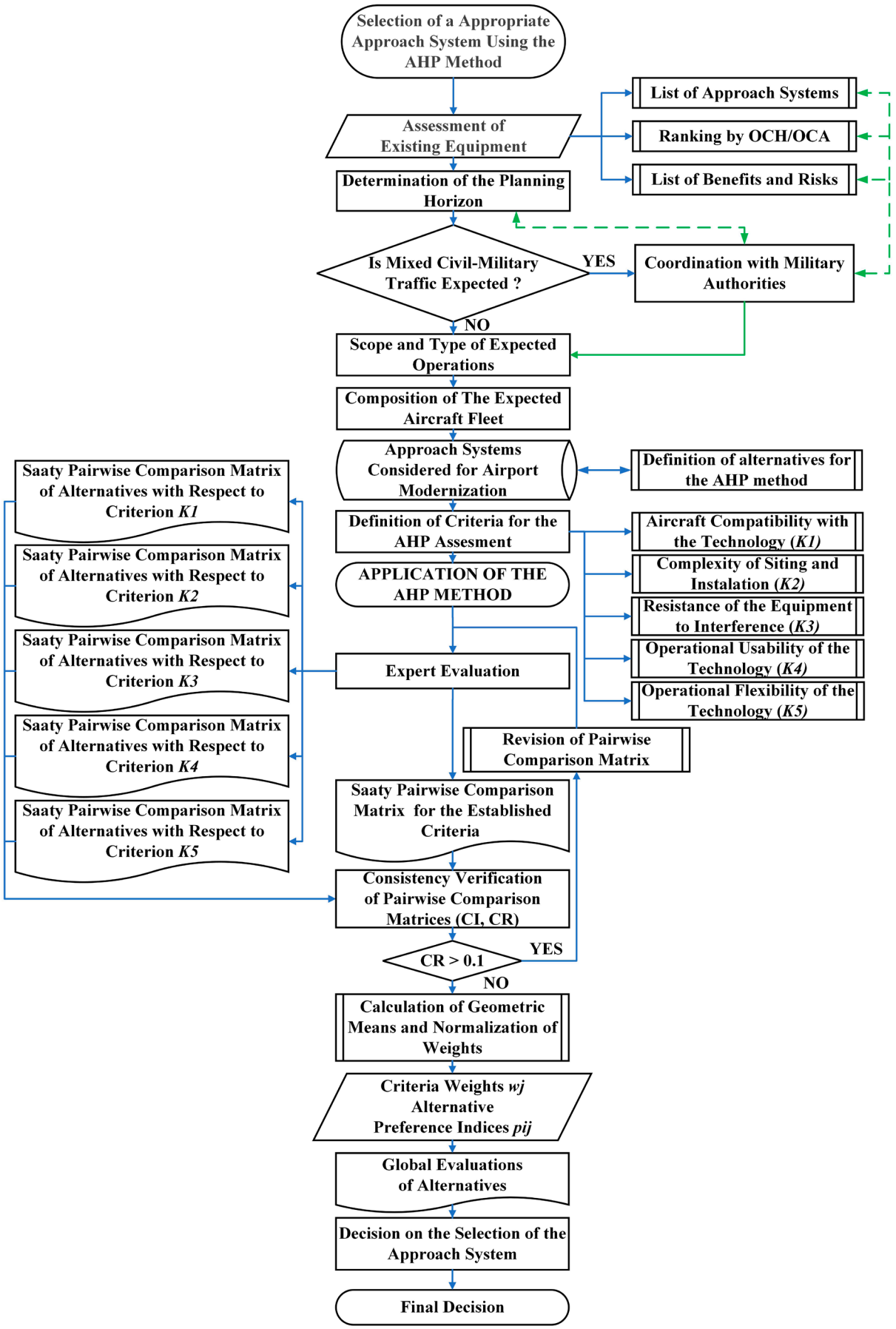


Figure 2 *Flowchart of the methodology based on AHP method for selecting an approach system*

Table 4 *An overview of minimum altitudes for individual approaches at LKMT Airport [12]*

OCA/OCH, Cat. C (ft)	RWY 04	RWY 22
ILS CAT III	N/A	---/50 (DH)
ILS CAT II	N/A	880/72
ILS CAT I	N/A	983/175
RNP (LPV)	1008/200	1008/200
VOR/DME	1210/370	1170/370

4 Case study of modernization - Ostrava/ Mosnov regional airport

Ostrava/Mosnov International Airport (LKMT) is a major regional transportation hub with international traffic. Thanks to its strategic location and advanced infrastructure, it facilitates the efficient operation of both passenger and cargo air transport. Ostrava/Mosnov Airport has a runway 3,511 metres long and 63 metres wide, which allows for takeoffs and landings of all types of aircraft, including wide-body commercial aircraft. The runway is used in both directions and is oriented 044°/224° (designation: RWY 04/22).

In the 1980s, the airport's movement areas were partially reconstructed and are now at the end of their service life. Administrative procedures related to their reconstruction are currently being finalized. In this context, the issue of a potential modernization of the safety equipment, including approach systems, has also been raised. In connection with the planned development of the airport, negotiations took place, followed by the signing of a Memorandum of Cooperation regarding the preparation of the site for the implementation of the "Mosnov Logistics Center of the Czech Army" project, between representatives of the Moravian-Silesian Region and the Ministry of Defense of the Czech Republic [36]. The operation of the military logistics center automatically presupposes mixed civil-military traffic, specifically the operation of military transport aircraft.

4.1 Application of the AHP method to approach-system selection at Ostrava/Mosnov airport

The first step of the proposed methodology involves compiling an overview of the approach systems available at the airport, for each runway direction. The approach equipment and systems currently installed and used at Ostrava Mosnov Airport for aircraft approach and landing are:

- ILS (Instrument Landing System) - at LKMT Airport, an ILS is installed only for RWY 22 and is certified for CAT III operations,
- VOR/DME (VHF Omnidirectional Range / Distance Measuring Equipment) - one VOR/DME unit designated as OTA is installed at LKMT Airport. The OTA VOR unit is located approximately at the centerline of the runway in its immediate vicinity and is usable for non-precision (2D) instrument approaches for both runways 04 and 22,
- RNAV/GNSS (Area Navigation / Global Navigation Satellite System) - the system is usable for both runways 04 and 22, for which RNP approaches utilizing GNSS navigation systems are published.

One of the most important parameters for individual approach aids, and their corresponding approach procedures, is the published minimum obstacle clearance altitude. The decision height, or minimum descent altitude, is derived from this. The lower this altitude is, the higher the probability that the pilot will establish a visual reference and complete the approach with a landing. When considering the modernization of an approach system, it is therefore important to include this criterion in the decision-making process and to assess how important the selected system's ability to enable the aircraft to approach and land in low visibility is for the final choice. An overview of the minimum altitudes for individual approach procedures at LKMT Airport is clearly presented in Table 4. The individual approaches are listed in ascending order from the most precise (ILS, RNP, VOR/DME). The data provided apply to Category C aircraft, which are commonly used for commercial flights at LKMT Airport.

The second step involves determining the time horizon for which the assessment and selection are being conducted. Another factor that can influence the determination of the time horizon, and which was also considered in this case-is the expected expansion and further technological development of the existing equipment. Given the dynamic technological development in the field of GNSS, the time horizon within which the selected approach system should, to the greatest extent possible, appropriately complement the existing installed approach systems and best meet the expected operational use of LKMT Airport was set at 15 years.

The third step involves determining the scope and type of operations and the expected aircraft mix. Ostrava/Mosnov Airport is a seasonally oriented airport with a high proportion of passenger charter air traffic during the summer months. The share of year-round scheduled passenger air transport is very small due to the high competition from the nearby Polish airports of Katowice and Krakow, and only slow development of

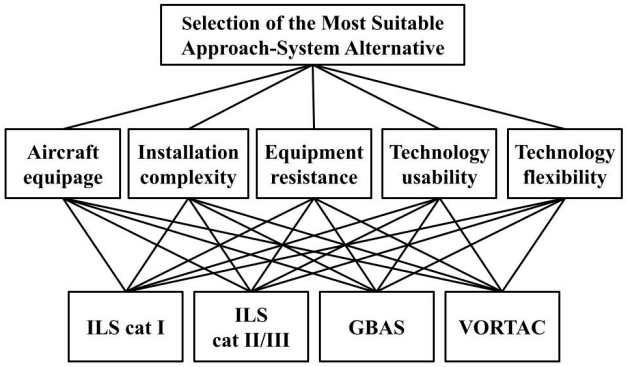


Figure 3 *Hierarchical structure of the problem under consideration*

additional scheduled routes can be expected within the assessed time horizon.

However, long-haul cargo air transport has been developing very dynamically in recent years and is gradually transforming into a year-round scheduled flight schedule. The cargo air transport is expected to play a dominant role in the airport's operational use in the coming period as well. Currently, it is carried out by older cargo aircraft equipped with standard radio navigation equipment used for approach and landing. The pressure on the operating costs of the airlines providing this transport does not allow for massive investment in modern approach technologies.

The planned military logistics center, which will be linked to military aircraft operations, is to be primarily focused on servicing and supplying international missions of the Czech Army and allied forces, or on providing rapid assistance in the distribution of humanitarian aid in the event of natural disasters and other humanitarian situations anywhere in the world. This purpose assumes the use of military transport aircraft, which are typically equipped with standard approach systems used in civil aviation. The operation of the logistics center does not involve the presence or deployment of military combat aircraft.

In addition to general aviation, the remaining existing air traffic consists of aircraft bound for the maintenance facilities located in the northern part of the airport. An area has been reserved at this location for the future expansion of aircraft painting capacity. However, all these activities are expected to involve predominantly older aircraft with conventional avionics and a relatively low level of adoption of the most advanced GNSS-based technologies.

Based on the preceding analysis and the available sources, the following modernization alternatives were identified for selecting an appropriate approach system capable of meeting the objective of modernizing the existing facilities at LKMT Airport:

- ILS CAT I RWY 04 - equipping Runway 04 with an ILS precision approach system enabling approaches and landings under CAT I conditions;
- ILS CAT II/III RWY 04 - equipping runway 04 with an ILS precision approach system enabling approaches and landings under CAT II/III conditions, including operations under low visibility conditions (LVO - Low Visibility Operation);
- GBAS - equipping the airport with a GBAS system, which will enable precision approaches and landings for both runways (RWY22 and RWY04), designated as GLS;
- VORTAC - equipping the airport with VORTAC equipment, which, when properly located, will enable non-precision instrument approaches for both runways (RWY22 and RWY04), with civilian aircraft using the VOR/DME portion of the equipment and military aircraft using the TACAN portion, both of which are included in the VORTAC system.

The next step is to establish the criteria for evaluating the most suitable option. The modernization options under consideration must be evaluated based on the significance of the identified criteria, which were proposed and described in the previous section. In combination with the established preference indices for the proposed approach systems at Ostrava/Mosnov Airport, the most suitable solution will then be identified.

The next step is application of the AHP method. The hierarchical structure of the decision-making problem is shown in Figure 3.

To evaluate the individual criteria and alternatives, an expert panel from the air transport sector was consulted. The experts were selected intentionally, based on their practical knowledge of airport operations, approach and landing procedures, aircraft equipage, operational limitations of regional airports, and the potential implications of mixed civil-military traffic. The expert group consisted of specialists familiar with the operational environment of LKMT Airport, including airport operations, aircraft operations, air traffic services, military aircraft operations, and aviation education and research. The composition of the expert panel is summarized in Table 5.

The expert evaluation was carried out in two steps. First, the experts assessed the relative importance of the proposed evaluation criteria using pairwise comparisons based on Saaty's scale. Second, they evaluated the local preferences of the approach-system alternatives with respect to each individual criterion. The assessed

Table 5 *Composition of the expert panel used for the AHP evaluation*

Expert	Professional background	Practical experience	Role in the AHP evaluation
E1	Airport operations / airport management	27 years	Airport infrastructure, operational impacts and implementation constraints
E2	Aircraft operations / pilot	35 years	Aircraft equipage and operational applicability of alternatives
E3	Air traffic services / ATC	26 years	ATC procedures, operational usability and impacts on airport operations
E4	Aviation education and research	21 years	Methodological structure, criteria formulation and consistency check
E5	Military aircraft operations / pilot	28 years	Military aircraft equipage, mixed civil-military usability and operational requirements

alternatives were ILS CAT I for RWY 04, ILS CAT II/III for RWY 04, GBAS and VORTAC. The expert evaluation was carried out as a consensus-based group assessment. The experts jointly discussed the relative importance of the criteria and the local preferences of the alternatives and agreed on the final values entered into the pairwise comparison matrices. This procedure was used to reflect a shared expert judgment rather than a statistical aggregation of independent individual assessments. The consistency of each matrix was verified using the Consistency Ratio (CR). Where the initial consistency ratio exceeded the recommended threshold, the relevant comparisons were reviewed by the expert group and revised only based on the professional judgment, without changing the calculation procedure or forcing a predetermined ranking of alternatives.

Based on the consolidated expert judgments, a Saaty pairwise comparison matrix was first compiled for the evaluation criteria. The criteria considered in the analysis were as follows: aircraft equipage with the given technology, complexity of locating and installing the technology at the airport, resistance of the equipment to interference, usability of the technology, and flexibility of the technology within the airport environment.

Before applying the AHP method to determine the final ranking of the proposed approach-system alternatives, the consistency of the original pairwise comparison matrix of the evaluation criteria was verified. The initial matrix did not meet Saaty's consistency requirement, as the calculated Consistency Ratio (CR) exceeded the generally accepted threshold value of 0.10 [33-34]. For this reason, the original expert assessment of the relative importance of the criteria was reviewed and revised by the expert group. The revision process was focused only on those pairwise comparisons that contributed most significantly to the inconsistency of the criteria matrix. The experts were therefore asked to reconsider these selected judgments while preserving the original decision-making logic and the operational meaning of the criteria. No changes were made to the AHP calculation procedure itself, and the revision was limited exclusively to the expert judgments expressed in the pairwise comparison matrix.

The revised pairwise comparison matrix preserved the original logic of the expert evaluation but adjusted selected pairwise comparisons so that the matrix would meet the required level of consistency. This procedure ensured that the final criteria weights were not obtained by arbitrary mathematical adjustment, but by a controlled revision of the expert assessment. The resulting criterion weights are presented in Table 6.

The consistency check of the revised criteria matrix confirmed its acceptability. The calculated values were λ_{max} = 5.4099; CI = 0.1025; RI = 1.12; CR = 0.0915. Since the resulting CR value is lower than 0.10, the revised matrix can be considered sufficiently consistent according to Saaty's recommended threshold. In addition to the revised criteria matrix, the local pairwise comparison matrices of the alternatives with respect to the individual criteria were also checked for consistency before calculating the final global preference scores.

The results show that, for the LKMT Airport, the most important criterion is the usability of the technology (K_4), with a weight of 0.4242. In the context of this study, this criterion primarily reflects the operational usability of the approach system with respect to the achievable approach and landing minima. The second most important criterion is the aircraft equipage with the given technology K_1, with a weight of 0.2769. This result indicates that the practical applicability of the selected approach system strongly depends on whether it can be used by a sufficiently broad range of aircraft expected to operate at LKMT Airport, including both civil aircraft and military transport aircraft in the case of possible future mixed civil-military operations.

In the next step, the expert group applied the AHP method to evaluate the proposed alternatives separately with respect to each criterion. The assessed alternatives were ILS CAT I for RWY 04, ILS CAT II/III for RWY 04, GBAS, and VORTAC. For each evaluation criterion, a separate local Saaty pairwise comparison matrix was created, and the local weights of the alternatives were calculated.

For illustrative purposes, the local Saaty matrix for the first criterion, the aircraft equipage with the given technology K_1 is presented in Table 7. This criterion

reflects the extent to which aircraft expected to operate at LKMT Airport are equipped to use the respective approach system. The results show that, with respect to this criterion, ILS CAT I and VORTAC achieved the highest local weights, both reaching 0.3478. ILS CAT II/III reached a local weight of 0.2068, while GBAS achieved the lowest local weight of 0.0975. This result reflects the current differences in aircraft equipage and operational readiness for the use of individual technologies.

The consistency of each local Saaty matrix was verified using the Consistency Ratio (CR). All the local matrices met Saaty's recommended consistency threshold, as the calculated CR values were lower than 0.10. The local weights of the alternatives obtained for the individual criteria are summarized in Table 8.

The global weights of the alternatives were subsequently calculated by multiplying the local weight of each alternative under each criterion by the corresponding criterion weight and summing these partial values across all criteria. This procedure expresses the overall preference for each alternative while considering both the importance of the criteria and the local performance of the alternatives under each criterion. The results of the global evaluation are listed in Table 9.

The final step was to evaluate the results obtained using the AHP method. The global evaluation showed that the most suitable alternative for the modernization and extension of radio navigation equipment at LKMT Airport is the installation of an ILS CAT II/III system for RWY 04, with a global weight of 0.2998. This result is mainly influenced by the high importance of criterion K_4 - usability of the approach system with respect to approach and landing minima, which achieved the highest criterion weight. Under this criterion, ILS CAT II/III obtained the highest local preference, confirming its operational advantage in low-visibility conditions and its ability to significantly increase the probability of completing an approach and landing under adverse meteorological conditions.

The second-ranked alternative was GBAS, with a global weight of 0.2390. Expanding the airport's equipment and utilizing GNSS through the implementation of GBAS technology would increase the redundancy and efficiency of navigation available for both runway directions, particularly for precision instrument approaches under CAT I conditions. The GBAS also offers important advantages in terms of lower requirements for critical and sensitive areas compared with ILS, as well as the potential to support multiple runway approach directions from a single ground-based station. These characteristics may contribute to greater operational flexibility and, in some cases, to increased airport capacity. However, the overall result of GBAS is limited by the lower aircraft equipage and by the fact that its current operational usability is primarily associated with CAT I minima. In the context of the present evaluation, this reduced its competitiveness compared with ILS CAT II/III, especially because criterion K_4 had the highest weight in the overall assessment.

The third-ranked alternative was ILS CAT I for RWY 04, with a global weight of 0.2366. This option would improve the availability of RWY 04 for instrument approaches and would provide a widely used, technically proven, and broadly compatible approach system. However, compared with ILS CAT II/III, it would not provide the same level of operational benefit in low-visibility conditions. Therefore, although ILS CAT I represents a feasible and operationally useful alternative, its contribution to reducing the approach and landing minima would be more limited.

The fourth-ranked alternative was VORTAC, with a global weight of 0.2246. The addition of VORTAC, or TACAN-based equipment, is currently being discussed in connection with the Czech Army's planned activities at LKMT Airport. This alternative may be beneficial primarily for the military component of the expected mixed civil-military operation. For the civilian segment of air traffic, however, such modernization would bring only limited improvement compared with the current situation, particularly in terms of approach and landing minima. Although the VORTAC achieved relatively strong results in the criteria related to aircraft equipage and resistance to interference, its low local weight under criterion K_4 significantly reduced its final global score. This indicates that from the perspective of improving the airport's usability under adverse meteorological conditions, VORTAC provides a lower operational benefit than the precision approach alternatives considered in the analysis.

The selection of VORTAC could be justified mainly if its implementation were explicitly required by the military component, for example if the establishment of a logistics facility or another form of military presence at LKMT Airport were made conditional upon such equipment. An indirect benefit could consist in synergies and cost-sharing resulting from the shared use of airport infrastructure under mixed civil-military operations. However, if the expected military component consists primarily of military transport aircraft that are generally capable of using standard civil approach systems, and if encrypted or coded approach guidance is not essential for their operation, VORTAC cannot be considered the preferred option for the purposes of airport modernization.

Particularly in view of the high importance assigned to approach-system usability with respect to approach and landing minima, the installation of an ILS CAT II/III system for RWY 04 can be considered the most suitable option for the modernization and extension of LKMT Airport's radio navigation equipment. This solution would increase the airport's operational usability and strengthen its competitiveness in regional and international air transport. Together with the existing ILS CAT II/III system for RWY 22, the proposed

Table 6 *Determination of criterion weights using the Saaty method*

Criterion	K_1	K_2	K_3	K_4	K_5	Geometric mean G_i	Weight of criterion w_i
K_1	1	4	3	$\frac{1}{3}$	4	1.7411	0.2769
K_2	$\frac{1}{4}$	1	1	$\frac{1}{5}$	3	0.6843	0.1088
K_3	$\frac{1}{3}$	1	1	$\frac{1}{3}$	3	0.8027	0.1277
K_4	3	5	3	1	3	2.6673	0.4242
K_5	$\frac{1}{4}$	$\frac{1}{3}$	$\frac{1}{3}$	$\frac{1}{3}$	1	0.3920	0.0624

Table 7 *Saaty Pairwise Comparison Matrix of Alternatives with Respect to Criterion K_1*

Approach System	ILS CAT I (RWY04)	ILS CAT II/III (RWY04)	GBAS	VORTAC	Geometric Mean G_i	Local Priority of Alternative p_i
ILS CAT I (RWY04)	1	1	3	1	1.5651	0.3478
ILS CAT II/III (RWY04)	$\frac{1}{2}$	1	3	$\frac{1}{2}$	0.9306	0.2068
GBAS	$\frac{1}{3}$	$\frac{1}{3}$	1	$\frac{1}{3}$	0.4387	0.0975
VORTAC	1	2	3	1	1.5651	0.3478

Table 8 *Summary of Local Weights of Alternatives with Respect to Evaluation Criteria p_{ij}*

Criterion	ILS CAT I (RWY04)	ILS CAT II/III (RWY04)	GBAS	VORTAC
Aircraft equipped with this type of technology	0.3478	0.2068	0.0975	0.3478
The complexity of locating and installing technology at an airport	0.1887	0.1089	0.3512	0.3512
The device's resistance to interference	0.2510	0.2050	0.1219	0.4222
Usability of the technology with respect to the landing minima	0.1901	0.4656	0.2814	0.0629
Flexibility in the use of technology within the airport	0.1125	0.1125	0.6225	0.1525

Table 9 *Global evaluation of alternatives S_i based on the AHP method*

Criterion	Weight w_i	ILS CAT I (RWY04)	ILS CAT II/III (RWY04)	GBAS	VORTAC
Aircraft equipped with this type of technology	0.2769	0.0963	0.0573	0.0270	0.0963
The complexity of locating and installing technology at an airport	0.1088	0.0205	0.0118	0.0382	0.0382
The device's resistance to interference	0.1277	0.0320	0.0262	0.0156	0.0539
Usability of the technology	0.4242	0.0806	0.1975	0.1194	0.0267
Flexibility in the use of technology within the airport	0.0624	0.0070	0.0070	0.0388	0.0095
Global Preference Indices for Alternatives		0.2366	0.2998	0.2390	0.2246
Results		3	1	2	4

ILS CAT II/III system for RWY 04 would provide mutual operational redundancy, particularly in situations where runway selection is affected by wind direction and tailwind limitations.

A disadvantage of this option is the need to establish the protection areas for the LOC and GP components serving RWY 04. However, given the existing experience with similar equipment installed for RWY 22, the implementation of such protection areas should be manageable from both procedural and operational perspectives. It should not create significant difficulties in terms of staff training or airport operating procedures.

The main operational disadvantage of this alternative is the need for regular maintenance, inspections, and flight checks, which will increase the financial costs associated with airport operation. Despite these disadvantages, the AHP results indicate that ILS CAT II/III for RWY 04 provides the most balanced and operationally beneficial solution for the modernization of approach-system infrastructure at LKMT Airport.

4.2 Sensitivity analysis of the AHP results

Since criterion K_4, representing the usability of the approach system with respect to approach and landing minima, obtained the highest criterion weight, a one-way sensitivity analysis was carried out to examine whether the final recommendation was excessively dependent on this dominant criterion. The purpose of the analysis was to verify whether the moderate changes in the weight of K_4 would change the preferred alternative.

The sensitivity analysis was performed by decreasing and increasing the weight of K_4 by ±10% and ±20%, while the weights of the remaining criteria were proportionally normalized so that the total sum of all criteria weights remained equal to 1. The local priorities of the alternatives with respect to individual criteria were kept unchanged.

The results showed that ILS CAT II/III for RWY 04 remained the preferred alternative in all tested scenarios. Although the order of the lower-ranked alternatives changed in some scenarios, the first position remained stable. This indicates that the final recommendation is influenced by the high importance assigned to operational usability, but it is not determined solely by this criterion.

The sensitivity analysis therefore confirmed that the preference for ILS CAT II/III is robust under moderate changes in the weight of K_4. The result follows from the combined effect of the criterion weights and the local priorities of the alternatives, rather than from the dominance of a single criterion alone.

5 Conclusion

In this article was addressed the operational and technical assessment of suitable approach-system alternatives for an international regional airport with anticipated mixed civil-military traffic in the event of future modernization. The theoretical part of the article provided a description of selected approach systems, summarized their basic advantages and disadvantages, and presented a methodological framework for the selection process, using the AHP method.

Within the proposed methodology, it was necessary to evaluate the current range of available approach systems, define the relevant time horizon, specify the scope and type of expected traffic, and determine the anticipated structure of the aircraft fleet, including possible military aircraft. In the article are presented the sample evaluation criteria intended for operational and technical assessment of approach-system alternatives. Those criteria could be modified or expanded according to the specific operational, technical, economic, or strategic conditions of the airport under consideration.

The practical part of the article was devoted to application of the proposed methodology at Ostrava/Mosnov Airport, where the runway reconstruction is expected in the coming years and where the mixed civil-military operations are currently being considered. The AHP result showed that, for the purposes of modernizing and expanding the airport's radio navigation equipment, the installation of a Category II/III ILS system for RWY 04 is the most suitable option. In addition to the basic AHP evaluation, a sensitivity analysis was carried out to verify the stability of the final ranking with respect to changes in the weight of the most influential criterion. The results confirmed that ILS CAT II/III for RWY 04 remains the preferred alternative even under moderate changes in criterion weights. This option increases the airport's operational usability, particularly with respect to approach and landing minima under adverse meteorological conditions. The results also showed that GBAS represents a promising alternative, mainly due to its flexibility and lower requirements for protection areas. However, its current operational limitations and lower aircraft equipage reduce its overall suitability in comparison to ILS CAT II/III. ILS CAT I remains a feasible but less operationally beneficial option, while the VORTAC appears to be the least suitable alternative for modernization focused on improving the airport's usability in low-visibility conditions.

The proposed methodology can be applied to other regional airports facing similar modernization decisions. However, the specific ranking of alternatives cannot be generalized automatically, as it depends on local operational conditions, expected traffic structure, aircraft equipage, meteorological characteristics, infrastructure constraints, and strategic requirements. Therefore, each application of the methodology should be based on airport-specific input data and expert assessment.

Acknowledgements

This work was supported by the research grant SP2025/065 Research, Development, and Innovation in Transportation and Logistics 2025.

Conflict of interest

The authors declare that they have no known competing financial interests or personal relationships that could have appeared to influence the work reported in this paper.

References

[1] PAUWELS, J., BUYLE, S., DEWULF, W. Regional airports revisited: unveiling pressing research gaps and proposing a uniform definition. *Journal of the Air Transport Research Society* [online]. 2024, **2**, 100008. eISSN 2941-198X. Available from: https://doi.org/10.1016/j.jatrs.2024.100008

[2] Airport authority complete ILS/DME replacement. Bernews [online] [accessed 2026-03-02]. 2024. Available from: https://bernews.com/2024/05/airport-authority-complete-ilsdme-replacement/

[3] NOVACKOVA, P. A new modern system for the safe landing of aircraft is now operational at all military airports. Army of the Czech Republic [online] [accessed 2026-05-04]. Prague: Ministry of Defence of the Czech Republic, 2023. Available from: https://acr.mo.gov.cz/informacni-servis/zpravodajstvi/novy-moderni-system-pro-bezpecne-pristani-letadel-uz-funguje-na-vsech-vojenskych-letistich-248061/

[4] ILS/DME precision instrument approach system - procurement: Contract No. 175210002. Register of Contracts - Czech Republic - Ministry of Defence [online] [accessed 2026-04-28]. Prague: Digital and Information Agency, 2021. Available from: https://smlouvy.gov.cz/smlouva/17154891

[5] Amendment No. 3 to the public contract "ILS/DME precision instrument approach system - procurement": Contract No. 175210002/3. Register of Contracts - Czech Republic - Ministry of Defence [online] [accessed 2026-04-28]. Prague: Digital and Information Agency, published 28 December 2023. Available from: https://smlouvy.gov.cz/smlouva/27077771

[6] AIP Czech Republic: AD 2 LKPD - Pardubice - Prague: air navigation services of the Czech Republic [online] [accessed 2026-04-28]. Available from: https://aim.rlp.cz/ais_data/www_main_control/frm_cz_aip.htm

[7] Krakow airport: information - Krakow: John Paul II International Airport Krakow-Balice Ltd. [online] [accessed 2026-04-28]. Available from: https://krakowairport.pl/en

[8] 8th Krakow transport aviation base named after Col. Pilot Stanislaw Jakub Skarzynski - Balice: Polish Armed Forces [online] [accessed 2026-04-28]. Available from: https://8bltr.wp.mil.pl/

[9] CASTELLI, L., PELLEGRINI, P. An AHP analysis of air traffic management with target windows. *Journal of Air Transport Management* [online]. 2011, **17**(2), p. 68-73. ISSN 0969-6997, eISSN 1873-2089. Available from: https://doi.org/10.1016/j.jairtraman.2010.05.006

[10] SENNAROGLU, B., CELEBI, G. V. A military airport location selection by AHP integrated PROMETHEE and VIKOR methods. *Transportation Research Part D: Transport and Environment* [online]. 2018, **59**, p. 160-173. ISSN 1361-9209, eISSN 1879-2340. Available from: https://doi.org/10.1016/j.trd.2017.12.022

[11] PIVAC, J., STIMAC, I., BARTULOVIC, D., VIDOVIC, A. Determining the optimal level of service of the airport passenger terminal for low-cost carriers using the analytical hierarchy process. *Applied Sciences* [online]. 2025, **15**(4), 1734. eISSN 2076-3417. Available from: https://doi.org/10.3390/app15041734

[12] European AIS database (EAD) - Brussels: Eurocontrol [online] [accessed 2026-04-28]. Available from: https://www.ead.eurocontrol.int/

[13] SmartPath ground-based augmentation system - Honeywell Aerospace Technologies [online] [accessed 2026-05-04]. Available from: https://aerospace.honeywell.com/us/en/products-and-services/product/hardware-and-systems/sensors/smartpath-ground-based-augmentation-system

[14] NOVAK, A., SKULTETY, F., BUGAJ, M., JUN, F. Safety studies on GNSS instrument approach at Zilina airport. In: 2019 Modern Safety Technologies in Transportation MOSATT: proceedings [online]. IEEE. 2019. ISBN 978-1-7281-5083-3, p. 122-125. Available from: https://doi.org/10.1109/MOSATT48908.2019.8944098

[15] NAS, A. Potential benefits of deploying a ground based augmentation system (GBAS) at Stockholm Arlanda airport [online] [accessed 2026-05-04]. Stockholm: Swedavia Airports, 2017. Available from: https://fudinfo.trafikverket.se/fudinfoexternwebb/Publikationer/Publikationer_003301_003400/Publikation_003333/GBAS%20Inflygningar%20p%C3%A5%20arlanda.pdf

[16] GUENTER, D., DENNIS, J. Initial operational experience with CAT I ground based augmentation system (GBAS). In: 2015 Integrated Communications Navigation and Surveillance ICNS Conference: proceedings. 2015. ISBN 978-1-4799-8952-2, p. S1-1-S1-14.

[17] GBAS Landing System (GLS). SKYbrary Aviation Safety - Skybrary [online] [accessed 2026-05-04]. Available from: https://skybrary.aero/articles/gbas-landing-system-gls

[18] AMBROZOVA, I., PLENINGER, S. Implementation of GBAS system at the Vaclav Havel airport. *Perner's Contacts* [online]. 2013, **8**(2), p. 5-14 [accessed 2026-05-04]. eISSN 1801-674X. Available from: https://pernerscontacts.upce.cz/index.php/perner/cs/article/view/726

[19] OLIVEIRA, P., SILVA, J., SOARES, J. P. A comparative study between ILS and GBAS approaches: the case of Viseu airfield. *Journal of Airline and Airport Management* [online]. 2020, **10**(2), p. 65-75 [accessed 2026-05-04]. ISSN 2014-4806, eISSN 2014-4806. Available from: https://doi.org/10.3926/jairm.168

[20] WANG, Z. P., MACABIAU, CH., ZHANG, J., ESCHER, A.-CH. Prediction and analysis of GBAS integrity monitoring availability at LinZhi airport. *GPS Solutions* [online]. 2014, **18**(1), p. 27-40 [accessed 2026-05-04]. ISSN 1080-5370, eISSN 1521-1886. Available from: https://doi.org/10.1007/s10291-012-0306-4
[21] Joint precision approach and landing system (JPALS) - Stanford Engineering GPS Lab [online] [accessed 2026-05-04]. Available from: https://gps.stanford.edu/research/early-gpspnt-research/joint-precision-approach-and-landing-system-jpals
[22] Joint precision approach and landing system (JPALS) - Collins Aerospace [online] [accessed 2026-05-04]. Available from: https://www.collinsaerospace.com/what-we-do/industries/military-and-defense/navigation/airborne-products/navigation-and-landing-systems/jpals
[23] Raytheon Technologies completes delivery of 23 joint precision approach and landing systems to the U.S. navy. Raytheon News Release Archive - Raytheon Technologies [online] [accessed 2026-05-04]. Available from: https://raytheon.mediaroom.com/2023-03-23-Raytheon-Technologies-completes-delivery-of-23-Joint-Precision-Approach-and-Landing-Systems-to-the-U-S-Navy
[24] A new navigation system is assisting American helicopters in Czech colours with landing at Namest - 22nd Helicopter Air Force Base [online] [accessed 2026-05-04]. 2024 Available from: https://lznamest.mo.gov.cz/aktuality/americkym-vrtulnikum-v-ceskych-barvach-pomaha-v-namesti-s-pristanim-novy-navigacni-system
[25] CNS SG/13-WP/27: Global navigation satellite system interference and contingency planning - International Civil Aviation Organization [online] [accessed 2026-05-04]. 2024. Available from: https://www.icao.int/sites/default/files/MID/MeetingDocs/2024/CNS%20SG13%20Meeting/WP/CNS-SG13-WP27.pdf
[26] Easy access rules for air operations: Revision 24, March 2026 - European Union Aviation Safety Agency [online] [accessed 2026-05-04]. 2026. Available from: https://www.easa.europa.eu/en/document-library/easy-access-rules/online-publications/easy-access-rules-air-operations
[27] A snapshot of State aircraft's on-board equipage for performance-based navigation (PBN) - Eurocontrol [online] [accessed 2026-05-04]. 2023. Available from: https://www.eurocontrol.int/sites/default/files/2023-11/eurocontrol-snapshot-state-aircraft-on-board-equipage-pbn.pdf
[28] REINES, P. SmartPath ground based augmentation system (GBAS): a new era in precision navigation. In: Poland Ground Based Augmentation System GBAS Seminar: proceedings [online] [accessed 2026-07-20]. 2015. Available from: https://www.pansa.pl/wp-content/uploads/GNSS/Honeywell%20SmartPath%20GBAS%20PANSA%2020150624%20v.0.pdf
[29] Airport benefit - cost analysis guidance - Federal Aviation Administration [online]. [accessed 2026-05-04]. 2026. Available from: https://www.faa.gov/regulations_policies/policy_guidance/benefit_cost/FAA-Airport-Benefit-Cost-Guidance.pdf
[30] Financing of Aviation System: CNS/ATM - Economic Aspects - International Civil Aviation Organization [online] [accessed 2026-05-04]. Available from: https://www.icao.int/sustainability/Pages/eap-im-cns-atm.aspx
[31] Standard Inputs for Economic Analyses: Edition 10 - Eurocontrol. Eurocontrol [online] [accessed 2026-05-04]. 2024. Available from: https://www.eurocontrol.int/sites/default/files/2024-05/eurocontrol-standard-inputs-economic-analyses-ed-10.pdf
[32] SESAR solution PJ.02-W2-21.1: cost benefit analysis (CBA) for V3 - Sesar Joint Undertaking [online] [accessed 2026-05-04]. 2023. Available from: https://www.sesarju.eu/sites/default/files/documents/solution/SolPJ.02-W2-21.1%20CBA%20V3.pdf
[33] SAATY, T. L. *The analytic hierarchy process: planning, priority setting, resource allocation*. New York: McGraw-Hill, 1980. ISBN 0-07-054371-2.
[34] SAATY, T. L. A scaling method for priorities in hierarchical structures. *Journal of Mathematical Psychology* [online]. 1977, **15**(3), p. 234-281 [accessed 2026-05-04]. ISSN 0022-2496, eISSN 1096-0880. Available from: https://doi.org/10.1016/0022-2496(77)90033-5
[35] KAYTON, M., FRIED, W. R. Avionics Navigation Systems. 2nd ed. New York: John Wiley & Sons, 1997. ISBN 978-0-471-54795-8
[36] Resolution of the Regional Assembly No. 8/719 of 16 June 2022. Resolutions of the Regional Assembly and Regional Council - Moravian-Silesian Region [online] [accessed 2025-09-24]. 2022. Available from: https://www.msk.cz/kraj/zastupitelstvo/usneseni.html?c=719&d=2022-06-16&s=8&t=z

This is an open access article distributed under the terms of the Creative Commons Attribution 4.0 International License (CC BY 4.0), which permits use, distribution, and reproduction in any medium, provided the original publication is properly cited. No use, distribution or reproduction is permitted which does not comply with these terms.

GENDER DIFFERENCES IN VISUAL ATTENTION AND STATED PREFERENCES DURING EVALUATION OF BATTERY ELECTRIC VEHICLES: AN EXPLORATORY EYE-TRACKING STUDY

Viktória Cvacho[1], Radovan Madleňák[1,*], Alessandro Pagano[2], Edward Kozłowski[3]

[1]University of Zilina, Faculty of Operation and Economics of Transport and Communications, Department of Communications, Zilina, Slovakia
[2]University of Bari Aldo Moro, Department of Computer Science, Bari, Italy
[3]Lublin University of Technology, Faculty of Management, Department of Quantitative Methods in Management, Lublin, Poland

*E-mail of corresponding author: radovan.madlenak@uniza.sk

Viktória Cvacho 0009-0006-1374-385X,
Radovan Madleňák 0000-0002-4376-0830,
Alessandro Pagano 0000-0002-7465-9778,
Edward Kozłowski 0000-0002-7147-4903

Resume

In this exploratory study were examined the gender differences in visual attention and stated preferences during the evaluation of battery electric vehicles (BEVs) using eye-tracking. Thirty-two participants (18 men, 14 women) viewed static images of the ten top-selling BEVs in Slovakia while eye movements were recorded across four predefined Areas of Interest (AOIs). Vehicle design attracted the greatest absolute dwell time in both groups. No gender difference reached conventional statistical significance (all $p > 0.05$), yet medium effect sizes were obtained for brand ($d = 0.69$), acceleration ($d = 0.67$), vehicle equipment ($d = 0.60$) and trunk capacity ($d = 0.53$), all rated higher by women, whereas men more often cited driving range as the main reason for model choice. The findings are hypothesis-generating and motivate confirmatory research with larger, purposively balanced samples.

Article info

Received 16 July 2026
Accepted 12 August 2026
Online 7 September 2026

Keywords:

battery electric vehicle
consumer behaviour
gender differences
eye-tracking
visual attention
areas of interest
exploratory study

Available online: https://doi.org/10.26552/com.C.2026.050

ISSN 1335-4205 (print version)
ISSN 2585-7878 (online version)

1 Introduction

The European Union's ambition to achieve climate neutrality by 2050 has accelerated the transition towards electromobility, positioning battery electric vehicles (BEVs) as a cornerstone of sustainable transport policy. In 2023, BEVs accounted for 14.6% of new car registrations in the EU, up from 12.1% in 2022 [1]. Despite this momentum, consumer hesitancy remains a structural challenge, particularly in Central and Eastern European markets characterised by lower average incomes, limited charging infrastructure, and high price sensitivity.

Slovakia presents a particularly instructive case. With only 2,227 newly registered BEVs in 2024, a 2.38% market share, Slovakia remains one of the lowest BEV-penetration markets in the EU [2]. Structural constraints, including underdeveloped public charging networks and fragmented policy incentives, impede mass-market adoption [3].

Affective responses play a central role in electric vehicle evaluation [4], and gender is among the most consistently identified moderators of automotive consumer behaviour [5]. Heterogeneity in consumer preferences, including pro-environmental orientation, is well established in vehicle-choice modelling [6], and European research documents systematic differences between male and female consumers in the attributes they prioritise when selecting a vehicle and in their responsiveness to brand and emotional cues [7]. However, the application of biometric methods, particularly eye-tracking, to examine gender-specific patterns within the BEV context has received limited attention.

This study is an extension of a prior research by the present authors [8], which identified overall visual attention patterns in BEV evaluation without disaggregating findings by gender. In the present study, the gender was treated as the primary analytical

variable, combining the eye-tracking data with a structured interview to reveal how men and women differ both in how they visually process commercial BEV imagery and in what attributes they prioritise when making model choices. Given the convenience sample and its size, the study was explicitly exploratory: its purpose is to estimate the direction and magnitude of gender-related differences and to generate hypotheses for subsequent confirmatory testing, rather than to test pre-specified hypotheses. No hypotheses were formulated in advance and no analysis plan was pre-registered.

2 Literature review

Research relevant to this study spans market-level analyses of electromobility adoption, behavioural work on the determinants of BEV choice, and the smaller literature applying biometric methods to consumer evaluation. Gender recurs across all three as a moderator, but rarely as the primary variable, and almost never in combination with eye-tracking in a Central European market.

2.1 Electromobility and the European market context

Electromobility has emerged as a structural priority within the EU's Green Deal framework, driven by binding CO_2 reduction targets and the proposed 2035 ban on new internal combustion engine vehicle sales [1]. The environmental case for electrification is the strongest in high-mileage applications: replacing a conventional ride-hailing vehicle with a BEV delivers approximately three times the emission-reduction benefit of replacing a privately used car [9]. Empirical analysis confirms that EU-level CO_2 targets for passenger cars are both technically achievable and economically feasible [10]. At the same time, the transition entails systemic sustainability challenges that extend beyond vehicle sales, notably end-of-life battery waste and recycling capacity [11]. Nevertheless, adoption trajectories diverge substantially across member states, reflecting heterogeneity in GDP per capita, fiscal policy, infrastructure density, and consumer readiness. Comparative analysis of BEV and PHEV market development across European countries indicates that electrification trajectories are linked not only to fiscal and infrastructural conditions but to the diffusion of vehicle automation technologies, as well [12].

Slovakia's BEV adoption remains structurally constrained. As of end-2024, only 15,476 BEVs were registered on Slovak roads, a 53% year-on-year increase, yet still representing a marginal fleet share [2]. The Slovak market remains highly price-sensitive: official new-BEV sales are among the lowest in the EU, and individually imported vehicles account for the majority of BEV additions [2]. Prior Slovak research on electromobility has primarily addressed infrastructure and policy frameworks [13], leaving consumer-level behavioural research underexplored.

2.2 Consumer behaviour in BEV adoption

Consumer decision-making in BEV contexts is shaped by a combination of instrumental, hedonic, and symbolic factors [14]. National fiscal policies strongly steer consumers' powertrain choices [15], while the price and range per charge consistently emerge as the most frequently cited functional barriers across European consumer studies [10, 16]. Charging speed and infrastructure availability are identified as the secondary but increasingly prominent concerns [17]. Beyond functional attributes, affective and symbolic dimensions play a significant role. Moons and De Pelsmacker [4] demonstrated that emotional responses towards electric vehicles are among the strongest predictors of BEV usage intention. Brand perception functions as a powerful heuristic cue, conveying implied quality and reducing perceived purchase risk [18]. Recent research confirms that design aesthetics, brand equity, and consumer trust jointly mediate BEV purchase intention [19].

2.3 Gender as a determinant of BEV preferences

Individual difference variables are established predictors of behaviour and outcomes across transport contexts: occupational stress and personality traits, for example, differentiate incident involvement among professional drivers [20]. Gender consistently moderates BEV adoption behaviour. Sovacool et al. [21] analysed data from five Nordic countries and found that gender significantly shapes electric mobility preferences: the male consumers exhibited stronger interest in performance-related attributes, such as acceleration and top speed, while the female consumers expressed greater concern about practical utility and environmental benefits. Haustein and Jensen [7] corroborated these findings in a Danish-Swedish sample, identifying BEV owners as predominantly male, highly educated, and higher-income.

More recent market research underscores the commercial significance of the gender gap. A 2024 industry study found that only 30% of women were familiar with BEVs compared to 55% of men, and that men comprised 71% of BEV owners [22]. Research on female new energy vehicle consumers reveals that brand loyalty, trust, and perceived performance drive female purchase intention [5], while men engage more extensively with technical specifications during the

Table 1 *Participant characteristics by gender*

Characteristic	Category	All n	All %	Women, n (%)	Men, n (%)
Gender	Female	14	43.8	-	-
	Male	18	56.3	-	-
Age group	18-28	9	28.1	4	5
	29-44	12	37.5	3	9
	45-60	9	28.1	7	2
	61-79	2	6.3	0	2
BEV experience	Yes	18	56.3	7 (50)	11 (61)
	No	14	43.8	7 (50)	7 (39)
Trips >200 km	Weekly	10	31.3	2 (14)	8 (44)
	Monthly	9	28.1	5 (36)	4 (22)
	Quarterly+	13	40.6	7 (50)	6 (33)

Note: Percentages may not sum to 100 due to rounding.

pre-purchase research [22]. Marketing communication itself influences EV purchase intention only indirectly, through perceived value and brand preference [23]. Range anxiety remains a central psychological barrier that also shapes willingness to pay for charging [24], and industry evidence indicates that women face a broader set of adoption barriers than men [22].

2.4 Eye-tracking in consumer and marketing research

Eye-tracking is a well-established biometric methodology in neuromarketing and consumer psychology, providing objective, real-time data on visual attention allocation [25]. Key metrics include fixation count, dwell time, first fixation duration, entry time, and revisit frequency [25-26]. Studies consistently demonstrate that certain visual elements, particularly brand logos and price information, capture attention rapidly [27]. Research in virtual retail environments confirmed that dwell time and fixation count are robust indicators of consumer engagement [28].

Research on gender differences in visual processing has revealed systematic variations in gaze patterns. A study found that men and women differ in how they allocate visual attention to advertising stimuli [29]. Neurophysiological research confirmed that female participants show longer visual attention to aesthetically rich stimuli [30]. In FMCG advertising contexts, gender-differentiated eye-tracking scan paths were found to shape attention capture and perceived trustworthiness [31]. The integration of eye-tracking with post-experimental structured interview methods provides methodological triangulation that captures both unconscious, bottom-up attentional processes and top-down deliberate evaluation [8]. More broadly, instrumental and sensor-based measurement methods have become increasingly established across transport research applications [32].

3 Methodology

The study combined two measurement modes applied to the same participants within a single session: an eye-tracking recording of visual attention to commercial BEV imagery, and a structured interview capturing the attributes that participants said mattered to them. The recording always preceded the interview, so that the questions could not direct attention during stimulus viewing.

3.1 Participants

A total of 32 participants took part in the study, comprising 18 men (56.3%) and 14 women (43.8%). Participants were recruited on a voluntary basis from the university and surrounding community without financial compensation. Fifty-six percent reported prior BEV experience. Men showed higher weekly travel frequency exceeding 200 km (44.4% vs. 14.3% of women). Detailed sample characteristics are presented in Table 1.

3.2 Stimuli and apparatus

Participants were shown the high-resolution static images of ten BEV models representing the best-selling electric vehicles in Slovakia during Q1 2024: Tesla Model Y, Tesla Model 3, Volvo EX30, MG 4, Volkswagen ID.4, Volkswagen ID.3, Skoda Enyaq, Volvo EX40, BMW iX1, and Audi Q4 e-tron. Each stimulus presented the vehicle image alongside the key commercial information (brand logo and name, range per charge, price, and vehicle specifications). Each image was displayed for 10 seconds on a 24-inch monitor at a viewing distance of approximately 65 cm. Eye movements were captured using the SMI RED remote eye-tracker with data recorded via SMI BeGaze software [33].

The five models subjected to gender-disaggregated

analysis, Audi Q4 e-tron, Skoda Enyaq, Volvo EX40, BMW iX1 and Tesla Model 3, were the five most frequently nominated models in a post-exposure structured interview asking which vehicle participants would realistically choose if making a purchase decision (n = 8, 7, 5, 5 and 3 respectively; Table 3). All five also featured in the European and national H1 2024 BEV sales rankings [34-35]. The remaining models attracted two or fewer nominations each (Tesla Model Y, n = 2; MG 4 and Volvo EX30, n = 2, in total) and were not analysed separately, because subgroup statistics based on so few preference-consistent responses would not be interpretable. This selection aligns the analysed stimulus set with both market relevance and participant purchasing intent. It was, however, applied after the data collection and is derived from the same participants whose gaze data are analysed; the resulting constraint on interpretation is addressed in the limitations.

3.3 Areas of interest and metrics

Four Areas of Interest (AOIs) were manually defined for each stimulus: (1) vehicle design: the visual representation of the car body; (2) brand: the manufacturer's logo and name; (3) range per charge: the displayed range figure; and (4) price: the retail price indicator. Figure 1 illustrates the AOI layout. Eye-tracking metrics extracted per AOI included dwell time, fixation count, first fixation duration, entry time, and revisit frequency. Tables 5 to 8 report the dwell time (in milliseconds and as a percentage of the 10 s exposure), fixation count, first fixation duration, and the number of revisits. First fixation duration denotes the length of the first fixation falling within the AOI; it does not indicate when that fixation occurred.

The four AOIs differed considerably in area and in position within the stimulus. The design AOI enclosed the whole vehicle body and occupied the central region of the image, whereas the brand, range, and price AOIs were small text fields located peripherally. Since both AOI area and eccentricity relative to the initial gaze position influence the dwell time and fixation count [25], absolute dwell times are not directly comparable between AOIs of unequal size, and the comparisons reported in Sections 4.3 to 4.6 should be read with this constraint in mind.

3.4 Post-experimental structured interview

Immediately after the eye-tracking session, each participant took part in an individual structured interview conducted by a member of the research team. The interview was governed throughout by a fixed questionnaire protocol and covered: (1) demographics; (2) mobility profile; (3) BEV experience; (4) importance ratings of nine EV selection attributes on a 7-point Likert scale (1 = not important, 7 = very important); (5) preferred model selection with up to three stated reasons, recorded as an open-ended response and subsequently coded into the attribute categories reported in Table 4; and (6) rated likelihood of choosing a BEV over an ICE vehicle (scale 1-10). All items except (5) had fixed response formats; the instrument is therefore described as a structured interview rather than an in-depth interview. The order of the two stages was fixed rather than counterbalanced: the eye-tracking measurement always preceded the interview, so that the questions could not direct participants' attention during stimulus viewing.

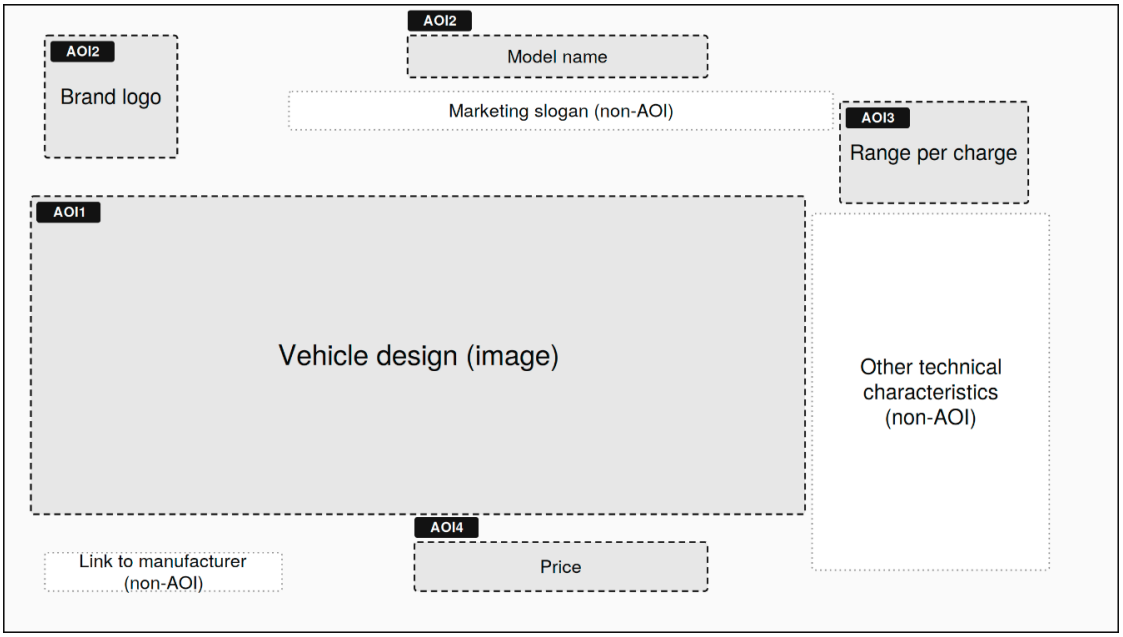


Figure 1 *Principal layout of the visual stimulus with the four defined AOIs*

3.5 Statistical analysis

Gender differences in attribute importance ratings (Table 2) were assessed using the Welch's independent-samples t-test, which does not assume equal variances and is robust to unequal sample sizes (n_2=14 women, n_1=18 men). Since the primary data export provided pooled and female subgroup statistics, the men's standard deviations were recovered algebraically from the pooled statistics (given n, M and SD of the total sample and the female subgroup, the male SD is uniquely determined); this recovery is exact, not an estimate. Effect size was quantified using Cohen's d, with conventional thresholds of 0.20 (small), 0.50 (medium), and 0.80 (large). Stated reasons for model choice were compared across genders by Spearman's rank correlation coefficient (ρ). Model preference distributions were examined using Pearson's chi-square test; where expected cell frequencies fell below five, results are reported descriptively. The significance threshold was set at $\alpha = 0.05$ (two-tailed). Since the study is exploratory, the nine comparisons were not corrected for multiple testing; the p-values are consequently nominal and are reported for descriptive purposes only. Analyses were performed in SMI BeGaze 3.7.59 and MS Excel 365.

4 Results

The stated and the recorded data are reported separately, so that what participants said mattered can be set against where they actually looked. In Sections 4.1 and 4.2 are presented the attribute importance ratings and the model preferences obtained in the interview. In Sections 4.3 to 4.6 are reported the eye-tracking metrics for each Area of Interest across the five models analysed in detail.

4.1 Gender differences in attribute importance

Table 2 presents importance ratings (M) and standard deviations (SD) for all nine BEV selection attributes disaggregated by gender, alongside the Welch t-test statistics, two-tailed p-values, and Cohen's d effect sizes. No comparison reached the $\alpha = 0.05$ threshold. Nevertheless, two attributes exhibited medium-to-large effect sizes: Acceleration ($d = 0.67$, $t(26) = 2.04$, $p = 0.052$) and Brand ($d = 0.69$, $t(30) = 1.99$, $p = 0.056$). Two further attributes, Vehicle equipment ($d = 0.60$) and Trunk capacity ($d = 0.53$), showed medium effect sizes, while Vehicle design ($d = 0.47$) fell just below the medium threshold. The absence of

Table 2 *Importance ratings of BEV selection attributes by gender (Likert scale 1-7, sorted by overall mean)*

Attribute	Women M (SD)	Men M (SD)	Δ (W-M)	t (df)	p	d
Fast charging time	6.21 (1.63)	6.44 (1.41)	-0.23	-0.42 (26)	0.678	0.15
Acceleration (0-100 km/h)	6.71 (0.73)	5.89 (1.49)	+0.82*	2.04 (26)	0.052	0.67
Brand	6.21 (1.12)	5.33 (1.38)	+0.88*	1.99 (30)	0.056	0.69
Top speed	5.86 (1.70)	5.44 (1.43)	+0.42	0.74 (25)	0.464	0.27
Range per charge	5.50 (1.70)	5.50 (1.70)	0.00	0.00 (28)	1.000	0.00
Price	5.14 (1.35)	5.17 (1.92)	-0.03	-0.05 (30)	0.959	0.02
Vehicle equipment	5.29 (1.73)	4.28 (1.64)	+1.01	1.68 (27)	0.105	0.60
Vehicle design	4.71 (1.38)	3.94 (1.80)	+0.77	1.37 (30)	0.181	0.47
Trunk capacity	4.57 (1.40)	3.83 (1.39)	+0.74	1.49 (28)	0.148	0.53

Note: Δ = women minus men; d = Cohen's d (absolute value); * denotes $0.05 < p \leq 0.10$. None of the nine comparisons reached the $\alpha = 0.05$ threshold. Acceleration ($d = 0.67$) and Brand ($d = 0.69$) yielded the largest point estimates, but at n = 32 the data do not distinguish between medium-sized gender differences and their absence. The p-values are nominal and are reported descriptively (Section 3.5).

Table 3 *Preferred BEV model by gender*

Model	All n	All %	Women, n (%)	Men, n (%)	Rank W/M
Audi Q4 e-tron	8	25.0	5 (35.7)	3 (16.7)	1st / 2nd
Skoda Enyaq	7	21.9	3 (21.4)	4 (22.2)	2nd / 1st
Volvo EX40	5	15.6	2 (14.3)	3 (16.7)	3rd / 3rd
BMW iX1	5	15.6	2 (14.3)	3 (16.7)	3rd / 3rd
Tesla Model 3	3	9.4	0 (0.0)	3 (16.7)	- / 3rd
Tesla Model Y	2	6.3	1 (7.1)	1 (5.6)	5th / 5th
MG 4 / Volvo EX30	2	6.3	1 (7.1)	1 (5.6)	5th / -

Table 4 *Frequency of stated reasons for BEV model choice by gender*

Attribute	Women n	Men n	Women rank	Men rank
Vehicle design	9	8	1st	4th
Brand	8	10	2nd	3rd
Price	7	11	3rd	2nd
Range per charge	5	12	4th	1st
Fast charging time	4	3	5th	5th
Vehicle equipment	3	3	6th	5th
Trunk capacity	3	1	6th	7th
Acceleration	1	1	8th	7th

Note: Participants stated up to three reasons; not all provided three, hence column totals (women n = 40, men n = 49) are below the theoretical maxima (42 and 54).

Table 5 *Eye-tracking metrics for AOI "Design"*

Model	Dwell Time, ms (%)	Fixations	First Fix. Duration (ms)	Revisits
Audi Q4 e-tron	2,668.5 (26.7)	9.8	176.0	2.2
BMW iX1	2,512.3 (25.1)	8.6	162.5	2.5
Skoda Enyaq	2,465.4 (24.6)	7.5	187.5	2.3
Volvo EX40	2,227.9 (22.3)	7.6	256.2	2.1
Tesla Model 3	1,645.7 (16.4)	5.8	204.2	1.8

statistical significance, despite the substantial effect sizes, reflects limited statistical power at n = 32; a post-hoc power analysis ($\alpha = 0.05$, $d = 0.65$) yields power ≈ 0.38, indicating the study was underpowered to detect these differences reliably. Fast charging time, Range per charge, and Price showed negligible gender differences ($d < 0.20$).

4.2 Model preference and purchase rationale by gender

Table 3 summarises model preferences by gender. Table 4 presents the frequency of attributes cited as the three main reasons for model choice.

Audi Q4 e-tron was the most preferred model overall (n=8; 25.0%), with disproportionate female preference (35.7% of women vs. 16.7% of men). Tesla Model 3 was selected exclusively by three male participants, while no female participant selected it. A Pearson chi-square test on the five-model preference distribution did not reach significance ($\chi^2(4) = 3.54$, $p = 0.471$); however, expected cell frequencies fell below five for several cells (min. expected = 1.29), precluding reliable inference. Results should therefore be interpreted descriptively. Regarding the attribute-level purchase rationale (Table 4), a Spearman rank correlation between women's and men's attribute citation frequencies indicated strong rank agreement in the overall ranking pattern ($\rho = 0.73$), suggesting that both genders share a common attentional hierarchy while differing in the relative emphasis placed on design versus range. With eight attributes and tied ranks, the associated p-value is approximate and is therefore not reported as evidence of statistical significance.

4.3 Eye-tracking AOI results: design

Vehicle design attracted the highest visual engagement across all five analysed models (Table 5). Dwell times ranged from 1,645.7 ms (Tesla Model 3; 16.4%) to 2,668.5 ms (Audi Q4 e-tron; 26.7%), with a near-universal hit ratio of 93.8%.

Figure 2 shows the gender-disaggregated eye-tracking outputs for the Audi Q4 e-tron, revealing that female participants concentrated gaze on the vehicle's front facade and brand emblem, consistent with their higher importance ratings for design and brand. Male participants' gaze was more spatially distributed across the stimulus.

4.4 Eye-tracking AOI results: brand

Brand AOIs elicited moderate but consistent engagement (Table 6). Tesla Model 3 generated the highest brand dwell time (654.1 ms; 6.5%), attributable to high global brand recognition. Audi Q4 e-tron recorded the lowest brand dwell time (455.2 ms; 4.5%), suggesting that Audi's brand identity may be inferred from design cues rather than requiring explicit logo verification.



***Figure** 2 Eye-tracking outputs for Audi Q4 e-tron – women (n = 14, top) vs. men (n = 18, bottom). Source of eye-tracking output: SMI BeGaze*

***Table 6** Eye-tracking metrics for AOI "Brand"*

Model	Dwell Time, ms (%)	Fixations	First Fix. Duration (ms)	Revisits
Tesla Model 3	654.1 (6.5)	2.2	202.1	1.2
Skoda Enyaq	613.5 (6.1)	1.8	246.8	0.5
BMW iX1	519.8 (5.2)	1.5	213.5	0.8
Volvo EX40	517.6 (5.2)	1.5	248.9	0.7
Audi Q4 e-tron	455.2 (4.5)	1.3	207.3	0.6

4.5 Eye-tracking AOI results: range

Despite being rated as highly important (M=5.50), the range AOI attracted comparatively modest visual attention (Table 7). Volvo EX40 and Audi Q4 e-tron attracted the most engagement (672.9 ms and 657.1 ms respectively), while BMW iX1 registered the lowest (492.7 ms). One possible explanation is that participants inferred range from brand reputation rather than verifying the displayed figures; this was not tested directly.

Table 7 *Eye-tracking metrics for AOI "Range"*

Model	Dwell Time, ms (%)	Fixations	First Fix. Duration (ms)	Revisits
Volvo EX40	672.9 (6.7)	1.6	264.6	0.7
Audi Q4 e-tron	657.1 (6.6)	1.6	349.9	0.8
Skoda Enyaq	609.3 (6.1)	1.4	264.5	0.8
Tesla Model 3	564.5 (5.6)	1.1	307.3	0.3
BMW iX1	492.7 (4.9)	1.1	304.1	0.5

Table 8 *Eye-tracking metrics for AOI "Price"*

Model	Dwell Time, ms (%)	Fixations	First Fix. Duration (ms)	Revisits
Tesla Model 3	603.1 (6.0)	1.7	212.5	0.4
BMW iX1	387.4 (3.9)	1.6	115.6	0.9
Audi Q4 e-tron	331.2 (3.3)	1.0	132.3	0.4
Skoda Enyaq	263.5 (2.6)	0.9	123.9	0.2
Volvo EX40	171.8 (1.7)	0.6	131.2	0.2

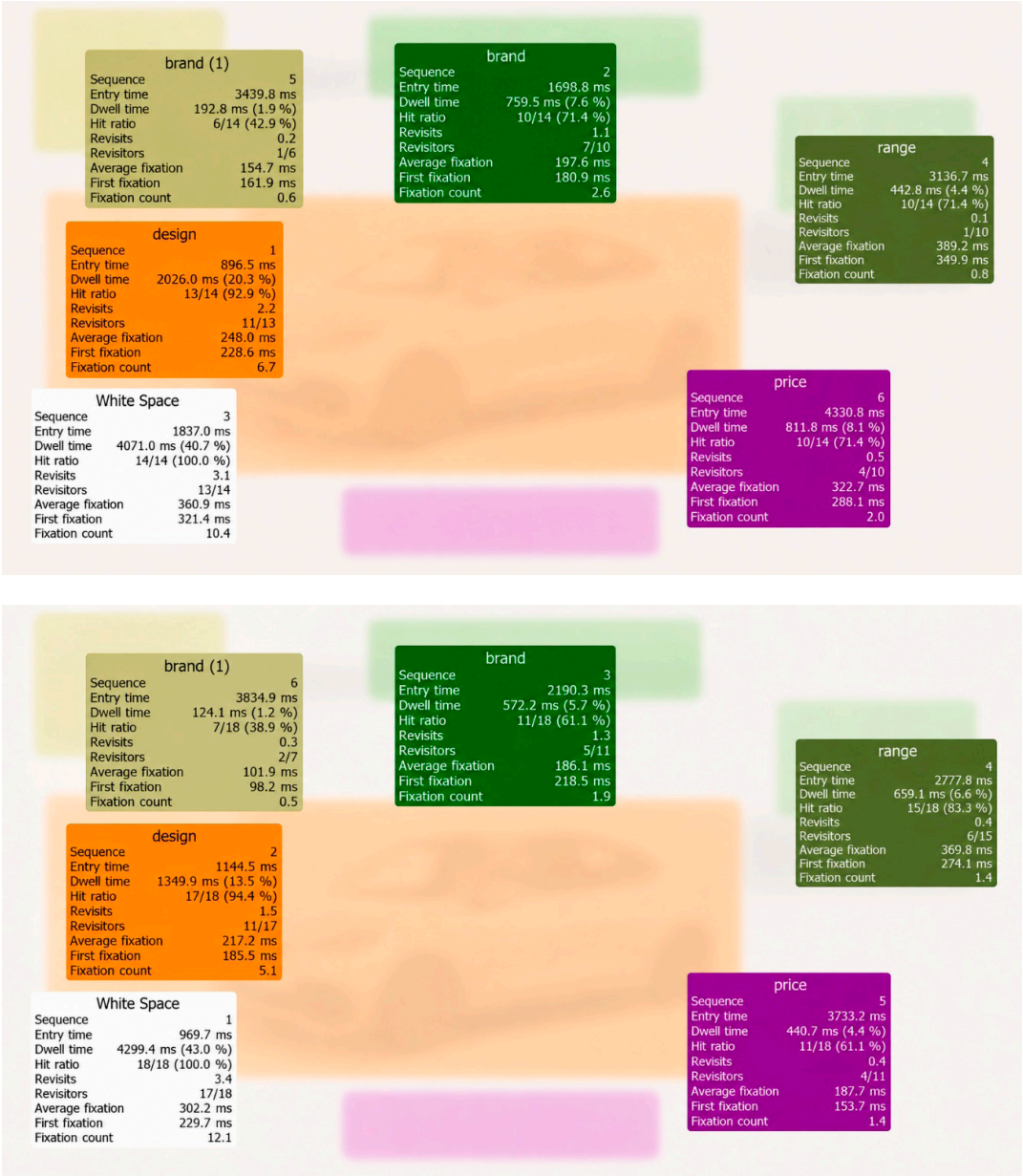


Figure 3 *Eye-tracking outputs for Tesla Model 3 – women (n = 14, top) vs. men (n = 18, bottom). Source of eye-tracking output: SMI BeGaze*

4.6 Eye-tracking AOI results: price

Price received the lowest visual engagement of all four AOIs despite being rated among the top three purchase reasons by both genders (Table 8). Tesla Model 3 generated the highest price-related dwell time (603.1 ms; 6.0%). Figure 3 illustrates gender-disaggregated outputs for Tesla Model 3, where female participants - who did not ultimately select this model - showed more diffuse attention across the stimulus, while male participants concentrated gaze on the vehicle body and brand.

5 Discussion

The dominance of vehicle design as the primary AOI across both genders aligns with the well-established primacy of aesthetic evaluation in consumer product assessment [19] and with recent market evidence: a 2026 survey of new-vehicle buyers found that interior and exterior design outrank brand, range, and charging performance as motivators of BEV choice [36]. It should also be noted that the design AOI was the largest region of each stimulus and the closest to the initial gaze position. Larger and more central regions accumulate dwell time and fixations partly for geometric reasons, so the observed ranking of AOIs is not attributable to informational content alone. The metrics reported here do not establish the time course of attention: first fixation duration measures the length of the first fixation within an AOI, not the moment at which it occurred. The present design does not permit a causal claim about the effect of design investment on consumer engagement, nor about the ordering of attentional and deliberative processes.

The gender-related tendencies observed in this sample are directionally consistent with international research but reveal potentially market-specific nuances. The female prioritisation of brand and design over range (reflected in stated reasons: design 1st vs. 4th for women and men respectively; range 4th vs. 1st) aligns with findings from Boscolo et al. [29] on gender differences in advertising attention and may suggest distinct entry points for targeted marketing communication. However, it should be noted, that these differences did not reach statistical significance (Brand: $p = 0.056$; Vehicle design: $p = 0.181$), and the limited sample precludes firm prescriptive conclusions. Replication with larger samples is warranted before these patterns are applied directly to commercial strategy.

The reversal of the expected acceleration preference - with women rating this attribute higher than men (6.71 vs. 5.89) - may reflect the age distribution: seven of fourteen women were aged 45-60, a group that may associate responsive acceleration with driving comfort and safety rather than performance signalling. This interpretation is consistent with evidence that gender shapes the weighting of instrumental and safety-related vehicle attributes: Lieven et al. [37] found that the female car buyers prioritise safety over performance symbolism, and Sovacool et al. [21] documented systematic gender differences in electric mobility preferences, with women placing greater emphasis on practical and safety-relevant attributes. This observation is a reminder that gender should not be treated as a monolithic segmentation variable, although a single non-significant comparison cannot itself support that conclusion.

The finding that Tesla Model 3 attracted zero female preference, while all male Tesla-preferring respondents cited brand, is compatible with the proposition that BEV brands may carry gendered associations, although it rests on three male and no female nominations and is reported as an observation only. Tesla's identity, centred on technological performance and minimalist design, appears more resonant with male participants in this study, consistent with prior work on symbolic vehicle attributes and gender [14, 37]. This is a descriptive observation based on small frequencies (n=3 male Tesla choosers, n=0 female), and should be treated as hypothesis-generating rather than confirmatory.

The implicit-explicit discrepancy for price and range, highly declared importance ($M > 5.1$) but low visual engagement (dwell times below 700 ms), is consistent with research documenting divergence between explicit and implicit consumer responses [27-28]. A comparable divergence between self-reported and behaviourally derived measures has been reported in other assessment domains, where skill levels inferred from observed behaviour differed from participants' own self-assessments [38]; this suggests a general property of self-report methods rather than a domain-specific artefact. A plausible interpretation is that participants had pre-formed price and range expectations anchored to brand associations, reducing the need for direct visual inspection. A second, non-exclusive interpretation concerns the mode of data collection: the stated measures were obtained in a face-to-face structured interview rather than through an anonymous self-completed instrument, and stated importance is exposed to social desirability in a way that visual attention is not. This finding is consistent across both genders (price: $d = -0.02$; range: $d = 0.00$) and may reflect a general heuristic rather than a gender-specific pattern.

6 Conclusions

In this exploratory study, gender differences in the visual evaluation of battery electric vehicles were examined using eye-tracking technology and post-experimental structured interviews with 32 participants. The following principal conclusions are drawn:

(1) Vehicle design attracted the most visual attention in this sample. Across all five analysed models, the design AOI recorded the highest dwell times

and fixation counts in the pooled data, exceeding the commercial information fields by a factor of between 2.5 and 13 depending on the model and the field. This ranking should, however, be read alongside the difference in AOI area and position noted in Sections 3.3 and 5.

(2) Gender-related tendencies in attribute importance and model preference were observed, though without reaching conventional statistical significance. Women tended to assign higher importance to brand identity (Δ = +0.88, d = 0.69, p = 0.056), vehicle equipment (Δ = +1.01, d = 0.60, p = 0.105), and vehicle design (Δ = +0.77, d = 0.47, p = 0.181) compared to men. Men cited range per charge as their primary stated purchase reason (66.7% of male respondents). The point estimates are compatible with the genuine gender differences of medium size, but the sample cannot discriminate between that possibility and the absence of any difference. Tesla Model 3 was chosen exclusively by men, while Audi Q4 e-tron was disproportionately preferred by women - a descriptive finding that warrants replication.

(3) Implicit attention and explicit preferences diverge for price and range. Despite both attributes being rated as highly important, they received the lowest visual engagement in the eye-tracking data. One plausible interpretation, not tested directly in this study, is that participants inferred price and range value from brand and design cues rather than verifying the displayed figures. If confirmed in subsequent research, this would have implications for the information architecture of digital BEV marketing environments.

(4) The exploratory findings suggest, but do not confirm, that gender-differentiated communication strategies may be effective in BEV marketing contexts. If the observed tendencies are borne out in larger, pre-registered studies, campaigns targeting female consumers could foreground brand heritage, design sophistication, and interior comfort, while campaigns targeting male consumers might provide transparent range comparisons and charging infrastructure assurances. Such strategies could contribute to broadening BEV appeal in Slovakia and comparable CEE markets, but this recommendation should be treated as hypothesis-generating pending confirmatory evidence.

Several limitations should be acknowledged. First, the sample size (n = 32; 14 women, 18 men) was relatively modest. Although this is consistent with sample sizes commonly reported in consumer eye-tracking research [25] and neuromarketing studies investigating gender differences (e.g., Vecchiato et al. [30], n = 28), where intensive within-subject measurement yields a large number of observations per participant, the post-hoc power analysis (power $\approx$ 0.38 for d = 0.65 at α = 0.05) indicates that the study was underpowered to reliably detect medium-to-large gender differences in attribute importance. Consequently, the observed effect sizes should be interpreted as exploratory and require confirmation in larger samples. Second, the study was conducted in the context of the Slovak market, and the findings may therefore reflect market-specific characteristics that cannot be directly generalised to other countries or cultural settings. Third, participants viewed each stimulus for a fixed exposure time of 10 seconds. While this ensured identical experimental conditions across all participants, it may not fully capture longer and more deliberate visual attention processes associated with real-world vehicle purchase decisions. Fourth, the five models subjected to gender-disaggregated analysis were selected after data collection based on the participants' own stated preferences, rather than being specified in advance. This procedure keeps the analysed stimulus set close to participants' purchase intentions, but it makes the selection conditional on an outcome measured in the same sample. One consequence is that Tesla Model Y, the best-selling BEV in Slovakia in the reference period, was excluded despite its market position. Fifth, the AOIs were not equated for area or for eccentricity. The design AOI necessarily encompassed the whole vehicle and occupied the central part of the stimulus, whereas the commercial information fields were small and peripheral. Comparisons of absolute dwell time across AOIs are therefore confounded with stimulus geometry. The future research should employ larger and more diverse samples, extend the study to different national contexts, pre-specify the analysed models or analyse the full stimulus set, equate AOI areas or apply a spatial-bias correction, and further examine the robustness of the observed gender-related visual attention patterns using confirmatory research designs. Subsequent studies could also overcome the constraints of static, fixed-exposure stimuli by employing immersive virtual-reality showrooms or wearable eye-tracking glasses during on-road test drives, approaches that have proven feasible in virtual retail environments [28].

Overall, the present results should be read as exploratory evidence intended to inform the design of future confirmatory studies on gender-differentiated BEV marketing communication, rather than as prescriptions for practice.

Acknowledgements

This research was supported by grant project I-24-028-09 of the University of Zilina.

Conflicts of Interest

The authors declare that they have no known competing financial interests or personal relationships that could have appeared to influence the work reported in this paper.

References

[1] Europe's BEV market defies odds but more affordable models needed - Transport and Environment [online] [accessed 2026-04-09]. 2024. Available from: https://www.transportenvironment.org/articles/europes-bev-market-defies-odds-but-more-affordable-models-needed

[2] Electric vehicle fleet Slovakia surpasses 15,000 units - SEVA [online] [accessed 2026-04-10]. 2025. Available from: https://seva.sk/en/bev-sk-2024/

[3] DUDAS, T. Government strategies for the transition to battery electric vehicles production in Slovakia. In: International Scientific Conference International Economy, Politics and Law in 2024: Trends, Challenges, Perspectives: proceedings [online] [accessed 2026-05-25]. 2024. ISBN 978-80-225-5205-9, p. 116-123. Available from: https://vgi.krtk.hu/wp-content/uploads/2025/04/Dudas-2024-Government-Strategies-for-the-Transition-to-Battery-Electric-Vehicles-Production-in-Slovakia.pdf

[4] MOONS, I., DE PELSMACKER, P. Emotions as determinants of electric car usage intention. *Journal of Marketing Management* [online]. 2012, **28**(3-4), p. 195-237 [accessed 2026-05-21]. ISSN 0267-257X, eISSN 1472-1376. Available from: https://doi.org/10.1080/0267257X.2012.659007

[5] ZHAO, J., SU, Y., FANG, M., SU, M. Embracing new energy vehicles: an empirical examination of female consumer perspectives. *Journal of Retailing and Consumer Services* [online]. 2024, **80**, 103945 [accessed 2026-04-28]. ISSN 0969-6989, eISSN 1873-1384. Available from: https://doi.org/10.1016/j.jretconser.2024.103925

[6] DAZIANO, R. A., BOLDUC, D. Incorporating pro-environmental preferences towards green automobile technologies. *Transportmetrica A: Transport Science* [online]. 2013, **9**(1), p. 74-106 [accessed 2026-04-10]. ISSN 2324-9935, eISSN 2324-9943. Available from: https://doi.org/10.1080/18128602.2010.524173

[7] HAUSTEIN, S., JENSEN, A. F. Factors of electric vehicle adoption. *International Journal of Sustainable Transportation* [online]. 2018, **12**(7), p. 484-496 [accessed 2026-05-06]. ISSN 1556-8318, eISSN 1556-8334. Available from: https://doi.org/10.1080/15568318.2017.1398790

[8] CVACHO, V., MADLENAK, R. The role of visual attention in evaluating electric vehicles: an eye-tracking perspective. In: International Scientific Conference Transport Means 2025: proceedings. 2025. eISSN 2351-7034, p. 120-125.

[9] EVs are three times better for the environment in ride-hailing fleets - Transport and Environment [online] [accessed 2026-04-09]. 2021. Available from: https://www.transportenvironment.org/articles/evs-three-times-better-environment-when-ride-hailing

[10] The drive to 2025: Carmakers' progress towards their EU CO2 target in H1 2024 -Transport and Environment [online] [accessed 2026-04-09]. 2024. Available from: https://www.transportenvironment.org/articles/the-drive-to-2025-why-eus-2025-car-co2-target-is-reachable-and-feasible

[11] SKEETE, J.-P., WELLS, P., DONG, X., HEIDRICH, O., HARPER, G. Beyond the "EVent horizon": battery waste, recycling, and sustainability in the United Kingdom electric vehicle transition. *Energy Research and Social Science* [online]. 2020, **69**, 101581 [accessed 2026-05-21]. eISSN 2214-6326. Available from: https://doi.org/10.1016/j.erss.2020.101581

[12] DUDZIAK, A., DROZDZIEL, P., STOMA, M., CABAN, J. Market electrification for BEV and PHEV in relation to the level of vehicle autonomy. *Energies* [online]. 2022, **15**(9), 3120 [accessed 2026-08-02]. eISSN 1996-1073. Available from: https://doi.org/10.3390/en15093120

[13] MADLENAKOVA, L., MADLENAK, R. Electromobility and the prospects for its development / Elektromobilita a perspektivy jej rozvoja (in Slovak). *Post, Telecommunications and Electronic Commerce / Posta, Telekomunikacie a Elektronicky obchod* [online]. 2021, **16**(2), p. 70-78 [accessed 2026-04-13]. ISSN 1336-8281. Available from: https://doi.org/10.26552/pte.C.2021.2.11

[14] SCHUITEMA, G., ANABLE, J., SKIPPON, S., KINNEAR, N. The role of instrumental, hedonic and symbolic attributes in the intention to adopt electric vehicles. *Transportation Research Part A: Policy and Practice* [online]. 2013, **48**, p. 39-49 [accessed 2026-04-28]. ISSN 0965-8564, 1879-2375. Available from: https://doi.org/10.1016/j.tra.2012.10.004

[15] Are European countries steering drivers to go electric? Transport and Environment [online] [accessed 2026-04-09]. 2025. Available from: https://www.transportenvironment.org/articles/are-european-countries-steering-drivers-to-go-electric-or-stick-to-polluting-suvs

[16] EGBUE, O., LONG, S. Barriers to widespread adoption of electric vehicles. *Energy Policy* [online]. 2012, **48**, p. 717-729 [accessed 2026-04-28]. ISSN 0301-4215, eISSN 1873-6777. Available from: https://doi.org/10.1016/j.enpol.2012.06.009

[17] RAINIERI, G., BUIZZA, C., GHILARDI, A. The psychological, human factors and socio-technical contribution: a systematic review towards range anxiety of battery electric vehicles' drivers. *Transportation Research Part F: Traffic Psychology and Behaviour* [online]. 2023, **97**, p. 52-70 [accessed 2026-04-28]. ISSN 1369-8478, eISSN 1873-5517. Available from: https://doi.org/10.1016/j.trf.2023.10.001

[18] UIKEY, A. A., BABER, R., MARAK, Z. R. Transforming green transparency into green brand loyalty and repurchase intentions: the role of brand image and credibility among electric vehicle users. *Journal of Applied Structural Equation Modelling* [online]. 2025, **9**(1), p. 1-24 [accessed 2026-04-10]. eISSN 2590-4221. Available from: https://doi.org/10.47263/JASEM.9(1)02

[19] CHEN, Y., HOU, Y. Impacts of design aesthetics, brand equity, and trust on electric vehicle purchase intention: an empirical study. *Journal of Brand Management* [online]. 2026, **33**, p. 54-72 [accessed 2026-04-29]. ISSN 1350-231X, eISSN 1479-1803. Available from: https://doi.org/10.1057/s41262-025-00408-w

[20] MAMCARZ, P., DROZDZIEL, P., MADLENAKOVA, L., SIERADZKI, A., DROZDZIEL, P. Level of occupational stress, personality and traffic incidents: comparative study of public and freight transport drivers. *Transportation Research Procedia* [online]. 2019, **40**, p. 1453-1458 [accessed 2026-08-02]. eISSN 2352-1465. Available from: https://doi.org/10.1016/j.trpro.2019.07.201

[21] SOVACOOL, B. K., KESTER, J., NOEL, L., ZARAZUA DE RUBENS, G. The demographics of decarbonizing transport: the influence of gender, education, occupation, age, and household size on electric mobility preferences in the Nordic region. *Global Environmental Change* [online]. 2018, **52**, p. 86-100 [accessed 2026-05-21]. ISSN 0959-3780, eISSN 1872-9495. Available from: https://doi.org/10.1016/j.gloenvcha.2018.06.008

[22] BEV market growth hinges on closing the gender gap - Escalent [online] [accessed 2026-04-10]. 2024. Available from: https://escalent.co/news/bev-market-growth-hinges-on-closing-the-gender-gap/

[23] SONG, Y., SUPASETTAYSA, G., RATCHATAKULPAT, T. Influence of marketing communication on purchase intention of the luxury electric vehicles in China: mediating role of consumer brand preference and perceived value. *Journal of Logistics, Informatics and Service Science* [online]. 2025, **12**(2), p. 287-310 [accessed 2026-04-29]. ISSN 2409-2665. Available from: https://doi.org/10.33168/JLISS.2025.0218

[24] PEI, M., HUANG, Z., ZHANG, Z., WANG, K., YE, X. Range anxiety and willingness to pay: psychological insights for electric vehicle. *Journal of Renewable and Sustainable Energy* [online]. 2025, **17**(1), 015902 [accessed 2026-04-30]. eISSN 1941-7012. Available from: https://doi.org/10.1063/5.0220237

[25] HOLMQVIST, K., NYSTROM, M., ANDERSSON, R., DEWHURST, R., JARODZKA, H., VAN DE WEIJER, J. *Eye tracking: a comprehensive guide to methods and measures*. Oxford: Oxford University Press, 2011. ISBN 978-0-19-873859-6.

[26] SMI Begaze Software. User guide and technical specifications. SensoMotoric Instruments (SMI), 2016.

[27] PIETERS, R., WEDEL, M. Attention capture and transfer in advertising. *Journal of Marketing* [online]. 2004, **68**(2), p. 36-50 [accessed 2026-04-30]. ISSN 0022-2429, eISSN 1547-7185. Available from: https://doi.org/10.1509/jmkg.68.2.36.27794

[28] KIM, N., LEE, H. Assessing consumer attention and arousal using eye-tracking technology in virtual retail environment. *Frontiers in Psychology* [online]. 2021, **12**, 665658 [accessed 2026-04-29]. eISSN 1664-1078. Available from: https://doi.org/10.3389/fpsyg.2021.665658

[29] BOSCOLO, J. C., OLIVEIRA, J. H. C., MAHESHWARI, V., GIRALDI, J. D. M. E. Gender differences: visual attention and attitude toward advertisements. *Marketing Intelligence and Planning* [online]. 2021, **39**(2), p. 300-314 [accessed 2026-04-28]. ISSN 0263-4503, eISSN 1758-8049. Available from: https://doi.org/10.1108/MIP-11-2019-0598

[30] VECCHIATO, G., MAGLIONE, A. G., CHERUBINO, P., WASIKOWSKA, B., WAWRZYNIAK, A., LATUSZYNSKA, A., LATUSZYNSKA, M., NERMEND, K., GRAZIANI, I., LEUCCI, M. R., TRETTEL, A., BABILONI, F. Neurophysiological tools to investigate consumer's gender differences during the observation of TV commercials. *Computational and Mathematical Methods in Medicine* [online]. 2014, **2014**, 912981 [accessed 2026-04-30]. ISSN 1748-670X, eISSN 1748-6718. Available from: https://doi.org/10.1155/2014/912981

[31] SINHA, M., MISRA, M., MISHRA, S. Gender selection dilemma in fast moving consumer goods (FMCG) advertising: Insights from eye-tracking research. *Journal of Eye Movement Research* [online]. 2024, **17**(2), p. 1-27 [accessed 2026-04-27]. eISSN 1995-8692. Available from: https://doi.org/10.16910/jemr.17.2.6

[32] KUDELA, P., FANDAKOVA, M., PALCAK, M., KORDEK, J. Utilization of modern methods for documentation of traffic accidents in road transport. In: International Scientific Conference Transport Means 2021: proceedings. 2021. eISSN 2351-7034, p. 584-588.

[33] SMI Red Eyetracker. Technical specifications. SensoMotoric Instruments (SMI), 2016.

[34] European demand for BEVs slowed in H1 as Tesla and Volkswagen lost ground to BMW and Chinese OEMs - Jato Dynamics [online] [accessed 2026-04-10]. 2024. Available from: https://www.jato.com/resources/media-and-press-releases/european-bev-demand-slows-tesla-volkswagen-lose-ground

[35] The number of electric vehicles is growing slowly / Elektromobily pribudaju pomaly - Seva (in Slovak) [online] [accessed 2026-04-10]. 2024. Available from: https://seva.sk/vozidla-h1-24/

[36] Seven in ten BEV buyers demand style over specs - Globenewswire [online] [accessed 2026-05-04]. 2026. Available from: https://www.globenewswire.com/news-release/2026/01/12/3217281/0/en/seven-in-ten-bev-buyers-demand-style-over-specs.html

[37] LIEVEN, T., MUHLMEIER, S., HENKEL, S., WALLER, J. F. Who will buy electric cars? An empirical study in Germany. *Transportation Research Part D: Transport and Environment* [online]. 2011, **16**(3), p. 236-243 [accessed 2026-04-28]. ISSN 1361-9209, eISSN 1879-2340. Available from: https://doi.org/10.1016/j.trd.2010.12.001

[38] MARENGO, A., PAGANO, A., SANTAMATO, V. A machine learning framework for soft skills assessment: leveraging serious games in higher education. *Computers and Education: Artificial Intelligence* [online]. 2025, **9**, 100469 [accessed 2026-04-30]. eISSN 2666-920X. Available from: https://doi.org/10.1016/j.caeai.2025.100469

This is an open access article distributed under the terms of the Creative Commons Attribution 4.0 International License (CC BY 4.0), which permits use, distribution, and reproduction in any medium, provided the original publication is properly cited. No use, distribution or reproduction is permitted which does not comply with these terms.

SYNCHRONIZING PUBLIC TRANSPORT SCHEDULES WITH GENETIC ALGORITHMS: CHOOSING THE HEURISTIC PARAMETERS

Vitalii Naumov[1,*], Assyl Tazhmuratova[2], Ihor Taran[3], Yuliia Melnikova[4], Daniel Kapica[1]

[1]Krakow University of Technology, Krakow, Poland
[2]Mukhamedzhan Tynyshbayev ALT University, Almaty, Kazakhstan
[3]Rzeszow University of Technology, Rzeszow, Poland
[4]Dnipro University of Technology, Dnipro, Ukraine

*E-mail of corresponding author: vitalii.naumov@pk.edu.pl

Vitalii Naumov 00-0001-9981-4108,
Ihor Taran 0000-0002-3679-2519,
Daniel Kapica 0009-0005-5453-6307
Assyl Tazhmuratova 0000-0002-1139-1006,
Yuliia Melnikova 0000-0001-7023-023X,

Resume
Synchronized timetables are crucial for public transportation, yet optimizing them remains complex. While Genetic Algorithms (GAs) address this challenge effectively, their success depends on parameter tuning. In this study was examined how the GA parameters affect schedule synchronization, using a stochastic simulation model to evaluate the fitness of alternative solutions. It is found that the larger population sizes improve solution quality, and higher crossover probabilities enhance overall performance. Conversely, increasing mutation rates or the number of attempted mutations reduces the algorithm's ability to converge on optimal timetables. Those findings provide researchers and practitioners with data-driven insights for efficiently deploying GAs in public transit optimization.

Article info
Received 1 June 2026
Accepted 26 August 2026
Online 14 September 2026

Keywords:
public transport timetables
network synchronization
genetic algorithm
parameter tuning

Available online: https://doi.org/10.26552/com.C.2026.051

ISSN 1335-4205 (print version)
ISSN 2585-7878 (online version)

1 Introduction

One key determinant of public transportation efficiency is schedule synchronization. Synchronized timetables minimize passenger waiting times, reduce transfer costs, and enhance the overall attractiveness of public transit. Achieving optimal synchronization is a complex combinatorial optimization problem, often characterized by a vast search space and multiple, conflicting objectives. Consequently, researchers have employed a variety of heuristic and metaheuristic approaches, such as Simulated Annealing (SA), Tabu Search, and Ant Colony Optimization (ACO), to find the high-quality solutions within reasonable computational limits [1]. Genetic algorithms (GAs) are widely used to tackle scheduling challenges because of their robustness and ability to explore a diverse solution space.

While the GAs have shown considerable potential for public transport synchronization, their performance depends critically on selecting the right heuristic parameters. Parameters such as population size, crossover rate, mutation rate, and selection mechanisms significantly influence the algorithm's convergence speed and solution quality. Suboptimal parameter choices can lead to premature convergence, an inability to find near-optimal solutions, or excessively long computation times, thereby diminishing the practical utility of the GA-based approach to synchronizing schedules within the public transport system.

In this paper is addressed the crucial role of heuristic parameter selection in synchronizing public transport schedules using GAs. Within this research was investigated how different parameters affect the effectiveness of GAs in this domain. By analyzing how parameter settings affect optimization performance, this study aim was to provide insights for researchers and practitioners seeking to deploy GAs to solve the

synchronization problem within a public transport network. Ultimately, this study's objective is to enhance the performance of GA-based solutions, thereby supporting the development of more efficient public transportation systems.

As a tool to evaluate the efficiency of the public transport system, the simulation model was first proposed and described in the paper [2]. The authors applied this tool while solving the synchronization problem for the public transport network in Verkhniodniprovsk, Ukraine [3]. The simulation model generates random trip demand within the public transport system, mimics the servicing process, and returns the estimated total waiting time for passengers.

This paper is organized as follows. In Section 2, the literature on applying the GA to public transport timetable synchronization is reviewed. The proposed approach, which combines GA with system simulations, is described in Section 3. The methodology for investigating the impact of GA parameters on the results is outlined in Section 4. The findings from the experimental studies are presented in Section 5, and a summary and recommendations for future research are provided in Section 6.

2 Literature review

Previously, research on timetable synchronization was focused on optimizing a single objective, such as minimizing passenger waiting time or total costs, including operational costs. Yet a significant shift is occurring, with more recent studies adopting a multi-criteria approach. This broader perspective allows researchers to address the problem's full complexity by considering objectives such as minimizing passenger time (waiting and travel), reducing schedule deviations, minimizing vehicle requirements, and maximizing transfer opportunities. This evolution reflects a deeper understanding of the interrelated factors crucial to effective timetable synchronization [1].

The GAs have been widely applied to the complex problem of public transport schedule synchronization, addressing a broad range of optimization objectives. A primary focus in many studies has been minimizing passenger inconvenience. For instance, Chakroborty et al. used GAs to minimize the combined transfer and initial waiting times [4]. Similarly, Wu et al. sought to reduce total passenger waiting times in the Beijing metro network, with an added emphasis on equitable waiting times across stations [5], while Tuzun and Yılmaz formulated an objective to minimize both passenger waiting times and missed transfers [6]. Building on this passenger-centric approach, Niu et al. addressed passenger waiting time while innovatively incorporating an in-train crowding factor to enhance comfort and maximize operator profits [7]. The challenge of the last-train synchronization, crucial for extending network accessibility, has also been tackled, with Kang et al. focusing on minimizing passenger transfer connection headways in Beijing, China, demonstrating that this approach is more effective than solely minimizing waiting time for successful transfers [8]. Yin et al. also addressed the last-train schedules, formulating an objective to balance extended operating hours and associated costs while reducing missed transfers and average waiting times [9].

Beyond passenger time, GAs have been used to optimize operational aspects and overall network efficiency. Ngamchai and Lovell addressed minimizing combined fleet operating costs, in-vehicle passenger time, and waiting time [10]. Vehicle utilization was a key concern for Ataeian et al., who used GAs to maximize simultaneous arrivals and minimize the vehicle count in the bus rapid transit network of Tehran, Iran [11]. Similarly, Naeini, Shafahi, and Taherkhani incorporated the skip-stop operations in their GA-based synchronization for the Tehran subway, aiming to reduce travel times and operating costs while considering passenger waiting time, in-vehicle travel time, and operational expenses [12]. The scope of GA applications extends to diverse network types, including bus networks, as optimized by Bielli, Caramia, and Carotenuto in Parma, Italy, achieving a 90% improvement in a multi-criteria fitness function [13], and by Shafahi and Khani in Mashad, Iran [14]. Integrated systems have also been a focus, with Shrivastava et al. synchronizing bus and train networks with penalties for excessive transfer times [15], and Yu, Yang, and Yao optimizing the multimodal public transport network in Dalian, China, while maintaining the existing fleet [16]. More recently, Wang, Zhou, and Yan applied GAs to synchronize timetables for autonomous buses in Singapore, integrating passenger assignment into the optimization [17].

Comparative studies have often highlighted GAs' strengths. Nachtigall and Voget found that GAs initialized with solutions from a greedy algorithm yielded better results for minimizing passenger waiting time than random initialization [18]. Shafahi and Khani demonstrated that GAs outperformed the Branch and Bound (B&B) algorithm for the bus network synchronization [14]. In a study of the Beijing metro network, Kang et al. compared SA, Tabu Search, B&B, and GA to minimize passenger travel time and schedule deviations, finding GA superior in objective function value and computational speed [19]. Cao et al. also reported that their GA for synchronized and coordinated scheduling optimization outperformed the CPLEX model in speed and solution quality for maximizing synchronized meetings at Beijing metro stations [20]. However, the performance advantage is not without trade-offs; Wang, Li, and Cao, while finding the GA superior to the Gray Wolf Optimizer in solution quality for timetable synchronization (minimizing origin waiting time, transfer waiting

time, and missed connection penalties), noted that GA required significantly more computation time [21]. Further applications include Chen et al., who used GAs to maximize accessible origin-destination pairs [22].

The consistent success of GAs across these varied applications, objective functions, and transport contexts underscores their robustness and utility for solving complex schedule synchronization problems. The literature shows that GAs can effectively handle multi-criteria objectives, diverse operational constraints, and large-scale networks. Given this widespread adoption and proven efficacy, optimizing GA performance itself is a critical research direction. The choice of heuristic parameters within a GA framework significantly influences search efficiency and solution quality. While many studies report successful GA implementations, a detailed investigation into the systematic selection of these parameters for the public transport synchronization problems is essential to harness the full potential of this powerful optimization tool.

When configuring the GA parameters, researchers often set a crossover rate between 50% and 60%. Similarly, a mutation probability of 10% is common because it balances the need to explore new solutions with the need to exploit promising ones within the search space. Regarding population size, research commonly suggests using fewer than 100 chromosomes. This is because, while larger populations can offer more diversity, the resulting increase in computational time often outweighs these benefits.

3 Implementation of GA to synchronize the timetables

The fundamental stages of a GA include evaluating current solutions via a fitness function applied to each population individual, selecting the most fit individuals for propagation, and the reproductive process itself, involving crossover and mutation operators. To address the timetable synchronization problem, the GA population must encode distinct public transport schedule configurations as chromosomes. Next, a fitness-quantification method is needed to support the selection phase. Explicit selection rules must then be established to define the cohort of individuals designated for reproduction in subsequent GA iterations. Furthermore, a crossover procedure that enables the formation of novel individuals from parental pairs must be formulated to underpin the reproduction stage. Finally, a mutation routine tailored to the chosen chromosome is indispensable for mitigating premature convergence to local optima during GA operation. The procedure for encoding timetables as binary chromosomes, along with the corresponding operators, was developed and described in [3].

3.1 Proposed approach to represent the problem

A streamlined method is proposed for representing public transport schedules, particularly effective for the peak-hour timetables where vehicle arrivals at a given stop occur at fixed, predetermined intervals. This common scenario allows for a highly efficient representation. Under this assumption, the entire timetable for a specific transport line can be derived from a single core parameter: the time shift from the service's commencement. This time shift parameter serves as an offset, defining all subsequent arrival times for that line. Consequently, to represent a complete set of timetables across the entire public transport system, a vector of these time shifts can be used, with each element corresponding to a specific transport line.

At its most granular level, a schedule element $S_k^{(\lambda,\nu)}$ for the vehicle ν on the line λ at its k-th sequential position is defined as:

$$S_k^{(\lambda,\nu)} = \left\langle p_k^{(\lambda,\nu)}, t_k^{(\lambda,\nu)} \right\rangle, \tag{1}$$

where: $p_k^{(\lambda,\nu)}$ represents the specific public transport line stop (spatial component), and $t_k^{(\lambda,\nu)}$ denotes the moment of arrival of vehicle ν at that stop (temporal component); this dual-component representation is crucial for real-world applications of timetable synchronization as it links geographic locations (public transport stops) with time-based events (vehicle arrivals).

The complete schedule for a vehicle ν on a given line λ, denoted as s_ν, is constructed as a union of these individual schedule elements:

$$s_\nu = \cup_{k=1}^{N_s^{(\lambda,\nu)}} s_k^{(\lambda,\nu)} = \cup_{k=1}^{N_s^{(\lambda,\nu)}} \left\langle p_k^{(\lambda,\nu)}, t_k^{(\lambda,\nu)} \right\rangle, \tag{2}$$

where: $N_s^{(\lambda,\nu)}$ is the total number of scheduled stops for the vehicle ν on the line λ; an important constraint is that every scheduled position $p_k^{(\lambda,\nu)}$ must belong to the set of defined stops N_λ for line λ: $\lambda: \forall p_k^{(\lambda,\nu)} \in N_\lambda$.

The planned arrival time $t_k^{(\lambda,\nu)}$ for the vehicle ν on the line λ at its k-th scheduled stop is formulated as a linear function of three key parameters:

$$t_k^{(\lambda,\nu)} = t_0 + \phi_\lambda + (k-1)\cdot\delta_\lambda, \tag{3}$$

where: t_0 represents the system-wide reference start time (e.g., midnight or a defined operational start of the day); ϕ_λ denotes the line-specific initial time shift for line λ, expressed in minutes; this parameter quantifies any offset from the global system start time t_0 for the commencement of service on a particular line; δ_λ signifies the constant interval (headway) between successive vehicle departures on line λ, in minutes; this parameter directly defines the service frequency of line λ and is a critical determinant of service capacity; the term $(k-1)\cdot\delta_\lambda$ accounts for the cumulative travel time based on the sequential progression through stops.

Since the public transport timetables are typically

established with minute-level precision, the elements of the time-shift vector are integers.

In its simplest application, the public transport schedule synchronization can be achieved by adjusting the initial service start time for each line. These adjustments, central to the schedule synchronization problem, are compactly represented by the vector Ψ:

$$\Psi = \langle \phi_1, \phi_2, \ldots, \phi_{N_\Lambda} \rangle, \tag{4}$$

where N_Λ denotes the total number of public transport lines operating within the network.

The vector Ψ serves as a primary control parameter. By manipulating its integer elements, the relative start times of passenger service across all lines in the transport system can be adjusted. This targeted control enables the coordination of passenger service processes, facilitating synchronization with minimal alteration to established operational patterns.

The primary performance metric for assessing the effectiveness of schedule synchronization within the public transport network is the average passenger waiting time $T^{(w)}$ across all public transport stops. This indicator quantifies the cumulative inconvenience and inefficiency passengers experience due to misaligned schedules. Building upon established approaches for synchronization, the $T^{(w)}$ value is proposed to be determined in the following way:

$$T^{(w)} = f(\Psi) = \frac{1}{|D|} \cdot \sum_{\pi \in D} t_\pi^{(w)} \rightarrow \min, \tag{5}$$

where: $t_\pi^{(w)}$ represents the individual waiting time (in minutes) for a passenger π using public transportation; D denotes the set of all passengers or passenger demand instances within the system under consideration, whereas $|D|$ stands for the set's power - the number of elements within a set, representing the total number of intended trips within a transport system.

Minimizing $T^{(w)}$ addresses the core problem of reducing passenger inconvenience and improving the overall efficiency and attractiveness of the public transport system by aligning service provisions more closely with passenger travel needs.

The transport network model, crucial for simulating passenger service based on provided schedules and estimating total waiting time, is thoroughly detailed in [3]. The program implementation of this simulation model is openly accessible on GitHub [23].

The core logic of this simulation model unfolds in the following sequence:

- Given a public transport network graph and the input vector Ψ (representing line-specific initial time shifts), timetables for all lines are calculated using Equation (3).
- Passenger demand for transport services is generated stochastically. Passenger arrival times are determined by a random variable representing inter-arrival intervals. The destination stop for each trip is then randomly selected or assigned according to a predefined origin-destination matrix.
- For each generated trip, the optimal travel route is determined using Dijkstra's algorithm. If the origin and destination are not on the same line, the transfer nodes are identified for that trip.
- The passenger-servicing process is simulated for each vehicle on every line. The simulation follows the calculated timetable and accommodates the generated passenger demand.
- Upon completion of the simulation, the waiting time for each passenger is computed. Subsequently, the mean waiting time $T^{(w)}$ is aggregated using Equation (5).

Note that the obtained values of $T^{(w)}$ are random due to the stochastic nature of demand generation. Consequently, multiple simulation runs are required to estimate the expected total waiting time.

3.2 Polygon for conducting experimental studies

To demonstrate the computational capabilities of the proposed timetable synchronization approach, a case study was conducted using the public transportation network of Verkhniodniprovsk, Ukraine. This city, located in the Dnipropetrovsk Oblast, was selected for its manageable size and representative urban transport characteristics, making it an ideal environment for validating the developed model without excessive computational overhead.

Verkhniodniprovsk has a population of approximately 17,000 and is served by a compact yet comprehensive public transportation system. The network consists of 5 public transport lines, spanning approximately 80 km. These lines serve 47 bus stops. The fleet comprises 5 vehicles, with one dedicated vehicle per line. Vehicle capacities range from 18 to 50 passengers.

A more granular breakdown of each public transport line in Verkhniodniprovsk's network is presented in Table 1. This detailed information underpins the parameters used in the simulation, enabling the authors to assess how the synchronization methodology can optimize passenger flow and minimize waiting times in a real-world setting.

Within the context of public transport systems, a transfer node is formally defined as any public transport stop served by more than one distinct line, thereby enabling passengers to interchange between different routes. This capability is crucial for passengers navigating the network, allowing them to reach destinations not directly served by a single line.

4 Methodology of studying the influence of GA parameters on synchronization results

The GA performance in optimization is strongly influenced by its heuristic parameters, a critical

factor that requires careful consideration for effective application. Some parameters have a straightforward impact; for instance, increasing the number of generations generally improves results until the algorithm converges on a stable solution. Conversely, other GA parameters are highly context-dependent, directly shaped by the problem being solved. A prime example is the genetic encoding of a solution, such as the number of bits used to represent it. This depends on the problem domain's attributes, such as the total number of lines in a network and the maximum possible headways allowed on those lines.

In the conducted study was analyzed the influence of the four key GA parameters on the effectiveness of timetable synchronization: population size S_p, crossover probability p_c, mutation probability p_m, and the number of attempted mutations per chromosome t_m. To evaluate their impact, the experimental studies define bounds and step sizes for each GA parameter, as detailed in Table 2.

For each experimental series, 300 model replications were executed to ensure a 5% statistical significance level for the obtained results. During each series, the GA parameters not currently under investigation were held constant at the midpoint of their respective evaluated ranges.

To quantitatively estimate the influence of each GA parameter on the optimization results, a regression-based methodology was applied. This approach allows to determine the statistical significance of each parameter's individual or combined impact. If a regression coefficient for a specific GA parameter is statistically significant, it provides evidence that adjusting that parameter's value can measurably improve schedule optimization results.

Specifically, the following linear regression models were utilized, where the explained variable $T^{(w)}$ represents the average waiting time. This metric serves as the primary performance indicator for assessing the quality of the generated public transport schedules, with lower values indicating better optimization. The following regression models were calculated based on the data obtained within the computational experiment:

$$T^{(w)} = \beta_0 + \beta_s \cdot S_p\,, \tag{6}$$

$$T^{(w)} = \beta_0 + \beta_c \cdot p_c\,, \tag{7}$$

$$T^{(w)} = \beta_0 + \beta_m \cdot p_m + \beta_t \cdot t_m\,, \tag{8}$$

where: β_0 represents the intercept that establishes the baseline for the predicted average waiting time, from which the effects of the GA parameters are then added or subtracted according to their respective coefficients; $\beta_s, \beta_c, \beta_m,$ and β_t are regression coefficients that quantify the specific impact of population size, crossover probability, mutation probability, and the number of mutation turns per chromosome, respectively, on the GA's optimization results.

The joint analysis of p_m and t_m in Equation (8) is justified because both parameters define the mutation process's characteristics, frequency, and intensity. Their interplay is particularly crucial for understanding the overall impact of mutation on the GA's ability to explore the solution space and avoid local optima, providing a more holistic view than analyzing them separately.

The statistical significance of each regression coefficient is assessed by examining its confidence interval. For this study, a conventional 5% significance level was used. If a regression coefficient's confidence interval did not include zero, it was deemed statistically significant.

Beyond mere significance, the sign of a significant coefficient indicates the direction of the influence. A negative value for a significant coefficient indicates that increasing the parameter's value would improve the optimization results, as reflected in a desirable reduction in average waiting time. Conversely, a positive value for a significant coefficient suggests that increasing the parameter's value would worsen the GA results, leading to an undesirable increase in waiting time.

Table 1 *Characteristics of public transport lines in Verkhniodniprovsk*

Line number	The number of stops (direct + return)	Route length [km] (direct + return)	Vehicle capacity [pax.]
#1	14 + 10	5.95 + 4.8	18
#2	18*	9.34*	50
#3	8 + 8	5.1 + 5.05	18
#4	8 + 8	13.35 + 13.35	38
#5	9 + 9	11.77 + 11.77	38

* Line #2 has a loop route

Table 2 *Bounds and step for GA parameters within the experiment*

GA parameter	Minimum	Maximum	Step
Population size	20	200	20
Crossover probability	0.1	1.0	0.1
Mutation probability	0.05	0.5	0.05
Mutations per chromosome	1	10	1

5 Results and discussion

In this section, the experimental results are presented, specifically illustrating how the GA parameters influence the average waiting time achieved in the public transport synchronization process. The figures depict the relationships between each GA parameter and three key performance indicators: the smallest, mean, and largest values of average waiting time recorded throughout the entire GA routine.

The largest value of $T^{(w)}$ typically emerges during the GA's initial generations. This early occurrence suggests that this value primarily reflects the GA parameter's immediate impact on the optimization results during the heuristic's starting phase. Conversely, the smallest $T^{(w)}$ value is almost invariably found in the final generation, representing the best possible result discovered and returned by the heuristic procedure. Consequently, its dependence on a given parameter highlights that parameter's critical influence on the optimized solution the GA can produce. Finally, the mean $T^{(w)}$ value serves as a crucial indicator of the GA's overall efficiency. Its dependence on a specific GA parameter explains how that parameter influences the convergence speed of the optimization routine.

Figure 1 illustrates the observed empirical relationships between $T^{(w)}$ and population size, along with their corresponding regression models. Table 3 presents the regression coefficients and their respective confidence intervals. As shown in Figure 1, a consistent negative correlation emerges between the increasing population size and all three mean waiting-time metrics. This empirically demonstrates that, within the tested range, larger population sizes generally lead to lower average waiting times. Further reinforcing these observations, the calculated confidence intervals confirm the statistical significance of the regression coefficient for all tracked $T^{(w)}$ levels. This significance indicates that increasing the population size positively impacts both the initial and final solutions derived from GA iterations.

Figure 2 illustrates the empirical relationships between average waiting time and varying crossover probabilities. Complementing this graphical analysis, Table 4 provides the numerical details of these relationships, presenting the calculated regression coefficients for the crossover probability. It also includes their respective confidence intervals to evaluate the statistical significance and reliability of the observed impacts on $T^{(w)}$. As follows from Figure 2, the overall trend for the smallest and mean waiting times suggests a slight improvement as the crossover probability

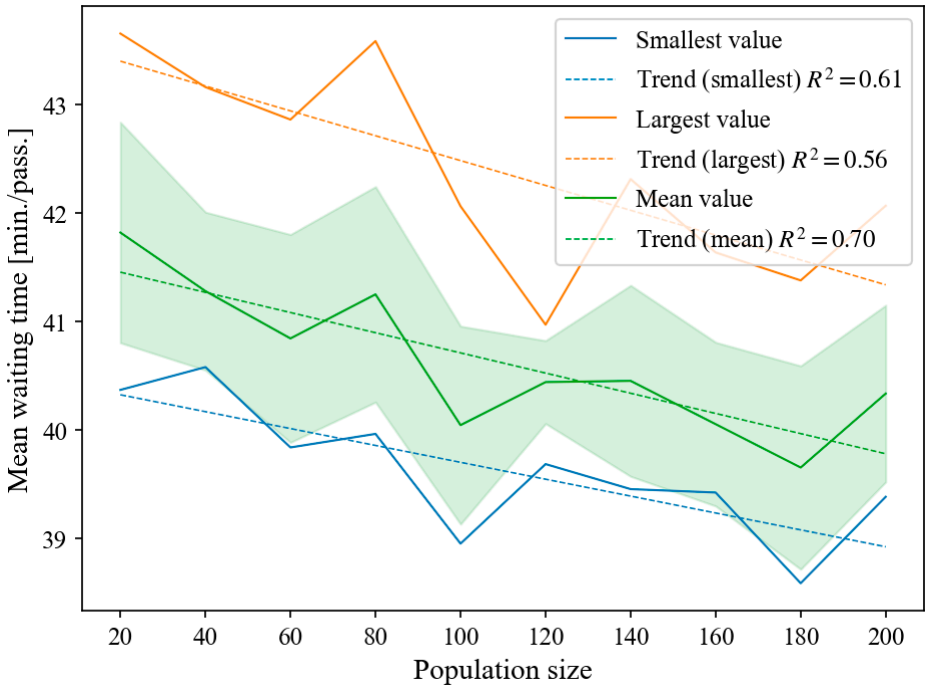


Figure 1 *Dependence of the waiting time on the population size*

Table 3 *Significance of population size in GA performance*

Level of the $T^{(w)}$ value	Regression coefficient β_s	Confidence interval	Parameter significance
Smallest	-0.008	(-0.010; -0.005)	True
Largest	-0.011	(-0.015; -0.008)	True
Average	-0.009	(-0.012; -0.007)	True

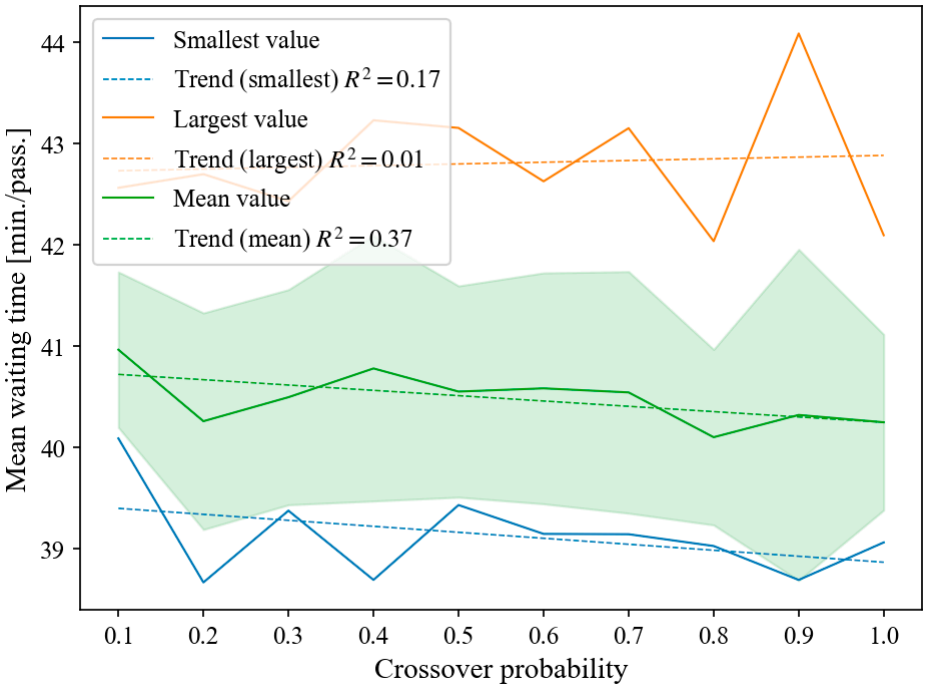


Figure 2 *Dependence of the waiting time on the crossover probability*

Table 4 *Significance of crossover probability in GA performance*

Level of the $T^{(w)}$ value	Regression coefficient β_c	Confidence interval	Parameter significance
Smallest	-0.591	(-1.083; -0.100)	True
Largest	0.168	(-0.596; 0.933)	False
Average	-0.526	(-0.785; -0.266)	True

increases. In contrast, the largest waiting time shows a relatively stable or slightly worsening trend, indicating that higher crossover probabilities might not consistently mitigate the initial high waiting times or the variability of less successful runs, even as the best outcomes slightly improve. However, the confidence interval for the coefficient shows that crossover probability does not influence average waiting time at the initial stage of GA, whereas the experimental results confirm a statistically significant impact of this parameter.

Figure 3 provides a visual overview of how the average waiting time varies with mutation probability (the figure presents results for $t_m = 4$). To complement this graphical representation, Table 5 reports the regression coefficients for mutation probability, along with their confidence intervals and statistical significance. As shown in Figure 3, the linear trends have very low determination coefficients R^2, indicating that mutation probability explains only a small share of the variance in the waiting time metrics across the tested range.

However, a crucial finding emerges when examining the statistical significance of these relationships. As with the crossover probability, the impact of the mutation rate on waiting time during the GA's initial stages (the largest value) is not statistically significant. Conversely, the influence of mutation probability on both the final optimized results (the smallest value) and overall algorithm performance (the average value) is statistically significant. Notably, the corresponding regression coefficients are positive. Since the objective is to minimize the waiting time, these positive coefficients indicate that increasing the mutation rate leads to a quantifiable increase in passenger waiting time. Consequently, higher mutation probabilities hurt optimization outcomes, hindering the GA's ability to refine solutions as it progresses.

In Figure 4 is presented an examination of the relationship between the average waiting time and the number of attempted mutations per chromosome, with results for p_m = 0.2. Table 6 complements this by providing the calculated regression coefficients for t_m and their confidence intervals to assess statistical significance.

As shown in Figure 4, the number of mutations per chromosome appears to have a relatively minor and inconsistent impact on all three mean waiting time metrics. The corresponding trends for these metrics remain largely flat, suggesting that varying t_m within the explored range does not yield substantial linear improvements in the GA's overall operational performance. The significance test for β_t indicates that changes in the number of mutation turns do not significantly affect results during the GA's initial phase, nor do they affect overall performance. However, the

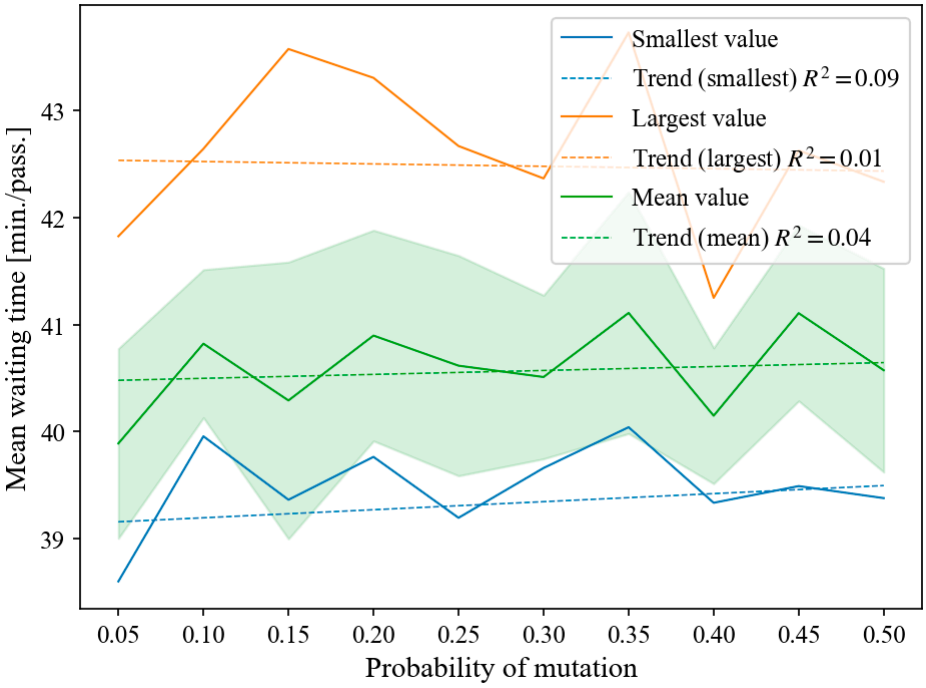


Figure 3 *Dependence of the waiting time on the mutation probability*

Table 5 *Significance of mutation probability in GA performance*

Level of the $T^{(w)}$ value	Regression coefficient β_m	Confidence interval	Parameter significance
Smallest	0.753	(0.300; 1.206)	True
Largest	-0.222	(-0.922; 0.478)	False
Average	0.368	(0.055; 0.681)	True

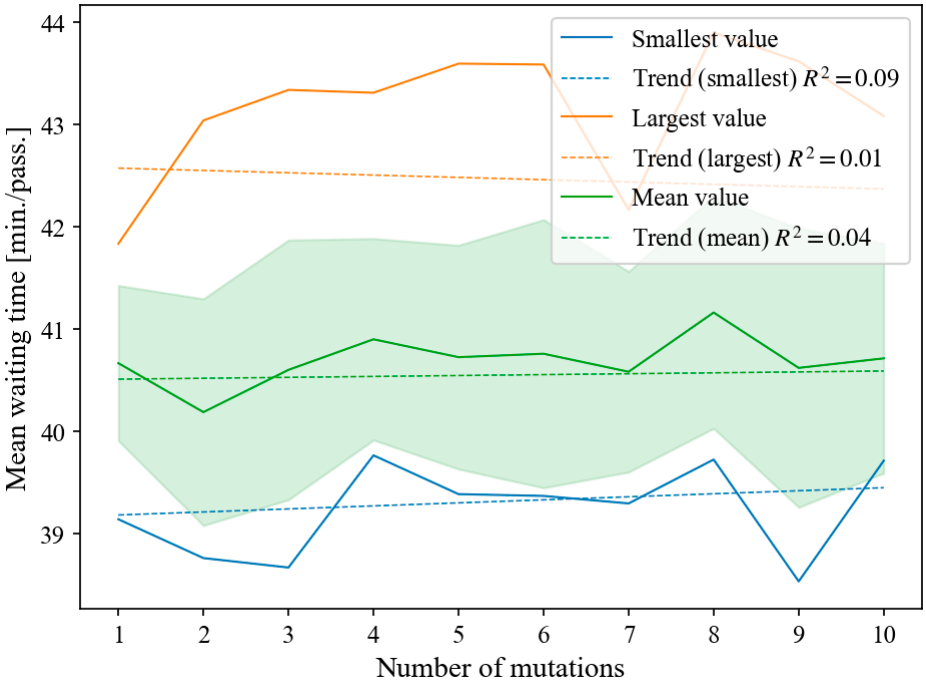


Figure 4 *Dependence of the waiting time on the mutation turns*

Table 6 *Significance of mutation turns in GA performance*

Level of the $T^{(w)}$ value	Regression coefficient β_t	Confidence interval	Parameter significance
Smallest	0.030	(0.007; 0.052)	True
Largest	-0.023	(-0.058; 0.012)	False
Average	0.009	(-0.007; 0.025)	False

analysis reveals a statistically significant impact on the GA procedure's results. This implies that while t_m doesn't broadly shape the GA's average performance, it does cumulatively influence the quality of the best solution found.

To address the explained variance, the determination coefficient values have been integrated into Figures 1-4. These values reflect the proportion of variance explained by each parameter. Predictably, lower R^2 values correspond to statistically insignificant relationships, confirming the lack of a meaningful linear trend, while higher values align with significant parameters.

6 Conclusions

In this study was addressed the critical role of heuristic parameter selection in optimizing public transport timetables using GAs. A GA-based heuristic was developed that uses a binary chromosome representation for schedule time-shifts and was integrated with a simulation model to evaluate fitness, with the objective of minimizing passenger waiting times under stochastic demand.

The completed investigation into how GA parameters influence effectiveness yielded several insights for deploying GAs in public transport network synchronization:

- a larger population consistently improved both the initial and final solution quality, significantly enhancing overall GA performance; therefore, using population sizes at the upper bound of the tested range (e.g., 200 individuals) is recommended for optimal results;
- while the crossover probability had minimal impact on early GA stages, it had a statistically significant positive effect on overall performance, suggesting that high crossover rates (e.g., approaching 1.0) are highly beneficial;
- increasing the mutation rate led to poorer solution quality, suggesting a detrimental effect on the GA's ability to converge toward optimal timetables; thus, a minimal mutation probability (e.g., 0.05) is recommended;
- the number of mutation turns had no significant effect on the initial phase of the GA or its overall performance; however, a higher number of mutations had a cumulative effect on the quality of the best solution, indicating that restricting the algorithm to a single mutation per chromosome is preferable.

It is important to acknowledge a genuine limitation of this manuscript: the empirical findings and subsequent parameter recommendations are based on a single, small-city case study. While this setting provided a clear and manageable baseline for evaluating the GA parameters, it does not fully capture the operational complexities and multimodal interactions characteristic of major metropolitan transit networks.

Based on these insights and limitations, future research should test the proposed GA procedure and validate the identified parameter regularities across diverse, larger-scale public transport networks and geographical locations; and investigate dynamic or adaptive parameter-tuning strategies that can adjust GA parameters during the optimization process.

Acknowledgements

The authors received no financial support for the research, authorship and/or publication of this article.

Conflicts of interest

The authors declare that they have no known competing financial interests or personal relationships that could have appeared to influence the work reported in this paper.

References

[1] KAPICA, D., MELNIKOVA, Y., NAUMOV, V. Synchronization in public transportation: a review of challenges and techniques. *Future Transportation* [online]. 2025, **5**(1), 6 [accessed 2026-06-01]. eISSN 2673-7590. Available from: https://doi.org/10.3390/futuretransp5010006

[2] NAUMOV, V., SAMCHUK, G. Class library for simulations of passenger transfer nodes as elements of the public transport system. *Procedia Engineering* [online]. 2017, **187**, p. 77-81 [accessed 2026-06-01]. ISSN 1877-7058. Available from: https://doi.org/10.1016/j.proeng.2017.04.352

[3] NAUMOV, V., TARAN, I., MELNIKOVA, Y., KAPICA, D. Minimizing passenger waiting in public transport: a genetic algorithm approach to bus schedule synchronization. In: 28th International Scientific Conference Transport Means: proceedings [online] [accessed 2026-06-01]. 2024. p. 91-96. Available from: https://doi.org/10.5755/e01.2351-7034.2024.P91-96

[4] CHAKROBORTY, P., DEB, K., SUBRAHMANYAM, P. Optimal scheduling of urban transit systems using genetic algorithms. *Journal of Transportation Engineering* [online]. 1995, **28**(1), p. 544-553 [accessed 2026-06-01]. ISSN 2473-2907, eISSN 2473-2893. Available from: https://doi.org/10.1061/(ASCE)0733-947X(1995)121:6(544)

[5] WU, J., LIU, M., SUN, H., LI, T., GAO, Z., WANG, D. Equity-based timetable synchronization optimization in urban subway network. *Transportation Research Part C* [online]. 2015, **51**, p. 1-18 [accessed 2026-06-01]. ISSN 0968-090X, eISSN 1879-2359. Available from: https://doi.org/10.1016/j.trc.2014.11.001

[6] TUZUN, A., YILMAZ, S. Transit coordination with heterogeneous headways. *Transportation Planning and Technology* [online]. 2014, **37**(5), p. 450-465 [accessed 2026-06-01]. ISSN 0308-1060, eISSN 1029-0354. Available from: https://doi.org/10.1080/03081060.2014.912419

[7] NIU, H., TIAN, X., ZHOU, X. Demand-driven train schedule synchronization for high-speed rail lines. *IEEE Transactions on Intelligent Transportation Systems* [online]. 2015, **16**(5), p. 2642-2652 [accessed 2026-06-01]. ISSN 1524-9050, eISSN 1558-0016. Available from: https://doi.org/10.1109/TITS.2015.2415513

[8] KANG, L., WU, J., SUN, H., ZHU, X., GAO, Z. A case study on the coordination of last trains for the Beijing subway network. *Transportation Research Part B: Methodological* [online]. 2015, **72**, p. 112-127 [accessed 2026-06-01]. ISSN 0191-2615, eISSN 1879-2367. Available from: https://doi.org/10.1016/j.trb.2014.09.003

[9] YIN, H., WU, J., SUN, H., KANG, L., LIU, R. Optimizing last trains timetable in the urban rail network: social welfare and synchronization. *Transportmetrica B: Transport Dynamics* [online]. 2019, **7**(1), p. 473-497 [accessed 2026-06-01]. ISSN 2168-0566, eISSN 2168-0582. Available from: https://doi.org/10.1080/21680566.2018.1440361

[10] NGAMCHAI, S., LOVELL, D. Optimal time transfer in bus transit route network design using a genetic algorithm. *Journal of Transportation Engineering* [online]. 2003, **129**(5), p. 510-521 [accessed 2026-06-01]. ISSN 2473-2907, eISSN 2473-2893. Available from: https://doi.org/10.1061/(ASCE)0733-947X(2003)129:5(510)

[11] ATAEIAN, S., SOLIMANPUR, M., AMIRIPOUR, S., SHANKAR, R. Synchronized timetables for bus rapid transit networks in small and large cities. *Scientia Iranica* [online]. 2021, **28**(1), p. 477-491 [accessed 2026-06-01]. ISSN 1026-3098, eISSN 2345-3605. Available from: https://doi.org/10.24200/sci.2019.51501.2220

[12] NAEINI, H., SHAFAHI, Y., TAHERKHANI, M. Optimizing and synchronizing timetable in an urban subway network with stop-skip strategy. *Journal of Rail Transport Planning and Management* [online]. 2022, **22**, 100301 [accessed 2026-06-01]. ISSN 2210-9706, eISSN 2210-9714. Available from: https://doi.org/10.1016/j.jrtpm.2022.100301

[13] BIELLI, M., CARAMIA, M., CAROTENUTO, P. Genetic algorithms in bus network optimization. *Transportation Research Part C: Emerging Technologies* [online]. 2002, **10**(1), p. 19-34 [accessed 2026-06-01]. ISSN 0968-090X, eISSN 1879-2359. Available from: https://doi.org/10.1016/S0968-090X(00)00048-6

[14] SHAFAHI, Y., KHANI, A. A practical model for transfer optimization in a transit network: Model formulations and solutions. *Transportation Research Part A: Policy and Practice* [online]. 2010, **44**(6), p. 377-389 [accessed 2026-06-01]. ISSN 0965-8564, eISSN 1879-2375. Available from: https://doi.org/10.1016/j.tra.2010.03.007

[15] SHRIVASTAVA, P., DHINGRA, S., GUNDALIYA, P. Application of genetic algorithm for scheduling and schedule coordination problems. *Journal of Advanced Transportation* [online]. 2002, **36**, p. 23-41 [accessed 2026-06-01]. eISSN 2042-3195. Available from: https://doi.org/10.1002/atr.5670360103

[16] YU, B., YANG, Z., YAO, J. Genetic algorithm for bus frequency optimization. *Journal of Transportation Engineering* [online]. 2010, **136**(6), p. 576-583 [accessed 2026-06-01]. ISSN 2473-2907, eISSN 2473-2893. Available from: https://doi.org/10.1061/(ASCE)TE.1943-5436.0000119

[17] WANG, Y., ZHOU, Y., YAN, X. Autonomous bus timetable synchronization for maximizing smooth transfers with passenger assignment. *Expert Systems with Applications* [online]. 2022, **193**, p. 478-492 [accessed 2026-06-01]. ISSN 0957-4174, eISSN 1873-6793. Available from: https://doi.org/10.1016/j.eswa.2021.116430

[18] NACHTIGALL, K., VOGET, S. A genetic algorithm approach to periodic railway synchronization. *Computers and Operations Research* [online]. 1996, **23**(5), p. 453-463 [accessed 2026-06-01]. ISSN 0305-0548, eISSN 1873-765X. Available from: https://doi.org/10.1016/0305-0548(95)00032-1

[19] KANG, L., WU, J., SUN, H., ZHU, X., WANG, B. A practical model for last train rescheduling with train delay in urban railway transit networks. *Omega* [online]. 2015, **50**, p. 29-42 [accessed 2026-06-01]. ISSN 0305-0483, eISSN 1873-5274. Available from: https://doi.org/10.1016/j.omega.2014.07.005

[20] CAO, Z., CEDER, A., LI, D., ZHANG, S. Optimal synchronization and coordination of actual passenger-rail timetables. *Journal of Intelligent Transportation Systems* [online]. 2019, **23**(3), p. 231-249 [accessed 2026-06-01]. ISSN 1547-2450, eISSN 1547-2442. Available from: https://doi.org/10.1080/15472450.2018.1488132

[21] WANG, Y., LI, D., CAO, Z. Integrated timetable synchronization optimization with capacity constraint under time-dependent demand for a rail transit network. *Computers and Industrial Engineering* [online]. 2020, **142**, 106374 [accessed 2026-06-01]. ISSN 0360-8352, eISSN 1879-0550. Available from: https://doi.org/10.1016/j.cie.2020.106374

[22] CHEN, Y., MAO, B., BAI, Y., HO, T., LI, Z. Timetable synchronization of last trains for urban rail networks with maximum accessibility. *Transportation Research Part C: Emerging Technologies* [online]. 2019, **99**(2), p. 110-129 [accessed 2026-06-01]. ISSN 0968-090X, eISSN 1879-2359. Available from: https://doi.org/10.1016/j.trc.2019.01.003

[23] Class library for simulations of technological processes in a public transport network [online] [accessed 2026-06-01]. Available from: https://github.com/naumovvs/publictransportnet

This is an open access article distributed under the terms of the Creative Commons Attribution 4.0 International License (CC BY 4.0), which permits use, distribution, and reproduction in any medium, provided the original publication is properly cited. No use, distribution or reproduction is permitted which does not comply with these terms.

THE ESG-ORIENTED APPROACHES TO DEVELOPING A SUSTAINABLE RAIL FREIGHT MARKET: METHODOLOGY AND EFFECTIVENESS ASSESSMENT

Bibizhan Aimagambetova[1], Olga Kisselyova[1,*], Roza Mussaliyeva[2], Yerzhan Karsybayev[2], Marzhan Chazhabayeva[3]

[1]Satbayev University, Almaty, Republic of Kazakhstan
[2]Mukhametzhan Tynyshpayev ALT University, Almaty, Republic of Kazakhstan
[3]Yessenov University, Aktau, Republic of Kazakhstan

*E-mail of corresponding author: o.kisselyova@satbayev.university

Bibizhan Aimagambetova 0009-0000-0271-7847,
Roza Mussaliyeva 0000-0002-5154-2374,
Marzhan Chazhabayeva 0000-0003-2676-2807
Olga Kisselyova 0000-0002-1569-7731,
Yerzhan Karsybayev 0000-0001-7942-716X,

Resume

In this paper, the sustainability of Kazakhstan's rail freight market was analyzed in the context of the influence of ESG (Environmental, Social, Governance) variables. The data used (secondary data 2018-2024) and the expert surveys (regression, SEM (Structural Equation Modelling), DEA (Data Envelopment Analysis)) revealed that ESG factors have a significant impact on performance ($R^2 = 0.85$), competitiveness ($R^2 = 0.82$), and stability ($R^2 = 0.84$). The most powerful factors were corridor efficiency ($\beta = 0.421$) and service quality ($\beta = 0.370$) with negative effects being energy consumption ($\beta = -0.312$) and emissions ($\beta = -0.275$). The SEM path coefficients ranged 0.597-0.652; DEA scores ranged 0.87-0.94.

Article info

Received 17 May 2026
Accepted 21 August 2026
Online 24 September 2026

Keywords:

data envelopment analysis
ESG (environmental, social and governance)
structural equation modelling (SEM)
rail freight
sustainability
Kazakhstan

Available online: https://doi.org/10.26552/com.C.2026.053

ISSN 1335-4205 (print version)
ISSN 2585-7878 (online version)

Nomenclature

AVE - Average Variance Extracted
CB-SEM - Covariance-Based Structural Equation Modelling
CE - Corridor Efficiency
CFA - Confirmatory Factor Analysis
CFI - Comparative Fit Index
CI - Community Impact
CR - Composite Reliability
DEA - Data Envelopment Analysis
EC - Energy Consumption
EFF - Efficiency Score
EM - Emissions
ESG - Environmental, Social, and Governance
IT - Investment Transparency
KPI - Key Performance Indicator
KTZ - Kazakhstan Temir Zholy (national railway operator)
LPI - Logistics Performance Index
LTS - Long-Term Stability
MC - Market Competitiveness
OECD - Organisation for Economic Co-operation and Development
PLS-SEM - Partial Least Squares Structural Equation Modelling
RC - Regulatory Compliance
RFP - Rail Freight Performance
RMSEA - Root Mean Square Error of Approximation
SEM - Structural Equation Modelling
SP - Strategic Planning
SQ - Service Quality
SRMR - Standardized Root Mean Square Residual
TBL - Triple Bottom Line
UIC - International Union of Railways
VIF - Variance Inflation Factor
WS - Workforce Safety

1 Introduction

The rail freight sector has seen rapid growth in Kazakhstan over the last decade, with the pace of growth being somewhat uneven. Although it carries a large amount of traffic in the transit between China and Europe, a lot of infrastructure is still aged and loaded with ESG obstacles. Major routes are under threat due to increasing stress on the environment and erratic investment cycles [1-2]. While numerous studies have shown that the current rail planning governance is inadequate and there is a need for new sustainability tools [3-4], only a few consider ESG evaluation methods for rail freight.

In the field of transport sustainability theory, attention is drawn to the issue of governance, environmental performance, network efficiency and community implications [5-7]. Experts believe that the ESG factors have an impact on rail performance, while the infrastructure sustainability has an impact on freight reliability [8-9]. The problems of governance impede improvement [10] and there is no public study of the sustainability of Kazakhstani rail infrastructure by ESG. An environmental scorecard without social and governance information [11] was suggested while other study concentrated on economic resilience [12] or could not find any safety risk-ESG association [13]. Whereas, with the competition from other transport corridors, the high efficiency of the corridor is crucial to maintain market share and to shift the traffic to the corridor [14]

This gap was addressed by presenting an ESG-based analysis model of the Kazakhstan rail freight market. The goals are to (1) assess the impact of ESG on market performance, competitiveness, and long-term stability; (2) assess the empirical validity of the proposed ESG methodology; and (3) develop a repeatable framework to incorporate ESG indicators in a rail corridor sustainability index. This study is an addition to the quantitative evaluation to the ESG integration in a rail project in Central Asia. In this paper, a unified analytical framework is introduced and empirically validated for the first time, integrating Structural Equation Modelling (SEM) and Data Envelopment Analysis (DEA) to assess sustainability performance of Kazakhstan's rail freight sector, as opposed to previous studies, which examined either one of these dimensions separately or generic frameworks. To our knowledge, this is one of the first studies to carry out such a methodological synthesis in the context of a transitional economy, providing an instrument which is replicable for policymakers and infrastructure managers...

2 Literature review

In this section, the theoretical and empirical literature on the link between ESG factors and rail freight sustainability is summarized. It starts with the theoretical literature, continues with empirical evidence on the ESG performance and finally ends with the methods for sustainability assessment and the creation of analytical frameworks based on ESG principles. The section ends with the definition of the research gap addressed in this study.

2.1 Theoretical literature review

The theoretical basis is sustainable development theory, which focuses on economic development, social needs, and environmental conservation [15].

This balance is relevant to the rail systems with high externalities [16]. The Triple Bottom Line (TBL) is a relationship between the people, the planet and economic performance, forming an ESG-based index [17].

Stakeholder theory addresses workers, shippers, communities and regulators in relation to service quality and trust [18].

Planning stability has been shown to influence investment decisions by institutional theory and the resource-based view, which explain why safe, efficient assets contribute to competitiveness [19-20].

These theories support a model in which the relationships between the ESG indicators mediate freight performance and stability in Kazakhstan's rail market.

2.2 Empirical literature review

The empirical literature is reviewed in three subsections, each of which is relevant to one of the objectives of the study. In the first part, the evidence on the impact of ESG on rail freight performance and stability is discussed. In the second part, the current sustainability-assessment approaches and their efficacy are reviewed. In the third part, the empirical underpinnings for building an ESG-oriented analytical framework are examined.

2.2.1 Empirical evidence on how the ESG factors shape rail freight performance and stability (Objective 1)

A triple bottom line analysis [21] shows that environmental and social issues are influencing the efficiency of railways. The ESG related key performance indicator (KPI) based network reliability differences between countries were highlighted in the IRES report [22]. The polls revealed that the cargo density and environmental stress in Kazakhstan has increased [23], while results of Organisation for Economic Co-operation and Development (OECD) study suggest that governance effects the rail planning and funding

[24]. While in a number of studies was highlighted the rail performance in developed economies or individual ESG elements, ESG considerations influence the rail performance. The integrated environmental, social and governance implications of transitioning economies, such as Kazakhstan, are poorly researched. It is necessary to establish a broad ESG framework for the rail freight sector of Kazakhstan.:

H_1: Higher ESG performance in rail operations and infrastructure improves performance, competitiveness, and long-term stability of the rail freight market in Kazakhstan.

2.2.2 Empirical studies on the effectiveness of sustainability-assessment methods (Objective 2)

It is known that the multi-indicator techniques can assess the performance of the rail freight, but need sufficient data [25]. Composite index research has shown that the weights of indicators do influence scores [26] and a systematic evaluation for the built environment has been developed for application in the rail sector [27]. A review of Kazakhstan's policy has shown that sustainability assessment tools remain underdeveloped and that local experimentation is needed [28]. Kazakhstan is in need of an ESG approach, but it is not structured and does not have institutions. There are general approaches to sustainability assessment that do not take into account operational conditions in a particular sector. Few empirical evidence exist on Central Asian rail networks about their usefulness in data-limited settings and institutional capacity limitations. Current sustainability assessment frameworks are largely based in mature economies where there is good data provisioning and institutional resources. Transitional economies (like Kazakhstan) have specific issues such as difficulty in accessing data, a lack of historical data, or developing regulatory frameworks. This opens up a disconnection between the general sustainability tools and real-world requirements of infrastructure managers and policy makers in the region. This gap is addressed by developing a context-sensitive ESG framework that takes these data and institutional realities into account. So, Hypothesis 2 is formulated as:

H_2: The ESG-oriented methodology will show the empirical validity when applied to Kazakhstan's rail infrastructure, but will also reveal the measurable data and institutional limitations.

2.2.3 Empirical foundations for constructing an ESG-oriented analytical framework (Objective 3)

The global assessments promote use of rail sustainability tools [29]. Composite indicator trials aid multidimensional sustainability assessments [30]. A study conducted in Central Asia suggests an ESG hybrid approach using region-specific parameters to tackle the challenges posed by the large-scale railways environment and governance aspects [31]. Policy and financial changes are illustrated in Kazakhstan's ESG articles [32]. Some research focus was on specific ESG aspects, or did not measure the ESG indicators at the level of rail freight performance. There is no empirical-based, comprehensive ESG strategy for Kazakhstan's transitional economy that is provided by any of them. Indicators are recommended in studies for different sectors on environmental, social and governance. Hypothesis 3 is as follows:

H_3: An ESG-oriented analytical framework that integrates environmental, social, and governance indicators can be developed for Kazakhstan's rail network and will generate a meaningful sustainability index.

2.3 Research gap

Based on the literature search, gaps in the field are identified. In the transitional economy, studies of rail sustainability separate out the environmental, social and governance factors [21, 29]. Second, there is a wide variety of suggested ESG frameworks that have not been tested in Central Asian institutions [11, 31]. Thirdly, the quantitative assessments of the rail infrastructure in Kazakhstan focus on economic or technical aspects, without reflecting the integration of ESG [23, 28, 32]. There is no accepted way to measure and correlate ESG performance with market outcomes. To address this, an ESG framework specifically adapted to Kazakhstan's rail freight industry is proposed, introduced and implemented.

3 Materials and methods

In this section, the data sources, variables, and the methodology used to analyze the data are explained. It begins with the presentation of the data and variables utilized and then specifies the regression models. Then, estimation method is then explained, and descriptive statistics, correlation analysis, multiple regression analysis and Data Envelopment Analysis (DEA) are described.

3.1 Data and variables

The secondary data for the years 2018-2024 come from Kazakhstan Temir Zholy (KTZ), government statistics, International Union of Railways (UIC), OECD and expert surveys. January-March 2024 structured expert surveys collected primary data. Out of the 42

Table 1 *List of variables*

Variable	Symbol	Explanation	Primary Source
Rail Freight Performance	RFP	Measures operational efficiency (tonnage, punctuality, capacity use)	KTZ Operational Reports
Market Competitiveness	MC	Assesses the market share, pricing and intermodal competition	World Bank Logistics Performance Index (LPI); Market Reports
Long-Term Stability	LTS	Captures financial resilience, service reliability and regulatory support	Ministry Reports; KTZ Annual Finance
Energy Consumption	EC	Total energy used by rail freight (GWh/fuel equivalent)	Ministry of Energy; KTZ Sustainability Reports
Emissions	EM	CO_2 and pollutant emissions from operations	Ministry of Ecology Reports
Corridor Efficiency	CE	Transit time, throughput, infrastructure utilization	UIC Data; KTZ Network Performance
Workforce Safety	WS	Accident rates, safety protocol compliance	KTZ Safety Records; Expert Survey
Community Impact	CI	Noise, land use and local economic effects	Expert Survey: Regional Environmental Data
Service Quality	SQ	Customer satisfaction, timeliness and reliability	Expert and Shipper Survey
Investment Transparency	IT	Budget disclosure, reporting accountability	Expert Survey; Public Investment Reports
Regulatory Compliance	RC	Adherence to safety, environmental and operational standards	Regulatory Audits; Expert Survey
Strategic Planning	SP	Effectiveness of long-term planning and modernization	Expert Survey; Strategic Documents

invited experts, 83.3% (35) responded (KTZ managers n = 12, Ministry n = 8, logistics professionals n = 7, academics n = 5 and consultants n = 3). All replied to the question 7+ years of experience. Purposive sampling, which involves including the people who are relevant and have professional experience and institutional affiliation, was used for the selection of participants. Such a methodology allowed the survey to collect the informed opinion of stakeholders directly involved in the Kazakhstan rail freight sector, such as operational, regulatory and academic. The selection criteria included that they have a minimum of 7 years of professional experience within the rail industry to ensure reliability and depth of responses. Responses were anonymous 5-point Likert scale responses. Ethics approval and informed consent was obtained. There are 35 observations in total (5 train lines × 7 years). Most of the Perceptual ESG indicators from the 2024 expert survey were applied panel-wide, with the quantitative aspects playing a secondary role. All variables are given in Table 1.

3.2 Models of the study

Three multiple regression models were formulated to examine the relationship between the ESG variables and the rail freight outcomes. The effects of nine explanatory variables (EC, EM, CE, WS, CI, SQ, IT, RC, SP) on three dependent variables (RFP, MC, LTS) ere estimated. The equations are given below.

$$RFP_i = \alpha_0 + \alpha_1 EC_i + \alpha_2 EM_i + \alpha_3 CE_i + \\ + \alpha_4 WS_i + \alpha_5 CI_i + \alpha_6 SQ_i + \alpha_7 IT_i + \alpha_8 RC_i + \\ + \alpha_9 SP_i \ \epsilon_I, \quad (1)$$

$$MC_i = \alpha_0 + \alpha_1 EC_i + \alpha_2 EM_i + \alpha_3 CE_i + \\ + \alpha_4 WS_i + \alpha_5 CI_i + \alpha_6 SQ_i + \alpha_7 IT_i + \alpha_8 RC_i + \\ + \alpha_9 SP_i \ \gamma_I, \quad (2)$$

$$RFP_i = \alpha_0 + \alpha_1 EC_i + \alpha_2 EM_i + \alpha_3 CE_i + \\ + \alpha_4 WS_i + \alpha_5 CI_i + \alpha_6 SQ_i + \alpha_7 IT_i + \alpha_8 RC_i + \\ + \alpha_9 SP_i \ \mu_I, \quad (3)$$

where all the explanatory variables (EC, EM, CE, WS, CI, SQ, IT, RC, SP) and dependent variables (RFP, MC, LTS) are defined in Table 1; α_0 is the constant (intercept) term; α_1 through α_9 are the regression coefficients for each explanatory variable, respectively; and ε_i, γ_i, and μ_i are the error terms for Equations (1), (2), and (3), respectively.

3.3 Estimation strategy

Descriptive statistics was used to describe the trends in ESG and performance. Pearson correlation tests were used to evaluate if a linear relationship existed [33]. Multiple linear regression [34] was used to estimate the effects of ESG variables on competitiveness and stability. The underlying assumptions of linearity, homoscedasticity, normality of residuals and independence were tested and confirmed before

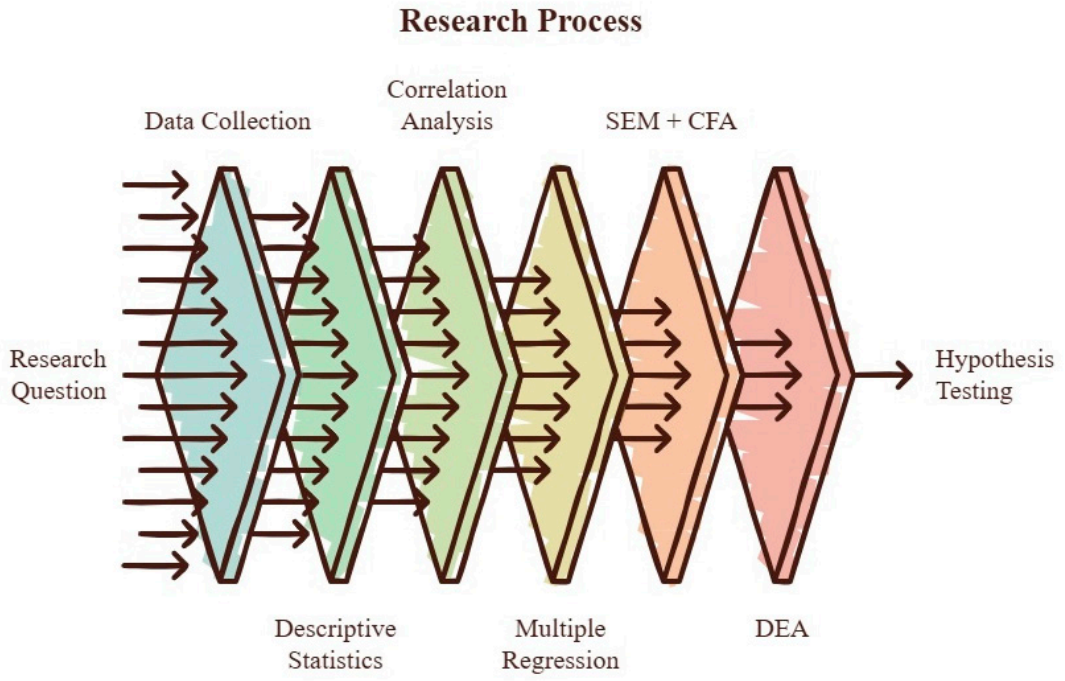


Figure 1 *Methodological framework of the study*

regression estimation.

To determine the relationship between the ESG dimensions and the sustainability outcomes, the Structural Equation Modelling (SEM) was used to examine the complex causal relationships between them [35]. The covariance-based SEM (CB-SEM) with maximum likelihood was selected because the model is parsimonious and the fit indices - the Comparative Fit Index (CFI), the Root Mean Square Error of Approximation (RMSEA) and the Standardized Root Mean Square Residual (SRMR) - enable a comprehensive evaluation of the model fit [35] although partial least squares SEM (PLS-SEM) is recommended for small samples. Based on simulation study [36], CB-SEM with maximum likelihood can perform adequately with sample sizes as small as 30 when the model is just-identified, the indicators are normally distributed, and the factor structure is clear. The latent construct of "ESG" was conceptualized as the second-order reflective construct composed of three dimensions: environmental (EC, EM), social (WS, CI, SQ), and governance (IT, RC, SP). The quality of the Measurement model was estimated by using Confirmatory Factor Analysis (CFA) with the following fit indices: CFI, RMSEA, and SRMR. Acceptable model fit was defined as CFI ≥ 0.90, RMSEA ≤ 0.08, and SRMR ≤ 0.08 [35]

The relative efficiency of the rail corridors to transform the ESG inputs to operational outputs was measured using DEA [37]. Through the sensitivity analysis, the most significant ESG variables that affect the outcomes are identified and taken into consideration for strategic prioritization [38] These methods for testing the hypothesis are shown in Figure 1.

All the indicators in the ESG composite index were normalized using the min-max scaling to ensure comparability of different scales of measurement. All indicators within each ESG dimension (environmental, social, and governance) were given equal weight and the three ESG dimensions were equally weighted (1/3 each) to create the overall ESG composite score. The method was selected for its interpretability and transparency, and, as in infrastructure research, similar composite indices for ESG.

4 Results

The findings of the research are obtained through a series of quantitative analyses aimed at testing the three hypotheses developed at the beginning of the research.

The first step is the descriptive statistics, which should provide a picture of the data, followed by correlation analysis, which should show how strong and in which direction the relations between variables are.

The effects of the ESG-related factors on rail freight performance, market competitiveness, and long-term stability were tested using multiple regression analysis.

Lastly, the effectiveness of the ESG-oriented methodology and the sustainability efficiency of rail corridors were evaluated using structural equation modelling (SEM) and Data Envelopment Analysis (DEA), respectively (Table 2).

As can be seen from the descriptive statistics presented in Table 2, the average of the state indicators of the rail freight performance (RFP = 78.42) and

Table 2 *Descriptive statistics of rail freight market variables*

Variable	Mean	Standard Deviation	Min	Max
RFP	78.42	12.36	55.1	98.4
MC	65.21	10.54	42.3	85
LTS	71.35	11.12	50.5	90.2
EC	320.15	45.67	250	420.5
EM	45.22	8.34	30.1	60.5
CE	82.1	9.21	65	95.3
WS	91.05	5.34	80	98
CI	68.2	7.89	55	82
SQ	74.5	6.72	60.5	88.3
IT	65.75	8.21	50	78.5
RC	78.9	7.12	62	90.2
SP	72.4	7.85	58	86

Note: N = 35 (5 rail corridors × 7 years, 2018-2024)

Table 3 *Correlation matrix for ESG variables and rail freight outcomes*

Variable	RFP	MC	LTS	EC	EM	CE	WS	CI	SQ	IT	RC	SP	VIF
RFP	1	0.72	0.65	-0.4	-0.5	0.61	0.58	0.41	0.69	0.6	0.63	0.62	-
MC	0.72	1	0.68	-0.4	-0.5	0.57	0.55	0.38	0.65	0.58	0.6	0.59	-
LTS	0.65	0.68	1	-0.4	-0.4	0.53	0.5	0.35	0.62	0.55	0.57	0.56	-
EC	-0.4	-0.4	-0.4	1	0.79	-0.4	-0.3	-0.3	-0.4	-0.3	-0.3	-0.3	2.85
EM	-0.5	-0.5	-0.4	0.79	1	-0.4	-0.3	-0.3	-0.4	-0.4	-0.3	-0.4	2.78
CE	0.61	0.57	0.53	-0.4	-0.4	1	0.5	0.4	0.6	0.5	0.5	0.5	1.85
WS	0.58	0.55	0.5	-0.3	-0.3	0.5	1	0.4	0.6	0.5	0.5	0.5	1.72
CI	0.41	0.38	0.35	-0.3	-0.3	0.4	0.4	1	0.4	0.3	0.3	0.3	1.42
SQ	0.69	0.65	0.62	-0.4	-0.4	0.6	0.6	0.4	1	0.5	0.6	0.5	2.1
IT	0.6	0.58	0.55	-0.3	-0.4	0.5	0.5	0.3	0.5	1	0.5	0.5	1.68
RC	0.63	0.6	0.57	-0.3	-0.3	0.5	0.5	0.3	0.6	0.5	1	0.5	1.55
SP	0.62	0.59	0.56	-0.3	-0.4	0.5	0.5	0.3	0.5	0.5	0.5	1	1.6

corridor efficiency (CE = 82.10) are relatively high, which indicates the high operational performance of Kazakhstan's rail corridors. Workforce safety (WS = 91.05) has the highest mean and the lowest standard deviation (5.34), thus showing consistently good safety practices. The range of energy consumption (EC = 320.15) is quite large (250.00 - 420.50), indicating that there is a significant variability in energy intensity in corridors. The governance dimensions with moderate are strategic planning (SP = 72.40) and investment transparency (IT = 65.75).

Table 3 indicates that the ESG factors are significantly positively correlated with rail freight performances, particularly with RFP, MC and LTS. The negative correlations with EC and EM confirm the better performance as the less energy consumed and the less emissions produced, which is consistent with previous studies on sustainable railway transport [39]. Variance Inflation Factor (VIF) values were calculated to see if there was multicollinearity among the explanatory variables and were included in Table 3. All the VIF values are below 5.0, which is the accepted value and are far less than the maximum value of 5.0. The highest VIF value is for the EC (VIF = 2.85) and EM (VIF = 2.78) which is logical, however, both values are within acceptable limits, which means that multicollinearity does not unduly affect the regression estimates [39].

The results in Table 4 clearly indicate that the rail freight has a significant impact on ESG factors and how they affect its performance, competitiveness and long term stability. The models exhibit strong explanatory power (R^2 = 0.85 for RFP, 0.82 for MC, 0.84 for LTS), with adjusted R^2 values of 0.80, 0.76, and 0.78, respectively. The F-statistics (15.73, 12.65, and 14.58; $p < 0.05$) confirm the overall model significance at N=35, k=9. Corridor efficiency (CE) is the strongest positive driver (β = 0.421-0.395), followed by service quality (SQ; β = 0.355-0.370), while energy consumption (EC; β = -0.290 to -0.312) and emissions (EM; β = -0.255 to

Table 4 *Regression results*

Variables	RFP Coeff.	RFP SE	MC Coeff.	MC SE	LTS Coeff.	LTS SE
EC	-0.312***	0.056	-0.290***	0.059	-0.305***	0.057
EM	-0.275***	0.062	-0.255***	0.065	-0.268***	0.063
CE	0.421***	0.058	0.395***	0.061	0.408***	0.059
WS	0.312***	0.051	0.295***	0.054	0.308***	0.052
CI	0.178***	0.047	0.165***	0.05	0.172***	0.048
SQ	0.355***	0.052	0.370***	0.055	0.362***	0.053
IT	0.212***	0.049	0.225***	0.052	0.218***	0.05
RC	0.240***	0.051	0.228***	0.054	0.235***	0.052
SP	0.198***	0.048	0.188***	0.051	0.193***	0.049
Const.	10.500***	2.1	9.800***	2.21	11.200***	2.15
R^2	0.85		0.82		0.84	
Adj. R^2	0.8		0.76		0.78	
F	15.73*		12.65*		14.58*	

*Dependent variables: Rail Freight Performance (RFP), Market Competitiveness (MC), and Long-Term Stability (LTS). *** indicates statistical significance at the 1% level ($p < 0.01$). The adjusted R^2 and F-statistics reported are based on N = 35 observations and k = 9 predictors. All values have been verified for internal consistency.*

Table 5 *SEM results*

Path	Coefficient	Std. Error	t-Value	p-Value
ESG → RFP	0.652	0.041	15.90	0.000
ESG → MC	0.611	0.045	13.58	0.000
ESG → LTS	0.597	0.048	12.44	0.000

P-Value 0.0000 indicates 1% level of significance, Model Fit Indices: CFI = 0.92, RMSEA = 0.07, SRMR = 0.06.

Table 6 *DEA results for hypothesis 3: Sustainability efficiency of rail corridors*

Corridor	Efficiency Score (EFF)
North-South	0.91
East-West	0.87
Central	0.94
Western	0.88
Southern	0.90

-0.275) exhibit significant negative effects. Workforce safety (WS; β = 0.295-0.312) also positively affects. The results are consistent with previous studies on the implementation of ESG principles in railway transportation and are applied to the economy of Kazakhstan. These findings are consistent with studies, which showed that the integration of ESG is a crucial part of the sustainability of rail operations [39] and it has been expanded to the context of the transitional economy in Kazakhstan.

The data on the SEM is shown in Table 5. Before the estimation of the structural model, the measurement model was evaluated by CFA. The Fit indices were acceptable (CFI = 0.92, RMSEA = 0.07 and SRMR = 0.06; the acceptable threshold values are given in [35]). The results validate the latent ESG construct as a predictor of rail freight outcomes. The structural paths of the latent construct of ESG to RFP, MC and LTS were found to be statistically significant, thus proving the predictive validity of the ESG framework [40]. The assessment of the measurement model was performed by CFA. The reliability and validity of the scale were measured by all the factor loadings being greater than 0.70, the composite reliability (CR) values between 0.82 and 0.89, and the average variance extracted (AVE) values between 0.58 and 0.67, which demonstrated internal consistency and convergent validity . Fit indices (CFI = 0.92, RMSEA = 0.07, SRMR = 0.06) also corroborated the goodness of fit of the measurement model.

The DEA analysis given in Table 6 shows that implementing a holistic ESG framework to identify areas for enhancement is applicable, in line with related efficiency analyses of transport infrastructure [41]. Due to the small number of corridors analyzed, (N = 5), the DEA results for the corridors presented in

Table 6 should be interpreted with caution. DEA is a useful tool to determine relative efficiency differences between decision making units but the small number of units limits the generalizability of the results. The efficiency scores (between 0.87 and 0.94) are indicative, not definitive, of corridor performance. However, the variation observed between corridors is the first-level diagnostic tool that will help to identify the operational improvement areas, especially in the East-West (0.87) and Western (0.88) corridors, as compared to the Central corridor (0.94).

5 Discussions

In this study, an ESG-oriented model for the sustainability of rail freight in Kazakhstan was developed and tested.

From the perspective of Objective 1, the ESG variables are important factors to predict the rail freight performance, market competition, and long term stability. The most influential positive drivers were corridor efficiency (CE) and service quality (SQ); energy consumption (EC) and emissions (EM) had fairly regular overall negative impacts. This is in line with theoretical considerations that operational excellence enhances market position and environmental inefficiencies sabotage long-term sustainability [42]. The workforce safety (WS) plays a positive role in stakeholder theory, which strengthens the case for the performance benefits of investments in human capital and safety practices.

The dominance of CE as the strongest driver is especially important for Kazakhstan as a transit route on the way from China to Europe. The EC and EM highlight the conflict between the goals of economic growth and environmental protection, which is typical of resource-based economies with the ambition of becoming sustainable [28].

With respect to Objective 2, the mixed-method had a high level of empirical validity.

The SEM established that the internal consistency of the framework is a strong predictor of three market outcomes (RFP, MC, LTS) using a latent ESG construct. The DEA revealed quantifiable efficiency differences between corridors, enabling diagnosis of the operations' strengths and weaknesses.

Nevertheless, when it comes to social-governance indicators, the use of secondary data and expert surveys exposes institutional and data limitations assumed in H2, i.e., transparency and time-series limitations [43].

With regard to Objective 3, the efficiency scores (0.87 to 0.94) assigned to DEAs, along with other indicators, are a preliminary sustainability index. The results should also be interpreted with caution, however, because of the small number of corridors (N=5). This deviation is used to tentatively identify some corridors (East-West, Western) as less efficient, thus indicating the potential areas for intervening at the corridor level. The results of this study should be considered in an exploratory way and to be validated in light of the extension of the data set and alternative efficiency measurement methods.

Theoretically, one ESG framework (TBL, stakeholder, institutional and resource-based views) was successfully operationalized. In practice, a replicable evaluation tool is provided [41] that links ESG advocacy to quantifiable infrastructure management [44].

Infrastructure and safety studies, conducted over the past few years also contribute to the practical application of energy saving related assessment in railway operations, such as railway traffic safety approaches [45-46] and energy saving approaches for dynamic performance of traction rolling stock [47], railway section integrity through georadar techniques and sustainable designs of railway infrastructures [48] and optimization of logistics [49] which supports the methodological and operational basis of the ESG approach proposed in this paper.

6 Conclusions

In this paper, the ESG framework designed and tested for the sustainability assessment of Kazakhstan's rail freight was used. The findings validate the use of the ESG indicators as effective predictors of the rail freight performance and competitiveness as well as its long-term stability. The most positive correlations were with efficiency in the corridor and the quality of service provided, whereas the most negative correlations were with energy consumption and emissions. The DEA results indicated differences in the efficiency scores by corridors, indicating that corridors should be focused for improvement: East-West and Western.

The resulting policy recommendations are: Promotion of energy efficient technologies and emissions control equipment in poorly performing corridors, better service quality and staff safety in the corridors, and greater transparency in governance through increased disclosure of investments and regulatory compliance. The framework has been tested using a repeatable and evidence-based tool that allows operators and policymakers to measure the ESG performance and make strategic investments, which proves the significance of integration of ESG in the competitiveness of Kazakhstan's rail freight market [50-51].

There are several limitations to the study. The social-governance variables are subject to interpretation since they have been based on the secondary data and expert surveys. The data in the cross-section do not allow for causal inference. The study focuses on main Kazakhstan roads, so there may be limitations to transferability to other contexts in the region without adaptations. Due to data constraints, some constructs were measured with proxy measures.

The future research needs to use panel and longitudinal datasets to strengthen causal arguments, validate results in other transitional economies, use spatial analysis and/or life-cycle analysis for environmental assessment, and create qualitative case studies to explain quantitative scores, and the institutional and managerial factors that drive them. Additionally, while the sample size of N=35 was justified for the parsimonious CB-SEM model employed [36], the application of SEM to small samples remains a methodological consideration. The ”N=30” threshold cited in the literature applies to simple, single-factor models with high factor loadings (~0.80), whereas the present model is more complex, involving the second-order construct with three dimensions and three simultaneous structural paths. Future research with larger samples would further strengthen the robustness of the findings.

Acknowledgements

The authors received no financial support for the research, authorship and/or publication of this article.

Conflicts of interest

The authors declare that they have no known competing financial interests or personal relationships that could have appeared to influence the work reported in this paper.

References

[1] RAHMAN, S. M. Human resource management in the transport sector: a systematic literature review of strategic approaches and sectoral impacts. *American Journal of Interdisciplinary Studies* [online]. 2025, **6**(1), p. 1-39. ISSN 3067-5146. Available from: https://doi.org/10.63125/c625ef08

[2] WANG, J., ZHANG, Y., YANG, X., FANG, R., ZHANG, J., BOBYLEV, N., LI, J., LI, S. Impact of environmental and operational stress on defect formation in China’s high-speed rail subgrades. *Communications Earth and Environment* [online]. 2025, **6**(1), 310. eISSN 2662-4435. Available from: https://doi.org/10.1038/s43247-025-02287-0

[3] CHOUDHARY, S., SINGH, D., KUMAR, M. Assessment of infrastructure and service supply on sustainable urban transport systems in Delhi-NCR: implications of last-mile connectivity for government policies. *Future Transportation* [online]. 2025, **5**(4), 134. eISSN 2673-7590. Available from: https://doi.org/10.3390/futuretransp5040134

[4] CLEMENTS, R., SEARLE, G., ALIZADEH, T. Epistemic silences in settler-colonial infrastructure governance literature. *Geographical Research* [online]. 2025, **63**(2), p. 221-235. ISSN 1745-5863, eISSN 1745-5871. Available from: https://doi.org/10.1111/1745-5871.12601

[5] DA FONSECA-SOARES, D., ELIZIARIO, S. A., GALVINCIO, J. D., RAMOS-RIDAO, A. F. Greenhouse gas emissions in railways: systematic review of research progress. *Buildings* [online]. 2024, **14**(2), 539. eISSN 2075-5309. Available from: https://doi.org/10.3390/buildings14020539

[6] HANDOYO, S., ANAS, S. The effect of environmental, social, and governance (ESG) on firm performance: the moderating role of country regulatory quality and government effectiveness in ASEAN. *Cogent Business and Management* [online]. 2024, **11**(1), 2371071. eISSN 2331-1975. Available from: https://doi.org/10.1080/23311975.2024.2371071

[7] KUANALIYEV, A. AI regulation for sustainable business: legal challenges in Eastern and Central Asian emerging economies. *Law, Business and Sustainability Herald* [online]. 2025, **5**(1), p. 4-24. ISSN 2787-9356. Available from: https://www.lbsherald.org/index.php/journal/article/download/73/66

[8] CHEN, S., CHI, X., ZHANG, Q., TANG, Y., LIU, Z., TAN, W. Cascading reliability assessment of international railway freight network based on coupled map lattices: a case study of China railway express. *Journal of Advanced Transportation* [online]. 2024, **2024**(1), 1436605. eISSN 2042-3195. Available from: https://doi.org/10.1155/2024/1436605

[9] IZTELEUOVA, M., ARIMBEKOVA, P., MURZABEKOVA, K., ALIK, A. Features of development and efficiency of transport logistics infrastructure. *Acta Commercii* [online]. 2024, **24**(1), p. 1-11. ISSN 2413-1903, eISSN 1684-1999. Available from: https://doi.org/10.4102/ac.v24i1.1235

[10] HUSSAIN, O. A., MOEHLER, R. C., WALSH, S. D., AHIAGA-DAGBUI, D. D. Minimizing cost overrun in rail projects through 5D-BIM: a conceptual governance framework. *Buildings* [online]. 2024, **14**(2), 478. eISSN 2075-5309. Available from: https://doi.org/10.3390/buildings14020478

[11] ROSSI, C., BYRNE, J. G., CHRISTIAEN, C. Breaking the ESG rating divergence: an open geospatial framework for environmental scores. *Journal of Environmental Management* [online]. 2024, **349**, 119477. eISSN 1095-8630. Available from: https://doi.org/10.1016/j.jenvman.2023.119477

[12] ZHU, R., TAN, K., XIN, X. Speed up for sustainable development: high-speed rail and corporate ESG performance. *Energy Economics* [online]. 2024, **138**, 107821. ISSN 0140-9883, eISSN 1873-6181. Available from: https://doi.org/10.1016/j.eneco.2024.107821

[13] TRUANT, E., BORLATTO, E., CROCCO, E., SAHORE, N. Environmental, social and governance issues in supply chains: a systematic review for strategic performance. *Journal of Cleaner Production* [online]. 2024, **434**, 140024. ISSN 0959-6526, eISSN 1879-1786. Available from: https://doi.org/10.1016/j.jclepro.2023.140024

[14] MOHSENI, S., VAN HASSEL, E., VANELSLANDER, T. Assessing the impact on mode competitiveness of improvements of the Trans-Eurasian railway network. *Journal of Shipping and Trade* [online]. 2025, **10**(1), 3. eISSN 2364-4575. Available from: https://doi.org/10.1186/s41072-025-00193-4

[15] GANDHI, N., KANT, R., THAKKAR, J. J., SHANKAR, R. Prioritizing solutions to mitigate the risks due to adoption of intermodal railroad freight transportation for achieving sustainable development goals. *Journal of Cleaner Production* [online]. 2024, **435**, 140535. ISSN 0959-6526, eISSN 1879-1786. Available from: https://doi.org/10.1016/j.jclepro.2023.140535

[16] DJORDJEVIC, B., STAHLBERG, A., KRMAC, E., MANE, A. S., KORDNEJAD, B. Efficient use of European rail freight corridors: current status and potential enablers. *Transportation Planning and Technology* [online]. 2024, **47**(1), p. 62-88. ISSN 0308-1060, eISSN 1029-0354. Available from: https://doi.org/10.1080/03081060.2023.2294344

[17] YU, L., XU, J., YUAN, X. Sustainable digital shifts in Chinese transport and logistics: exploring green innovations and their ESG implications. *Sustainability* [online]. 2024, **16**(5), 1877. eISSN 2071-1050. Available from: https://doi.org/10.3390/su16051877

[18] HO, A., GIANNOPOULOS, D., PILORGE, H., PSARRAS, P. Opportunities for rail in the transport of carbon dioxide in the United States. *Frontiers in Energy Research* [online]. 2024, **11**, 1343085. eISSN 2296-598X. Available from: https://doi.org/10.3389/fenrg.2023.1343085

[19] AROSO, A., BUGARIN, M. R. Energy efficiency improvement on railway lines: an overview. *Energy Science and Engineering* [online]. 2024, **12**(12), p. 5753-5764. ISSN 2050-0505, eISSN 2050-0505. Available from: https://doi.org/10.1002/ese3.1971

[20] GENIN, A. L., TAN, J., SONG, J. State governance and technological innovation in emerging economies: state-owned enterprise restructuration and institutional logic dissonance in China's high-speed train sector. *Journal of International Business Studies* [online]. 2021, **52**(4), p. 621-645. ISSN 0047-2506, eISSN 1478-6990. Available from: https://doi.org/10.1057/s41267-020-00342-w

[21] KUMAR, A., R, A. An MCDM framework for assessment of social sustainability indicators of the freight transport industry under uncertainty: a multi-company perspective. *Journal of Enterprise Information Management* [online]. 2020, **33**(5), p. 1023-1058. ISSN 1741-0398, eISSN 1758-7409. Available from: https://doi.org/10.1108/JEIM-09-2019-0272

[22] PAN, J. Y. Understanding high-speed rail users in the US - environmental and sustainability perspectives. *Travel Behaviour and Society* [online]. 2024, **34**, 100670. ISSN 2214-367X, eISSN 2214-3688. Available from: https://doi.org/10.1016/j.tbs.2023.100670

[23] SULTANBEK, M., ADILOVA, N., SLADKOWSKI, A., KARIBAYEV, A. Forecasting the demand for railway freight transportation in Kazakhstan: a case study. *Transportation Research Interdisciplinary Perspectives* [online]. 2024, **23**, 101028. eISSN 2590-1982. Available from: https://doi.org/10.1016/j.trip.2024.101028

[24] KNOX, C., ORAZGALIYEV, S. Public administration country study: Kazakhstan - post-Soviet legacy, modernisation, and hybridity. *Public Administration Review* [online]. 2025, **85**(6), p. 1888-1900. ISSN 0033-3352, eISSN 1540-6210. Available from: https://doi.org/10.1111/puar.70030

[25] ZENG, J., GUO, S., ZENG, J., JIN, K. Deep learning based method for early warning of price risk in railroad bulk freight transport with consideration of time series of comprehensive impact index. *Transportation Research Record: Journal of the Transportation Research Board* [online]. 2024, **2678**(7), p. 434-449. ISSN 0361-1981, eISSN 2169-4052. Available from: https://doi.org/10.1177/03611981231207842

[26] KALEM, A., TADIC, S., KRSTIC, M., CABRIC, N., BRANKOVIC, N. Performance evaluation of railway infrastructure managers: a novel hybrid fuzzy MCDM model. *Mathematics* [online]. 2024, **12**(10), 1590. eISSN 2227-7390. Available from: https://doi.org/10.3390/math12101590

[27] SAKR, A. M., ELMASRY, H., BIRHANE, F., EL-BASYOUNY, K. Assessing the built environment of light rail transit stations to encourage active transportation: a multi-criteria GIS-based analysis. *Transactions in GIS* [online]. 2025, **29**(4), e70082. ISSN 1361-1682, eISSN 1467-9671. Available from: https://doi.org/10.1111/tgis.70082

[28] RAKHYMZHAN, G., DABYLTAYEVA, N. E., SAKHANOVA, G., RUZIYEVA, E. A., BEKMUKHAMETOVA, A. B. Navigating Kazakhstan's sustainable economic future: a study of tech innovation, infrastructure, and resource management. *Economies* [online]. 2024, **12**(5), 104. eISSN 2227-7099. Available from: https://doi.org/10.3390/economies12050104

[29] CORAZZA, M. V. A comprehensive research agenda for integrating ecological principles into the transportation sector. *Sustainability* [online]. 2024, **16**(16), 7081. eISSN 2071-1050. Available from: https://doi.org/10.3390/su16167081

[30] HAN, F., LIU, Z., WANG, C., WEI, H., WANG, B. Research on optimization method of railway construction scheme based on multidimensional combination weighting and improved grey theory. *Scientific Reports* [online]. 2024, **14**(1), 3023. eISSN 2045-2322. Available from: https://doi.org/10.1038/s41598-023-50098-0

[31] HE, Y., LIU, X., SUN, E., WU, D. Balancing economic growth and environmental conservation through the optimization of rail transit routes for sustainable development. *Scientific Reports* [online]. 2024, **14**(1), 31926. eISSN 2045-2322. Available from: https://doi.org/10.1038/s41598-024-83462-9

[32] NURGALIYEVA, K. Evaluating the impact of ESG on regional development in Kazakhstan: empirical analysis. *Eurasian Journal of Economic and Business Studies* [online]. 2025, **69**(1), p. 5-17. ISSN 2789-8253, eISSN 2789-8261. Available from: https://doi.org/10.47703/ejebs.v69i1.459

[33] FIELD, A. *Discovering statistics using IBM SPSS statistics*. 6. ed. London: SAGE Publications, 2024. ISBN 9781529668704.

[34] MONTGOMERY, D. C., PECK, E. A., VINING, G. G. *Introduction to linear regression analysis*. 4. ed. Hoboken: John Wiley and Sons, 2021. ISBN 978-0470125069.

[35] HAIR, J. F., RINGLE, C. M., SARSTEDT, M. PLS-SEM: indeed a silver bullet. *Journal of Marketing Theory and Practice* [online]. 2011, **19**(2), p. 139-152. ISSN 1069-6679, eISSN 1944-7175. Available from: https://doi.org/10.2753/MTP1069-6679190202

[36] WOLF, E. J., HARRINGTON, K. M., CLARK, S. L., MILLER, M. W. Sample size requirements for structural equation models: an evaluation of power, bias, and solution propriety. *Educational and Psychological Measurement* [online]. 2013, **73**(6), p. 913-934. ISSN 0013-1644, eISSN 1552-3888. Available from: https://doi.org/10.1177/0013164413495237

[37] COOPER, W. W., SEIFORD, L. M., TONE, K. *Data envelopment analysis: a comprehensive text with models, applications, references and DEA-solver software* [online]. 2. ed. New York: Springer, 2007. eISBN 978-0-306-47541-2. Available from: https://doi.org/10.1007/b109347

[38] SALTELI, A., RATTO, M., ANDRES, T., CAMPOLONGO, F., CARIBONI, J., GATELLI, D., SAISANA, M., TARANTOLA, S. *Global sensitivity analysis: the primer* [online]. Chichester: John Wiley and Sons, 2008. ISBN 9780470059975, eISBN 9780470725184. Available from: https://doi.org/10.1002/9780470725184

[39] REIS, B. L., PUGLIERI, F. N., PIEKARSKI, C. M. A roadmap approach to enhancing ESG and operational performance in road freight logistics. *Logistics* [online]. 2026, **10**(4), 71. eISSN 2305-6290. Available from: https://doi.org/10.3390/logistics10040071

[40] BALDI, F., LAMBERTIDES, N. Exploring the role of ESG for the performance and risks of infrastructure investing: evidence from the international funds' market. *Managerial Finance* [online]. 2024, **50**(1), p. 92-117. ISSN 0307-4358, eISSN 1758-7743. Available from: https://doi.org/10.1108/MF-01-2023-0024

[41] CHEN, Y., KISSELYOVA, O., ABZHAPBAROVA, A., ALIAKBARKYZY, D., KARSYBAYEV, Y. Comparing intermodal and synchromodal transport systems to enhance efficiency and sustainability at the Port of Aktau, Kazakhstan. *International Journal of Transport Development and Integration* [online]. 2025, **9**(2). ISSN 2058-8305, eISSN 2058-8313. Available from: https://doi.org/10.18280/ijtdi.090201

[42] MEESIT, R. Factors affecting the future utilisation of high-speed train services in Eastern Economic Corridor (EEC). *Transportation Research Interdisciplinary Perspectives* [online]. 2024, **26**, 101162. eISSN 2590-1982. Available from: https://doi.org/10.1016/j.trip.2024.101162

[43] MOHAMMAD AL EBBINI, M., FARHAN ALSHIRAH, A., HANNA ZAWAI DEH, F., SALEH ENAIZAN BATAYNEH, M., ALQUDAH, H. Modelling the impact of ESG orientation on business continuity through IS audit effectiveness: evidence from financial institutions using SPSS-PLS. *EDPACS* [online]. 2025, latest articles. ISSN 0736-6981, eISSN 1936-1009. Available from: https://doi.org/10.1080/07366981.2025.2576312

[44] KISSELYOVA, O., IZBAIROVA, A., ALTAYEVA, Z., KULMAGAMBETOVA, Z. Ensuring secure transport infrastructure in supply chains. *E3S Web of Conferences* [online]. 2025, **640**, 02002. eISSN 2267-1242. Available from: https://doi.org/10.1051/e3sconf/202564002002

[45] ORALBEKOVA, Z., TYULEPBERDINOVA, G., GAZIZ, G., ADAMOVA, A., SHOLPANBAEV, B. Results of experimental georadar surveys of railway sections. *International Journal of GEOMATE* [online]. 2023, **25**(109), p. 189-196. ISSN 2186-2982, eISSN 2186-2990. Available from: https://doi.org/10.21660/2023.109.m2320

[46] BOGDANOVICH, S., KISELEVA, O., KOSENKO, S., KABANOV, A. A systematic approach to ensuring traffic safety of railway transport. In: International Scientific Siberian Transport Forum: proceedings [online]. Springer. 2022. ISBN 978-3-030-96382-8, eISBN 978-3-030-96383-5, p. 170-179. Available from: https://doi.org/10.1007/978-3-030-96383-5_19

[47] MUSAYEV, J., ZHAUYT, A., ISMAGULOVA, S., YUSSUPOVA, S. Theory and practice of determining the dynamic performance of traction rolling stock. *Applied Sciences* [online]. 2023, **13**(22), 12455. eISSN 2076-3417. Available from: https://doi.org/10.3390/app132212455

[48] YANG, Y., ORR, J., SPADEA, S. Shear behavior of variable-depth concrete beams with wound fiber-reinforced polymer shear reinforcement. *Journal of Composites for Construction* [online]. 2018, **22**(6), 04018058. ISSN 1090-0268, eISSN 1943-5614. Available from: https://doi.org/10.1061/(asce)cc.1943-5614.0000899

[49] MULIAREVYCH, O. The serverless computing for acceptance and shipping warehouse zones optimization. *CEUR Workshop Proceedings* [online]. 2023, **3384**, p. 87-97. ISSN 1613-0073. Available from: https://ceur-ws.org/Vol-3384/Paper_8.pdf

[50] NAMOZOV, J., ARABOV, N., ADURAMANOV, X., NASIMOV, D., MAKHMUDOVA, M., IBRAGIMOV, L. Dynamics of transformation and economic resilience in agricultural lands: An anthropogenic perspective. *E3S Web of Conferences* [online]. 2024, **541**, 03003. eISSN 2267-1242. Available from: https://doi.org/10.1051/e3sconf/202454103003

[51] ARABOV, N., NASIMOV, D., ABDURAMANOV, X., UTEMURATOVA, G., LUTFULLO, I. Addressing the economic impacts of climate change in Uzbekistan: challenges and strategies. *E3S Web of Conferences* [online]. 2024, **542**, 04006. eISSN 2267-1242. Available from: https://doi.org/10.1051/e3sconf/202454204006

This is an open access article distributed under the terms of the Creative Commons Attribution 4.0 International License (CC BY 4.0), which permits use, distribution, and reproduction in any medium, provided the original publication is properly cited. No use, distribution or reproduction is permitted which does not comply with these terms.

MODELLING AND OPTIMIZATION OF HYDROGEN FUEL SYSTEMS IN RAILWAY VEHICLES USING DATA ANALYSIS AND MACHINE LEARNING

Oleksandra Shepel[1], Ján Dižo[2,*], Miroslav Blatnický[2], Martin Bučko[2]

[1]Independent researcher, Vilnius, Lithuania
[2]University of Zilina, Faculty of Mechanical Engineering, Department of Trasport and Handling Machines, Zilina, Slovakia

*E-mail of corresponding author: jan.dizo@fstroj.uniza.sk

Ján Dizo 0000-0001-9433-392X,
Miroslav Blatnický 0000-0003-3936-7507,
Martin Bučko 0009-0006-0566-4430

Resume

Hydrogen fuel cell systems offer a zero-emission alternative to diesel-powered trains, combining high energy density with the potential for renewable energy integration. A hybrid data-driven modelling and optimization approach of improving the efficiency, reliability, and cost-effectiveness of hydrogen fuel systems for rail applications is developed in this research. Using operational and thermodynamic data from simulated and experimental sources, a predictive model of fuel cell performance based on non-linear regression and machine learning methods was developed. Results indicate that the data-driven model predicts system efficiency with a mean absolute error (MAE) of 1.9%, while the optimization framework reduces fuel consumption by up to 12.4% compared to reference operation strategies. The study proves the value of machine learning in optimizing hydrogen energy systems.

Article info

Received 12 May 2026
Accepted 7 July 2026
Online 20 August 2026

Keywords:

hydrogen railway transport
environmental optimization
machine learning
fuel cell system
sustainability

Available online: https://doi.org/10.26552/com.C.2026.045

ISSN 1335-4205 (print version)
ISSN 2585-7878 (online version)

1 Introduction

The railway transport remains among the most energy-efficient modes of terrestrial mobility. It is supposed to be the most effective and economical mode for transport of goods and it is also favorite mode of transport of passengers in many countries. It is a quite fast, comfortable and reliable transportation system, which allows movement of people for shorter (urban railway transport) to long distances [1-2]. The huge amount of goods is transported by freight railway wagons [3-4]. There are many types of freight railway wagons, which are intended to transport various types of goods [5-7]. Similarly, passengers are transported by various kind of railway vehicle, such as passenger wagons, trams, metro vehicles and others [8].

Due to relative purity of produced gas emissions mainly on electrified railway lines, it is also supposed to be one of the most environmentally friendly modes of transport [9-12]. The European continent is one of the leading regions, where the efforts and emphasis is placed on massive reduction of gas emission production by transport means [13-16].

It is necessary to ensure reliable and sufficient sources of energy to power rail vehicles. This energy is obtained by thermal conversion of fuel in internal combustion engines in the case of railway vehicles for railway lines with an independent traction system. It is considered an older traction system. Electrified railway lines have a dependent traction system, which requires a suitable infrastructure and this kind of traction is supposed to be more environmentally friendly kind of traction system [17]. In this case, trains are towed by electric locomotives powered by electric traction system equipped with modern electric motors of a high efficiency [18-20]. Although the older option still dominates the modern transport system, considerable efforts are being made to find the new, innovative and environmentally friendly energy sources as a source of



a)



b)

Figure 1 *a) A multiple unit by Alstom equipped by hydrogen fuel powertrain known as Coradia iLint, b) an illustration of a layout of the components of the hydrogen powertrain on a vehicle roof [39]*

energy for rail vehicles [21-22]. The chemical energy, which is contained in fuels with a carbon base, such as oil, is converted during the combustion process into mechanical work. Carbon dioxide (CO_2) as an associated result and the direct consequence of the combustion process is released into the air [23-24]. Therefore, continuous development of railway vehicles is aimed at the reduction of the proportion of pollutants emitted into the air. Moreover, this phenomenon is connected not only with actual operation, but with the production, distribution and storage of used fuel, as well. As a possible and perspective alternative to hydrocarbon fuels, alternative fuels, as well as power plants are currently being developed and introduced in railway vehicles in large quantities [25-26]. It is mainly in a form of electromobility, hydrogen fuel cells and other methods.

Railway transport is recently one of the most dominant sector, where the electric energy is used and consumed for powering railway vehicles. Although electrification of railway lines seems to be the most effective way to reduce a production of harmful exhaust gases, full electrification of all railway lines is not possible. Therefore, a substantial share of the world's rail lines remains non-electrified, leading to persistent reliance on diesel traction. Additionally, electrification of railway lines can be too costly and even unprofitable [27-28]. Therefore, there are rather efforts to find innovative and at the same time suitable technical solutions of sources of energy for railway vehicles with an independent traction system [29]. One of the possible options is to apply hydrogen fuel systems to the railway vehicles design as a source of energy [30-32]. In such a case, electricity is produced from hydrogen. The main advantage of this technical solution is practically zero exhaust emissions, which are released into the air during the operation of railway vehicles [33-37].

Hydrogen fuel cell technology offers a sustainable alternative [38-39] capable of providing the high power density and long range without direct emissions of CO_2 or NO_x. Several demonstration projects, such as Alstom's Coradia iLint in Germany and HydroFLEX in the UK, have established the technical viability of hydrogen-powered rail systems. As it is known, the Alstom Coradia iLint multiple-unit was the first railway vehicle, which was equipped by hydrogen fuel-cells and presented at the International railway exhibition Innotrans in 2016. It is shown in Figure 1.

Besides that, other important manufacturers of railway vehicles, such as Siemens within the project Mireo Plus H [40], shown in Figure 2, Alstom with Eversholt Rail with the model Project Breeze and also Stadler and its model Flirt H2 [41] (Figure 3), consider application of hydrogen powertrains with fuel-cells.

A Slovak producer ZOS Vrutky, Inc. [42] also tried to reflect current trends in the field of alternative fuels for a multiple unit 862 class. It is a railway vehicle with independent traction systems, and it is shown in Figure 4. They proposed to replace an original diesel traction powertrain by a powertrain including hydrogen fuel cells.

An example of a layout of components in a multiple



Figure 2 *An illustration of multiple units Mireo Plus H produced by the Siemens company [40]*



Figure 3 *An illustration of the multiple unit by Stadler known as Flirt H2 [41]*



Figure 4 *The multiple unit 861 class produced by the ZOS company originally powered by diesel powertrain [42]*

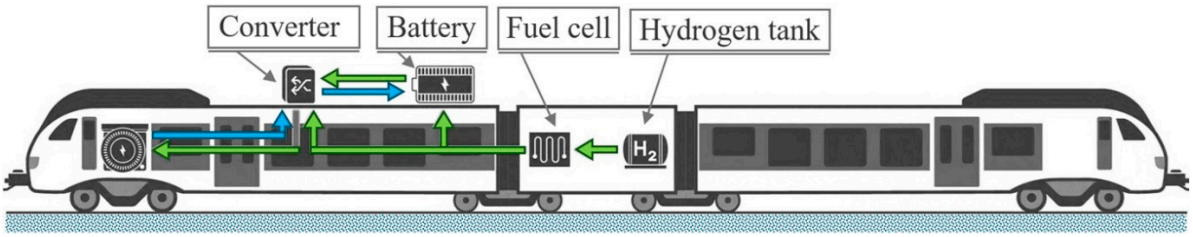


Figure 5 *A layout of hydrogen powertrain components in the Stadler Flirt H2 [41]*

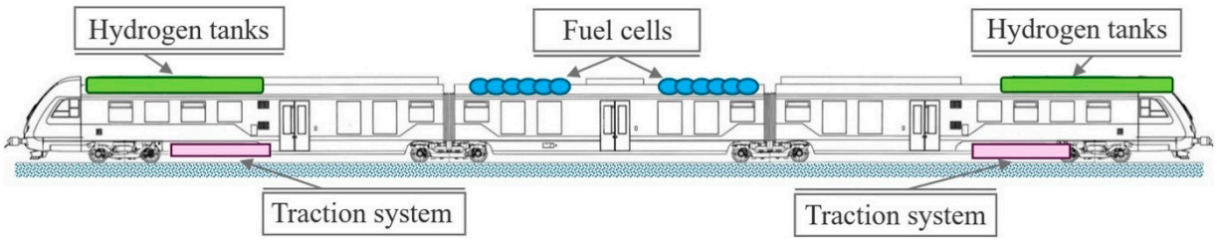


Figure 6 *A layout of hydrogen powertrain components in the multiple unit 861 class multi [42]*

unit powered by hydrogen fuel cells is illustrated in Figure 5 on an example of the Stadler Flirt H2 vehicle and a proposed layout of components of the hydrogen powertrain installed in the ZOS multiple unit 861 class is depicted in Figure 6. As it can be seen, the vehicle by Stadler, as well as the vehicle by the ZOS, include components, which need to implement hydrogen fuel cells as a source of power.

Nevertheless, optimizing system efficiency and lifetime under real-world conditions remains a major challenge.

Machine learning has emerged as a transformative tool for modelling the complex, non-linear processes in energy systems [43-44]. The application of machine learning to hydrogen fuel cell systems in the rail transport can aid in both system design and operational optimization, leveraging large datasets obtained from real-time monitoring. A systematic approach to modelling and optimizing hydrogen fuel systems for railway applications, integrating experimental data, thermodynamic modelling, and machine learning-based optimization is presented in this research. Moreover, a hybrid framework, combining a Proton Exchange Membrane Fuel Cell (PEMFC) performance predictor trained on a mixed simulated-experimental dataset, and a multi-objective genetic optimization strategy simultaneously minimizing hydrogen consumption and stack degradation under realistic hybrid train duty cycles in presented in this research. The proposed method yields route-relevant operating policies improving efficiency, while explicitly accounting for the long-term degradation risks compared to the conventional single-objective or purely physics-based approaches.

2 Background and related work

Hydrogen fuel cells convert chemical energy directly into electricity via electrochemical reactions between hydrogen and oxygen. The overall efficiency depends on multiple dynamic parameters: stack temperature, pressure, humidity, hydrogen flow rate, and load fluctuations. Conventional modelling approaches, such as equivalent circuit or empirical models, depend on simplifying assumptions that do not capture non-linear operational dynamics.

In contrast, the machine learning techniques enable data-driven inference of system relationships without explicit physical modelling. Previous research has demonstrated the use of artificial neural networks for predicting polymer electrolyte membrane fuel cell (PEMFC) performance [45-46] and genetic algorithms for optimizing fuel utilization [47]. However, these methods are rarely tailored for railway conditions, where the transient loads, regenerative braking, and hybrid power management with batteries create unique optimization challenges.

This research bridges that gap by combining the empirical data from simulated railway duty cycles with supervised machine learning models and multi-objective optimization algorithms to minimize hydrogen consumption and degradation rate simultaneously.

3 Hydrogen combustion engines and local pollutant control

Hydrogen fuelled or hydrogen blended internal combustion engines can serve as a cost effective transitional option in rail, especially through retrofits [48-49] Matlab (ML) models such as artificial neural networks, random forest, XGBoost, CatBoost, and other ensemble techniques accurately predict brake specific fuel consumption, efficiency, and emissions (CO_2, HC, particulates, NO_x), enabling optimization of injection, Exhaust Gas Recirculation (EGR), and after treatment strategies [48-49]. Studies on hydrogen enriched engines report:

- Substantial reductions in CO_2 and smoke, accompanied by NO_x increases that must be controlled via combustion tuning and after treatment [50-51].
- High fidelity ML predictors that support the real time Electronic Control Unit (ECU) optimization while highlighting risks of overfitting and data bias [50].

These methods are directly applicable to hydrogen rail engines to balance fuel efficiency with stringent NO_x and air quality targets.

4 Hydrogen production, storage, and refuelling for railway vehicles

Hydrogen production dominates the lifecycle environmental profile of hydrogen rail [52]. The ML is increasingly used to optimize both gray/blue (e.g., steam methane reforming) and green (electrolysis based) hydrogen systems [53-58]:

- Artificial Neural Network (ANN) based process models for Steam Methane Reforming (SMR) capture complex heat transfer phenomena with $R^2 \approx 0.999$ and are used to optimize nine operating variables, achieving thermal efficiencies of ~85.6% [55].
- For renewable powered electrolysis, the ML models, such as K-Nearest Neighbor (KNN), Random Forest (RF), XGBoost, Long Short-Term Memory (LSTM), Artificial Neural Network (ANN) and Lasso trained on decade scale meteorological data accurately predict green hydrogen yields and associated CO_2 savings; one study estimates nearly 400,000 kg CO_2 avoided per year for a single wind powered site [59].
- Bibliometric and technical reviews show ML widely applied to catalyst discovery, operating point

optimization, and cost/emission reduction across electrochemical, thermochemical, and biological hydrogen production routes [53-54, 56-57].

Integrated Reinforcement Learning - Internet of Things (Integrated RL-IoT) systems for hydrogen infrastructure demonstrate that combining real time sensing with Reinforcement Learning (RL) dispatch can reduce emissions up to 97.8% and costs by 40% in renewable hydrogen scenarios, with additional 30% emission reductions through the RL logistics optimization [59]. Such architectures are directly relevant to hydrogen rail refuelling corridors.

5 Methodology

This section includes a presentation of the applied methodology to the research. An overview of the of the system is presented together with collection of the data, processing of the data, a used model for machine learning and a framework for optimization.

5.1 System overview

The hydrogen fuel cell powertrain considered consists of:

- Proton Exchange Membrane Fuel Cell (PEMFC) stack: providing primary traction power.
- Lithium-Ion Battery: supplying transient and peak loads.
- Hydrogen Storage Tank: compressed at 350 bar.
- Power Management System (PMS): balancing the fuel cell and battery contributions.

The analyzed data represent a hybrid multiple-unit (HMU) rail vehicle with the gross mass of 120 tons operating over typical European regional routes.

5.2 Data collection

Data were derived from two sources:

1. Simulated Data: MATLAB/Simulink model of the hybrid multiple-unit energy system under variable duty cycles.
2. Experimental Data: Controlled PEMFC test bench including parameters such as voltage, current density, temperature, humidity, and degraded performance over time.

The combined dataset included 42,000 data points divided into training (70%), validation (15%), and testing (15%) sets.

Key variables:

- Input: Current density, hydrogen flow rate, cell temperature, pressure, and relative humidity.
- Output: Stack voltage, power output, hydrogen consumption rate, and degradation index.

The output voltage of a hydrogen fuel cell can be expressed as:

$$V = E - \eta_{act} - \eta_{ohmic} - \eta_{conc}\,, \tag{1}$$

where:
E is open-circuit voltage [V],
η_{act} are activation losses,
η_{ohmic} are ohmic losses,
η_{conc} are concentration losses.

The hydrogen consumption rate is defined as:

$$\dot{m}_{H_2} = \frac{1}{2 \cdot F} \cdot M_{H2}\,, \tag{2}$$

where:
I is electric current [A],
F equals to the value of 96,485 [kg/mol],
M_{H2} equals to the value of 2 [kg/mol],

The total environmental impact is estimated as:

$$EI = \alpha \cdot \dot{m}_{H_2} + \beta \cdot D_{stack}\,, \tag{3}$$

where:
EI is environmental impact index,
$\dot{m}_{H_2}$ is hydrogen consumption,
D_{stack} is degradation index,
α, β are weighting coefficients.

The simulated dataset was generated using a MATLAB/Simulink model of a hybrid multiple-unit (HMU) energy system operating under variable European regional duty cycles (urban, intercity, and steep gradient profiles). The Simulink model includes a PEMFC stack representation, hydrogen mass-flow dynamics, a compressor/power-management subsystem, and battery buffering to capture the transient load sharing during acceleration and regenerative braking.

The experimental data was obtained from a controlled PEMFC test-bench. Measured signals included stack voltage, current density, cell temperature, inlet hydrogen pressure, relative humidity, hydrogen flow rate, and long-term degradation indicators. The dataset covers both quasi-steady operation points and transient excitation regimes. An empirical degradation index was derived from the evolution of performance loss over time (e.g., capacity/voltage decay trends under comparable operating conditions) to support degradation-aware learning.

5.3 Data processing

The data were standardized and filtered for outliers using the Hampel identifier. Non-stationary time-series components were decomposed using Discrete Wavelet Transform (DWT) to isolate the steady-state and transient behavior. Missing data (≈1%) were imputed through K-nearest neighbor interpolation.

5.4 Machine learning models

Two supervised regression models were employed:

1. Random Forest Regression (RFR): robust against noise and capable of modelling non-linearities.
2. Support Vector Regression (SVR): optimized via radial basis function Kernel for generalization.

A Random Forest regression model was used to predict fuel cell voltage:

$$\hat{V} = f(T, j, \dot{m}_{H_2}, P), \tag{4}$$

where:
T is stack temperature,
J is current density,
P is pressure.

Hyperparameter tuning was conducted using the Bayesian optimization with 5-fold cross-validation. Performance metrics included Root Mean Squared Error (RMSE), Mean Absolute Error (MAE), and Coefficient of Determination (R^2).

5.5 Optimization framework

A multi-objective genetic algorithm (MOGA) was formulated to minimize the two competing objectives:

Minimize:
f_1 = hydrogen consumption (g/s),
f_2 = stack degradation index. (5)

The formulation of minimization of the two competing objectives in Equation (5) can be written as follows:

$$f_1 = \dot{m}_{H_2}, f_2 = D_{stack}. \tag{6}$$

Further, the multi-objective optimization problem is subjected to:

$$\begin{aligned} &P_{demand} = P_{fuel\ cell} + P_{battery} \\ &SOC_{\min} \le SOC \le SOC_{\max} \end{aligned}, \tag{7}$$

at which, the decision variables are considered as follows:

- fuel cell load ratio: $x_1 \in [0\ 1]$,
- battery State of Charge (SOC) threshold: $x_2 \in [0.2, 0.9]$,
- compressor speed: x_3.

The Pareto-optimal solutions were evaluated based on the weighted sum of normalized objectives, emphasizing the hydrogen economy. An optimal solution based on the Pareto-optimal approach is achieved using MOGA. A weighted objective function is also used:

$$F = w_1 \cdot f_1^{norm} + w_2 \cdot f_2^{norm}, \tag{8}$$

with $w_1 > w_2$.

6 Environmental impact reduction

When the baseline hydrogen consumption is assumed:

$$\dot{m}_{H_2}^{base} = 1.0\ \mathrm{g/s}, \tag{9}$$

then the optimized hydrogen consumption is as follows:

$$\dot{m}_{H_2}^{base} = 0.876\ \mathrm{g/s}, \tag{10}$$

and the reduction of hydrogen consumption is calculated by means of the following formulation:

$$\Delta H_2 = 1.0 - 0.876 = 0.124\ \mathrm{g/s}. \tag{11}$$

Annual savings of fuel (for 3000 h operation) is given:

$$0.124 \cdot 3600 \cdot 3000 = 1.34 \cdot 10^6 = 1.34\ \mathrm{tons}\ . \tag{12}$$

6.1 Emission equivalent

A calculation of emission equivalent is evaluated based on the following statement. When the hydrogen is produced via electrolysis, then the production of carbon dioxide is given as follows:

$$CO_2^{eqv} = 9\frac{\mathrm{kg}(CO_2)}{\mathrm{kg}(H_2)}. \tag{13}$$

When the value from Equation (12) is considered, then:

$$1.34 \cdot 9 = 12.06\frac{\mathrm{t}(CO_2)}{\mathrm{year}}. \tag{14}$$

7 Results and data analysis

This section includes a presentation of the obtained results based on the model performance, further the optimization results and validation of the research based on the operational scenarios.

7.1 Model performance

The Random Forest model demonstrated superior accuracy and stability. The Random Forest model outperformed SVR across all metrics, with less overfitting in transient regimes (Table 1). An important feature analysis indicated that stack temperature (37%) and current density (31%) were the most influential parameters, followed by hydrogen flow rate (18%) and pressure (9%).

The dependences of the values listed in Table 1 are shown in Figure 7. The dependence of the predicted voltage on the measured voltage is depicted. The value

Table 1 *The results of the model*

Error	Random Forest	SVR
RMSE [V]	0.045	0.057
MAE [V]	0.019	0.023
R^2	0.985	0.974

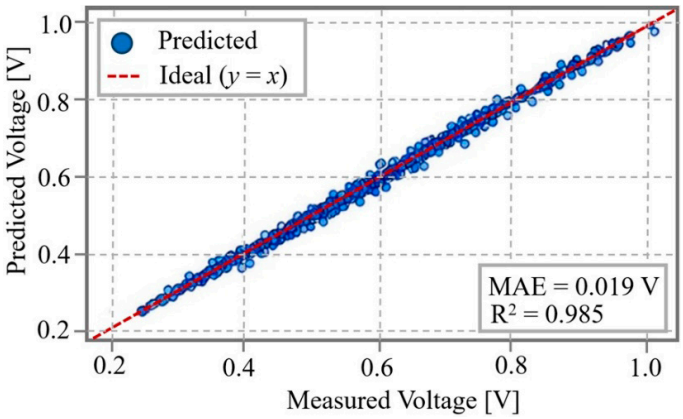


Figure 7 *The dependence of the predicted and measured voltage (on the test set)*

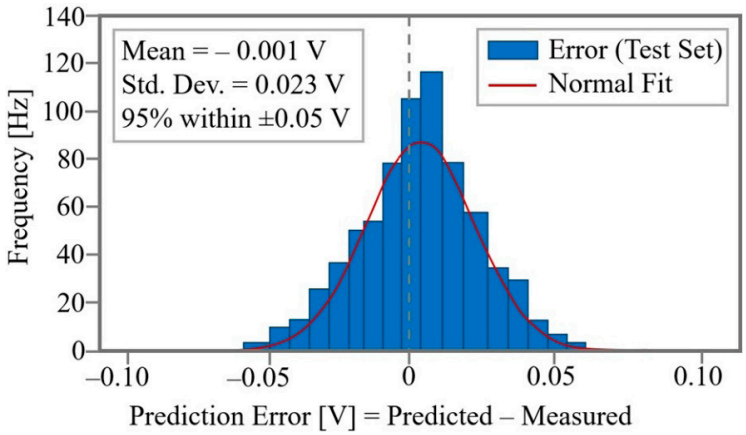


Figure 8 *The error distribution (The Error histogram)*

MAE represents the mean absolute error and R^2 is the coefficient of determination.

Then, a distribution of the predicted error of the predicted value and the measured value is depicted in Figure 8. It has a character of the centered distribution. The error distribution, i.e., the error histogram is centered near the zero value. It indicates no systematic bias.

7.2 Optimization results

MOGA produced a Pareto front illustrating the trade-off between the hydrogen efficiency and stack degradation. The optimal configuration (fuel cell load share ≈ 70%) resulted in:

- 12.4% reduction in hydrogen consumption
- 8.7% extension of projected stack lifetime
- 5.3% improvement in overall energy efficiency compared to baseline control.

The MOGA Pareto front is presented in Figure 9.

A trade-off between hydrogen consumption (a function f_1) and a degradation index (a function f_2) is depicted. The selected optimal point corresponds to a fuel cell load share of 70%.

7.3 Validation under operational scenarios

Three simulated railway duty cycles - urban, intercity, and steep gradient routes-were tested. The optimized controller demonstrated the stable SOC management, maintaining the battery levels between 35-85% and preventing voltage undershoot during acceleration peaks:

$$35\% \leq SOC \leq 85\%. \tag{15}$$

The machine learning model was further validated using experimental bench data, yielding a

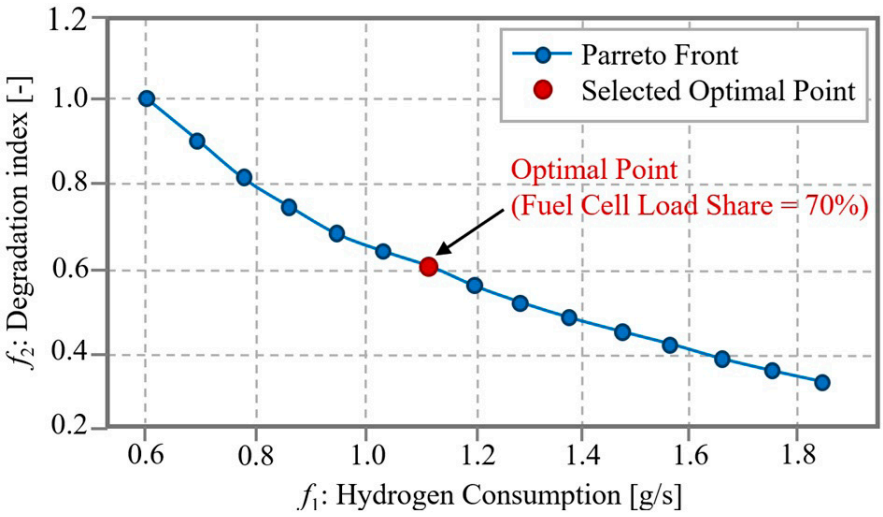


Figure 9 *An illustration of the Pareto front (MOGA) waveform*

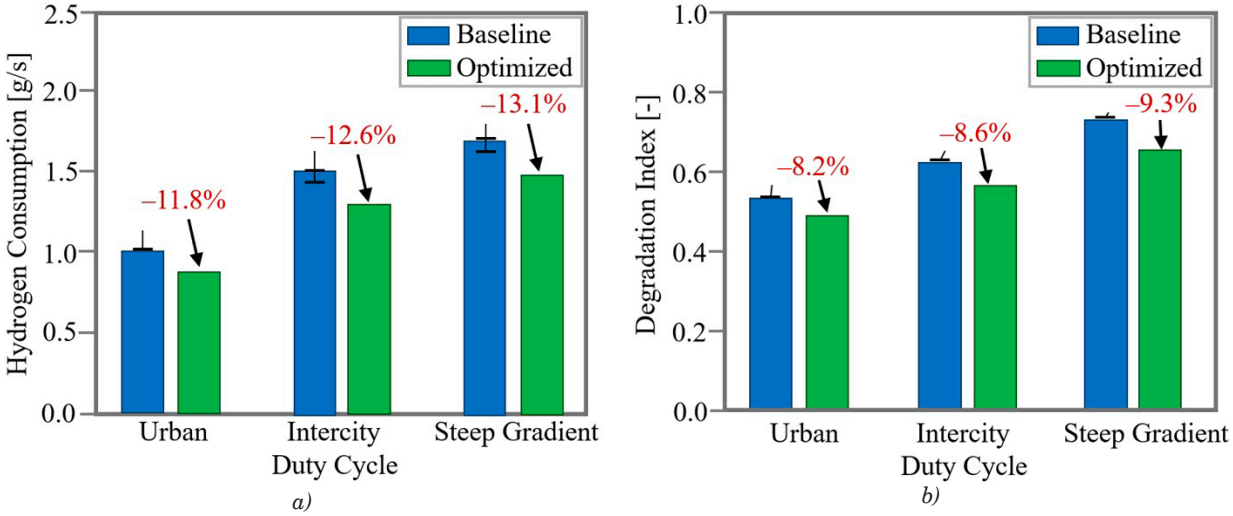


Figure 10 *Duty-cycle comparison: baseline vs. optimized: a) hydrogen consumption [g·s-1], b) the degradation index*

prediction error below 2% under dynamic load cycles, confirming the generalization capability of the proposed framework.

Figure 10 includes a comparison of duty-cycle for the baseline and optimized strategy. The optimized strategy reduces both hydrogen consumption and degradation index across all duty cycles, i.e. urban, intercity and steep gradient.

8 Discussion

The results highlight three main insights:

1. Data-driven modelling complements physical models. Traditional thermodynamic approaches often struggle with parameter uncertainty; the ML provides reliable performance prediction with minimal explicit modelling effort.
2. Hybrid optimization improves lifetime and efficiency. The multi-objective approach balances immediate fuel economy against long-term degradation, providing a framework adaptable to route-specific requirements.
3. Practical implementation requires online adaptability. Integrating the model into the real-time PMS would enable adaptive operation based on continuous feedback from onboard sensors.

In a real practical application, the proposed ML predictor would be embedded into the on-board Power Management System (PMS) to estimate the stack voltage and hydrogen consumption rate from sensor measurements (current density, temperature, pressure, humidity, hydrogen flow). The optimization module would generate updated references for the fuel-cell load share and battery SOC threshold at a fixed control interval (e.g., every few seconds/minutes), while the battery remains the fast-acting buffer for transient power peaks. Safety constraints, such as SOC limits,

compressor operating bounds, and stack temperature thresholds should be enforced as hard constraints in the optimization problem to prevent unsafe operating points.

Since the railway conditions are variables in time (ambient temperature, altitude, humidity, aging state), continuous monitoring is required. Model monitoring can include tracking prediction residuals and triggering a re-calibration/re-training step when the concept drift or data distribution shift is detected. For reliability assurance, a fallback strategy (e.g., conservative baseline controller) should be activated if the model confidence drops below a predefined threshold.

The main limitation is dependency on hydrogen production pathways. Challenges remain in ensuring robustness to unmodeled conditions, long-term data drift, and environmental variability (temperature, humidity, altitude). Future efforts should integrate reinforcement learning for adaptive control and consider digital twin architectures for real-time health monitoring.

9 Conclusion

A comprehensive data-driven methodology for modelling and optimization of hydrogen fuel systems in railway transport is presented in this research. Combining machine learning with multi-objective optimization leads to significant gains in hydrogen efficiency and fuel cell durability. The Random Forest-based predictive model achieved high accuracy (R^2 = 0.985), while optimization reduced hydrogen consumption by 12.4%. Moving forward, coupling the ML models with the real-time control architectures will be key to realizing intelligent zero-emission railway propulsion. The results confirm that:

- Machine learning improves system predictability,
- Optimization reduces both fuel use and degradation,
- Environmental impact is significantly reduced.

Acknowledgements

This publication was realized with support of Operational Program Integrated Infrastructure 2014 - 2020 of the project: Concept, safety and related industrial research for the replacement of diesel traction by hydrogen fuel cell traction in the railway vehicles series 861 (code ITMS2014+: 313011BVC2), co-financed by the European Regional Development Fund.

This publication was also supported by the Cultural and Educational Grant Agency of the Ministry of Education of the Slovak Republic in the project KEGA 028ZU-4/2026: Integration of advanced modelling methods and simulation computations into university education of future specialists in vehicles' design.

Conflicts of interest

The authors declare that they have no known competing financial interests or personal relationships that could have appeared to influence the work reported in this paper.

References

[1] ALI, Y., MEHMOOD, B., HUZAIFA, M., YASIR, U., KHAN, A.U. Development of a new hybrid multi criteria decision-making method for a car selection scenario. *Facta Universitatis Series Mechanical Engineering* [online]. 2020, **18**(3), p. 357-373 [accessed 2026-04-13]. ISSN 2335-0164. Available from: https://doi.org/10.22190/FUME200305031A

[2] AL-LAMI, A., TOROK, A. Economic growth and transport emissions: testing the environmental Kuznets Curve in Austria and the Netherlands. *Transportation Research Procedia* [online]. 2026, **93**, p. 71-76 [accessed 2026-04-17]. ISSN 2352-1465. Available from: https://doi.org/10.1016/j.trpro.2025.11.011

[3] FOMIN, O., LOVSKA, A., PISTEK, V., KUCERA, P. Research of stability of containers in the combined trains during transportation by railroad ferry. *MM Science Journal* [online]. 2020, **2020**, p. 3728-3773 [accessed 2026-05-02]. ISSN 1805-0476. Available from: https://doi.org/10.17973/MMSJ.2020_03_2019043

[4] GERLICI, J., LOVSKA, A., PAVLIUCHENKOV, M. Study of the dynamics and strength of the detachable module for long cargoes under asymmetric loading diagrams. *Applied Sciences* [online]. 2024, **14**(8), 3211 [accessed 2026-03-13]. ISSN 2076-3417. Available from: https://doi.org/10.3390/app14083211

[5] FOMIN, O., LOVSKA, A., KUCERA, P., PISTEK, V. Substantiation of improvements for the bearing structure of an open car to provide a higher security during rail/sea transportation. *Journal of Marine Science and Engineering* [online]. 2021, **9**(8), 873 [accessed 2026-05-02]. ISSN 2077-1312. Available from: https://doi.org/10.3390/jmse9080873

[6] PANCHENKO, S., GERLICI, J., VATULIA, G., LOVSKA, A., RYBIN, A., KRAVCHENKO, O. Strength assessment of an improved design of a tank container under operating conditions. *Communications - Scientific Letters of the University of Zilina* [online]. 2023, **25**(3), p. B186-B193 [accessed 2026-03-13]. ISSN 1335-4205, eISSN 2585-7878. Available from: https://doi.org/10.26552/com.C.2023.047.

[7] FOMIN, O., GERLICI, J., LOVSKA, A., KRAVCHENKO, K., PROKOPENKO, P., FOMINA, A., HAUSER,

V. Durability determination of the bearing structure of an open freight wagon body made of round pipes during its transportation on the railway ferry. *Communications - Scientific Letters of the University of Zilina* [online]. 2019, **21**(1), p. 28-34 [accessed 2026-04-07]. ISSN 1335-4205, eISSN 2585-7878. Available from: https://doi.org/10.26552/com.c.2019.1.28-34

[8] BAJOR, I., TOROK, A., ROZIC, T., NOVACKO, L. The EU logistics sector. *Periodica Polytechnica Transportation Engineering* [online]. 2024, **52**(3), p. 229-234 [accessed 2026-04-15]. ISSN 1587-3811. Available from: https://doi.org/10.3311/PPtr.23694

[9] FISCHER, S., HERMAN, B., SYSYN, M., KURHAN, D., KOCSIS SZURKE, S. Quantitative analysis and optimization of energy efficiency in electric multiple units. *Facta Universitatis, Series: Mechanical Engineering* [online]. 2025, **23**(2), p. 351-375 [accessed 2026-04-14]. ISSN 2335-0164. Available from: https://doi.org/10.22190/FUME241103001F

[10] MAN, D.-W., ZHANG, Y., TANG, L.-P., XU, Q.-H., CHEN, D., JIANG, B.-D., HAN, T.-T., XU, T., LI, J.-B. Nonlinear dynamical characteristics of hybrid tri-stable piezoelectric energy harvester based on rotational motion. *Facta Universitatis, Series: Mechanical Engineering* [online]. 2024, **22**(2), p. 257-273 [accessed 2026-04-13]. ISSN 2335-0164. Available from: https://doi.org/10.22190/FUME240118033M

[11] MIKUSOVA, M., TOROK, A., BRIDA, P. Technological and economical context of renewable and non-renewable energy in electric mobility in Slovakia and Hungary. In: Lecture Notes in Computer Science Including Subseries Lecture Notes in Artificial Intelligence and Lecture Notes in Bioinformatics ICCCI 2018: proceedings [online] [accessed 2026-04-29]. 2018. ISBN 978-3-319-98445-2, eISBN 978-3-319-98446-9, p. 429-436. Available from: https://doi.org/10.1007/978-3-319-98446-9_40

[12] TOROK, A., ZOLDY, M. Energetic and economical investigation of greenhouse gas emission of Hungarian road transport sector. *Pollack Periodica* [online]. 2010, **5**(3), p. 123-132 [accessed 2026-03-02]. ISSN 1788-3911. Available from: https://doi.org/10.1556/pollack.5.2010.3.10

[13] BAJEC, P., PIVTORAK, H., SVADLENKA, L., VRBA, R. Analyzing the characteristics of potential last-mile crowdshippers: insights from survey data in Slovenia, Ukraine, and the Czech Republic. *Transportation Research Procedia* [online]. 2025, **83**, p. 1-10 [accessed 2026-04-28]. ISSN 2352-1465. Available from: https://doi.org/10.1016/j.trpro.2025.02.003

[14] FICZERE, P. The role of artificial intelligence in the development of rail transport. *Cognitive Sustainability* [online]. 2023, **2**(4), p. 1-5 [accessed 2026-05-04]. ISSN 2939-5240. Available from: https://doi.org/10.55343/CogSust.81

[15] KURHAN, M., FISCHER, S., TIUTKIN, O., KURHAN, D., HMELEVSKA, N. Development of high-speed railway network in Europe: a case study of Ukraine. *Periodica Polytechnica Transportation Engineering* [online]. 2024, **52**(2), p. 151-158 [accessed 2026-04-16]. ISSN 1587-3811. Available from: https://doi.org/10.3311/PPtr.23464

[16] ŁUCZYSZYN, K. Sustainable transport - development and goals. *Cognitive Sustainability* [online]. 2024, **3**(1), p. 1-6 [accessed 2026-04-17]. ISSN 2939-5240. Available from: https://doi.org/10.55343/CogSust.92

[17] GOOLAK, S., GOROBCHENKO, O., HOLUB, H., KULBOVSKIY, I., PETRYCHENKO, O. Traction drive control system for railway electric rolling stock based on the application of power factor as an optimization criterion, *Problems of the Regional Energetics / Problemele Energeticii Regionale* [online]. 2025, **3**(67), p. 1-12 [accessed 2026-07-02]. ISSN 1857-0070. Available from: https://doi.org/10.52254/1857-0070.2025.3-67.01.

[18] GOOLAK, S., KYRUCHENKO, M. Thermal model of the output traction converter of an electric locomotive with induction motors, *Problems of the Regional Energetics / Problemele Energeticii Regionale* [online]. 2022, **3**(55), p. 1-16 [accessed 2026-06-30]. ISSN 1857-0070. Available from: http://doi.org/10.52254/1857-0070.2022.3-55.01

[19] GOOLAK, S., TKACHENKO, V., KYRYCHENKO, M., KOZLOV, S. Hybrid reactive power compensator with adaptation of the operation of the control system to the parameters of the mains voltage, *Problemele Energeticii Regionale* [online]. 2023, **57**(1), p. 1-16 [accessed 2026-06-30]. ISSN 1875-0070. Available from: https://doi.org/10.52254/1857-0070.2023.1-57.01

[20] LUKOSEVICIUS, V., GOOLAK, S., DEREHUZ, I., NEDUZHA, L., KERSYS, A., DZERKELIS, V. Conceptual basis of adaptation of a field-oriented control system for traction induction motors to the operating parameters of a locomotive, *Energies* [online]. 2026, **19**(2), 298 [accessed 2026-07-04]. ISSN 1996-1073. Available from: https://doi.org/10.3390/en19020298

[21] FISCHER, S., KOCSIS SZURKE, S. Detection process of energy loss in electric railway vehicles, *Facta Universitatis, Series: Mechanical Engineering* [online]. 2023, **21**(1), p. 81-99 [accessed 2026-04-10]. ISSN 2335-0164. Available from: https://doi.org/10.22190/FUME221104046F

[22] SZURKE, S. K., KOVACS, G., SYSYN, M., LIU, J., FISCHER, S. Numerical optimization of battery heat management of electric vehicles. *Journal of Applied and Computational Mechanics* [online]. 2023, **9**(4), p. 1076-1092 [accessed 2026-04-05]. ISSN 2383-4536. Available from: https://doi.org/10.22055/jacm.2023.43703.4119

[23] JABBAR, M. Y., AHMED, S. Y., KHAFAJI, S. O. W. A scoping review of the thermoelectric generator systems designs (heat exchangers and coolers) with locations of application to recover energy from internal combustion

engines. *Journal of Applied and Computational Mechanics* [online]. 2024, **10**(3), p. 547-583 [accessed 2026-05-02]. ISSN 2383-4536. Available from: https://doi.org/10.22055/jacm.2024.45491.4376

[24] TOROK, A. Theoretical estimation of the environmental impact of biofuel mixtures. *Transport* [online]. 2009, **24**(1), p. 26-29 [accessed 2026-04-20]. ISSN 1648-3480. Available from: https://doi.org/10.3846/1648-4142.2009.24.26-29

[25] KONDOR, P. Limitations of using hydrogen as a sustainable fuel in gas turbines. *Cognitive Sustainability* [online]. 2026, **5**(1), p. 1-6 [accessed 2026-05-02]. ISSN 2939-5240. Available from: https://doi.org/10.55343/Cogsust.21702

[26] AZIM, R. M., TORII, S. Exploring the potential of ammonia and hydrogen as alternative fuels for transportation. *Open Engineering* [online]. 2024, **14**(1), 20240024 [accessed 2026-04-03]. ISSN 2391-5439. Available from: https://doi.org/10.1515/eng-2024-0024

[27] MALEK, A., TACCANI, R., KASPAREK, D., HUNICZ, J. Optimization of energy management in a city bus powered by the hydrogen fuel cells. *Communications - Scientific Letters of the University of Zilina* [online]. 2021, **23**(4), p. E56-E67 [accessed 2026-04-10]. ISSN 1335-4205, eISSN 2585-7878. Available from: https://doi.org/10.26552/com.C.2021.4.E56-E67.

[28] MEILUS, L., MASKELIUNAITE, L., SIVILEVICIUS, H. Economical comparison of passenger rail traction rolling stock alternatives. *Lecture Notes in Intelligent Transportation and Infrastructure* [online]. 2025, **Part F230**, p. 423-435 [accessed 2026-04-17]. ISSN 2523-3459. Available from: https://doi.org/10.1007/978-3-031-85390-6_39.

[29] FABRI, G., OMETTO, A., LI, H, D'OVIDIO, G. Redesign of a non-electrified urban railway line with hydrogen-fuelled trains. *Lecture Notes in Civil Engineering* [online]. 2024, **526 LNCE**, p. 640-648 [accessed 2026-05-02]. ISSN 2366-2565. Available from: https://doi.org/1007/978-981-97-4355-1_62.

[30] FISCHER, T., REINOLD, S., LICHTEBERG, M., SAHBA, M.-A. Farewell diesel: on the way to climate neutrality using alternative drives and fuels in rail passenger service and rail transport. *Proceedings of the Institution of Mechanical Engineers, Part F: Journal of Rail and Rapid Transit* [online]. 2023, **238**(3), p. 284-291 [accessed 2026-05-03]. ISSN 2041-3017. Available from: https://doi.org/10.1177/09544097231174487.

[31] DE ABREU, V. H. S., DA ROS HOLLANDA, D. L., PROENCA, L. F. C., BAHIENSE, L., SANTOS, A. S. A systematic review on renewable hydrogen application in the land transportation sector. *Energy, Environment, and Sustainability* [online]. 2024, **Part F2419**, p. 9-31. [accessed 2026-04-16]. ISSN 2522-8374. Available from: https://doi.org/10.1007/978-981-97-0515-3_2.

[32] RAHIM MARJANI, S., MOTAMAN, S., VARASTEH, H., YANG, Z., CLEMENTSON, J. Assessing hydrogen as an alternative fuel for rail transport - a case study. *Scientific Reports* [online]. 2025, **15**(1), 6449 [accessed 2026-04-11]. ISSN 2045-2322. Available from: https://doi.org/10.1038/s41598-025-90887-3.

[33] WALLINGTON, T. J., WOODY, M., LEWIS, G. M., KEOLEIAN, G. A., ADLER, E. J., MARTINS, J. R. R. A., COLLETTE, M. D. Hydrogen as a sustainable transportation fuel. *Renewable and Sustainable Energy Reviews* [online]. 2025, **217**, 115725 [accessed 2026-04-02]. ISSN 1879-0690. Available from: https://doi.org/10.1016/j.rser.2025.115725, 115725.

[34] WIESER, S., BRUNNER, L., BOHM, M., SOTO, M., RODRIGUEZ, E. J. Development, application and optimization of hydrogen refuelling processes for railway vehicles. *International Journal of Hydrogen Energy* [online]. 2025, **124**, p. 331-344 [accessed 2026-03-29]. ISSN 0360-3199. Available from: https://doi.org/10.1016/j.ijhydene.2025.04.040

[35] EMRAN, A., GARG, S., MERTES, S., GAUTAM, A., SCHMIDT, M., WICK, M., WALTERS, M., WAGH, S., SHARMA, V. Fuel cell electric metro train concept - zero emission rail transport solution for Indian cities. *SAE International Journal of Advances and Current Practices in Mobility* [online]. 2024, **6**(6), 197403 [accessed 2026-05-03]. Available from: https://doi.org/10.4271/2024-26-0179.

[36] NQODI, A., MOSETLHE, T. C., YUSUF, A. Advances in hydrogen-powered trains: a brief report. *Energies* [online]. 2023, **16**(18), 6715 [accessed 2026-03-23]. ISSN 1996-1073. Available from: https://doi.org/10.3390/en16186715, no. 18, 6715.

[37] XU, Z., ZHAO, N., YAN, Y., GAO, S., HILLMANSEN, S. Electric-thermal collaborative system and control for hydrogen-fuel cell passenger trains in the UK's winter. *Energy Conversion and Management* [online]. 2025, **328**, 119629 [accessed 2026-04-09]. ISSN 1879-2227. Available from: https://doi.org/10.1016/j.enconman.2025.119629

[38] TANCZOS, K. Adapting the ITF's transport policy with a focus on the EU's strategy of sustainable mobility. *Periodica Polytechnica Transportation Engineering* [online]. 2025, **53**(2), p. 222-225 [accessed 2026-04-29]. ISSN 1587-3811. Available from: https://doi.org/10.3311/PPtr.39780

[39] Alstom. Coradia iLint hydrogen train performance report. Alstom Mobility. 2020.

[40] Siemens Mireo Plus [online]. Available from: https://www.mobility.siemens.com/global/en/portfolio/rolling-stock/commuter-and-regional-trains/mireo/mireo-plus.html

[41] Stadler Flirt H2 [online]. Available from: https://www.stadlerrail.com/en/solutions/rolling-stock/mainline-flirt-h2

[42] ZOS Vrutky Inc. [online]. Available from: https://www.zos-vrutky.sk/
[43] KANCHAN, M., MANIYERI, R., POWAR, O. S. Numerical analysis of two side-by-side flexible filaments in shear flow and orbit class prediction using immersed boundary method and machine learning techniques. *Journal of Applied and Computational Mechanics* [online]. 2026, **12**(1), p. 238-254 [accessed 2026-03-17]. ISSN 2383-4536. Available from: https://doi.org/10.22055/jacm.2025.48275.5112
[44] NWACHUKWU, U., AIKHUELE, D. O., SOROOSHIAN, S. Dynamic concept drift detection using an integrated machine learning model with error-based Page-Hinkley test for enhanced predictive accuracy in adhesive manufacturing process. *Open Engineering* [online]. 2026, **16**(1), 20250158 [accessed 2026-02-28]. ISSN 2391-5439. Available from: https://doi.org/10.1515/eng-2025-0158
[45] PUKRUSHPAN, J. T., STEFANOPOULOU, A. G., PENG, H. *Control of fuel cell power systems: principles, modelling, analysis and feedback design*. 1. ed. London, UK: Springer, 2004. ISBN 978-1-4471-3792-4.
[46] OU, S., ACHENIE, L. E. K. Artificial neural network modelling of PEM fuel cell. *Journal of Fuel Cell Science and Technology* [online]. 2005, **2**(4), p. 1-24 [accessed 2026-05-01]. ISSN 1551-6989. Available from: https://doi.org/10.1115/1.2039951
[47] LIM, H. S., KANG, B., AHN, M., KIM, M. S. Optimizing hydrogen utilization in fuel cell hybrid vehicles: modelling fuel cell systems and managing energy between batteries and fuel cells. *International Journal of Hydrogen Energy* [online]. 2025, **99**, p. 819-835 [accessed 2025-04-20]. ISSN 1879-3487. Available from: https://doi.org/10.1016/j.ijhydene.2024.12.150
[48] MARJANI, S., MOTAMAN, S., VARASTEH, H., YANG, Z., CLEMENTSON, J. Assessing hydrogen as an alternative fuel for rail transport - a case study. *Scientific Reports* [online]. 2025, **15**, 6449 [accessed 2026-05-02]. ISSN 2045-2322. Available from: https://doi.org/10.1038/s41598-025-90887-3
[49] NQODI, A., MOSETLHE, T., YUSUFF, A. Advances in hydrogen-powered trains: a brief report. *Energies* [online]. 2023, **16**(18), 6715 [accessed 2026-02-27]. ISSN 1996-1073. Available from: https://doi.org/10.3390/en16186715
[50] ZBIKOWSKI, M., TEODORCZYK, A. Machine learning for internal combustion engine optimization with hydrogen-blended fuels: a literature review. *Energies* [online]. 2025, **18**(6), 1391 [accessed 2026-04-02]. ISSN 1996-1073. Available from: https://doi.org/10.3390/en18061391
[51] BAI, F. J. J. S. A Machine learning approach for carbon di oxide and other emissions characteristics prediction in a low carbon biofuel-hydrogen dual fuel engine. *Fuel* [online]. 2023, **341**, 127578 [accessed 2026-02-16]. ISSN 1873-7153. Available from: https://doi.org/10.2139/ssrn.4231208
[52] SIM, L. C., YEO, W. H., PURBOLAKSONO, J., SAW, L. H., TEY, J. Y., LEE, J.V., YEW, M. C. Thermomechanical stresses of multilayered wellbore structure of underground hydrogen storage - a simplified solution based on recursive algorithm. *Journal of Applied and Computational Mechanics* [online]. 2022, **8**(4), p. 1287-1298 [accessed 2026-02-18]. ISSN 2383-4536. Available from: https://doi.org/10.22055/jacm.2022.39453.3411
[53] DU, X., GAO, S., YANG, G. Machine learning applications in gray, blue, and green hydrogen production: a comprehensive review. *Gases* [online]. 2025, **5**(2), 9 [accessed 2026-04-20]. ISSN 2673-5628. Available from: https://doi.org/10.3390/gases5020009
[54] IQBAL, S., AFTAB, K., JANNAT, F., BAIG, M., KALSOOM, U. A bibliographic analysis of optimization of hydrogen production via electrochemical method using machine learning. *Fuel* [online]. 2024, **372**, 132126 [accessed 2026-04-22]. ISSN 1873-7153. Available from: https://doi.org/10.1016/j.fuel.2024.132126
[55] LEE, J., HONG, S., CHO, H., LYU, B., KIM, M., KIM, J., MOON, I. Machine learning-based energy optimization for on-site SMR hydrogen production. *Energy Conversion and Management* [online]. 2021, **244**, 114438 [accessed 2026-04-23]. ISSN 0196-8904. Available from: https://doi.org/10.1016/j.enconman.2021.114438
[56] SALEHMIN, M., KIONG, T., MOHAMED, H., UMAR, D., YU, K., ONG, H., NOMANBHAY, S., LIM, S. Navigating challenges and opportunities of machine learning in hydrogen catalysis and production processes: beyond algorithm development. *Journal of Energy Chemistry* [online]. 2024, **99**, p. 223-252 [accessed 2026-04-24]. ISSN 2096-885X. Available from: https://doi.org/10.1016/j.jechem.2024.07.045
[57] SETHI, H., AHMAD, I., KHAN, M., QAZI, A., AYUB, A., ZULKEFAL, M., SHUTAYWI, M. Applications of computer intelligence in hydrogen production. *ACS Omega* [online]. 2025, **10**(31), p. 33982-33998 [accessed 2026-04-24]. ISSN 2470-1343. Available from: https://doi.org/10.1021/acsomega.5c01602
[58] URHAN, B., ERDOGMUS, A., DOKUZ, A., GOKCEK, M. Predicting green hydrogen production using electrolyzers driven by photovoltaic panels and wind turbines based on machine learning techniques: A pathway to on-site hydrogen refuelling stations. *International Journal of Hydrogen Energy* [online]. 2025, **101**, p. 1421-1438 [accessed 2026-04-20]. ISSN 1879-3487. Available from: https://doi.org/10.1016/j.ijhydene.2025.01.017
[59] BEKMYRZA, K., KUTERBEKOV, K., KABYSHEV, A., KUBENOVA, M., BARATOVA, A., AIDARBEKOV, N., VINCESLAS, F. Integrating machine learning and IoT in hydrogen production, storage, and distribution for a decarbonized transport future. *International Journal of Low-Carbon Technologies* [online]. 2025, **20**, p. 1554-1570 [accessed 2026-04-21]. ISSN 1748-1325. Available from: https://doi.org/10.1093/ijlct/ctaf103

This is an open access article distributed under the terms of the Creative Commons Attribution 4.0 International License (CC BY 4.0), which permits use, distribution, and reproduction in any medium, provided the original publication is properly cited. No use, distribution or reproduction is permitted which does not comply with these terms.

ADAPTING D-FMEA TO INCREASING PRODUCT COMPLEXITY: A STUDY OF CONVENTIONAL AND MECHATRONIC SHOCK ABSORBERS

Łukasz Rudolf[1,*], Marek Roszak[2], Lenka Kuchariková[3]

[1]Silesian University of Technology, Faculty of Mechanical Engineering, Gliwice, Poland
[2]Silesian University of Technology, Faculty of Mechanical Engineering, Department of Engineering, Materials and Biomaterials, Gliwice, Poland
[3]University of Zilina, Faculty of Mechanical Engineering, Department of Materials Engineering, Zilina, Slovakia

*E-mail of corresponding author: lukasz.rudolf@outlook.com

Łukasz Rudolf 0000-0001-9430-8513, Marek Roszak 0000-0002-4035-8360, Lenka Kuchariková 0000-0002-2688-1075

Resume
The risk analysis is essential in product development, particularly as technical complexity increases. In this article the focus was on Design Failure Mode and Effects Analysis (D-FMEA) in the automotive industry. The conventional and electronically controlled shock absorbers as examples of a transition from a mechanical-hydraulic product to a more complex mechatronic system, are compared. In the study was considered how increasing complexity affects analysis boundaries, decomposition level, function description, interactions between components and subsystems, and the link between risk analysis and product validation. Based on industrial practice, a model is proposed to show how D-FMEA should evolve with product complexity.

Article info
Received 22 May 2026
Accepted 14 July 2026
Online 21 August 2026

Keywords:
D-FMEA
product complexity
shock absorber
mechatronic product
risk analysis

Available online: https://doi.org/10.26552/com.C.2026.046

ISSN 1335-4205 (print version)
ISSN 2585-7878 (online version)

Nomenclature

FMEA: Failure Mode and Effects Analysis; a preventive method used to identify potential failure modes, their effects and causes, in order to reduce risk.
D-FMEA: Design Failure Mode and Effects Analysis; a type of FMEA focused on product design and design-related risk.
BOM: Bill of Materials; a structured list of product components, used here as an indicator of product complexity.
RPN: Risk Priority Number; an index based on Severity, Occurrence and Detection, used in D-FMEA and applied here to compare product-related risk.
AP: Action Priority; a priority level in AIAG & VDA FMEA indicating how urgently risk-reduction action should be considered.
APQP: Advanced Product Quality Planning; a structured automotive framework supporting product and process development from planning to serial production.
PLM: Product Lifecycle Management; an organizational approach to managing product data, processes, engineering changes, and traceability throughout the product lifecycle, typically supported by an integrated digital environment.

1 Introduction

The subject of this study were the automotive shock absorbers, which are analysed into two product groups: conventional and mechatronic. The first group includes shock absorbers with a classical mechanical-hydraulic architecture, while the second includes electronically controlled shock absorbers, in which the damping function requires the interaction of mechanical, hydraulic, and electronic components and subsystems [1-2]. The differences between the analysed products concern not only their design, but the scope of the functions performed, the degree of connections with other subsystems, and the validation requirements, as well. This makes them a suitable subject for analysing

how design risk assessment should be adapted to increasing product complexity.

The Failure Mode and Effects Analysis (FMEA) is one of the basic preventive methods of technical risk analysis used in product and process development. Its origins can be traced back to reliability analyses developed for military applications; one of the earliest formal reference points is the MIL-P-1629 procedure from 1949, which structured the identification of potential failures, their effects, and their criticality. In the following decades, the method was further developed in the aerospace sector, where particular emphasis was placed on a system-level understanding of function, reliability, and safety. The FMEA was then widely adopted in many branches of industry, including the automotive sector, where it evolved from a tool originally focused mainly on component reliability into a structured method supporting quality planning, product development, and risk reduction during product preparation [3]. According to the current automotive approach presented by AIAG & VDA, FMEA is a structured method carried out by an interdisciplinary team to identify potential failure modes, their effects, causes, and actions intended to reduce risk [4]. In automotive practice, two main areas of application are usually distinguished: Design Failure Mode and Effects Analysis (D-FMEA), which addresses risks associated with product design, and Process Failure Mode and Effects Analysis (P-FMEA), which addresses risks associated with the manufacturing process. In this article, the main focus is on D-FMEA, because it is at the design stage that the analysis boundaries, product architecture, functions, and relationships between components, subsystems, and the system are defined.

Despite the widespread use of FMEA in industrial practice, there are relatively few empirical studies that show how D-FMEA should be performed as the product complexity increases [5-6]. This is especially important in cases where the product evolves, as in the development of shock absorbers from a conventional architecture to a mechatronic one, where not only the number of components changes, but also the scope of functions, the number of relationships between subsystems, and the validation requirements. The research gap, therefore, concerns not the use of D-FMEA itself, but the principles for adapting it to increasing product complexity. The aim of this article was to provide a comparative analysis of the two groups of automotive shock absorbers, conventional and mechatronic products, based on research conducted in industrial conditions, and to develop a model showing how the way D-FMEA is performed changes as product complexity increases. In the following sections, product complexity is considered not only descriptively, but in relation to product structure, the organisation of risk analysis, and the scope of activities related to quality planning and its validation, as well.

2 Research background and methodology

In this study, the logic of D-FMEA was adopted in line with the AIAG & VDA approach, in which design risk analysis is not limited only to the assessment of Severity (S), Occurrence (O), and Detection (D), but is treated as a structured process including planning and preparation, structure analysis, function analysis, failure analysis, risk analysis, optimisation, and documentation of product-related results [7-8]. This means that a reliable risk assessment requires the proper definition of the analysis boundaries, the level of the analysed product, and the relationships between the function, the potential failure mode, its effect, and its cause. According to the AIAG & VDA methodology, the priorities of the risk-reduction actions should be determined using the Action Priority (AP) approach, rather than only on the basis of the Risk Priority Number (RPN). At the same time, for the purposes of this study, the RPN values were retained as a supporting analytical indicator for comparing the two product groups in terms of overall design risk burden. In this article, therefore, the RPN does not serve a decision-making function, but a comparative and reference function, while the logic for interpreting the need for action remains consistent with the AP approach.

The research material used in this article comes from the authors own studies conducted in industrial conditions at Tenneco Automotive Eastern Europe as part of an implementation-oriented doctoral project. The comparative analysis covered two product groups: conventional shock absorbers, treated as the reference group, and electronically controlled shock absorbers, hereinafter referred to as mechatronic products. It was assumed that the second group represents solutions from the Monroe Intelligent Suspension product family, in which damping is achieved through the interaction of mechanical, hydraulic, and electronic subsystems, along with control via an ECU (Electronic Control Unit) and sensor signals [9-10]. This research setting enabled comparison of two levels of product architecture complexity in a real development and industrialisation environment, while maintaining alignment with the quality requirements typical of the automotive industry.

In this study, product complexity was not assessed solely descriptively, but rather using comparable data on both product structure and the scope of activities associated with quality planning [11]. This approach made it possible to analyse product complexity not only from the perspectives of the number of components and the organisation of the product structure, but also from the perspectives of the activities required to confirm the performed product functions and to plan and carry out product validation [12]. As a result, it was possible to link the features of product architecture with the way D-FMEA is conducted.

The research procedure included four main stages.

In the first stage, the comparison scope and the analysis boundaries were defined for both product groups. In the second stage, the available D-FMEA studies for selected shock absorber types were analysed, with a focus on product structure, function description, potential failure modes, and the interpretation of design risk. In the third stage, the data describing product complexity were compiled and then subjected to the comparative analysis. In the final stage, the results were interpreted in accordance with the D-FMEA methodology, and a model was developed to organise the observed changes in the way D-FMEA is conducted as product complexity increases.

3 Results

The results of the analysis show that the studied product groups differ not only in design, but also in the scope of the functions performed, the degree of relationships between components and subsystems, and the validation requirements. These differences are reflected in both the product's structural features and the way D-FMEA results are developed and interpreted. The research results are presented in a structure that covers successive aspects of the complexity of the analysed products and their significance for design risk assessment. In the final part of the section, a model is presented to organise these observations from the perspective of D-FMEA.

3.1 System-level context relevant to D-FMEA

The comparative analysis began at the vehicle level, with the vehicle understood as the final product intended for use by the end user. This perspective allows the shock absorber to be considered not as an isolated component, but as part of a wider system responsible for functions related to vehicle behaviour, ride comfort, and driving stability.

Figure 1 presents an illustrative comparison of components and subsystems found in vehicles equipped with conventional shock absorbers and in vehicles using the KINETIC® solution from the Monroe Intelligent Suspension product family [13]. The radial scale indicates the number of elements of each type included in the analysed vehicle-level system. The presented data are illustrative and are intended to show the typical level of complexity of both solutions at the system level, without fully representing all variants of the analysed products. This comparison indicates that, for the mechatronic product, the damping function is implemented within a broader system that includes more interacting components and subsystems than in the conventional solution.

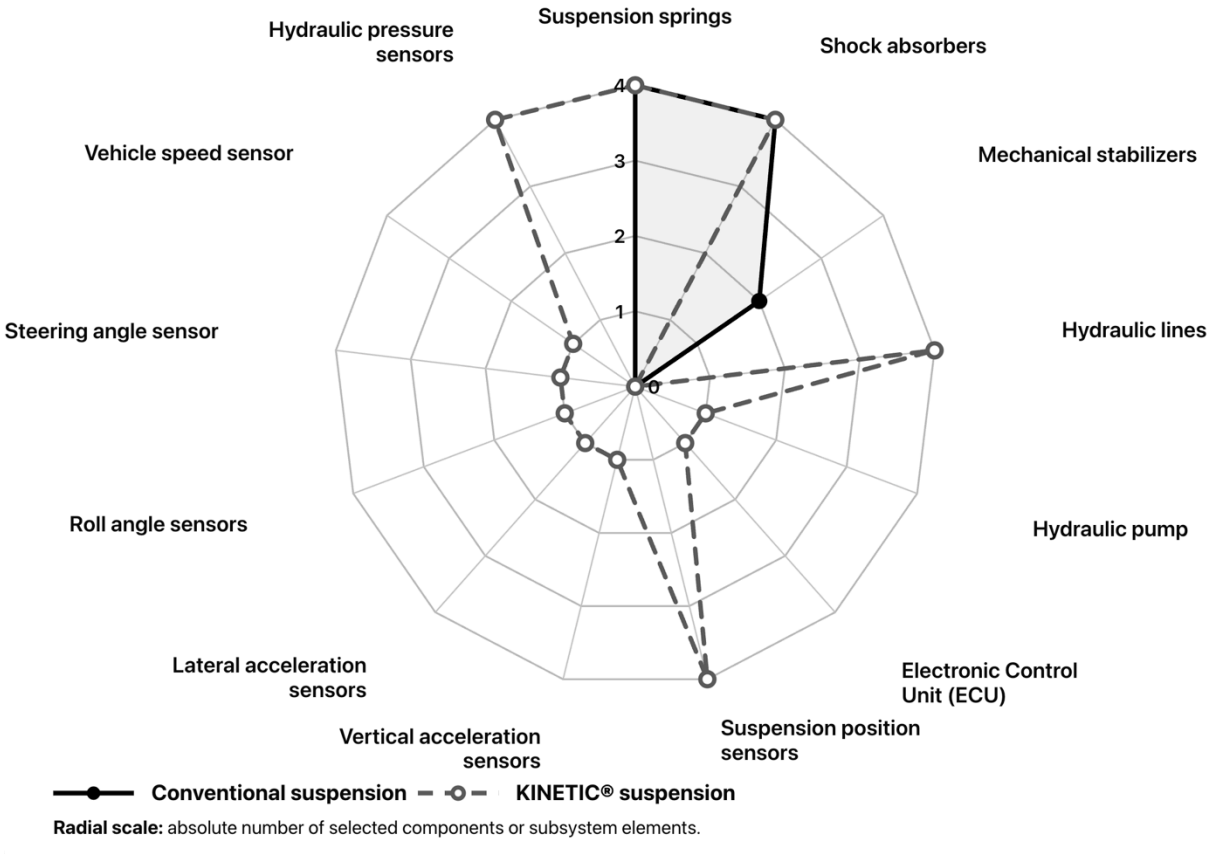


Figure 1 *Comparison of selected components and subsystems in conventional suspension and the KINETIC® system*

In the context of D-FMEA, the above is important mainly for defining the analysis boundaries. In the conventional product, the shock absorber's damping function can be analysed in greater detail within the component itself and its direct hydraulic subsystem. In the mechatronic product, however, it becomes necessary to consider a broader system context, since the way the function is performed also depends on the interaction of mechanical, hydraulic, electronic, and control subsystems, not only within the product itself [14]. This means that the difference between the analysed product groups is not only structural, but the system-related as well which directly affects how the scope of further design risk analysis should be defined.

3.2 Product-level complexity relevant to D-FMEA

At the shock absorber level, the differences between the conventional product and the mechatronic product can be presented using indicators directly related to product structure, functional scope, and the burden placed on the quality planning process. The compiled data include the number of components listed in the

Table 1 *Comparison of selected damper-level complexity and D-FMEA-relevant indicators for conventional and electronically controlled dampers*

Area	Parameter	Conventional shock absorbers	Electronically controlled shock absorbers	Implication for DFMEA and quality planning
Product and function	Product architecture	Simple mechanical architecture: cylinder body, piston rod, piston with flow valves; steel structural components.	Integrated mechatronic system: mechanics, hydraulics, electronics and control software; more extensive system architecture.	The broader set of dependencies between components and subsystems requires a more comprehensive DFMEA structure and validation strategy.
Product and function	Damping characteristic adjustment	Fixed damping characteristic; no adjustment during operation.	Real-time damping adjustment based on sensor inputs and ECU control.	Functional requirements should be linked to the control algorithm and verified across multiple operating states.
Product and function	Subsystems affecting shock absorber performance	No additional control subsystems beyond the hydraulic system of the shock absorber.	Hydraulic, electronic and mechanical subsystems operate concurrently; the ECU communicates with other vehicle systems.	Quality planning should cover cross-domain dependencies and consistency between cooperating subsystems.
Validation	Verification of damping characteristics	Assessment of a single fixed damping curve.	Higher number of functional measurements; analysis of characteristic curves for different current levels supplied to the active valve.	The test burden increases, as does the importance of a consistent validation plan.
Special characteristics	Significant characteristic	min = 28 ; max = 56	min = 30 ; max = 68	This category predominates in both groups; the range is broad and depends on shock absorber architecture and OEM requirements.
Special characteristics	Critical characteristic	min = 0 ; max = 2	min = 0 ; max = 0	Critical characteristics occur rarely; none were identified in the analysed electronically controlled shock absorbers.
Design complexity	Average number of BOM components	103	133	A higher component count broadens the scope of DFMEA and quality planning and increases the number of control points requiring coordination and verification.
Risk	Average RPN value	91	98	RPN is used here as a comparative indicator only; the observed increase does not imply that product complexity directly determines S, O or D ratings.

BOM, the number of significant characteristics, the scope of validation, and, as a supporting indicator, the average RPN values. This approach allows the moving beyond a general product description and showing its complexity at the shock absorber level, which is directly relevant to the further interpretation of D-FMEA results.

The mechatronic product shows higher values for both the number of components and the number of significant characteristics. The average values are 103 components and 42 significant characteristics for the conventional group, and 133 components and 49 significant characteristics for the electronically controlled group. These differences indicate a broader scope of controlled characteristics and a greater burden on the quality planning process, but they should not be interpreted as an automatic increase in risk in every analysed case. In this study, the RPN values were retained solely as a comparative indicator to support the analysis of the two product groups.

The comparison presented in Table 1 shows that the differences between the two analysed product groups concern not only the number of components, but the way the function is performed, the number of interacting subsystems, and the scope of confirming product performance, as well. In the conventional product, the damping function can be analysed primarily at the component and its direct hydraulic subsystem levels. In the mechatronic product, however, it is necessary to account for the interactions among mechanical, hydraulic, electronic, and control components and subsystems. From the D-FMEA perspective, this means that a broader function description is needed, together with a more developed analysis of relationships between subsystems and a stronger link between the analysis and validation.

The scope of activities used to confirm that the product meets its requirements is also an important factor. A typical validation plan included 25 to 38 tests, supplemented by additional subsystem tests where required. However, in the more complex solutions, not only did the number of tests change, but above all the scope of testing and the way the results were interpreted. In addition, separate tests were required for further subsystems. This means that, at the shock absorber level, product complexity is reflected in the product structure, the scope of functions, the number of parameters requiring control, and the scope of confirmation of compliance with requirements. This provides a direct basis for further analysis of how the preparation and execution of D-FMEA should change as product complexity increases.

Table 2 *Selected D-FMEA entries illustrating the evolution of risk interpretation for conventional and mechatronic products*

Category of Failure	Failure	Product	S	O	D	RPN	AP	Explanation of Differences
Mechanical Hydraulic	Hydraulic fluid leakage	P_1	6	4	3	72	Medium	Simple design minimizes leakage points and ensures easy detection.
		P_2	8	6	6	288	High	Advanced system critical to rollover control; leakage impacts safety significantly.
Functional	Lack of pressure control in the system	P_1	-	-	-	-	-	Not applicable to products without dynamic pressure control.
		P_2	9	5	6	270	High	Pressure imbalance destabilizes rollover control, reducing vehicle safety.
	Failure to achieve damping targets	P_1	5	3	4	60	Medium	Simple mechanical system limits the causes of damping deviations.
		P_2	7	4	6	168	High	Precision of dynamic damping control may be reduced in specific driving conditions.
Electronic	Disruptions in control system	P_1	-	-	-	-	-	Not applicable to products without electronic components.
		P_2	8	5	6	240	High	The lack of coordination between the pump and ECU disrupts the system's ability to control vehicle roll, reducing stability, can affect safety.
Assembly	Installation difficulties	P_1	5	3	3	45	Medium	Simple design ensures easy installation, with minimal risk of errors.
		P_2	8	6	7	336	High	System complexity (hydraulics, electronics) and space requirements significantly increase risk.

3.3 Selected D-FMEA entries showing the evolution of risk interpretation

The differences presented in Sections 3.1 and 3.2 are directly reflected in the way the selected D-FMEA entries are interpreted. In this subsection, the full D-FMEA analyses for both product groups are not presented; instead, a selected set of entries is used to illustrate the differences in the approach to design risk analysis between the conventional and mechatronic products. The designations P1 and P2 refer, respectively, to the two product types analysed in this article: P1 denotes the conventional product, that is, a shock absorber with a classical mechanical-hydraulic architecture, while P2 denotes the mechatronic product, that is, an electronically controlled shock absorber.

The examples presented in Table 2 show that the evolution of D-FMEA is not limited to increases in ratings for the S, O, and D criteria, but primarily involves changes in the logic of the risk interpretation. In the conventional product, many potential nonconformities can be analysed within a single component and its basic function. In the mechatronic product, the same or similar risk areas gain a broader functional context because they affect the interaction among several subsystems, the control system, and functions that depend on operating conditions. For this reason, Table 2 includes both entries common to both product types and entries not present in the conventional solution but relevant to the mechatronic product. This comparison shows that, as product complexity increases, D-FMEA must cover a broader range of functions, a larger number of relationships, and a more developed interpretation of the effects and causes of nonconformities.

3.4 Proposed approach to D-FMEA adaptation based on increasing product complexity

The proposed model (Figure 2) is termed a model because it does not define a rigid algorithm but instead provides a structured representation of the decision logic by which D-FMEA should be adapted to increasing product complexity. Its purpose is to show how the level of analysis should be selected according to the range of functional impact of a potential product failure, and how this affects the scope of review and update across component, subsystem, and system levels. The basic assumption of the model is that the analysis boundary should not be determined only by the number of components, but by the assessed range of the effects of a given failure mode, that is, whether they remain at the component level, extend to the subsystem level, or affect the function of the whole system [15]. In this approach, increasing product complexity does not mean that each D-FMEA entry must automatically be expanded, but rather that the level of review and the scope of analysis update must be selected more consciously.

The model is based on a three-level logic: component-level, subsystem-level, and system-level reviews. If the impact of a potential failure is limited to a single component, the analysis may remain at the component level. If the effects involve interactions among several components and affect the function of a subsystem, the analysis should be extended to the subsystem level. If, however, the potential failure affects the interaction between subsystems, control functions, or the fulfilment of a system-level function, a system-level review is required. The model, therefore, shows that the scope of D-FMEA should be determined primarily by the propagation of functional impact.

The second important element of the model is the link between the review level and the corresponding scope of D-FMEA review and update. In simpler solutions, the review and update may be limited to a single component and its direct function. In more complex products, however, it becomes necessary to also include the relationships among mechanical, hydraulic, electronic, and control components and subsystems. This means a shift from a local update to an update covering the broader functional context of the product, including the relationships between subsystems.

The model also defines the relationship between the D-FMEA and validation. Validation results do not serve only as confirmation but may also signal the need to extend the analysis from the component level to the subsystem or system level. In practice, this means that in more complex products, the D-FMEA should be updated not only after a component change, but when the function of a subsystem changes, when the interaction between subsystems changes, or when the scope of confirmation of product performance changes, as well. In a PLM-supported digital engineering environment, traceable links among requirements, product structures, D-FMEA records, engineering changes, and validation results can automatically flag potentially affected risks across component, subsystem, and system levels, while the final S, O, D, and AP assessments remain subject to expert evaluation. As a result, the model presents D-FMEA as a structured process, moving from component-level to multi-level analysis, carried out in line with the actual range of potential nonconformity effects.

4 Discussion

The results indicate that, as the product complexity increases, the importance of D-FMEA as a quality planning tool increase, helping structure the analysis throughout the product development process. In the case of the conventional product, many issues can still be considered within a relatively narrow scope, whereas in the mechatronic product, risk analysis requires a broader functional view of the product and consideration of the relationships between cooperating subsystems. From the perspective of industrial practice, this means

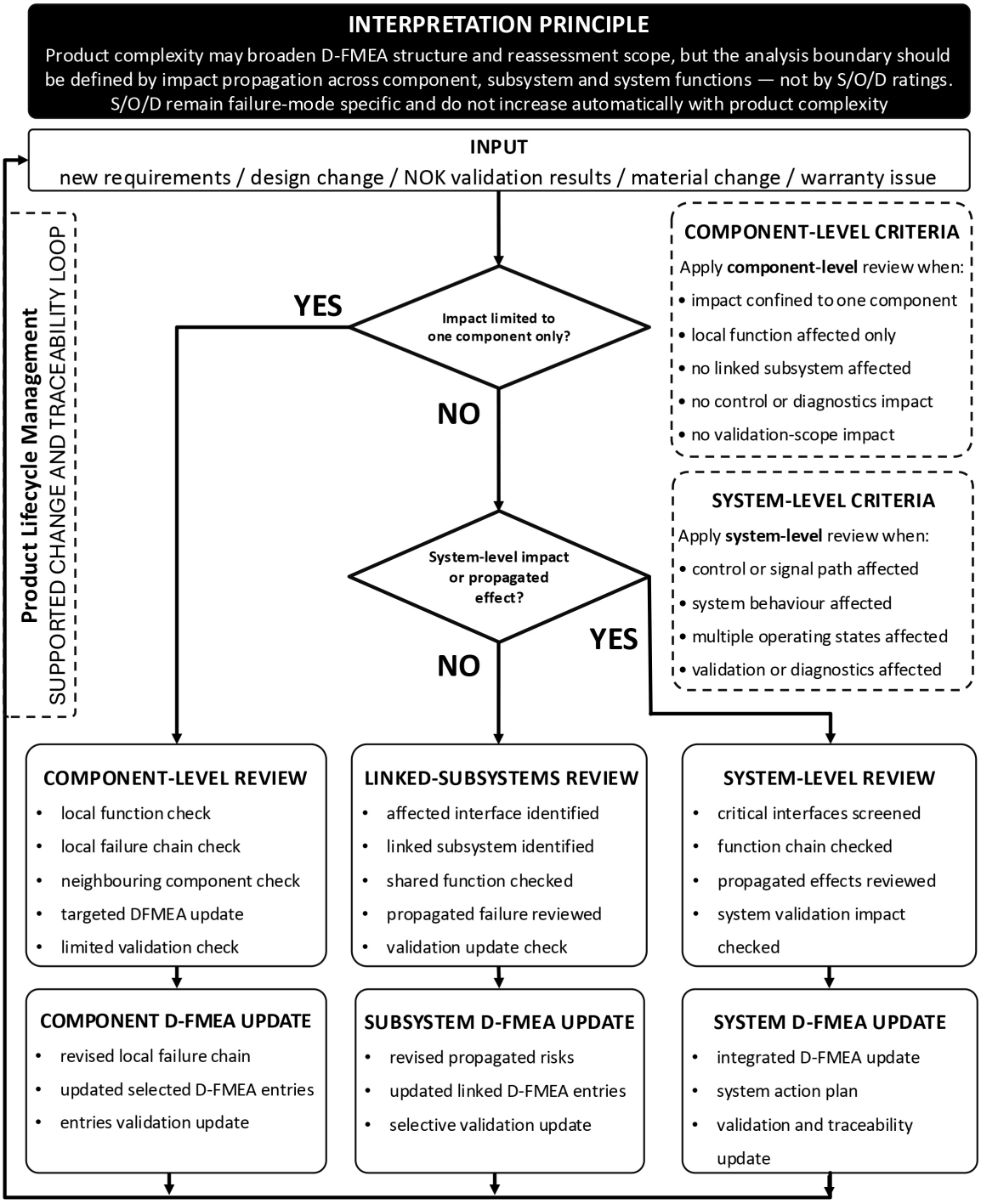


Figure 2 *Proposed model for adapting D-FMEA review and update to increasing product complexity*

that the usefulness of D-FMEA is determined not by the number of records included in the analysis, but by the consistency of the analysis structure, the correct assignment of functions, and the proper link between the analysis and verification and validation activities.

This interpretation is consistent with the approach presented by Henshall, Campean, and Rutter [16], who indicated that, for complex automotive products, one of the main problems in D-FMEA is maintaining a consistent analysis structure across the hierarchy of system, subsystems, and components, and ensuring clear links between product functions, dependencies at the boundaries between the subsystems, and verification activities. The authors also emphasised that overly extensive and inconsistent analyses, which combine different levels of detail reduce the usefulness of D-FMEA both for design improvement and for verification planning. These conclusions are reflected in the results of the present study. For the analysed shock absorbers, the difference between the conventional product and the mechatronic product is not limited to a higher number of components, but it requires extending the analysis

to areas arising from subsystem interactions as well. For this reason, the proposed model may be viewed as a practical clarification of how D-FMEA should be developed in the face of increasing product complexity, while remaining consistent with the AIAG & VDA approach.

An additional consequence of increasing the product complexity concerns the composition of the D-FMEA team. For conventional shock absorbers, the core team may be dominated by mechanical and hydraulic expertise, whereas electronically controlled products require systematic participation of specialists in electronics, embedded software, control logic, systems engineering, and validation. The team should therefore evolve not merely by increasing its size, but by aligning its expertise with the interfaces and failure-propagation paths included within the analysis boundary. A stable core team, supplemented by domain experts when subsystem- or system-level effects are reviewed, can improve the completeness of failure chains while maintaining analytical consistency. In this arrangement, the moderator should ensure that assumptions, interfaces, and responsibilities remain traceable across engineering domains [4,16].

It is also important to note that increasing the product complexity should not be interpreted as a direct cause of higher ratings for the S, O, and D criteria. In the presented results, the number of components increased by 29.1%, the number of significant characteristics by 16.7%, and the number of validation activities by 52.0%, whereas the average RPN value changed only slightly, by 7.7%. This means that greater product complexity does not automatically determine a higher risk rating in every case; rather, it changes the conditions for analysis and interpretation. From a practical point of view, the key issue is therefore not only the identification of individual failure modes, but also the proper recognition of functional relationships, which determine how detailed the D-FMEA analysis should be for a given product.

Looking ahead, the increasing dependence of mechatronic suspension systems on embedded software and networked control suggests that the proposed D-FMEA adaptation model could be complemented by Software FMEA (S-FMEA) and cybersecurity risk assessment. The S-FMEA would address unintended software failure modes related to control algorithms, timing, interfaces, and diagnostics, whereas cybersecurity analysis would consider threat-driven scenarios affecting data integrity, communication availability, or control authority. These analyses should remain methodologically distinct since the software faults and cybersecurity threats arise from different causal mechanisms, but their results should be linked at shared functions and interfaces. Such a coordinated approach could extend the proposed model towards a more complete assessment of software-intensive automotive products and constitutes a relevant direction for future research [17].

5 Conclusions

The conducted study conclusion is that increasing the product complexity primarily affects how D-FMEA is organised and carried out. The comparison of the conventional product and the mechatronic product showed that, as complexity increases, greater importance is placed on the correct definition of analysis boundaries, the level of analysis development, and the links between function analysis, risk assessment, and validation. This means that, for more complex products, D-FMEA should be developed in a more structured, multi-level manner.

At the same time, the obtained results indicate that product complexity should not be understood as an automatic increase in the values of the S, O, and D criteria. For the analysed products, a higher number of components, significant characteristics, and validation activities did not lead to a proportional increase in RPN risk ratings; rather, they mainly changed the conditions for their analysis and interpretation. Therefore, as product complexity increases, the scope and structure of the D-FMEA analysis change the most, while the ratings remain dependent on the specific failure mode, its effect, the probability of occurrence, and the possibility of detection.

Based on the obtained results, a practical conclusion can be drawn that the effective adaptation of D-FMEA to products of increasing complexity requires consistency across component, subsystem, and system levels, as well as between risk analysis and validation. The proposed model provides a structured view of the differences in the D-FMEA approach for conventional and mechatronic products and may serve as useful support for quality planning and product quality development activities.

Acknowledgment

The study was conducted as part of doctoral studies at the Joint Doctoral School under the Ministry of Science and Higher Education's 'Implementation Doctorate' program.

Conflicts of interest

The authors declare that they have no known competing financial interests or personal relationships that could have appeared to influence the work reported in this paper.

References

[1] WANG, Z., LIU, C., ZHENG, X., ZHAO, L., QIU, Y. Advancements in semi-active automotive suspension systems with magnetorheological dampers: a review. *Applied Sciences* [online]. 2024, **14**(17), 7866 [accessed 2026-03-28]. eISSN 2076-3417. Available from: https://doi.org/10.3390/app14177866

[2] YU, M., EVANGELOU, S. A., DINI, D. Advances in active suspension systems for road vehicles. *Engineering* [online]. 2024, **33**, p. 160-177 [accessed 2026-03-28]. eISSN 2096-0026. Available from: https://doi.org/10.1016/j.eng.2023.06.014

[3] RUDOLF, L., ROSZAK, M. KUCHARIKOVA, L. Evolution of the product and process requirements during the project lifetime. *Communications - Scientific Letters of the University of Zilina* [online]. 2024, **26**(4), p. B252-B259 [accessed 2026-04-11]. ISSN 1335-4205, eISSN 2585-7878. Available from: https://doi.org/10.26552/com.C.2024.049

[4] Automotive industry action group Verband der Automobilindustrie. AIAG & VDA FMEA Handbook: Design FMEA, Process FMEA, Supplemental FMEA for monitoring and system response. 1. ed. Southfield, MI: AIAG, 2019. ISBN 9781605343679.

[5] WU, Z., LIU, W. NIE, W. Literature review and prospect of the development and application of FMEA in manufacturing industry. *The International Journal of Advanced Manufacturing Technology* [online]. 2021, **112**(5-6), p. 1409-1436 [accessed 2026-03-28]. ISSN 0268-3768, eISSN 1433-3015. Available from: https://doi.org/10.1007/s00170-020-06425-0

[6] KOLOSSVARY, T., FESZTY, D. DORY, T. Systems engineering in automotive product development: a guide to initiate organisational transformation. *Journal of Open Innovation: Technology, Market, and Complexity* [online]. 2023, **9**(4), 100160 [accessed 2026-03-28]. eISSN 2199-8531. Available from: https://doi.org/10.1016/j.joitmc.2023.100160

[7] International Electrotechnical Commission. IEC 60812:2018. Failure modes and effects analysis (FMEA and FMECA). Geneva: IEC, 2018.

[8] PLINTA, D., GOLINSKA, E. DULINA, L. Practical application of the new approach to FMEA method according to AIAG and VDA reference manual. *Communications - Scientific Letters of the University of Zilina* [online]. 2021, **23**(4), p. B325-B335 [accessed 2026-03-28]. ISSN 1335-4205, eISSN 2585-7878. Available from: https://doi.org/10.26552/com.C.2021.4.B325-B335

[9] DE CARVALHO, R. A., DA HORA, H. FERNANDES, R. A process for designing innovative mechatronic products. *International Journal of Production Economics* [online]. 2021, **231**, 107887 [accessed 2026-03-28]. ISSN 0925-5273, eISSN 1873-7579. Available from: https://doi.org/10.1016/j.ijpe.2020.107887

[10] UHRI, E. ISENHARDT, I. Function-oriented development of complex mechatronic products from an HTO perspective: a systematic literature review. *Proceedings of the Design Society* [online]. 2023, **3**, p. 2085-2094 [accessed 2026-03-28]. eISSN 2732-527X. Available from: https://doi.org/10.1017/pds.2023.203

[11] RUDOLF, L. ROSZAK, M. T. Tools of product quality planning in the production part approval process. *Archives of Materials Science and Engineering* [online]. 2022, **118**(2), p. 67-74 [accessed 2026-03-28]. ISSN 1897-2764. Available from: https://doi.org/10.5604/01.3001.0016.2591

[12] MAROPOULOS, P. G. CEGLAREK, D. Design verification and validation in product lifecycle. *CIRP Annals - Manufacturing Technology* [online]. 2010, **59**(2), p. 740-759 [accessed 2026-03-28]. ISSN 0007-8506, eISSN 1726-0604. Available from: https://doi.org/10.1016/j.cirp.2010.05.005

[13] Monroe Ride Solutions - KINETIC® [online]. [accessed 2026-03-28]. Available from: https://www.monroeridesolutions.com/products/kinetic/

[14] YILDIRIM, U. CAMPEAN, F. Functional modelling of complex multi-disciplinary systems using the enhanced sequence diagram. *Research in Engineering Design* [online]. 2020, **31**, p. 429-448 [accessed 2026-03-28]. ISSN 0934-9839, eISSN 1435-6066. Available from: https://doi.org/10.1007/s00163-020-00343-8

[15] MUNK, P. NORDMANN, A. Model-based safety assessment with SysML and component fault trees: application and lessons learned. *Software and Systems Modelling* [online]. 2020, **19**, p. 889-910 [accessed 2026-03-28]. ISSN 1619-1366, eISSN 1619-1374. Available from: https://doi.org/10.1007/s10270-020-00782-w

[16] HENSHALL, E., CAMPEAN, I. F. RUTTER, B. A systems approach to the development and use of FMEA in complex automotive applications. *SAE International Journal of Materials and Manufacturing* [online]. 2014, **7**(2), p. 280-290 [accessed 2026-03-28]. ISSN 1946-3979, eISSN 1946-3987. Available from: https://doi.org/10.4271/2014-01-0740

[17] SCHMITTNER, C., GRUBER, T., PUSCHNER, P. SCHOITSCH, E. Security application of failure mode and effect analysis (FMEA). In: Computer Safety, Reliability, and Security SAFECOMP 2014: proceedings [online]. Vol. 8666. 2014. ISBN 978-3-319-10505-5, eISBN 978-3-319-10506-2, p. 310-325 [accessed 2026-07-11]. Available from: https://doi.org/10.1007/978-3-319-10506-2_21

This is an open access article distributed under the terms of the Creative Commons Attribution 4.0 International License (CC BY 4.0), which permits use, distribution, and reproduction in any medium, provided the original publication is properly cited. No use, distribution or reproduction is permitted which does not comply with these terms.

TOWARDS THE DIGITAL TWIN-ENABLED V2I MONITORING OF SHIP POWER PLANTS UNDER REAL OPERATING CONDITIONS

Andrii Holovan[1,*], Igor Gritsuk[2,3,*], Iryna Honcharuk[4], Olena Volska[5], Andrii L. Simanenkov[6], Artem A. Ivanov[6]

[1]Odessa National Maritime University, Department of Shipbuilding and Ship Repair, Odesa, Ukraine
[2]Alexander Dubcek University of Trencin, Faculty of Special Technology, Trencin, Slovakia
[3]Chernihiv Polytechnic National University, Department of Automobile Transport and Industrial Engineering, Chernihiv, Ukraine
[4]Odessa National Maritime University, Department of Navigation and Control of the Ship, Ukraine
[5]Kherson National Technical University, Department of Public Administration and Local Self-Government, Khmelnytskyi, Ukraine
[6]Kherson State Maritime Academy, Department of Ship Electrical Equipment and Automation Appliances Operation, Kherson, Ukraine

*E-mail of corresponding author: ai.onmu@ukr.net, gritsuk_iv@ukr.net

Andrii Holovan 0000-0001-6589-4381,
Iryna Honcharuk 0000-0002-5306-4206,
Andrii L. Simanenkov 0000-0003-0797-5276,
Igor Gritsuk 0000-0001-7065-6820,
Olena Volska 0000-0001-5047-4579,
Artem A. Ivanov 0000-0002-1919-2570

Resume

In this paper is presented an ITS-oriented framework for monitoring and predictive assessment of ship power plants based on V2I communication and digital twin principles. The framework integrates onboard sensor data with environmental and operational information in a unified cyber-physical environment. A mathematical model and structured algorithm support state estimation, prediction, diagnostics, and decision-making under non-stationary conditions. The distributed architecture combines onboard systems, communication networks, and infrastructure-level processing. Validation using real operational data demonstrates that the framework captures variations in vessel speed, fuel consumption, and engine performance while providing reliable parameter estimates. The results confirm its feasibility for maritime monitoring, digital twin development, and predictive maintenance.

Article info

Received 10 May 2026
Accepted 21 July 2026
Online 20 August 2026

Keywords:

intelligent transport systems
V2I communication
digital twin
remote monitoring
maritime transport
condition monitoring
cyber-physical systems

Available online: https://doi.org/10.26552/com.C.2026.047

ISSN 1335-4205 (print version)
ISSN 2585-7878 (online version)

1 Introduction

The rapid digitalization of maritime transport has stimulated the development of intelligent monitoring systems aimed at improving operational efficiency, safety, and sustainability. Modern vessels operate under dynamically changing conditions where the technical, environmental, and operational factors continuously interact. Under such non-stationary conditions, traditional onboard monitoring systems remain limited due to their reliance on isolated data sources and insufficient situational awareness.

The evolution of Intelligent Transport Systems (ITS) has enabled the integration of communication, control, and information technologies across transport domains. In maritime applications, Vehicle-to-Infrastructure (V2I) communication supports continuous data exchange between the vessels and shore-based infrastructure, enabling real-time monitoring and decision-making. However, existing maritime V2I approaches remain constrained by fragmented data integration, limited consideration of operating conditions, and communication instability.

At the same time, Digital Twin technologies have emerged as an effective approach for representing physical systems in virtual environments. By continuously synchronizing physical assets with digital counterparts, digital twins support predictive analytics,

anomaly detection, and operational optimization. Nevertheless, the integration of digital twin principles with V2I-enabled maritime monitoring systems remains insufficiently explored.

In this study is proposed an ITS-oriented framework for remote monitoring and predictive assessment of ship power plants based on V2I communication and digital twin principles. The proposed approach integrates onboard, environmental, and infrastructure-level data into a unified cyber-physical monitoring environment capable of operating under constrained communication conditions.

The main contributions of this paper include:

- development of a unified V2I-based information model for ship power plant monitoring;
- integration of environmental, transport, and human-related operating conditions into the monitoring process;
- formulation of a mathematical model for state estimation and prediction under non-stationary conditions;
- development and experimental validation of an ITS-oriented monitoring architecture using real operational data.

The remainder of the paper is organized as follows. In Section 2, related work on maritime monitoring, V2I communication, and digital twin technologies is reviewed. In Section 3, the proposed monitoring architecture is presented. In Section 4, the mathematical model is described, while in Section 5, the monitoring algorithm is introduced. In Section 6, the system implementation is discussed. In Section 7, the experimental validation results are presented, whereas in Sections 8 and 9, the discussion and conclusions are provided, respectively.

2 Related work

Ship condition monitoring is a key component of reliable maritime operation. Traditional approaches mainly rely on onboard sensor data and predefined diagnostic thresholds; however, their effectiveness is limited under the non-stationary operating conditions [1-3]. Existing systems often depend on static models and offline analysis, reducing their ability to detect unexpected faults and respond to dynamically changing conditions [3].

Recent studies indicate that insufficient integration of environmental and operational factors significantly affects monitoring accuracy [4].

In addition, measurement uncertainty, variable load conditions, and limited operational data complicate the condition assessment and predictive maintenance implementation [5]. Moreover, limited availability of detailed usage data and operational profiles restricts the effectiveness of predictive maintenance strategies.

To improve monitoring performance, recent research has explored multivariate modelling, intelligent diagnostics, and advanced sensor configurations [6-7]. Nevertheless, subsystem-level diagnostics and vibration-based monitoring still face limitations under the variable operating conditions [8-9]. As a result, the integration of heterogeneous data sources for reliable real-time monitoring remains an open research problem.

The development of ITS has enabled new approaches to maritime monitoring through distributed communication and data processing technologies. Modern maritime systems increasingly rely on IoT networks, multi-sensor data fusion, and advanced situational awareness tools to support real-time decision-making [10-14].

However, the majority of existing studies focus on individual aspects of maritime monitoring, including visualization [15], satellite-based analysis [16], or onboard situational awareness systems [17-18], rather than integrated vessel-infrastructure interaction. Although the role of interconnected sensor networks and real-time data exchange was emphasized in several studies [11-12], the comprehensive V2I-enabled monitoring architectures for maritime ITS applications remain insufficiently developed.

Digital twin technologies have emerged as an effective approach for monitoring, prediction, and optimization in maritime transport systems. By continuously synchronizing physical assets with virtual models, digital twins support predictive maintenance and operational decision-making [19-21].

Recent studies demonstrated the integration of artificial intelligence, IoT technologies, and data-driven analytics into digital twin frameworks to improve prediction accuracy and operational efficiency [22]. Several researchers also highlighted the potential of combining digital twins with communication technologies, including V2I systems, to enhance situational awareness and distributed monitoring capabilities.

Despite these advances, the majority of existing approaches addressed the digital twins and communication infrastructures separately. Therefore, integrated frameworks combining digital twin methodologies with V2I-enabled ITS architectures for real-time maritime monitoring and prediction remain insufficiently explored.

The analysis of existing studies shows that the ship condition monitoring, ITS technologies, and digital twin applications are still largely developed independently. Current approaches lack comprehensive integration of onboard and external data, reliable operation under non-stationary conditions, and unified predictive capabilities.

In this study are addressed these limitations by proposing an ITS-oriented monitoring framework that integrates V2I communication and digital twin principles for remote monitoring and predictive assessment of ship power plants under real operating conditions.

3 System concept and ITS architecture

The proposed monitoring framework is developed as a cyber-physical component of an Intelligent Transport System (ITS), enabling continuous interaction between the vessel, onboard systems, and transport infrastructure through V2I communication. The ship is considered as an integrated system combining the power plant, onboard information systems, operators, operating conditions, and maritime infrastructure.

The general interaction scheme of the proposed ITS-based monitoring framework is presented in Figure 1.

The core of the proposed framework is a V2I communication layer that enables the data exchange between the onboard and infrastructure-level systems. The monitoring architecture consists of three interconnected levels:

- onboard level, including sensors and local processing modules;
- V2I communication level responsible for data

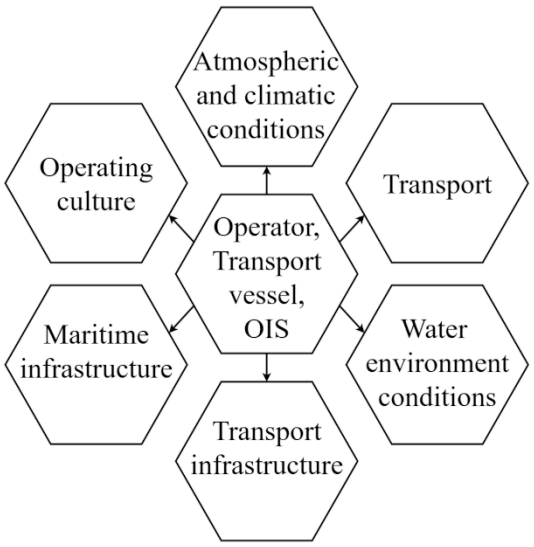


Figure 1 *General scheme of system interaction in the ITS-based monitoring framework*

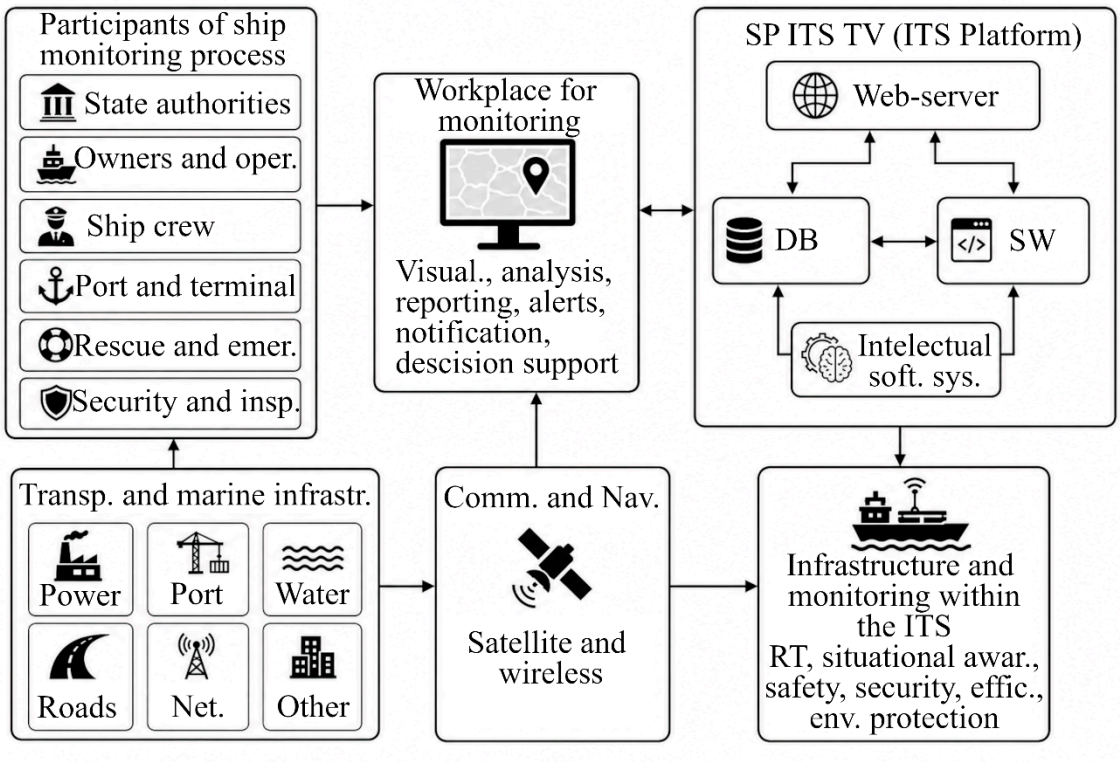


Figure 2 *The V2I-based information exchange between onboard systems and transport infrastructure*

transmission;

- infrastructure level, including servers, databases, and analytical tools.

This distributed architecture enables the continuous monitoring under limited communication bandwidth by allocating processing tasks between onboard and shore-based components. The information exchange structure is shown in Figure 2.

A key feature of the proposed approach is the integration of operating conditions into the monitoring process. The framework considers environmental, transport, atmospheric, and human-related factors affecting the ship power plant performance, including sea state, traffic density, climatic conditions, and operator-related influences.

The classification of operating conditions and their integration into the monitoring framework are summarized in Table 1.

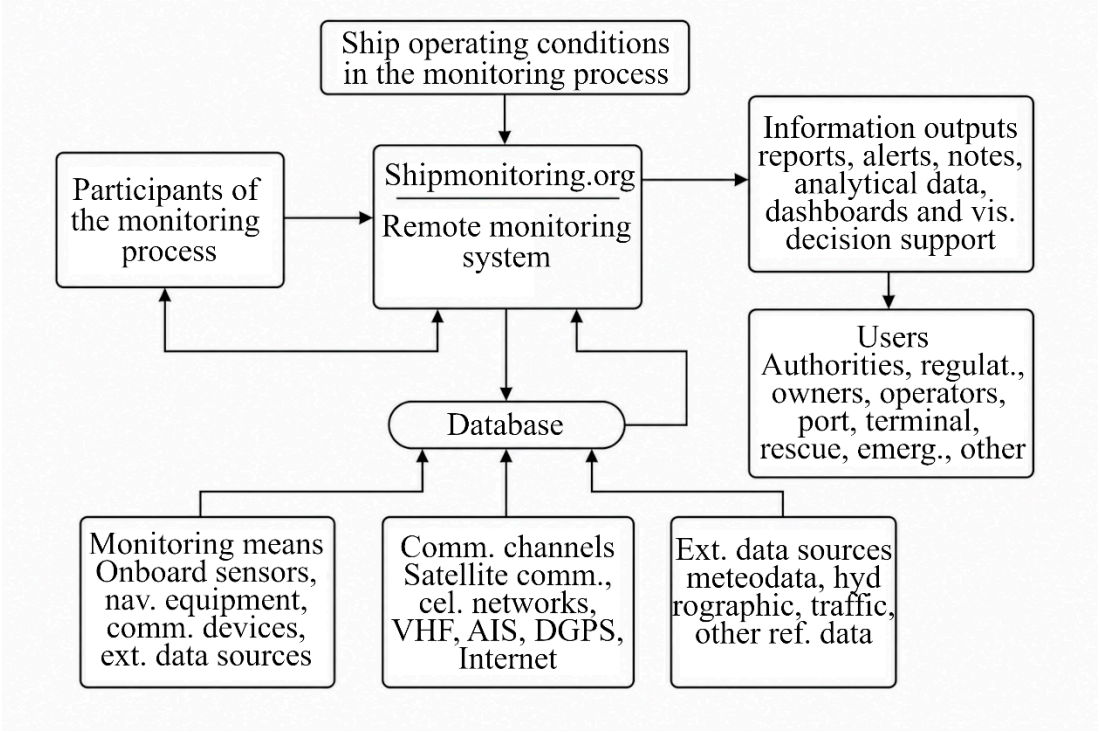


Figure 3 *Data flow diagram of the ITS-based ship monitoring system*

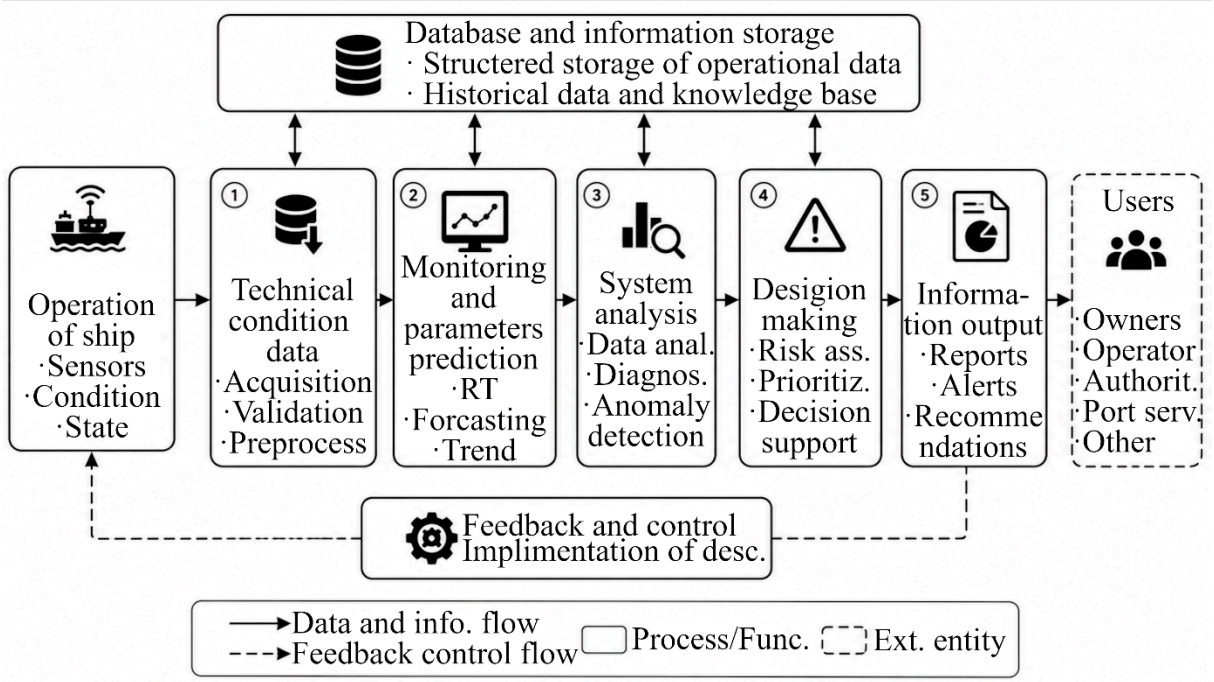


Figure 4 *Structured V2I-based information model of the transport ship monitoring system*

Table 1 *Classification of operating conditions and their integration within the ITS monitoring framework*

Main classification features of the operating conditions		ITS Information opportunities		Notes
		OIS	Maritime and transport infrastructure	
Water environment conditions	Seawater temperature	+	+ (-)	*
	Seawater density	+ (-)	- (+)	*
	Presence of undercurrents	-	+ (-)	*
	Altitude	+	+	
	Depth under the vessel keel	+	-	
	Fairway Width	-	+	
	The presence of resistance to movement (physical objects of artificial and natural origin)	- (+)	+ (-)	*
	Ship's hull fouling	- (+)	+ (-)	
Transport conditions	Type of cargo carried	+	- (+)	*
	Ship traffic density	- (+)	+	*
	Driving mode	+	- (+)	*
	Movement speed	+	+	
Atmospheric and climatic conditions	Air temperature	+	+	
	Air pressure	+	-	
	Air humidity	+	+	
	Precipitation	-	+	
	Visibility	-	+	
Operating culture	Level of work organization and management	- (+)	+	*
	Operator(s) qualifications and diligence	- (+)	-	*
	Compliance with the provisions of technical regulations and rules of technical operation	- (+)	+	*
	Repair and maintenance material and technical base of the vessel and transport infrastructure	+ (-)	+	
	Quality of shipboard maintenance materials	- (+)	- (+)	*

The monitoring framework is implemented as a distributed information system combining onboard data acquisition modules, communication subsystems, databases, and data processing tools. Information exchange between the system components is represented using a data flow approach, as illustrated in Figure 3.

The monitoring process includes vessel identification, acquisition of technical parameters, integration of operating conditions, state prediction, diagnostics, and decision support. The structured V2I information model describing these interactions is presented in Figure 4.

The proposed framework forms a basis for the development of a digital twin of the ship power plant. Continuous acquisition and processing of real-time data enable synchronization between physical and digital system states, supporting predictive analysis and operational optimization.

Thus, the proposed ITS-oriented architecture provides a foundation for the future integration of advanced digital twin technologies into maritime transport systems.

4 Mathematical model of monitoring and prediction

The monitoring of a ship power plant under the real operating conditions is considered as a dynamic process within a cyber-physical transport system integrating onboard, environmental, and infrastructure-level data through V2I communication.

The technical state of the ship power plant is represented as a multidimensional vector:

$$Y(t) = \{y_1(t), y_2(t), \ldots, y_m(t)\}, \quad (1)$$

where $y_i(t)$ denotes measurable parameters such as engine speed, fuel consumption, exhaust gas temperature, and load characteristics.

Operating conditions are represented as:

$$O(t) = \{o_1(t), o_2(t), \ldots, o_p(t)\}, \quad (2)$$

including environmental, transport, and human-related factors.

The monitoring process is defined as the integration

of technical and operating condition data into a unified system representation:

$$Y_{TCP,VOP}(t) = A_{TCP}(Y_{TCP}(t)) \circ A_{VOP}(Y_{VOP}(t)), \quad (3)$$

where: Y_{TCP} - technical condition parameters, Y_{VOP} - operating condition parameters, A_{TCP},A_{VOP} - transformation operators, $\circ$ - composition operator.

The estimated technical state is obtained as:

$$\hat{Y}(t) = f(S(t), O(t)), \quad (4)$$

where: $S(t)$ - onboard sensor data, $O(t)$ - operating conditions, $f(\cdot)$ - estimation function.

Future system behavior is predicted using the historical and current state data:

$$\hat{Y}(t + k\Delta t) = F(\hat{Y}(t), H(t - n : t)), \quad (5)$$

where: $H(t - n : t)$ - historical data, k - prediction horizon, Δt - time step.

The system operates within a distributed information environment:

$$I = \{C, L, N\}, \quad (6)$$

where: C - cloud-based infrastructure, L - local onboard data sources, N - networked databases.

The proposed model forms a functional basis for a digital twin of the ship power plant. The estimated state $\hat{Y}(t)$ represents the digital counterpart of the physical system, while the prediction model supports forward simulation and scenario analysis.

5 Monitoring algorithm and data processing

Algorithm 1: V2I-Based Monitoring and Prediction of Ship Power Plant State

Input:

- Onboard sensor data $S(t)$
- Operating conditions data $O(t)$
- Historical data $H(t - n : t)$;

Output:

- Estimated technical state $\hat{Y}(t)$
- Predicted technical state $\hat{Y}(t + k\Delta t)$.

Step 1: Data Acquisition.

Acquire the real-time onboard sensor and navigation data together with external information obtained via V2I communication.

Step 2: Data Synchronization and Preprocessing.

Synchronize the heterogeneous data streams, remove outliers, filter noise, and normalize parameters.

Step 3: Feature Extraction.

Generate derived indicators describing the current operating state of the ship power plant.

Step 4: State Estimation.

Integrate onboard and external data to estimate the current technical state of the power plant:

$$\hat{Y}(t) = f(S(t), O(t)). \quad (7)$$

Step 5: Prediction of Technical State.

Use historical observations and current state estimates to predict future system behavior:

$$\hat{Y}(t + k\Delta t) = F(\hat{Y}(t), H(t - n : t)). \quad (8)$$

Step 6: Diagnostics and V2I Exchange.

Detect anomalies, generate diagnostic indicators, and exchange processed data with infrastructure-level systems.

Step 7: Visualization and Decision Support.

Present monitoring results and operational recommendations to the operator.

6 Implementation of the V2I monitoring system

The proposed monitoring framework is implemented as a distributed cyber-physical system within an ITS environment, integrating onboard subsystems, communication channels, and infrastructure-level components. The system includes onboard data acquisition and diagnostic modules, an onboard information system (OIS), V2I communication interfaces, infrastructure-level servers and databases, and data visualization tools.

The monitoring framework operates as a distributed telecommunications network supporting continuous data collection, transmission, storage, and analysis under real operating conditions.

The system integrates heterogeneous onboard and external data sources obtained through the V2I communication, including:

- onboard sensor data (engine parameters, fuel consumption, diagnostics);
- navigation data (GPS-based position and speed);
- environmental data (weather conditions, sea state);
- infrastructure-based data (traffic conditions, maritime information systems).

These data sources form a unified information environment for monitoring and predictive analysis. Additional information sources include ship geolocation data, maritime infrastructure models, weather services, and ship tracking systems.

The data processing architecture is designed for operation under limited communication bandwidth by distributing computational tasks between onboard and infrastructure-level components.

The primary processing, including filtering, aggregation, and preliminary diagnostics, is performed onboard, while advanced analysis and storage are executed within infrastructure-level systems. This approach reduces communication load while preserving monitoring continuity.

6.1 Functional capabilities of the monitoring system

The implemented system supports: real-time monitoring of ship power plant parameters; integration of operating conditions into diagnostics; anomaly detection and diagnostic code generation; prediction of system behavior based on historical data; decision support for operational adjustments.

The framework also enables continuous archiving and visualization of monitoring results.

Within the ITS framework, the proposed system functions as a distributed monitoring node enabling interaction between vessels and transport infrastructure through V2I communication.

Continuous data acquisition and processing provide the basis for a digital twin of the ship power plant, supporting the state estimation, prediction, and scenario analysis. This enables the transition from reactive monitoring toward predictive and prescriptive maintenance strategies.

7 Experimental results and validation

Experimental validation of the proposed V2I-based monitoring framework was performed using the real operational data obtained from a transport vessel operating under varying environmental and transport conditions. The onboard information system collected time-series data from the key ship power plant subsystems, including engine rotational speed, exhaust gas turbocharger (EGT) parameters, auxiliary generator load, fuel consumption, and GPS-based vessel speed.

The initial data acquisition frequency was 1 s and it was later aggregated to 60 s intervals for stable analysis. External weather and navigation data were integrated via V2I communication channels. The dataset corresponds to a voyage segment of approximately 497 nautical miles (921 km) and contains more than 40,000 measurement points.

The dataset includes synchronized onboard and external data streams representing technical, operational, and environmental conditions. The monitored variables were grouped into technical parameters (engine speed, fuel consumption, EGT characteristics), operational parameters (vessel speed and load conditions), and environmental influences affecting system behavior.

The temporal variation of the key operational parameters is presented in Figures 5-7. The obtained results demonstrate: a strong dependency of fuel consumption on vessel speed and engine load; observable variations in engine performance under changing operating conditions; the capability of the monitoring system to capture transient behavior in non-stationary environments.

In Figure 8 are compared the measured and estimated fuel consumption values, demonstrating the consistency of the proposed monitoring model.

The performance of the proposed framework was evaluated using Mean Absolute Error (MAE), Root Mean Square Error (RMSE), and the correlation

Table 2 *Comparison of measured and estimated parameters*

Parameter	Measured (avg)	Estimated (avg)	MAE	RMSE	R
Vessel speed (knots)	9.8	9.5	0.32	0.41	0.96
Fuel consumption (kg/h)	1850	1790	65	82	0.94
EGT speed (rpm)	9200	9050	110	145	0.92

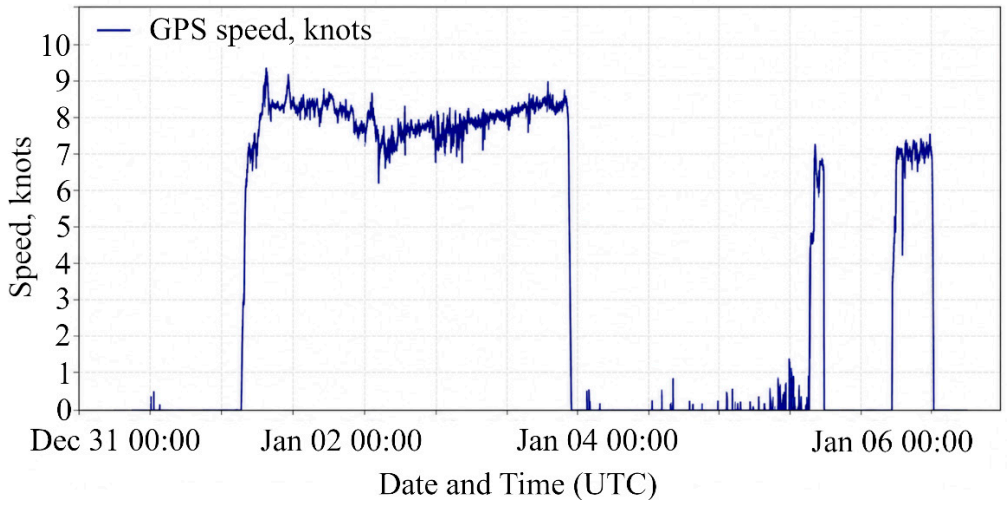


Figure 5 *Temporal variation of the vessel speed during the monitored voyage segment*

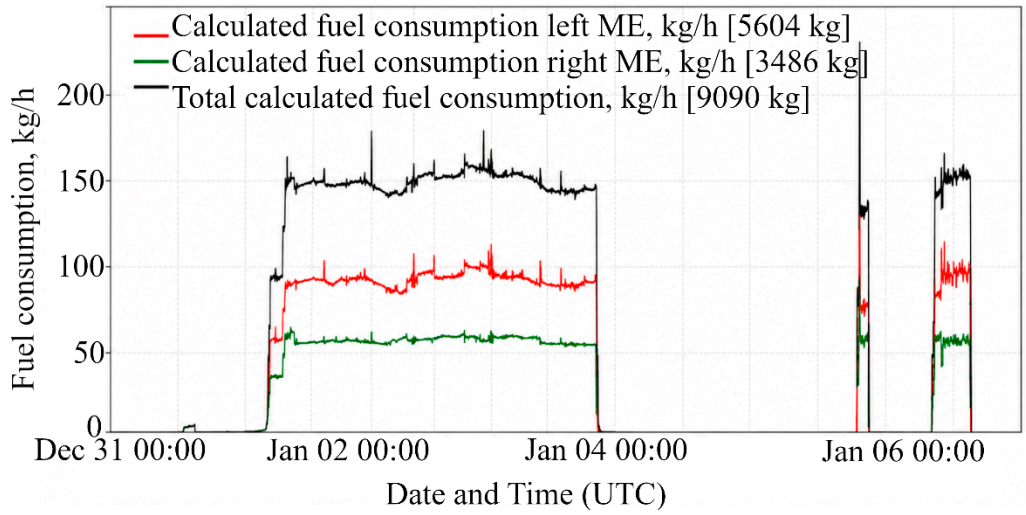


Figure 6 *Temporal variation of the fuel consumption during the monitored voyage segment*

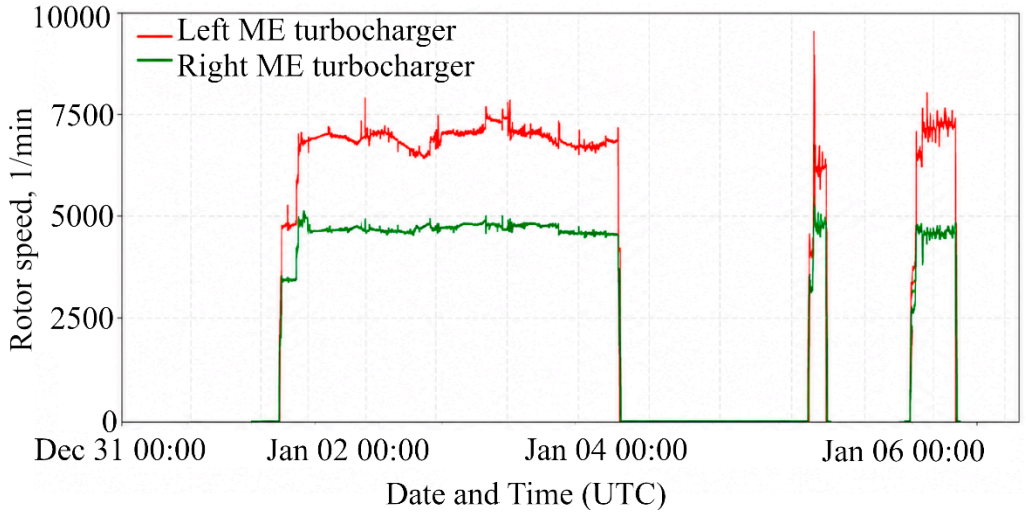


Figure 7 *Temporal variation of the main engine turbocharger rotor speed during the monitored voyage segment*

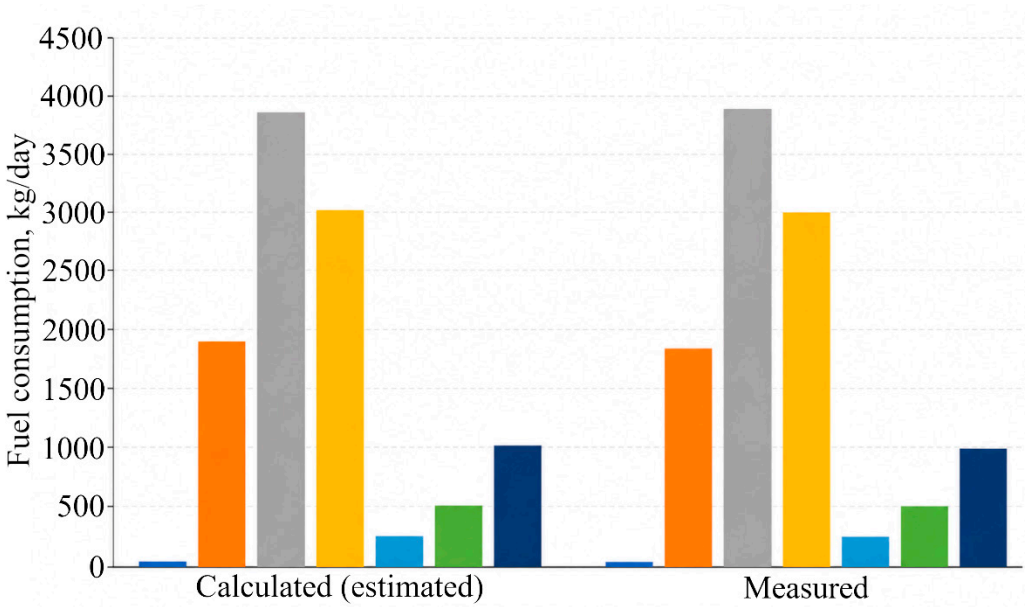


Figure 8 *Comparison of measured and model-estimated daily fuel consumption*

coefficient (R):

$$MAE = \frac{1}{N}\sum_{i=1}^{N}|Y_i - \hat{Y}_i|, \tag{9}$$

$$RMSE = \sqrt{\frac{1}{N}\sum_{i=1}^{N}(Y_i - \hat{Y}_i)^2}, \tag{10}$$

$$R = \frac{\sum(Y_i - \bar{Y})(\hat{Y}_i - \bar{\hat{Y}})}{\sqrt{\sum(Y_i - \bar{Y})^2 \sum(\hat{Y}_i - \bar{\hat{Y}})^2}}. \tag{11}$$

The calculated metrics are summarized in Table 2.

The results show a close agreement between the measured and estimated values, confirming the adequacy of the proposed model for representing the system behavior under real operating conditions. The results demonstrate the strong agreement between the measured and estimated values, with correlation coefficients exceeding 0.9 for all analyzed parameters. The results obtained confirm the capability of the proposed framework to integrate heterogeneous data sources and provide reliable estimation of ship power plant performance under non-stationary operating conditions.

From an ITS perspective, the proposed approach demonstrates the feasibility of distributed monitoring systems supporting real-time interaction between vessels and transport infrastructure.

8 Discussion

The obtained results demonstrate the feasibility of integrating V2I communication with onboard monitoring systems to create an ITS-oriented framework for maritime applications. The proposed approach enables continuous interaction between vessels and transport infrastructure while integrating onboard and external data into a unified monitoring environment.

A key advantage of the framework is its ability to operate under the non-stationary conditions and limited communication bandwidth through distributed onboard and infrastructure-level processing. In addition, the proposed approach introduces digital twin elements that support real-time monitoring and predictive assessment of ship power plant behavior.

However, the proposed model has several limitations. The prediction framework is based on simplified functional relationships and does not yet incorporate advanced machine learning methods. Moreover, experimental validation was conducted using data from a specific vessel and operational scenario, which may limit the generalizability of the results. System performance also depends on the availability and quality of the sensor data.

From an ITS perspective, the proposed framework contributes to the development of distributed cyber-physical maritime transport systems supporting situational awareness and data-driven decision-making. The approach can be further extended towards the fleet-level monitoring and integration with broader maritime transport infrastructures.

Future research should focus on integrating machine learning techniques, developing full-scale digital twin implementations, and extending the framework to multi-vessel and large-scale maritime transport systems.

9 Conclusions

In this paper is presented an ITS-oriented framework for the remote monitoring and predictive assessment of ship power plants based on V2I communication and digital twin principles. The proposed approach integrates onboard and external operating data into a unified cyber-physical monitoring environment.

A mathematical model for the state estimation and prediction under non-stationary operating conditions was developed together with a structured monitoring algorithm supporting real-time data acquisition, diagnostics, and decision-making. The monitoring architecture was implemented as a distributed system combining onboard subsystems, communication networks, and infrastructure-level components.

Experimental validation using real operational data demonstrated the capability of the proposed framework to capture variations in vessel speed, fuel consumption, and engine performance parameters under real operating conditions. Quantitative analysis confirmed strong agreement between the measured and estimated values, indicating the adequacy of the proposed model.

From an ITS perspective, the framework supports the development of distributed maritime monitoring systems that improve situational awareness and enable data-driven operational decision-making. In addition, the proposed approach provides a functional basis for the development of digital twins of ship power plants, supporting predictive analysis and advanced maintenance strategies.

Future work should focus on the integration of machine learning methods and the extension of the proposed framework to multi-vessel and large-scale maritime transport systems.

Acknowledgment

The authors received no financial support for the research, authorship and/or publication of this article.

Conflicts of interest

The authors declare that they have no known competing financial interests or personal relationships that could have appeared to influence the work reported in this paper.

References

[1] GRITSUK, I., ZAGLINSKIS, J. Features of the data collection and transmission technology in an intelligent thermal conditioning system for engines and vehicles operating on thermal energy storage technology based on a digital twin. *Machines* [online]. 2026, 14(1), 130. eISSN 2075-1702. Available from: https://doi.org/10.3390/machines14010130

[2] BILKA, M., GRITSUK, I., HOLOVAN, A., VOLSKA, O., HONCHARUK, I., KOHUTIAR, M., KRBATA, M. Digital twin-based assessment and forecasting of marine plate heat exchanger performance under variable operating conditions. *Machines* [online]. 2026, 14(5), 497. eISSN 2075-1702. Available from: https://doi.org/10.3390/machines14050497

[3] XU, X., YAN, X., YANG, K., ZHAO, J., SHENG, C., YUAN, C. Review of condition monitoring and fault diagnosis for marine power systems. *Transportation Safety and Environment* [online]. 2021, 3(2), p. 85-102. eISSN 2631-4428. Available from: https://doi.org/10.1093/tse/tdab005

[4] PARK, M., KIM, H., LEE, S., LEE, J. Anomaly detection and root cause analysis of ship main engines: explainable artificial intelligence-based methodology considering internal sensors and external environmental factors. *Journal of the Korean Institute of Industrial Engineers (JKIIE)* [online]. 2023, 49(5), p. 379-394. ISSN 1225-0988, eISSN 2234-6457. Available from: https://doi.org/10.7232/JKIIE.2023.49.5.379

[5] SHARKO, O., STEPANCHIKOV, D., SHARKO, A., YANENKO, A. Computer diagnostics of the condition of ship rolling bearings during their operation. *Science-Based Technologies* [online]. 2024, 63(3), p. 409-418. ISSN 2075-0781, eISSN 2310-5461. Available from: https://doi.org/10.18372/2310-5461.63.18952

[6] ZHANG, P., GAO, Z., CAO, L., DONG, F., ZOU, Y., WANG, K., ZHANG, Y., SUN, P. Marine systems and equipment prognostics and health management: a systematic review from health condition monitoring to maintenance strategy. *Machines* [online]. 2022, 10(2), 72. eISSN 2075-1702. Available from: https://doi.org/10.3390/machines10020072

[7] FU, C., LU, K., LI, Q., XU, Y., GU, F., BALL, A. D., ZHENG, Z. Physics-based modelling for on-line condition monitoring of a marine engine system. *Journal of Marine Science and Engineering* [online]. 2023, 11(6), 1241. eISSN 2077-1312. Available from: https://doi.org/10.3390/jmse11061241

[8] MAILULA, K. O., SAHA, A. K. A Comprehensive review of shaft voltages and bearing currents, measurements and monitoring systems in large turbogenerators. *Energies* [online]. 2025, 18(8), 2067. eISSN 1996-1073. Available from: https://doi.org/10.3390/en18082067

[9] SUN, J., SUN, P., LIN, B., LI, W. Evolution of shipboard motor failure monitoring technology: multi-physics field mechanism modelling and intelligent operation and maintenance system integration. *Energies* [online]. 2025, 18(16), 4336. eISSN 1996-1073. Available from: https://doi.org/10.3390/en18164336

[10] FORTI, N., D'AFFLISIO, E., BRACA, P., MILLEFIORI, L. M., CARNIEL, S., WILLETT, P. Next-gen intelligent situational awareness systems for maritime surveillance and autonomous navigation [point of view]. *Proceedings of the IEEE* [online]. 2022, 110(10), p. 1532-1537. ISSN 0018-9219, eISSN 1558-2256. Available from: https://doi.org/10.1109/JPROC.2022.3194445

[11] FLENKER, T., STOPPE, J. MARLIN: An IoT sensor network for improving maritime situational awareness. In: European Workshop on Maritime Systems Resilience and Security MARESEC 2021: proceeding [online]. 2021. Available from: https://doi.org/10.5281/ZENODO.5603378

[12] IBOKETTE, A. I., OGUNDARE, T. O., DANQUAH, E. O., ANYEBE, A. P., AGABA, J. A. Optimizing maritime communication networks with virtualization, containerization and IoT to address scalability and real - time data processing challenges in vessel - to - shore communication. *Global Journal of Engineering and Technology Advances* [online]. 2024, 20(2), p. 135-174. eISSN 2582-5003. Available from: https://doi.org/10.30574/gjeta.2024.20.2.0156

[13] MORANDO, E., DAFFINA, F. C., STAHL, T., CORVINO, M. M., PRATOLA, C. Multi-sensor data fusion to enhance maritime situational awareness. In: IEEE International Geoscience and Remote Sensing Symposium IGARSS 2023: proceedings [online]. IEEE. 2023. eISSN 2153-7003, eISBN 979-8-3503-2010-7, p. 6829-6831. Available from: https://doi.org/10.1109/IGARSS52108.2023.10282392

[14] PETERSEN, C., PIEPER, F., BOKERN, A., STEIDEL, M. Enhancing situation awareness in highly automated shipping using high-resolution electronic navigational charts. In: 4th European Workshop on Maritime Systems, Resilience and Security 2024 MARESEC 24: proceedings [online]. 2024. Available from: https://doi.org/10.5281/ZENODO.14214326

[15] CAMOSSI, E., LAVIGNE, V., MCKENZIE, M., RAY, C., TRABER-BURDIN, S., VARGA, M. Advancing maritime situational awareness with visual analytics and complex systems. In: 2025 29th International Conference Information Visualisation IV: proceedings [online]. IEEE. 2025. eISSN 2375-0138, eISBN 979-8-3315-7741-4, p. 32-37. Available from: https://doi.org/10.1109/IV68685.2025.00018

[16] DEL PRETE, R., SALVOLDI, M., BARRETTA, D., LONGEPE, N., MEONI, G., KARNIELI, A., GRAZIANO, M. D., RENGA, A. Enhancing maritime situational awareness through end-to-end onboard raw data analysis. *IEEE*

Journal of Selected Topics in Applied Earth Observations and Remote Sensing [online]. 2025, 18, p. 16997-17018. ISSN 1939-1404, eISSN 2151-1535. Available from: https://doi.org/10.1109/JSTARS.2025.3584999

[17] GONZALEZ, I. I., RAPADO, A. G., GARCIA, I. L., JIMENEZ, M. P. Situational awareness for maritime surveillance. In: European Workshop on Maritime Systems Resilience and Security MARESEC 2021: proceedings [online]. 2021. Available from: https://doi.org/10.5281/ZENODO.5604019

[18] TROUPIOTIS-KAPELIARIS, A., SPILIOPOULOS, G., GRIGOROPOULOS, G., FILIPPOU, E., CHAMATIDIS, I., VODAS, M., KALIORAKIS, M., ZISSIS, D. A digital twin for maritime situational awareness. In: IEEE/ACM 10th International Conference on Big Data Computing, Applications and Technologies BDCAT '23: proceedings [online]. ACM. 2023. ISBN 979-8-4007-0473-4, p. 1-2. Available from: https://doi.org/10.1145/3632366.3632378

[19] GOLOVAN, A., MATEICHYK, V., GRITSUK, I., LAVROV, A., SMIESZEK, M., HONCHARUK, I., VOLSKA, O. Enhancing information exchange in ship maintenance through digital twins and IoT: a comprehensive framework. *Computers* [online]. 2024, 13(10), 261. eISSN 2073-431X. Available from: https://doi.org/10.3390/computers13100261

[20] GRIGOROPOULOS, G., SPILIOPOULOS, G., CHAMATIDIS, I., KALIORAKIS, M., TROUPIOTIS-KAPELIARIS, A., VODAS, M., FILIPPOU, E., CHONDRODIMA, E., PELEKIS, N, THEODORIDIS, Y., ZISSIS, D., BERETA, K. A Scalable system for maritime route and event forecasting. In: 27th International Conference on Extending Database Technology EDBT/ICDT 2024 Joint Conference: proceedings [online]. 2024. ISSN 2367-2005, ISBN 978-3-89318-095-0, p. 762-769. Available from: https://doi.org/10.48786/edbt.2024.66

[21] FERNANDES, A., GUTIERRES, D., FUGIHARA, M., DE NORMAN, B. Port management digital twin and control tower integration: an approach to support real-time decision making. In: 2024 Winter Simulation Conference WSC 2024: proceedings [online]. IEEE. 2024. eISSN 1558-4305, eISBN 979-8-3315-3420-2, p 2821-2831. Available from: https://doi.org/10.1109/WSC63780.2024.10838965

[22] ILIAS, L., TSAPELAS, G., KAPSALIS, P., MICHALAKOPOULOS, V., KORMPAKIS, G., MOUZAKITIS, S., ASKOUNIS, D. Leveraging extreme scale analytics, AI and digital twins for maritime digitalization: the VesselAI architecture. *Frontiers in Big Data* [online]. 2023, 6, 1220348. eISSN 2624-909X. Available from: https://doi.org/10.3389/fdata.2023.1220348

This is an open access article distributed under the terms of the Creative Commons Attribution 4.0 International License (CC BY 4.0), which permits use, distribution, and reproduction in any medium, provided the original publication is properly cited. No use, distribution or reproduction is permitted which does not comply with these terms.

EVALUATION AND EXPERIMENTAL VALIDATION OF POWER CONVERTER TOPOLOGIES FOR A BIDIRECTIONAL GRID-CONNECTED BATTERY ENERGY STORAGE SYSTEM

Michal Praženica[1,*], Patrik Resutík[1], Slavomír Kaščák[1], Michal Prídala[2], Martin Kuchař[3]

[1]University of Zilina, Faculty of Electrical Engineering and Information Technology, Department of Mechatronics and Electronics, Zilina, Slovakia
[2]A2B s. r. o., Zilina - Povazsky Chlmec, Slovakia
[3]VSB - Technical University of Ostrava, Faculty of Electrical Engineering and Computer Science, Department of Applied Electronics, Ostrava, Czech Republic

*E-mail of corresponding author: michal.prazenica@uniza.sk

Michal Praženica 0000-0003-0894-7090, Patrik Resutík 0000-0001-6643-4045,
Slavomír Kaščák 0000-0001-7294-0438, Martin Kuchař 0000-0003-3390-5650

Resume

In this research is described the topology assessment, design, simulation, and experimental verification of bidirectional grid connected BESS. Several converter topologies were assessed based on the efficiency, power quality, bidirectional capability, electromagnetic compatibility, and ease of implementation. A bridgeless totem-pole PFC converter, together with bidirectional CLLLC resonant DC/DC converter, was chosen and implemented in 2 kW lab prototype. Experimental tests in both grid-to-battery and battery-to-grid modes yielded maximum power of 2.28 kW, a power factor of 1.0, total current harmonics of 1.43%, and maximum efficiency of around 96%. These results show the suitability of the architecture chosen for bidirectional energy storage systems and grid connected energy management, renewable energy integration, and electric vehicle charging and V2G applications.

Article info

Received 12 June 2026
Accepted 31 August 2026
Online 24 September 2026

Keywords:

active compensation system
battery storage system
bidirectional power flow
grid connected system

Available online: https://doi.org/10.26552/com.C.2026.055

ISSN 1335-4205 (print version)
ISSN 2585-7878 (online version)

1 Introduction

Active compensation systems (ACS) represent a modern approach to optimizing the electricity consumption, as they can play a key role in this process. These systems help to reduce harmonic distortions in electrical networks, losses in distribution networks, and increase a power system efficiency. Implementing these technologies allows not only to reduce costs but to stabilize electricity supplies, as well [1-3].

An important key element in saving electricity is energy storage, which allows the accumulation of energy in periods of excess and, conversely, its use when the energy demand is higher. In this way, it is also possible to contribute to stabilizing energy networks and support using renewable energy sources. These energy storages can be based on different technologies (mechanical, thermal, electrochemical, etc.). The current trend is storage based on batteries (especially lithium or lead) [4-5].

Another important aspect is the reuse and second-life utilization of battery systems or components, especially battery recycling (especially the possibility of using batteries from electric cars and the like) [6-8]. This attitude would primarily contribute to reducing the environmental impact by reducing waste and emissions created [9-11].

Active compensation systems (ACS) can be used in industrial facilities, commercial buildings, and even homes, helping to reduce operating costs. Another great benefit of these ACS systems is the possibility of connecting them with systems of renewable energy sources such as solar, wind, geothermal, or others [12-14].

Another area of use of ACS is residential urban and local areas. Current trends also indicate that the

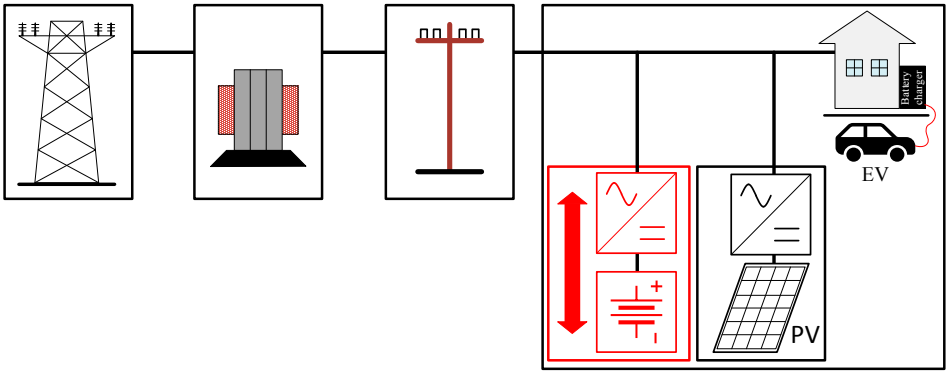


Figure 1 *Configuration of ACS for combined applications*

Table 1 *Main contributions of the paper*

Contribution	Description
Topology evaluation	Comparison of BLTP-PFC, DAB and CLLLC solutions
Experimental validation	Verification on 2 kW laboratory prototype
Bidirectional operation	Charging and discharging modes verified
Power quality analysis	PF = 1 and THD_i = 1.43 %
Transport applicability	Suitability for EV charging and V2G operation

importance of using the ACS systems is significantly more complex, as they enable applications in Grid-to-Vehicle (G2V) or Vehicle-to-Grid (V2G) modes and support applications with renewable energy sources, Figure 1, [12, 15-19].

In the presented article are compared converter topologies suitable for implementing an ACS system for electrical energy compensation consisting of several parts and presents its initial implementation and verification, Table 1.

Unlike many previously published ACS and BESS solutions that focus either on converter design or on simulation-based evaluation, the presented work provides a comprehensive comparison of bidirectional converter topologies and experimentally validates a complete ACS architecture combining a bridgeless totem-pole PFC (BLTP-PFC) stage and a bidirectional resonant converter (CLLLC).

The proposed architecture achieves high power quality (PF = 1, THDi = 1.43 %) together with bidirectional operation and high efficiency, which makes it suitable for future smart-grid and transport-energy applications.

The ACS prototype uses two operating modes for basic verification of the principle of operation:

1. Mode - accumulation of energy from the grid to the batteries (accumulation mode),

2. Mode - supply of energy from the batteries to the grid (generative mode).

Based on the test results of the ACS system prototype, further stages will continue, focused on active compensation of negative phenomena in the electrical grid and the possibilities of their optimization.

2 ACS components

Active compensation systems (ACS) using electrical energy storage systems represent very complex devices, especially in terms of technical implementation and equipment, measurement of necessary quantities and corresponding control algorithms. From the point of view of safe and correct operation of the electrical network, the development of ACS systems and the development of necessary control algorithms to control these complex systems to achieve the required properties is important [12].

From the point of view of the power electronic part, they can be generally divided into three basic parts, Figure 2. All used parts of the system must operate in bidirectional operation to achieve the highest possible efficiency, stability, safety and dynamics.

The first part of the ACS system consists of the input-output system, which forms the interface between the electrical network and the energy storage. These are suitable bidirectional PFC converters, or Four-Quadrant Converter (4QC) [20]. The converter operates as a controlled rectifier in Mode 1 (accumulation mode), and as an inverter in Mode 2 (generative mode).

The second part of the ACS system deals with the optimal transfer of DC energy to and from the battery storage, i.e., suitable DC/DC converters. As suitable DC/DC converters can be considered bidirectional CLLLC [21-23] or DAB converter [24-27]. The converter operates in BUCK mode in Mode 1 (accumulation mode), and in BOOST mode in Mode 2 (generative mode).

The last part of the ACS system concerns the

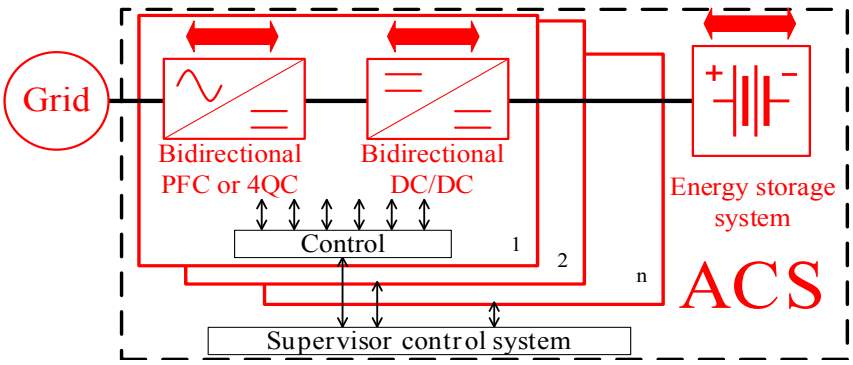


Figure 2 *Block configuration of the ACS system*

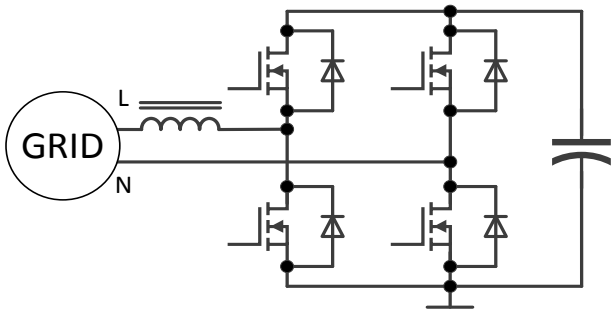


Figure 3 *Bridgeless totem-pole PFC*

battery storage systems themselves. Many professional and scientific articles are devoted to this issue [28-32].

2.1 PFC selection

As mentioned above, the first part of the ACS system consists of an input-output converter, which forms the interface between the electrical network and the energy storage. This converter operates as a controlled rectifier in Mode 1 (accumulation mode) and as an inverter in Mode 2 (generative mode). Based on these requirements, it is possible to choose a bidirectional PFC or 4QC topology for the first stage. Considering the nominal power, complexity, and overall requirements for the implemented system, the bidirectional PFC topology was chosen.

Within the used PFC converter topologies, one of the significant sources of power losses is the input bridge rectifier, which converts the AC input current into the high-voltage DC current required for the power factor correction (*PFC*) circuit. At lower AC voltages, high powers and at full load, the bridge rectifier can be responsible for 2% to 3% of the total output power loss due to line inefficiency [33-34].

For this reason, the bridgeless boost PFC topology has become popular. It has gained attention as a more efficient alternative because it eliminates the need for an input rectifier bridge, thereby reducing conduction losses [35-36].

The selection of a PFC converter topology for the DC power flow is usually a question of the need to achieve the required level of transmitted power. It is possible to choose from the following topologies: classic boost PFC, double boost PFC, or one of the latest totem-pole PFC topologies. However, the selection of a PFC topology suitable for bidirectional power flow and for application in ACS is not so difficult nowadays. The Bridgeless Totem-Pole Power Factor Corrector (*BLTP-PFC*), Figure 3, is a topology with the smallest number of switching elements, which allows for bidirectional power flow, which is essential for ACS systems, and at the same time provides high efficiency. However, to achieve the desired properties, it is necessary to properly design and select the PFC inductance, semiconductor switches, output filter capacitors and control circuit of the entire PFC system. Semiconductor switches can be further divided into slow (MOSFETs, switching with the frequency of the power grid) and fast (GaN, switching the detailed current waveform). Another important part is the circuit for measuring the mains voltages and currents that the converter draws from or supplies to the power grid.

2.2 DC/DC converter selection

The bidirectional DC/DC power stage works as a battery charger in one direction - accumulation mode (*BUCK mode - Mode 1*) and as a constant voltage converter when operating in the opposite direction - generative mode (*BOOST mode - Mode 2*). The battery voltage level depends upon the system power level. In addition to the necessity of bidirectional energy flow, high inverter efficiency is also an important feature. For

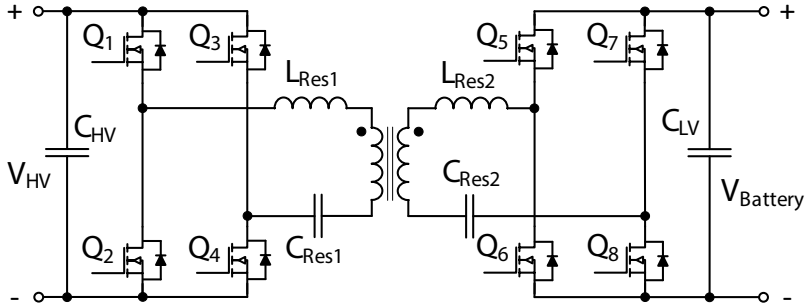


Figure 4 *CLLLC resonant topology*

isolated bidirectional power stages, resonant CLLLC converter and Dual Active Bridge (*DAB*) topologies are commonly used, providing suitable properties for ACS systems.

2.2.1 CLLLC resonant topology

The CLLLC resonant topology is a highly efficient, symmetric bidirectional DC-DC converter architecture widely used in modern power electronics. CLLLC, Figure 4, is derived from popular LLC and uses all its advantages. One major advantage is using the secondary switches to obtain bidirectional power transfer which is most important for ACS system applications. This topology can be used for power levels up to 10 kW.

The resonant tank must be symmetrical (symmetrical design will ensure similar behavior during both charge and discharge cycles). This topology achieves Zero-Voltage Switching (ZVS) on the primary bridge and Zero-Current/Zero-Voltage Switching (ZCS/ZVS) on the secondary bridge, which drastically lowers the switching losses and enables high-frequency operation. Capacitors used in the resonant tank naturally prevent the saturation of the transformer core. The integration of minimalized resonant components combined with high operating frequencies (often 500 kHz up to 1 MHz) minimizes the overall volume of the converter. Due to soft-switching characteristics, superior Electromagnetic Interference (EMI) performance is achieved. This topology uses identical transmission characteristics for both power flow directions, simplifying the control system. Frequency-pulse modulation is a standard control technique for CLLLC converters [21-23].

2.2.2 Dual Active Bridge (DAB) topology

Among different topologies, the Dual Active Bridge (DAB) converter, Figure 5, is increasingly popular for its isolation, natural bidirectional operation, high power density, and ability to perform soft switching. The DAB converter is well-suited for efficient bidirectional energy conversion with high power density, making it appropriate for applications where the power needs to be transferred over a wide voltage range, especially in low-voltage energy storage. The operation of the DAB converter relies on the phase difference between the primary and secondary bridge voltages and on the interaction of two active full bridges via the high-frequency transformer and the energy-transfer inductance. By controlling the power transfer through the phase difference, the conditions for soft-switching and for minimizing switching losses are achieved, leading to high efficiency.

Numerous publications were focused on the design of DAB converters for medium- and high-power applications, such as EV charging, energy storage systems, and the integration of renewable energy sources. They addressed issues related to the modulation scheme, efficiency, wide voltage regulation range, and the use of digital controllers. Low-power isolated DC-DC converters are discussed much less frequently and detailed guidelines for design, testing, and implementation are lacking [24-26].

At the same time, there are specific challenges associated with DAB converter design, including transformer optimization, leakage inductance selection, semiconductor switching loss reduction, control system stability, and cooling. The topology can operate with a wide range of battery voltages. However, it exhibits a high circulating current, which contributes significantly to reduction in efficiency. Another disadvantage of the topology is the loss of ZVS at low load. These disadvantages can be eliminated by using further modulation modes (Dual phase shift and triple phase shift), which increases the complexity of the system control [27].

Finally, based on the comparison in Table 2, based on the application requirements for low EMI and high efficiency, the CLLLC topology was selected for its superior performance in high-power applications where efficiency, low EMI, and thermal management are critical. The resonant design of the CLLLC enables the zero-voltage switching (ZVS) and zero-current switching (ZCS), significantly reducing switching losses and improving efficiency over a wide load range. In addition, its EMI suppression makes it suitable for noise-sensitive applications. Although it requires more complex control and potentially a larger number of passive components, the benefits in reliability, efficiency, and reduced cooling requirements justify these tradeoffs. This makes the

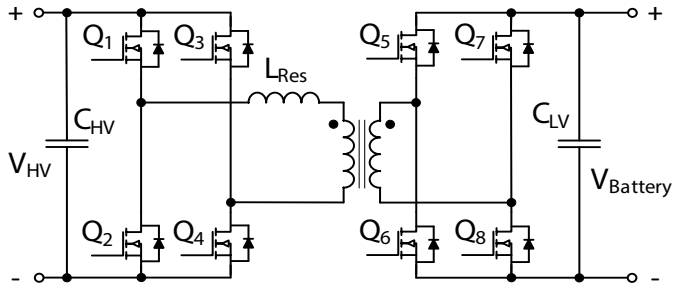


Figure 5 *Dual Active Bridge (DAB) topology*

Table 2 *DC/DC converters comparison*

Parameter	CLLLC	DAB
Soft switching	Excellent	Moderate
EMI	Low	Medium
Control complexity	Medium	High
Circulating current	Low	High
Efficiency	High	Medium-High
ACS suitability	Excellent	Good

CLLLC topology optimal for achieving high performance in demanding, high-power environments.

The resulting topology of the ACS system was a combination of bridgeless totem PFC (BLTP-PFC) and bidirectional CLLLC converter, which was subjected to simulation and experimental verification of operation.

2.2.3 Energy Storage Systems

The Energy storage systems (ESS) absorb electrical energy from the energy sources - such as solar panels, wind turbines or the electrical grid and store it. When needed, this energy can then be used for power generation. They play a key role in balancing supply and demand in the grid, mitigating the intermittency of renewable energy supplies and providing reliable backup power.

The Energy Storage Systems (ESS) can be implemented as purely battery-based (Battery Energy Storage Systems - BSS) or as hybrid (Hybrid Energy Storage Systems - HESS).

Battery energy systems (BSS) are a key pillar of modern energy transformation, grid stability and renewable energy integration (RES).

With the increasing share of solar and wind power plants, whose production is unstable and dependent on the weather, a backup (system) is needed to balance the mismatch between electricity production and consumption. BESS systems can absorb excess energy during times of overproduction and feed it back into the grid during times of deficit or peak. In addition to supporting RES, they serve to provide support services (frequency and voltage stabilization), optimize costs through charging during times of low tariffs (arbitrage), reduce reserved capacity (peak reduction), and ensure uninterrupted power supply (UPS) for critical infrastructure [28-32].

For the ACS system, a battery storage system was designed consisting of LiFePO4 batteries LFP48150U5E, V_{NOM} 48V, 150Ah, 7200Wh, capacity according to requirements (according to the number of battery modules), maximum 96kWh [37].

2.2.4 Final structure of ASC and control architecture

As mentioned in the previous sections, the final topology of the ACS system consists of an input EMI filter, BLTP-PFC and CLLLC converter and battery storage, Figure 6.

The ACS control system is very complex and intricate and its description is not the primary subject of this article. This issue will be addressed in detail in further research and the results will be published in detail.

The ACS control system must process a large amount of data in real time, for example: sensing of quantities - grid voltage and current, battery voltage and current, inverter and battery temperatures, relay control, BLTP-PFC and CLLLC converter control, CAN communication, sensing data from the superior system and defining the magnitudes and directions of power flows, parallelization, HW and SW protection, and many others.

The control architecture of the proposed ACS consists of two independently controlled power conversion stages (BLTP-PFC and CLLLC) interconnected by a common DC-link capacitor. The first stage (BLTP-PFC) is

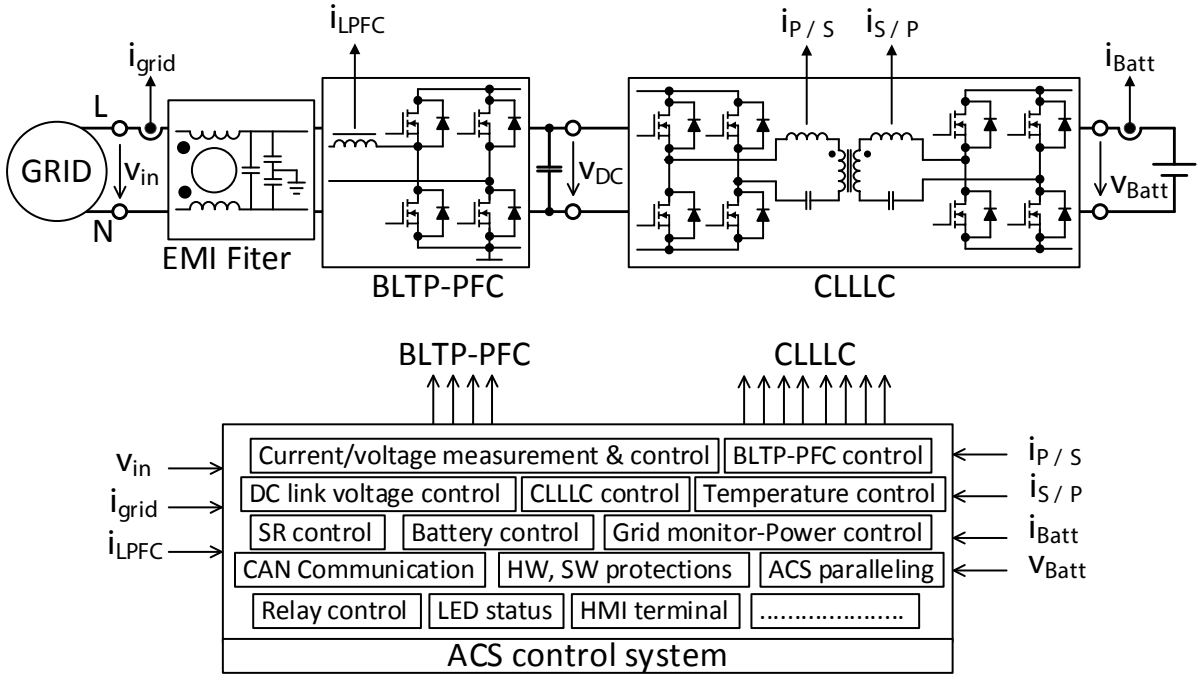


Figure 6 *Final structure of ASC system*

responsible for the grid interface, whereas the second stage (CLLLC) is responsible for battery charging and discharging. The overall control strategy follows a hierarchical structure. The BLTP-PFC converter controls the power exchange with the utility grid, while maintaining a regulated DC-link voltage. The CLLLC converter independently controls the battery current or battery voltage according to the selected operating mode. The DC-link capacitor therefore acts as an energy buffer separating the dynamics of the grid-side converter from the battery-side converter.

The complete control architecture consists of three principal control loops:

1. Grid synchronization and current control (BLTP-PFC),
2. DC-link voltage regulation,
3. Battery charging/discharging control (CLLLC converter).

This hierarchical arrangement allows both converters to operate independently while maintaining stable bidirectional power transfer.

The BLTP-PFC converter operates as a current-controlled voltage-source converter synchronized with the supply grid; switching frequency is 70 kHz. The grid voltage is continuously measured and processed using a Phase-Locked Loop (PLL), which generates the instantaneous phase angle required for current synchronization. The outer (slower) voltage-control loop regulates the DC-link voltage by comparing the measured DC-link voltage with its reference value. The resulting controller output defines the required active current reference. The inner (fast) current-control loop regulates the converter input current so that it accurately follows the sinusoidal reference synchronized with the grid voltage. Consequently, the converter achieves nearly unity power factor and very low harmonic current distortion. Depending on the operating mode, the sign of the reference current determines the direction of power flow. During the battery charging, the converter behaves as an active rectifier drawing sinusoidal current from the grid. During the battery discharging, the current reference is reversed, allowing the converter to inject active power back into the utility grid while maintaining synchronized operation.

The DC-link capacitor principally electrically decouples the grid-side converter from the battery-side converter and represents the main intermediate energy storage element. The DC-link voltage is continuously monitored and regulated to a constant reference value of approximately 415 V. A cascaded control structure is used. The outer voltage controller determines the required active power transferred through the BLTP-PFC converter, while the fast inner current controller ensures rapid dynamic current response.

The second stage (CLLLC) transmits power controlled by changing the switching frequency around the resonant frequency (140 kHz) of the resonant tank. During the battery charging, the converter operates in BUCK mode. The battery charging current is regulated according to the charging profile while maintaining stable DC-link operation. During the battery discharging, the converter operates in BOOST mode. The switching frequency is automatically adjusted to maintain the required DC-link power under varying battery voltage conditions. For battery voltages below the nominal value, the switching frequency decreases below the resonant frequency in order to increase the converter voltage gain. Conversely, operation above resonance

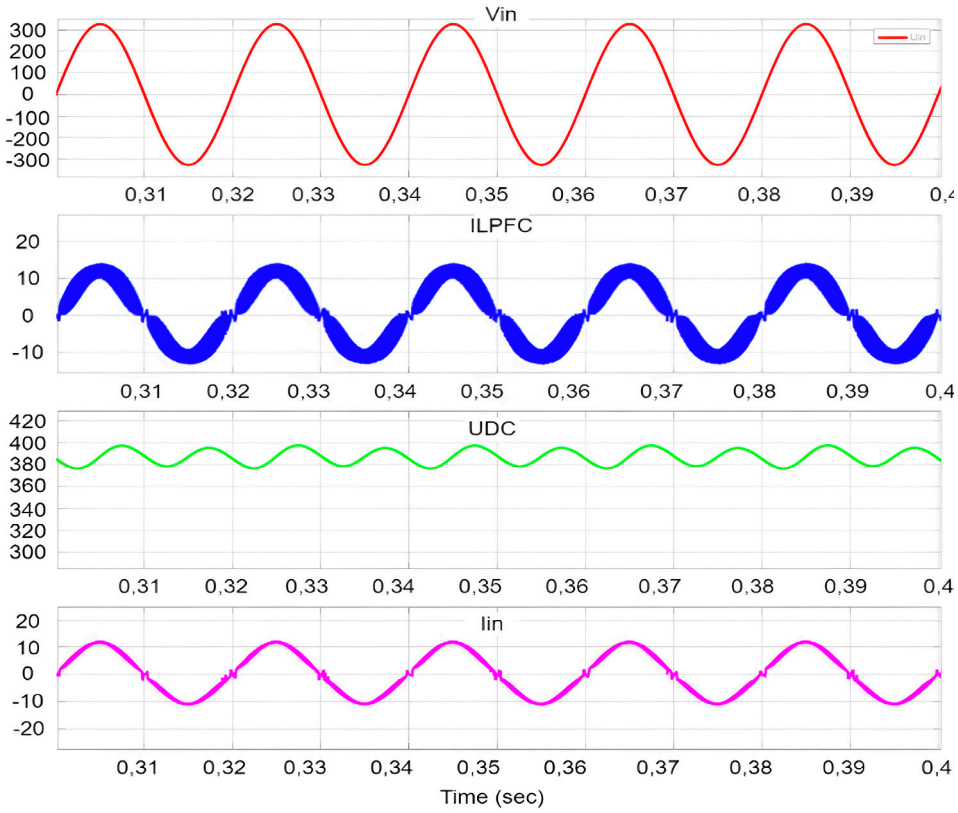


Figure 7 *Simulated BLTP-PFC waveforms, rectifier mode at full power*

reduces the voltage gain while preserving soft-switching conditions.

The frequency-control strategy enables Zero-Voltage Switching (ZVS) and Zero-Current Switching (ZCS) over a wide operating range, contributing to the high efficiency experimentally verified in this work (what is an advantage of this topology).

The advantage of this topology is that the switching frequency control strategy allows zero voltage switching (ZVS) and zero current switching (ZCS) over a wide operating range, which contributes to high efficiency, which is also verified in this paper.

3 Simulation verification

Simulation tests were performed to verify the correct function of the proposed solutions for individual inverter topologies of the ACS system. As a part of the simulation testing, models of the bidirectional BLTP-PFC and bidirectional CLLLC inverter were verified in both operating modes: Mode 1 (accumulation mode, battery charging) and Mode 2 (generative mode, inverter).

3.1 BLTP-PFC simulation

A BLTP-PFC simulation model was created to verify the PFC converter's functionality and features. This converter was tested in both work modes - in Mode 1 (accumulation mode, operates as a controlled rectifier) and in Mode 2 (generative mode, operates as an inverter). These waveforms show the input voltage v_{IN} (red), the i_{LPFC} inductor current (blue), the DC bus voltage v_{DC} (green), and the input current i_{IN} (magenta).

At the input, the inverter is connected to the grid, so it is important to focus on the shape of the input current i_{IN}, which is directly related to THD_i. Another quantity worth noting is the current through the main inductor of the i_{LPFC}.

The first waveforms represent the valid results for a total output power of 2 kW in the rectifier mode of the BLTP-PFC converter, Figure 7. Similar waveforms represent the results in the inverter mode at the same power 2 kW, Figure 8. In this case the BLTP-PFC works as a VSI inverter and transfers energy from DC bus back to the main grid. In this mode of operation, it is necessary to achieve the desired current shape, as well which directly determines the THD.

3.2 The CLLLC simulation

The resonant CLLLC converter was simulated in two modes of operation depending on the direction of the energy flow. In Mode 1 for the direction of energy flow to the battery, the DC/DC converter is in BUCK mode, Figure 9. This Figure shows the transformer primary current i_p (green) and the transformer secondary current

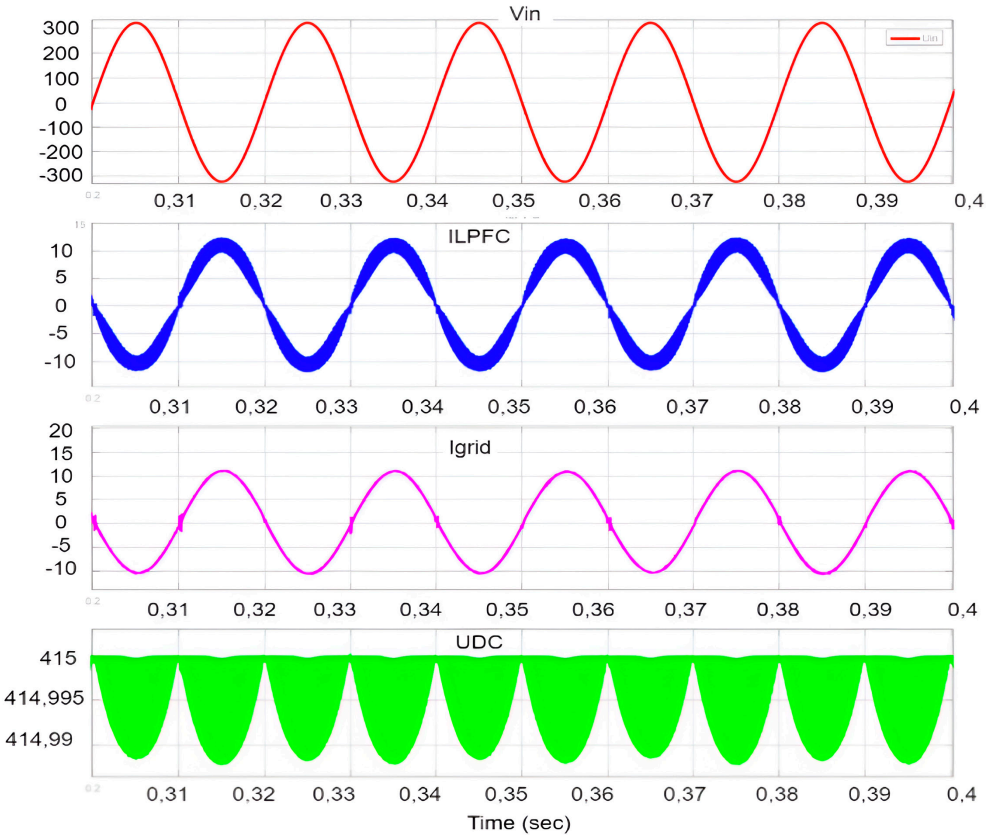


Figure 8 *Simulated BLTP-PFC waveforms, inverter mode at full power*

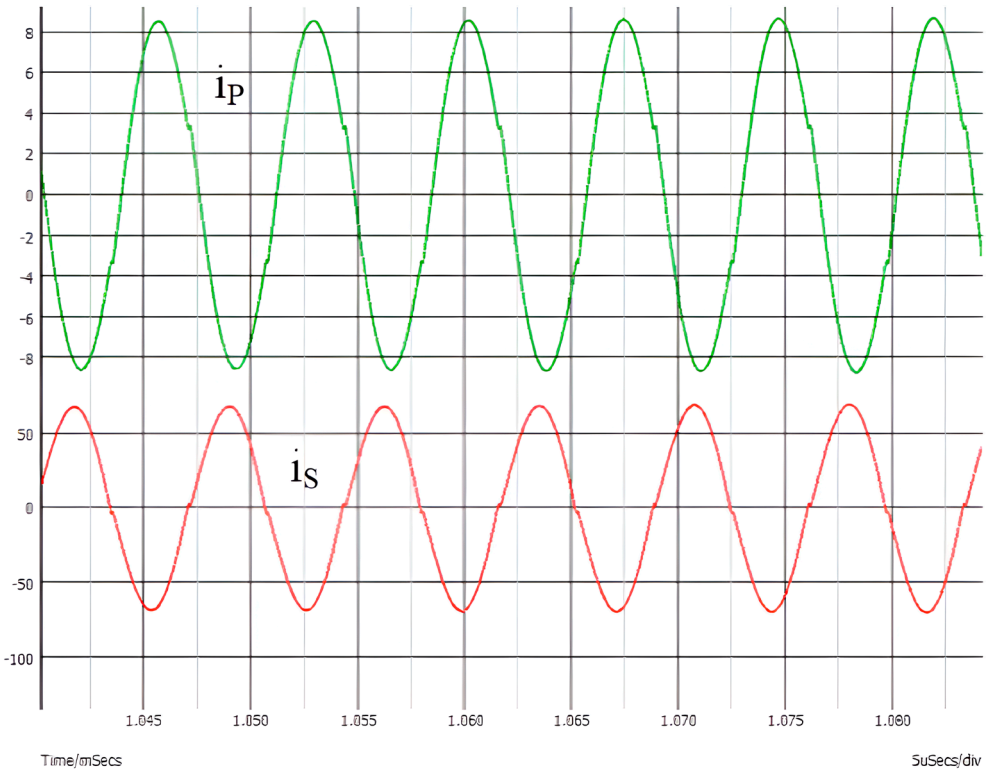


Figure 9 *The CLLLC converter BUCK mode*

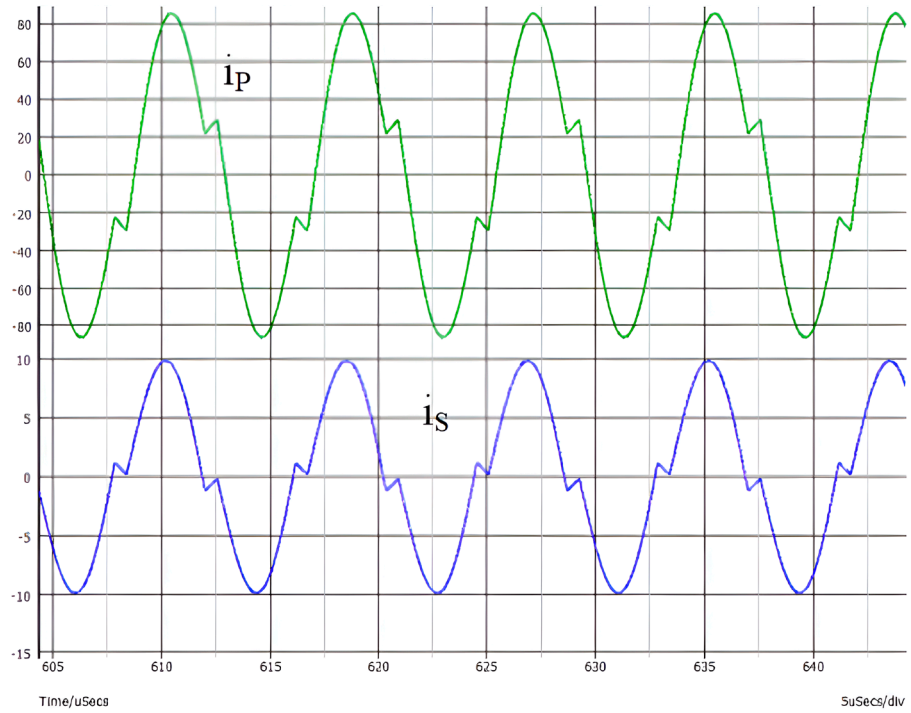


Figure 10 *The CLLLC converter BOOST mode*

Table 3 *Designed ACS prototype specification*

Parameter	Value
Nominal power [kW]	2
Nominal input voltage [V]	230
Nominal interlink capacitor voltage [V]	415
Switching frequency BLTP-PFC [kHz]	70
Switching frequency CLLLC [kHz]	140
Battery nominal voltage [V]	48
Battery capacity [Ah]	150

i_S (red) - battery charging current. Conversely, in Mode 2, the direction of energy flow is from the battery to the grid, which represents BOOST mode of converter. Figure 10 also shows the transformer primary current i_P (green) and the transformer secondary current i_S (blue) - battery discharging current (see Figure 4.)

From a control perspective, this condition in Mode 2 was simulated for the specific case where the converter is operating below the rated input voltage (below 48 V). In order for the control loop to provide the required power transfer at a lower input voltage, the switching frequency f_{SW} had to be reduced below the resonant frequency f_{RES} of the resonant circuit and thus the magnetizing component of the current is significantly more visible.

4 Experimental verification

Table 3 shows the parameters of the designed ASC system prototype. As described above, the experimental prototype of the ACS system consisted of a bidirectional BLTP-PFC and a bidirectional resonant CLLLC DC/DC converter. A LiFePo4 battery LFP48150U5E was used as an energy storage. To verify the correct operation, both converters were first independently verified and tested in laboratory conditions.

4.1 The BLTP-PFC verification

The BLTP-PFC converter was tested in both operating modes. The first measurement, Mode 1 - rectifier mode, was carried out at a nominal output power of 2 kW. Figure 11 shows the waveforms of the input voltage, which is also the grid voltage, i.e., $v_{IN} = V_{GRID}$ (magenta) and input current i_{IN} (yellow). The input voltage and current are in phase, so the inverter draws the necessary power from the grid (active power). The waveform of the consumed current shows a low content of higher harmonic components and almost zero phase shift.

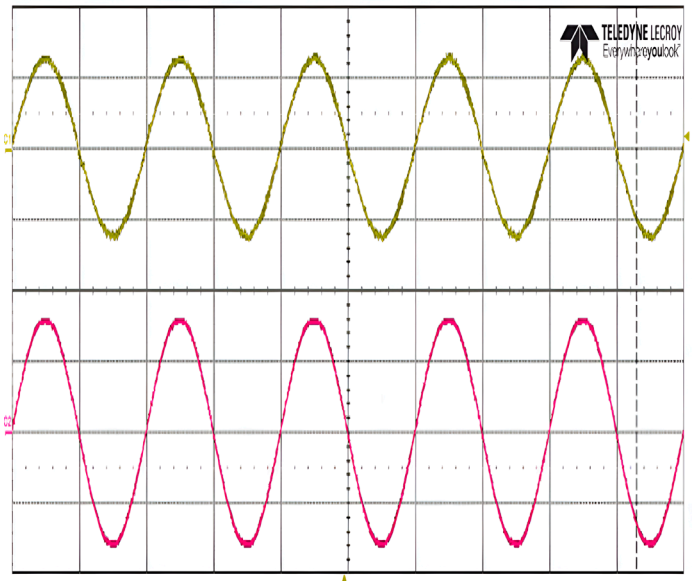


Figure 11 *Measured i_{IN} and v_{IN} in rectifier mode, output power 2 kW*

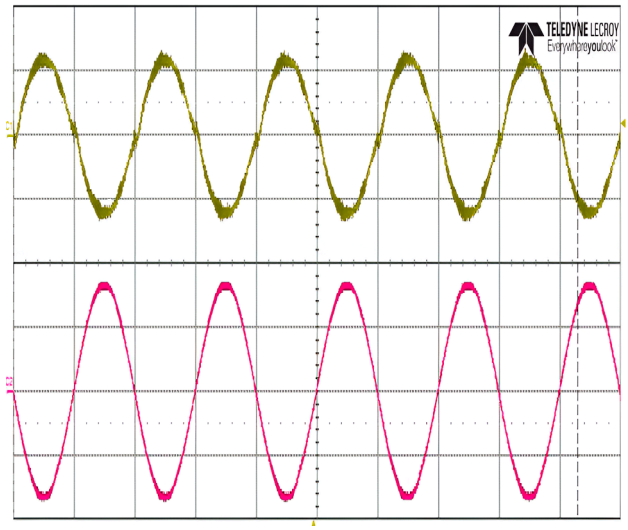


Figure 12 *Measured i_{OUT} and v_{GRID} in inverter mode, output power 2kW*

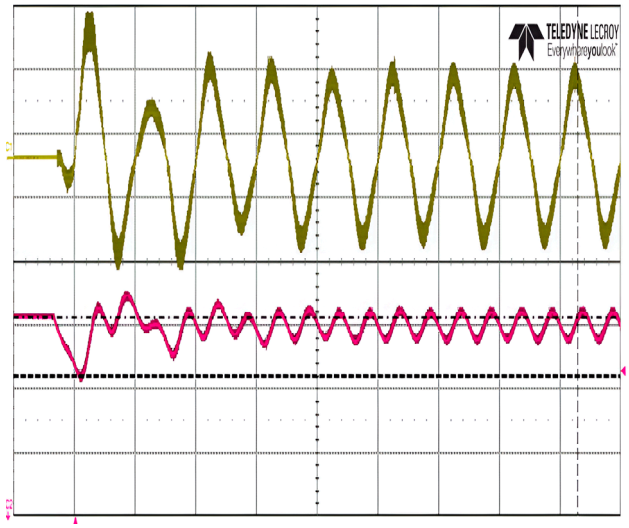


Figure 13 *Measured dynamic response during a step change in load power*

The second measurement, Mode 2 - inverter mode, was carried out similarly at a nominal power of 2 kW. Figure 12 shows the output voltage waveform, which in this case also represents the grid voltage $v_{OUT} = v_{GRID}$ (magenta) and the current supplied to the grid $i_{OUT} = i_{GRID}$ (yellow). The current supplied to the grid is in the opposite phase of the grid voltage so that the required power is provided to the grid (negative power). Again, the waveform of the consumed current shows a low content of higher harmonic components and almost 180° phase shift, which corresponds to the delivery of active power to the grid.

Within the BLTP-PFC operation, a mode based on synchronous switching of transistors has also been tested and is used. This mode replaces the classic diodes in the BLTP-PFC converter with actively controlled transistors (most often SiC MOSFETs or GaN HEMTs), which significantly reduces power losses and increases the overall efficiency of the device. During the conventional rectification, a high voltage drop occurs on the diodes, which generates significant heat at high currents. For this reason, it is more advantageous to switch on transistors with a significantly lower voltage drop and therefore lower losses.

The BLTP-PFC converter consists of two main branches (half-bridges): The High-Frequency Leg: Switches at a high frequency (tens to hundreds of kHz) and ensures the shaping of the current into a sinusoidal waveform. Synchronous switching here means that when the main transistor opens, the current flows through the parasitic diode of the opposite transistor. The control system immediately turns on this opposing transistor, redirecting the current through its low-resistance channel. The Low-Frequency Leg: Switches at the mains frequency (50 Hz) and serves to rectify the polarity (replaces the mains diode bridge). Controlled MOSFETs completely eliminate the losses of classic diodes here.

Main advantages: increased efficiency, bidirectional energy flow (key for the operating modes used), synchronous switching allows a smooth transition from Mode 1 (rectifier - grid consumption) to Mode 2 (inverter - grid supply), better thermal management (less losses = less heat produced = smaller heat sinks = higher power density).

The proposed BLTP-PFC converter was also tested in dynamic mode, Figure 13, with a step change in load. During this measurement, the power changed from 0 to P_{MAX} (2 kW). In Figure 13, the current i_{IN} (yellow) can be seen, and the V_{DC} voltage (magenta) drops by only 50 V. This is because a fast V_{DC} regulator is used in the control. When using a standard (slow) V_{DC} regulator, the voltage drop was more than 120 V.

4.2 The CLLLC verification

The CLLLC converter was also tested in both operating modes - Mode 1 - BUCK and Mode 2 - BOOST. Both modes were tested at a nominal power of 2 kW.

In the first measurement, the direction of energy flow is to the battery, i.e., the converter operates in mode - BUCK. Figure 14. shows the primary current of the transformer i_P (yellow) and the secondary current i_S (green).

In the second measurement, the direction of current flow is reversed; i.e. the current flows from the battery and the converter operates in mode - BOOST, Figure 15. Again, the Figure shows the primary current of the transformer i_P (green) and the secondary current i_S (yellow).

4.3 Complete ACS system verification

Further experimental measurements were performed on the complete unit of the designed ACS system with parameters according to Table 3. During

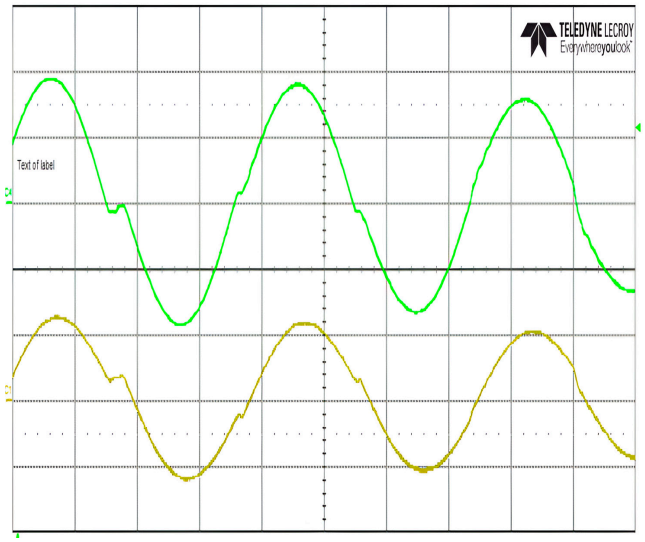


Figure 14 *The CLLLC converter in BUCK mode*

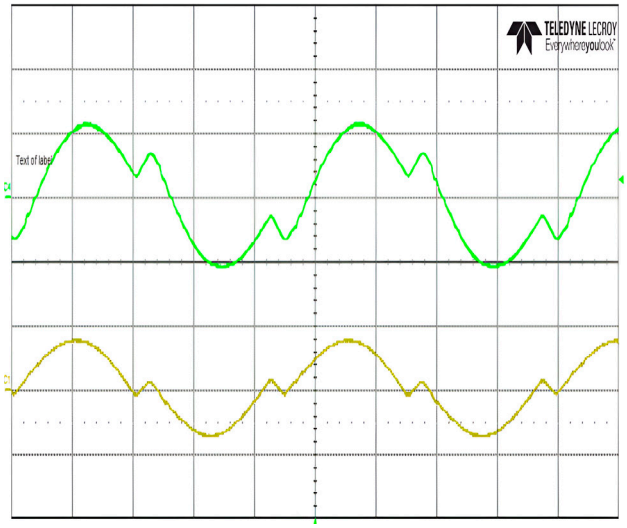


Figure 15 *The CLLLC converter in BOOST mode*

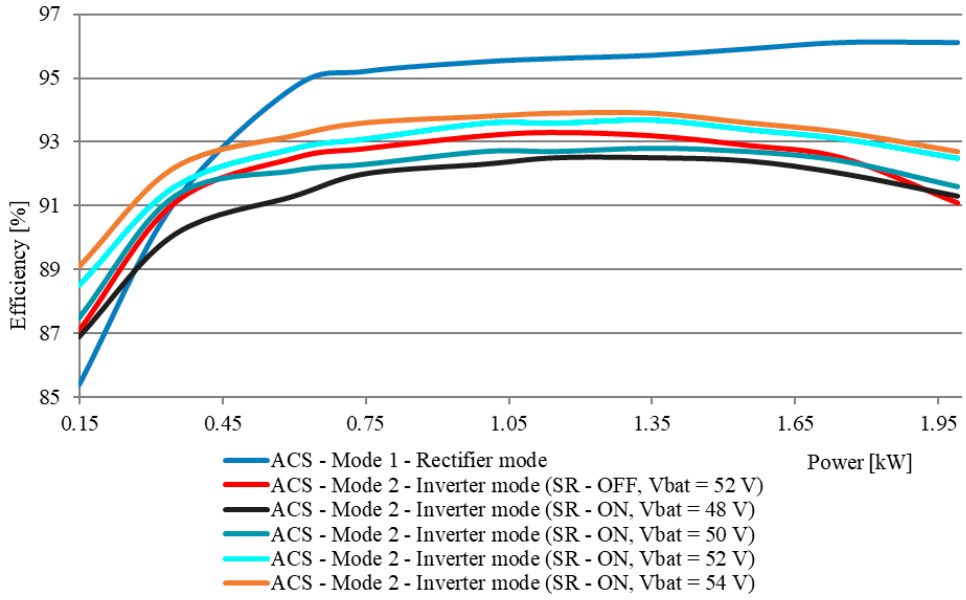


Figure 16 *Efficiency waveforms of the complete ACS system*

Table 4 *Complete ACS system harmonic analysis.*

Parameter	Value
Standard	EN 61000-3-2:2014
Frequency	50 [Hz]
Voltage	230.59 [V_{RMS}]
Current	9.892 [A_{RMS}]
Power Factor	1.000
Apparent power	2281.0 [VA]
Fundamental power component:	P1 = 2279.9 [W]
Fundamental harmonic factor:	cos φ1 = 1,000
Total voltage harmonic distortion	0.90 %
Total current harmonic distortion	1.43 %
Total harmonic voltage	0.047 [V]
Total harmonic currents	0.142 [A]
Partial harmonic voltage	0.014 [V]
Partial harmonic currents	0.079 [A]
Weighted voltage harmonic distortion	0.04 %
Weighted current harmonic distortion	5.66 %

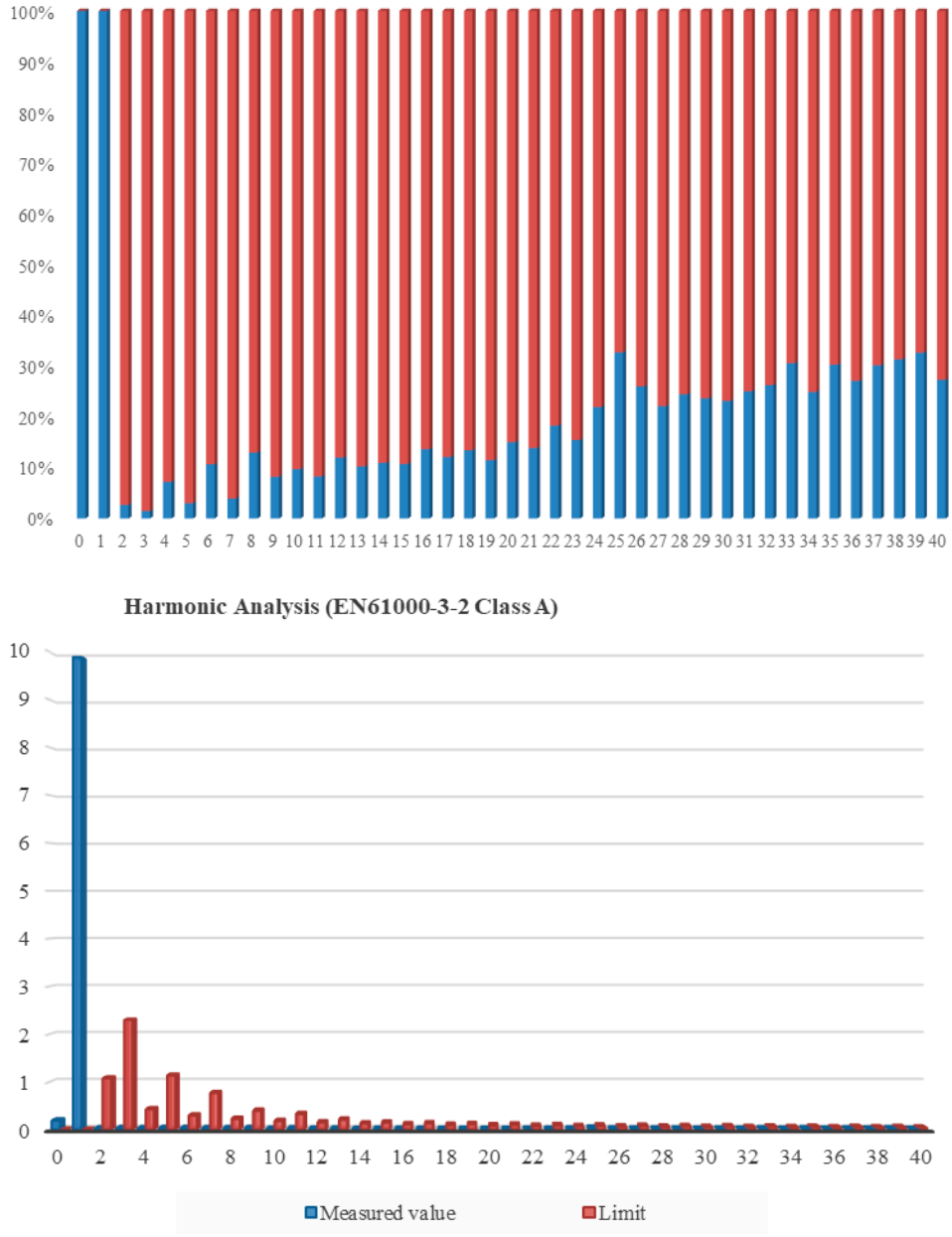


Figure 17 *Complete ACS system current harmonic analysis*

the measurements at the maximum achieved power P_{MAX} = 2180 W (apparent power S = 2181 VA), the values PF = 1, cos φ = 1, THD_i = 1.43% and THD_u = 0.90% were determined.

Figure 16 shows the results of measurements of efficiency of the entire ACS system in different operating modes. ACS operates in rectifier mode, in inverter mode - but without using the synchronous rectifier mode at a battery module voltage of U_{BAT} = 52 V and finally in the inverter mode by using the synchronous rectifier mode with the following battery module voltage values U_{BAT} = 48 V, 50 V, 52 V and 54 V.

The ACS system was also subjected to harmonic analysis tests in a certified laboratory based on the EN 61000-3-2:2014 standard. The EMC test results are shown in Table 4. A graphical interpretation of the harmonic analysis results is shown in Figure 17, where the blue columns represent the measured component and the red columns represent the limit of a given harmonic component for a given order of the harmonic component.

Final result of the harmonic analysis tests: The tested inverter achieved very low harmonic current distortion (THD_i = 1.43 %) at a power of approximately 2.28 kW and meets the requirements of the EN 61000-3-2:2014 standard, class A, with a significant margin against all harmonic current limits. The power factor reached a value of 1.000, which indicates practically ideal grid consumption.

4.4 Relevance of ACS for transport electrification

The proposed ACS architecture is directly applicable to transportation electrification systems, especially in bidirectional electric vehicle (EV) charging infrastructure. Modern charging stations require high efficiency, low harmonic distortion, and bidirectional power transfer capability to support Vehicle-to-Grid (V2G) and Grid-to-Vehicle (G2V) services [38-40].

The selected combination of BLTP-PFC and CLLLC converter provides several advantages for transport applications:

- unity power factor operation,
- low current harmonic distortion,
- galvanic isolation between the battery and a grid,
- bidirectional energy transfer,
- compatibility with second-life EV battery systems.

These features make the proposed ACS concept suitable for implementation in smart charging stations, electric bus depots, fleet charging hubs, railway auxiliary energy systems, and future smart transportation infrastructure.

5 Conclusion

In this paper are presented the design, simulation verification, and experimental validation of an Active Compensation System (ACS) prototype intended for bidirectional energy exchange between the electrical grid and battery storage. Based on a comparison of available converter topologies, the combination of a bridgeless totem-pole PFC (BLTP-PFC) converter and a bidirectional CLLLC resonant DC/DC converter was selected and implemented in the experimental prototype.

Simulation results confirmed the correct operation of both converter stages in accumulation and generative modes. The simulated waveforms demonstrated stable power transfer, proper current shaping, and expected converter behavior in both directions of energy flow. Experimental measurements showed a very good agreement with simulation predictions. The measured current and voltage waveforms corresponded closely to the simulated results, confirming the validity of the developed models and the selected control strategies.

The experimental verification demonstrated that the proposed ACS topology is capable of achieving high power quality and satisfactory efficiency. The BLTP-PFC converter maintained nearly unity power factor and low harmonic distortion in both rectifier and inverter operating modes. The complete ACS system achieved a maximum measured power of approximately 2.28 [kW] while maintaining PF = 1, $\cos \varphi = 1$, $THD_i = 1.43$ %, and $THD_u = 0.90$ %. Harmonic analysis performed according to EN 61000-3-2:2014 confirmed full compliance with the standard and significant reserve against all prescribed harmonic limits.

Efficiency measurements revealed that the highest efficiency was achieved in rectifier mode, reaching approximately 96 %. In inverter operation, the efficiency ranged between 91 % and 94 % depending on battery voltage and operating conditions. The results further confirmed the positive impact of synchronous rectification, which improved converter efficiency, especially at higher battery voltages. The best measured efficiency in inverter mode reached approximately 93.9 % at a battery voltage of 54 [V].

Overall, the obtained simulation and experimental results confirm that the proposed ACS topology represents a promising solution for future smart-grid applications requiring bidirectional power flow, energy storage integration, and active power quality management. Besides the stationary battery energy storage applications, the proposed ACS architecture can also be directly utilized in bidirectional EV charging stations, V2G infrastructures, electric public transport charging hubs, and transport-oriented microgrids. The obtained results confirm that the selected topology provides the power quality and efficiency required for the future transportation electrification systems.

Acknowledgements

This research was funded by APVV-22-0330 “Research of a system for active and optimal management of electrical energy using battery storage system” and Vega 1/0314/24 “Research of a system for active management of electrical energy using battery storage system.”

Conflicts of interest

The authors declare that they have no known competing financial interests or personal relationships that could have appeared to influence the work reported in this paper.

References

[1] YUAN, X., HUANG, X., GUO, L., ZHUO, D., CHEN, M., WANG, T. Implementation of a control strategy for harmonic suppression and dynamic voltage compensation in series active power filter. In: 23rd International Conference on Electrical Machines and Systems ICEMS: proceedings [online]. IEEE. 2020. eISSN 2642-5513, eISBN 978-4-8868-6419-2, p. 1739-1743. Available from: https://doi.org/10.23919/ICEMS50442.2020.9290862

[2] SZROMBA, A. Improvement of the source current quality for a shunt active power filter operating using hysteresis technique with stabilized switching frequency. *Energies* [online]. 2024, **17**, 5098. eISSN 1996-1073. Available from: https://doi.org/10.3390/en17205098

[3] WANG, T., GONG, L. D., HOU, Y. A Novel grid-connected inverter filtering method using series active power filter based on magnetic flux compensation. In: 23rd International Conference on Electrical Machines and Systems ICEMS: proceedings [online]. IEEE. 2020. eISSN 2642-5513, eISBN 978-4-8868-6419-2, p. 863-866. Available from: https://doi.org/10.23919/ICEMS50442.2020.9290930

[4] ADAMEC, J., DANKO, M., TARABA, M., DRGONA, P. Analysis of selected energy storage for electric vehicle on the lithium based. *Transportation Research Procedia* [online]. 2019, **40**, p. 127-131. eISSN 2352-1465. Available from: https://doi.org/10.1016/j.trpro.2019.07.021

[5] HUSSIEN, S. A., BAQAIS, A., AL-GABALAWY, M. Estimation of the residual useful life of EV batteries using advanced hybrid learning tools. *Electrical Engineering* [online]. 2024, **106**, p. 2651-2677. ISSN 0948-7921, eISSN 1432-0487. Available from: https://doi.org/10.1007/s00202-023-02071-3

[6] POLASEK, M., DANKO, M. Testing of batteries used in electric cars. In: 2022 ELEKTRO (ELEKTRO) [online]. IEEE. 2022. eISSN 2691-0616, eISBN 978-1-6654-6726-1, p. 1-5. Available from: https://doi.org/10.1109/ELEKTRO53996.2022.9803725

[7] DANKO, M., SIMCAK, M. Cyclic evaluation of capacity of recovered traction battery after short-circuit damage. *Advances in Science, Technology and Engineering Systems Journal* [online]. 2021, **6**(1), p. 879-885. ISSN 2415-6698. Available from: https://doi.org/10.25046/aj060197

[8] YAO, Q., SONG, X., XIE, W. State of health estimation of lithium-ion battery based on CNN-WNN-WLSTM. *Complex and Intelligent Systems* [online]. 2024, **10**, p. 2919-2936. eISSN 2198-6053. Available from: https://doi.org/10.1007/s40747-023-01300-3

[9] LI, J., ZHOU, J., WANG, W. ET AL. LCA for lithium battery recycling technology-recent progress. *Ionics* [online]. 2024, **30**, p. 4417-4428. ISSN 0947-7047, eISSN 1862-0760. Available from: https://doi.org/10.1007/s11581-024-05640-z

[10] ALTINER, M., TOP, S., KURSUNOGLU, S. Waste lead-acid battery recycling technologies. In: *Recycling technologies for secondary Zn-Pb resources. The minerals, metals and materials series* [online]. KAYA, M. (Ed.). Cham: Springer, 2023. ISBN 978-3-031-14684-8, eISBN 978-3-031-14685-5, p. 235-289. Available from: https://doi.org/10.1007/978-3-031-14685-5_7

[11] OUYANG, LA., HE, Y., HE, P., ZHOU, J., HUANG, H., GUO, Z. Emerging electrochemical techniques for recycling spent lead paste in lead-acid batteries. *Journal of Sustainable Metallurgy* [online]. 2024, **10**, p. 1905-1920. ISSN 2199-3823, eISSN 2199-3831. Available from: https://doi.org/10.1007/s40831-024-00928-w

[12] PRIDALA, M., SUPOLIK, M., PRAZENICA, M. Choosing right topology for bidirectional power converter used in a battery storage system based on efficiency and economic perspective. In: 2024 ELEKTRO (ELEKTRO): proceedings [online]. IEEE. 2024. p. 1-5. ISSN 2691-0616, eISBN 979-8-3503-7235-9. Available from: https://doi.org/10.1109/ELEKTRO60337.2024.10556932

[13] GHORPADE, S. J., SHARMA, R. B. A comprehensive review of demand-side management in smart grid operation with electric vehicles. *Electrical Engineering* [online]. 2024, **106**, p. 6495-6514. ISSN 0948-7921, eISSN 1432-0487. Available from: https://doi.org/10.1007/s00202-024-02330-x

[14] YADAV, G., SINGH, M. Real-time investigation of grid-interactive EV charger with two-stage bidirectional converter under wide voltage range scenarios. *Electrical Engineering* [online], 2024, **107**, p. 1993-2005. ISSN 0948-7921, eISSN 1432-0487. Available from: https://doi.org/10.1007/s00202-024-02609-z

[15] GAGO, G., PINTO, S. F., SILVA, J. F. G2V and V2G electric vehicle charger for smart grids. In: 2016 IEEE International Smart Cities Conference ISC2: proceedings [online]. IEEE. 2016. eISBN 978-1-5090-1846-8, p. 1-6. Available from: https://doi.org/10.1109/ISC2.2016.7580786

[16] ZGHEIB, R., AL-HADDAD, K., KAMWA, I. V2G, G2V and active filter operation of a bidirectional battery charger for electric vehicles. In: IEEE International Conference on Industrial Technology ICIT: proceedings [online]. IEEE. 2016. eISBN 978-1-4673-8075-1, p. 1260-1265. Available from: https://doi.org/10.1109/ICIT.2016.7474935

[17] ERTEKIN, D. ARVIN converter: a bidirectional DC/DC converter for grid-connected G2V/V2G energy storage and electrification approaches. *Electrical Engineering* [online]. 2024, **106**, p. 5785-5505. ISSN 0948-7921, eISSN 1432-0487. Available from: https://doi.org/10.1007/s00202-024-02295-x

[18] BHOSALE, P., KUMAR, R. Electric vehicle charging station design for V2G and G2V operation. In: 2023 4th International Conference for Emerging Technology INCET: proceedings [online]. IEEE. 2023. eISBN 979-8-3503-3575-0, p. 1-6. Available from: https://doi.org/10.1109/INCET57972.2023.10170188

[19] ESCODA, J., FONTANILLES, J., BIEL, D., REPECHO, V., CARDONER, R., GRINO, R. G2V and V2G operation 20 kW battery charger. In: World Electric Vehicle Symposium and Exhibition EVS27: proceedings [online]. IEEE. 2013. eISBN 978-1-4799-3832-2, p. 1-5. Available from: https://doi.org/10.1109/EVS.2013.6914939

[20] DOBRUCKY, B., SEDO, J., BRACINIK, P., LUSKOVA, M. Improving reliability of sensitive appliance supply combining DVR and UPS techniques: a new concept. In: 2020 ELEKTRO (ELEKTRO) [online]. IEEE. 2020. eISBN 978-1-7281-7542-3, p. 1-5. Available from: https://doi.org/10.1109/ELEKTRO49696.2020.9130327

[21] CHANG, H. T., LIANG, T. J., YANG, W. C. Design and implementation of bidirectional DC-DC CLLLC resonant converter. In: IEEE Energy Conversion Congress and Exposition ECCE: proceedings [online]. IEEE. 2018. eISSN 2329-3748, eISBN 978-1-4799-7312-5, p. 2712-2719. Available from: https://doi.org/10.1109/ECCE.2018.8557697

[22] WANG, S. Development of bi-directional CLLLC resonant converter. In: 4th International Conference on Mechatronics Technology and Intelligent Manufacturing ICMTIM: proceedings [online]. IEEE. 2023. eISBN 979-8-3503-1443-4, p. 39-44. Available from: https://doi.org/10.1109/ICMTIM58873.2023.10246744

[23] LIU, X., WU, X., WANG, H. Parameters analysis and control strategy combined with synchronous rectification technology for bidirectional CLLC resonant converter. *Electrical Engineering* [online]. 2023, **105**, p. 1397-1412. ISSN 0948-7921, eISSN 1432-0487. Available from: https://doi.org/10.1007/s00202-023-01745-2

[24] BASSO, CH. An introduction to the dual active bridge converter or DAB - Future Electronics [online]. 2024 Available from: https://powersimtof.com/Downloads/PPTs/Introduction%20to%20the%20DAB.pdf

[25] Bidirectional, dual active bridge reference design for level 3 electric vehicle charging stations. Design Guide: TIDA-010054, TI [online]. 2026. Available from: https://www.ti.com/lit/ug/tidues0f/tidues0f.pdf?ts=1779881084843

[26] 25 kW, dual active bridge bidirectional power converter for EV charging and battery energy storage systems. User manual UM3198 [online]. 2025. Available from: https://www.st.com/resource/en/user_manual/um3198-25-kw-dual-active-bridge-bidirectional-power-converter-for-ev-charging-and-battery-energy-storage-systems-stmicroelectronics.pdf

[27] HAN, S. High power bi-directional DC/DC converter with controlled device stresses. *Electrical Engineering* [online]. 2023, **105**, p. 233-242. ISSN 0948-7921, eISSN 1432-0487. Available from: https://doi.org/10.1007/s00202-022-01648-8

[28] BAQAR, A., CAMARA, M. B., DAKYO, B. Supercapacitors fast ageing control in residential microgrid based photovoltaic/fuel cell/electric vehicle charging station. *Energies* [online]. 2023, **16**, 5084. eISSN 1996-1073. Available from: https://doi.org/10.3390/en16135084

[29] KAMAGATE, Y., SHAH, H. A. Effective dynamic energy management algorithm for grid-interactive microgrid with hybrid energy storage system. *Scientific Reports* [online]. 2024, **14**, 20294. eISSN 2045-2322. Available from: https://doi.org/10.1038/s41598-024-70599-w

[30] UROOJ, A., NASIR, A. Review of hybrid energy storage systems for hybrid electric vehicles. *World Electric Vehicle Journal* [online]. 2024, **15**, 342. eISSN 2032-6653. Available from: https://doi.org/10.3390/wevj15080342

[31] LEI, H., LI, K., CHONG, CH. A review of hybrid energy storage system for heavy-duty electric vehicle. *Transportation Research Procedia* [online]. 2023, **70**, p. 234-240. eISSN 2352-1465. Available from: https://doi.org/10.1016/j.trpro.2023.11.024

[32] ABO-KHALIL, A. G., SOBHY, A., ABDELKAREEM, M. A., OLABI, A. G. Advancements and challenges in hybrid energy storage systems: components, control strategies, and future directions. *International Journal of Thermofluids* [online]. 2023, **20**, 100477. ISSN 2666-2027. eISSN 2666-2027. Available from: https://doi.org/10.1016/j.ijft.2023.100477

[33] ADRAGNA, C., BIANCO, A., GRITTI, G., SUCAMELI, M. State-of-the-art power factor correction: an industry perspective. *Encyclopedia* [online]. 2024, **4**, p. 1324-1354. eISSN 2673-8392. Available from: https://doi.org/10.3390/encyclopedia4030087

[34] AIELLO, G., NARDO, D., GENNARO, F., CACCIATO, M., SCELBA, G. Investigation on WBG power devices inside bidirectional PFC in on-board charger applications. In: ELEKTRO (ELEKTRO) [online]. IEEE. 2024. eISSN 2691-0616, eISSN 979-8-3503-7235-9, p. 1-6. Available from: https://doi.org/10.1109/ELEKTRO60337.2024.10557038

[35] ZHU, K., BHALLA, A., DODGE, J. Enabling 99.3% efficiency in 3.6 kW totem-pole PFC using new 750 V gen 4 SiC FETs. *IEEE Power Electronics Magazine* [online]. 2021, **8**(4), p. 30-37. ISSN 2329-9207, eISSN 2329-9215. Available from: https://doi.org/10.1109/MPEL.2021.3123757

[36] CHELLAPPAN, S. A comparative analysis of topologies for a bridgeless-boost PFC circuit - Texas Instruments [online]. 2018. Available from: https://www.ti.com/lit/an/slyt750/slyt750.pdf?ts=1729577763515&ref_url=https%253A%252F%252Fwww.ti.com%252Flit%252Fan%252Fsluaau2%252Fsluaau2.pdf%253Fts%253D1729570464919

[37] Vision, user manual LFP48 series [online]. 2025. Available from: https://techlux.com.br/storage/products/206/iIOQY50W2V7VCacjmwFc2rbUN2JNYY9zPd2iDTYq.pdf

[38] RAO, S. P., OLUSEGUN, T. S., RANGANATHAN, P., KOSE, U., GOVEAS, N. Vehicle-to-grid technology: opportunities, challenges, and future prospects for sustainable transportation. *Journal of Energy Storage* [online]. 2025, **110**, 114927. ISSN 2352-152X, eISSN 2352-1538. Available from: https://doi.org/10.1016/j.est.2024.114927

[39] RANA, R., SAGGU, T. S., LETHA, S. S., BAKHSH F. I. V2G based bidirectional EV charger topologies and its control techniques: a review. *Discover Applied Sciences* [online]. 2024, **6**, 588. eISSN 3004-9261. Available from: https://doi.org/10.1007/s42452-024-06297-z

[40] CHEN G, ZHANG Z. Control strategies, economic benefits, and challenges of vehicle-to-grid applications: recent trends research. *World Electric Vehicle Journal* [online]. 2024, **15**(5), 190. eISSN 2032-6653. Available from: https://doi.org/10.3390/wevj15050190

This is an open access article distributed under the terms of the Creative Commons Attribution 4.0 International License (CC BY 4.0), which permits use, distribution, and reproduction in any medium, provided the original publication is properly cited. No use, distribution or reproduction is permitted which does not comply with these terms.

NUMERICAL ASSESSMENT OF ELECTROMAGNETIC EXPOSURE FROM MOTORCYCLE HELMET COMMUNICATION SYSTEMS

Zuzana Pšenáková[1], Milan Smetana[1], Grazia Lo Sciuto[2], Denisa Dvončová[3]

[1]University of Zilina, Faculty of Electrical Engineering and Information Technology, Department of Electromagnetic and Biomedical Engineering, Zilina, Slovakia
[2]University of Catania, Department of Electrical Electronic and Computer Engineering, Catania, Italy
[3]Siemens Healthcare, Zilina, Slovakia

*E-mail of corresponding author: milan.smetana@uniza.sk

Zuzana Psenakova 0000-0001-8898-5438, Milan Smetana 0000-0002-8419-5428,
Grazia Lo Sciuto 0000-0001-9384-7232

Resume
In this study was numerically assessed electromagnetic exposure from a 2.4 GHz wireless communication system integrated into a motorcycle helmet. Using CST Studio Suite and an anatomically realistic human head model, the localized SAR were evaluated averaged over 10 g of tissue for five helmet shell materials at transmitter powers from 1 mW to 1 W. At 100 mW, polyimide produced the highest SAR (approximately 1.47 W/kg), whereas the carbon fibre produced the lowest (approximately 0.94 W/kg). All investigated configurations remained below the ICNIRP (International Commission on Non-Ionizing Radiation Protection) localized exposure limit of 2 W/kg for operating powers up to 100 mW, while higher-power scenarios exceeded this limit. The results demonstrate the importance of transmitter power, antenna placement, and helmet material properties for the electromagnetic safety of smart motorcycle helmets.

Article info
Received 23 June 2026
Accepted 26 September 2026
Online 21 October 2026

Keywords:
electromagnetic field
non-ionising radiation
specific absorption rate
CST studio suite
motorcycle helmet
human head model

Available online: https://doi.org/10.26552/com.C.2026.056

ISSN 1335-4205 (print version)
ISSN 2585-7878 (online version)

1 Introduction

The rapid evolution of intelligent transportation systems (ITS) and the paradigm shift towards smart mobility have fundamentally transformed the design requirements of modern transport safety infrastructure. In the contemporary automotive and vehicular sectors, safety is no longer evaluated solely through the lens of passive mechanical crashworthiness, such as impact absorption and structural integrity. Instead, active safety and real-time connectivity have become core pillars of rider protection. This technological revolution is particularly prominent in the motorcycle domain, where riders remain among the most vulnerable road users (VRUs). To mitigate the high risks of severe injuries in dense or high-speed traffic environments, the integration of advanced wireless communication hardware into personal protective equipment (PPE), specifically smart motorcycle helmets, has experienced an unprecedented surge over the past decade [1-3].

Modern smart helmets are no longer mere passive shells lined with expanded polystyrene; they are complex, wearable technological hubs. These advanced protective systems standardly incorporate short-range Bluetooth transceivers, dynamic mesh communication (DMC) modules for inter-rider coordination, GPS tracking units, and ambient noise-cancelling systems. In the context of vehicle-to-everything (V2X) and vehicle-to-vehicle (V2V) communication networks, these integrated antennas allow motorcyclists to receive *real*-time telemetry, hazard warnings, and collision-avoidance data directly from the transport infrastructure. While these wireless systems undeniably enhance active traffic safety by increasing riders' situational awareness, they simultaneously introduce a new, often-overlooked engineering challenge: continuous exposure of the human body to non-ionising radiofrequency electromagnetic (EM) radiation [4-6].

From a bioelectromagnetic perspective, a wireless communicator operating inside or mounted onto a motorcycle helmet acts as an intentional EM transmitter

situated in the immediate near field of the human head. Unlike commercial cellular smartphones, which are typically placed against the ear intermittently during calls, helmet communication systems often transmit continuously for hours of riding, remaining in proximity to the highly sensitive occipital and temporal lobes of the brain. At microwave frequencies, particularly within the 2.4 GHz industrial, scientific, and medical (ISM) band used by Bluetooth and wi-fi protocols, biological tissues in the head absorb a fraction of the radiated energy. This energy absorption can lead to localised dielectric heating and potential thermal stress in the underlying cranial structures, raising vital questions regarding long-term user health and compliance with international dosimetric safety standards [1, 7-8].

Furthermore, the physical presence of the motorcycle helmet itself introduces severe EM boundary conditions that complicate standard free-space antenna assumptions. The outer shell of a modern helmet is fabricated from specialised structural materials: ranging from cost-effective high-impact thermoplastics like polycarbonate to high-performance advanced composites such as carbon fibre and E-glass fibre. These materials possess drastically different dielectric constants and electrical conductivities. When the embedded antenna radiates, the surrounding helmet shell behaves as a secondary complex reflector and dielectric loader. It can induce wave refractions, surface eddy currents, and localised field focusing, which can significantly alter the near-field radiation pattern and potentially amplify energy deposition (hotspots) within the rider's biological tissues [9-10].

Consequently, evaluating the specific absorption rate (SAR) within an anthropomorphic head model under realistic helmet-loaded conditions is an essential requirement for modern transport safety engineering. In this study was addressed this critical intersection of wireless communication performance, material science, and public health compliance within transportation systems. By deploying the high-resolution numerical modelling using the CST studio suite software (Dassault Systemes SIMULIA, Velizy-Villacoublay, France), combined with the anatomical "HUGO" voxel phantom, in this paper was systematically investigated the localized SAR distribution triggered by a 2.4 GHz dipole communicator.

The primary objective of this article is to quantify how different structural helmet shell materials influence energy deposition across various standard input power levels. Ultimately, this research aims to provide vehicle designers and transport safety engineers with rigorous, predictive data to optimize the integration of wearable wireless hardware, guaranteeing that next-generation smart protective gear protects the rider not only from mechanical impacts but also from electromagnetic hazards.

2 Theoretical background

In this section are presented the foundational EM principles and a review of the existing scientific literature concerning radiofrequency exposure in transport environments. To rigorously evaluate the SAR inside the human head, it is essential to analyze the underlying physics of dielectric heating and frequency-dependent tissue interactions. Furthermore, in this part is provided a comprehensive overview of the biomedical classification of electromagnetic field (EMF) effects, along with the evolution of international regulatory frameworks governing public safety. By bridging fundamental bioelectromagnetic with modern computational dosimetry, this theoretical framework creates the necessary baseline for interpreting the numerical results presented later in this study.

Since the experimental measurement of SAR inside a living human head requires highly invasive procedures (inserting micro-probes into the cranial cavity), physical validation is ethically prohibited and technically restrictive. Consequently, modern dosimetric research relies almost exclusively on computational electromagnetics (CEM) combined with high-fidelity anatomical phantoms. The two most prominent numerical methods deployed for human EMF simulations are the finite-difference time-domain (FDTD) method and the finite integration technique (FIT), the latter being the core solver framework of CST studio suite [10-12]. The accuracy of these numerical models has evolved significantly. Early studies in the late 1990s used homogeneous spherical or elliptical models to approximate the human head, severely underestimating the localized field concentrations arising from the complex internal boundaries of bone and fluid. The development of voxel-based anthropomorphic datasets, such as the "virtual family" and the "HUGO" phantom, revolutionized the field by partitioning the human body into millions of individual cubic cells (voxels), each assigned distinct frequency-dependent permittivity and conductivity values [13-14]. Recent literature on smart protective gear indicates that when an antenna is operated within an enclosed structure, such as a motorcycle helmet, the helmet shell material acts as a secondary boundary condition, potentially causing reflections, dielectric loading, or partial shielding [9]. In the context of modern ITS, evaluating the EM compatibility of wearable rider accessories has transitioned from a secondary design consideration to a strict regulatory mandate. The spatial deformation of the antenna's radiation pattern inside a multi-layered helmet-head configuration underscores the insufficiency of analytical approximations. It justifies the use of advanced full-wave numerical solvers. Furthermore, the continuous structural variance between the standard high-permittivity thermoplastics and advanced conductive carbon composites introduces

complex boundary conditions that radically alter near-field interactions. Consequently, establishing a rigorous theoretical foundation that bridges the dielectric relaxation physics with international safety standards is essential for interpreting and evaluating the subsequent localized SAR behavior.

The interaction between high-frequency EMF and complex biological systems represents a fundamental topic in modern bioelectromagnetic and transport safety engineering. When an organism is subjected to non-ionizing radiation within the microwave spectrum, specifically the 2.4 GHz ISM frequency band utilized by commercial Bluetooth and DMC systems, the primary mechanism of physical interaction is dielectric heating. Biological tissues are fundamentally heterogeneous and contain a vast concentration of polar molecules, predominantly water. At microwave frequencies, the rapidly alternating electric field induces a torque on these dipoles, continuously forcing them to realign with the changing field. This high-frequency rotational movement and the subsequent molecular-level friction dissipate electromagnetic energy into thermal energy, causing a localized temperature to rise within the exposed anatomical structures [1, 15].

To quantitatively evaluate and standardize the amount of radiofrequency (RF) energy absorbed by biological entities, the scientific community universally deploys SAR. Mathematically, the local SAR value at any specific coordinate within a lossy dielectric medium is derived from Maxwell's equations and defined by the following expression:

$$SAR = \frac{\sigma |E|^2}{2\rho} = c_i \frac{dT}{dt}, \tag{1}$$

where σ [S/m] represents the electrical conductivity of the localized tissue layer, E is the peak amplitude of the internal electric field intensity [V/m], ρ [kg/m^3] denotes the mass density of the specific biological tissue, c_i is the specific heat capacity of the tissue [J/kg·°C], and dT/dt represents the initial time derivative of the temperature rise. Since the near-field radiation pattern of an embedded helmet antenna is inherently non-uniform, the local electric field exhibits strong spatial gradients. Consequently, international dosimetric standards require that the raw spatial SAR distribution be averaged over a standardized mass of continuous tissue, typically 1 g or 10 g, to smooth out extreme localized anomalies and provide a biologically relevant metric for thermal stress assessment [8, 16-17].

Biological tissues cannot be modelled as simple, ideal dielectrics. From an electromagnetic perspective, they represent a highly dispersive medium whose electrical conductivity and relative permittivity fluctuate dynamically with operating frequency. This frequency-dependent behavior is standardly quantified using the complex relative permittivity formula:

$$\varepsilon^*(\omega) = \varepsilon'(\omega) - j\varepsilon''(\omega) = \varepsilon'(\omega) - j\frac{\sigma}{\omega\varepsilon_0}, \tag{2}$$

Where ε' represents the real permittivity (a measure of the tissue's ability to store electrical energy), ε'' is the imaginary permittivity or loss factor (characterizing the energy dissipation), ω is the angular frequency, and ε_0 is the vacuum permittivity. At 2.4 GHz, the dielectric response of tissues is strongly governed by the dispersion phase, which arises from the dipolar relaxation of free water molecules. This relaxation process is mathematically modelled using the multi-frequency Cole-Cole or Debye formulation:

$$\varepsilon^*(\omega) = \varepsilon_\infty + \frac{\varepsilon_s - \varepsilon_\infty}{1 + (j\omega\tau)^{1-\alpha}}, \tag{3}$$

where ε_∞ is the relative permittivity at the high-frequency limit, ε_s is the static relative permittivity, τ represents the characteristic relaxation time of the tissue, and α is an empirical parameter describing the distribution of relaxation times [8, 13].

The literature comprehensively categorizes the biological consequences of RF exposure into two distinct domains: thermal (established) effects and non-thermal (low-level) effects. Thermal effects occur when the localized rate of EM energy deposition exceeds the biological organism's natural thermoregulatory capabilities. In the human head, metabolic heat dissipation is primarily regulated by forced convection via blood microcirculation. However, certain anatomical regions within the cranial structure, such as the crystalline lens of the eye or specific poorly vascularized areas of the skull, exhibit reduced blood flow and are highly susceptible to localized thermal stress. Prolonged exposure leading to a local temperature increase of more than 1°C can trigger cellular protein denaturation, alter enzyme activity, and cause irreversible tissue damage [18-19]. Conversely, non-thermal effects refer to biological alterations that occur at exposure levels well below those required to produce measurable temperature changes. Over the past decades, a significant body of epidemiological and in vitro research has investigated whether chronic low-level RF exposure can induce neurological symptoms, alter cognitive functions, or provoke electromagnetic hypersensitivity (EHS) [2, 5]. Recent experimental exposure systems using real telecommunication signals further demonstrate the importance of accurately controlled RF exposure conditions in bioelectromagnetic studies [20]. Some laboratory studies have reported subtle cellular transformations, including changes in calcium ion efflux across cell membranes, increased production of reactive oxygen species (ROS), and potential DNA strand breaks under specific exposure conditions [3]. Despite these isolated findings, the large-scale systematic reviews coordinated by the world health organization (WHO) maintain that a definitive, causal link between low-power microwave exposure and long-term carcinogenic or neurological pathologies has not been established conclusively [16]. Nevertheless, because wireless communicators mounted inside motorcycle helmets operate continuously in the immediate near

Table 1 *The public exposure SAR limits according to international guidelines [1, 9]*

Frequency range	Whole-body average SAR [W/kg]	Localized SAR (head and torso) [W/kg]	Localized SAR (extremities) [W/kg]
100 kHz - 10 MHz	0.08	2.0	4.0
10 MHz - 10 GHz	0.08	2.0	4.0

field of the brain's occipital and temporal lobes, rigorous numerical verification remains a vital precautionary requirement to ensure user safety in the transport sector [6].

As the EM wave emitted by the 2.4 GHz dipole antenna travels from free space into the multi-layered structure of the helmet and human head, it undergoes severe attenuation. The rate of this attenuation determines how deep radiation penetrates the human brain. The penetration depth δ, defined as the distance at which the amplitude of the EMF decays to e^{-1} (where e denotes Euler's number, corresponding to approximately 37% of the initial amplitude) of its initial value at the boundary, is calculated using the following expression:

$$\delta = \frac{1}{\omega}\left[\frac{\mu_0 \varepsilon_0 \varepsilon'}{2}\left(\sqrt{1+\left(\frac{\sigma}{\omega \varepsilon_0 \varepsilon'}\right)^2}-1\right)\right]^{-\frac{1}{2}}, \quad (4)$$

where μ_0 is the magnetic permeability of free space. At 2.4 GHz, the penetration depth in high-water-content tissues (such as muscle or grey matter) is approximately 15-20 mm. This implies that most of the RF energy from a helmet communicator is absorbed within the outermost layers of the head, namely the skin, subcutaneous fat, and the skull. This physical limitation underscores the absolute necessity of using high-fidelity voxel phantoms rather than simplified spheres; a simplified model cannot accurately track wave refraction through the thin layer of high-attenuation skin before encountering the low-attenuation skull bone.

To safeguard the public against the proven thermal hazards of RF radiation, specialized international organizations have developed comprehensive exposure limits based on decades of peer-reviewed dosimetric literature. The two primary bodies responsible for establishing these safety guidelines are the international commission on non-ionizing radiation protection (ICNIRP) and the institute of electrical and electronics engineers (IEEE) via the international committee on electromagnetic safety (ICES) [1, 7]. Historically, the exposure thresholds were derived by determining the lowest operational SAR level capable of producing adverse biological effects in animal models-identified as a whole-body average SAR of 4.0 W/kg. By applying a conservative safety factor of 50 for the general public, the global safety threshold for whole-body average exposure was established at 0.08 W/kg and for localized exposure (such as the head and trunk), where higher energy concentrations are permissible due to localized thermoregulation, a threshold of 2.0 W/kg was mandated by ICNIRP, averaged over a 10 g tissue mass. In contrast, early guidelines from the United States federal communications commission (FCC), based on ANSI/IEEE standards, adopted a stricter local threshold of 1.6 W/kg but averaged over a smaller mass of 1 g of tissue, creating a historical discrepancy in international compliance testing [17-18, 21]. In 2020, ICNIRP published updated guidelines that refined the exposure metrics for high-frequency fields above 6 GHz but maintained the local 2.0 W/kg limit for the 100 kHz to 10 GHz range, reaffirming its adequacy for protecting against localized tissue heating in consumer electronics [1]. In the Slovak republic, these international thresholds are legally codified and enforced via the decree of the ministry of health No. 534/2007 coll., ensuring that any electronic equipment deployed in transport and everyday life satisfies identical safety criteria [7]. Table 1 summarizes the current public exposure limits across the critical frequency domains relevant to consumer communications.

3 Numerical model and numerical simulation set-up

In this section are described the computational methodology and numerical configuration used to analyze EM interactions between the wireless communicator and the human body. To achieve high dosimetric accuracy, a complex simulation environment was established within CST studio suite, combining an advanced anthropomorphic phantom with precise geometric models of protective transport gear. The primary objective is to replicate realistic operational conditions of motorcycle communication systems and evaluate how different structural materials influence energy absorption in biological tissues.

To accurately evaluate the spatial distribution of the electromagnetic field and the resulting local SAR, a high-resolution anatomical voxel model, "HUGO", was deployed within the CST environment. The human head model was extracted from the high-fidelity voxel dataset to represent realistic biological boundaries. The tissue parameters, including electrical conductivity, mass density, and relative permittivity, were configured to match the international dielectric standard databases for human tissues at the targeted microwave frequency band of 2.4 GHz, Table 2.

The solver accounts for the distinct boundaries between these layers, as the high-water content in tissues like the muscle or brain significantly accelerates energy absorption compared to the low-conductivity bone structures. This high spatial resolution ensures

Table 2 *Dielectric properties of key human head tissues at f = 2.4 GHz [13]*

Tissue	Relative Permittivity ε_r [-]	Conductivity σ [S/m]	Mass Density ρ [kg/m³]
Skin	38.1	1.46	1100
Muscle	52.7	1.74	1040
Bone (Skull)	11.4	0.39	1850
Brain (Grey Matter)	48.9	1.81	1040
Brain (White Matter)	36.2	1.22	1040
CSF (Cerebrospinal Fluid)	66.2	3.46	1000

that the computational model can precisely determine the location of maximum energy deposition and calculate localized thermal stress without undergoing simplification errors.

The motorcycle helmet geometry was imported into the computational domain using a standardized stereolithography (STL) surface mesh format. To investigate the EM attenuation and potential shielding behavior of the outer protective gear, five frequently utilized structural materials for helmet shell manufacturing were assigned and compared, Table 3: polycarbonate, a widely used impact-resistant thermoplastic polymer; polyimide, a high-performance polymer known for its thermal stability and structural strength; teflon (PTFE, a synthetic fluoropolymer of tetrafluoroethylene), a low-permittivity fluoropolymer utilized as a comparative baseline; carbon fibre, a lightweight, highly rigid conductive composite matrix designed for premium impact absorption; e-glass fibre, an industrial glass-reinforced composite bound with epoxy resin.

The numerical helmet model was simplified to specifically investigate the influence of the helmet material on electromagnetic energy absorption in the human head. The helmet geometry was imported from an STL model and resized to fit the anatomical HUGO head model. The same helmet geometry was maintained across all simulations, while the helmet material was varied among polycarbonate, polyimide, PTFE, carbon fibre, and E-glass fibre. The numerical model did not explicitly include the expanded polystyrene (EPS) impact-absorbing liner as a separate dielectric layer. Consequently, the model represents a simplified single-material helmet configuration rather than the complete multilayer structure of a real motorcycle helmet. This simplification should be considered when the absolute SAR values are interpreted. However, because the geometry, antenna position, operating frequency, and excitation conditions were identical across all investigated configurations, the model enables a consistent comparative assessment of how the selected helmet materials affect the resulting SAR distribution. Future work will investigate the effect of a realistic multilayer helmet structure, including an EPS liner with defined thickness and dielectric properties.

The combined numerical model, consisting of the anthropomorphic head model, the motorcycle helmet shell, and the embedded dipole communicator, was analyzed using the high-frequency time-domain solver based on the FIT, Figure 1. The boundary conditions were explicitly set to "open (space)" in all directions to establish an unrestricted free-space radiation environment and prevent artificial reflections back into the simulation volume.

3.1 Antenna configuration and computational settings

To ensure reproducible numerical exposure assessments, the geometrical configuration of the radiating source relative to the anatomical head model were kept identical for all investigated helmet materials. A half-wave dipole antenna operating at 2.4 GHz was positioned inside the helmet adjacent to the ear region of the anatomical head model. The antenna had a total dipole length of 55.76 mm, a diameter of 1.5 mm, and a 10 mm long central feeding section. The feed impedance was set to 73 Ω. The minimum distance between the radiating element and the head phantom surface was approximately 10 mm. Since the original simulation documentation did not record the antenna's absolute Cartesian coordinates in the CST global coordinate system, its position was specified here by its anatomical location and separation from the head surface.

The centre of the dipole was set as the reference point, with the origin of the coordinate system O = (0, 0, 0) at the centre of the head; x-axis: left-right, y-axis: posterior-anterior, z-axis: inferior-superior, and the antenna positioned near the ear, at a distance of 10 mm from the head surface. The dipole was oriented approximately in the superior-inferior direction, corresponding to the actual situation.

The geometrical position of the antenna, the head phantom, and the helmet was fixed throughout the simulation series; only the material assigned to the helmet shell was changed. Consequently, differences in the calculated SAR distributions can be attributed primarily to the electromagnetic properties of the investigated helmet materials rather than to changes in source geometry. The anatomical head model was derived from the HUGO model of the CST Voxel Family and included heterogeneous biological structures such as skin, bone, muscle, brain tissue, and blood.

Table 3 *Physical and dielectric parameters of simulated motorcycle helmet shell materials [10]*

Material	Relative Permittivity ε_r [-]	Conductivity σ [S/m]	Mass Density ρ [kg/m³]
Polycarbonate	2.90	0.001	1200
Polyimide	3.40	0.002	1420
PTFE	2.10	0.000	2200
Carbon Fibre	5.50	10.500	1750
E-Glass Fibre	4.80	0.004	2580

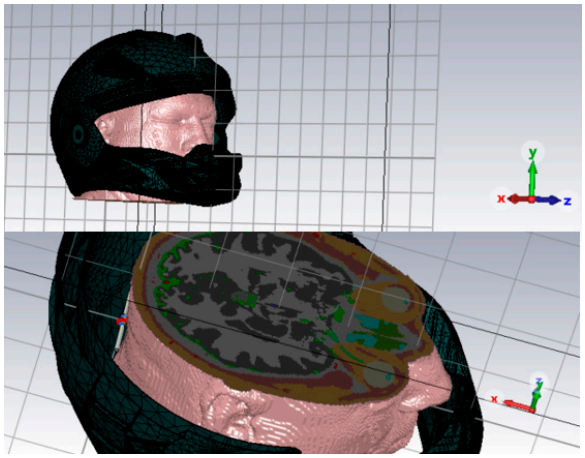


Figure 1 *Numerical simulation model: anthropomorphic human head phantom model with helmet, CST Studio Suite*

The dipole antenna was designed for operation at 2.4 GHz and evaluated over the frequency range of 2.3-2.5 GHz. Before the exposure simulations, the antenna model was verified separately by evaluating its reflection coefficient and radiation pattern. At the operating frequency of 2.4 GHz, the simulated reflection coefficient reached approximately –31.37 dB, indicating good impedance matching at the selected operating frequency. The antenna input power varied from 0.001 W to 1 W during the SAR calculations. The values of 0.001 W, 0.01 W, and 0.1 W represented the power levels considered for Bluetooth operation in the original simulation study. In contrast, we included higher power levels to investigate SAR dependence on increasing antenna power.

The computational domain was terminated using Open boundary conditions. The simulation included monitors for the far field, electric field (E-field), magnetic field (H-field), and power loss density. The specific absorption rate was evaluated using the CST SAR Calculation function with spatial averaging over 10 g of tissue.

To make the field interactions and calculate the SAR, localized field monitors were activated for the electric field, magnetic field, and power loss density. The internal SAR calculation routine was configured to average the power absorption over a standardized 10 g mass of continuous tissue, ensuring direct compatibility with regional public safety guidelines. The simulations were executed sequentially by sweeping the input power level across standard Bluetooth operational ranges.

3.2 Mesh and numerical settings

Electromagnetic simulations were performed at an operating frequency of 2.4 GHz. The computational domain used open (space) boundary conditions, allowing electromagnetic waves to propagate out of the domain with minimal artificial reflections. The numerical model included the anatomical HUGO head model, the helmet geometry, and the dipole antenna, and the same geometrical configuration was maintained for all investigated helmet materials. The electromagnetic field evaluation included electric-field (E-field), magnetic-field (H-field), far-field, and power-loss-density monitors. The specific absorption rate was calculated using the CST SAR evaluation procedure with spatial averaging over 10 g of tissue. The antenna excitation frequency, boundary conditions, head and helmet geometry, antenna position, and SAR averaging procedure remained unchanged throughout the simulation series to ensure consistent comparisons between the investigated material configurations. For an accurate analysis, the following mesh settings were applied: local mesh refinement in areas with intricate geometry, a minimum mesh step size of 0.2 mm, adaptive mesh refinement enabled, and a limit of 200 million mesh cells, ensuring a balance between accuracy and computation time.

The CST utilizes integrated full-wave electromagnetic solvers (specifically the Time Domain Solver) based on the Finite Integration Technique (FIT). The software calculates the electromagnetic field distribution across the entire discretized mesh

grid and then derives the resulting parameters during the post-processing using built-in analytical routines. Manual calculation was therefore unnecessary and less suitable, as the software accounts for complex boundary conditions, material losses, and high-frequency effects that standard analytical equations cannot fully capture.

All the helmet configurations were evaluated using an identical computational setup, keeping the head geometry, antenna position, excitation conditions, computational domain, and SAR evaluation procedure unchanged. The open boundary conditions were applied and the local SAR were evaluated using 10-g mass averaging. We assessed numerical consistency across twelve input-power levels from 0.001 to 1 W. For all materials, SAR exhibited the expected linear scaling with power; for example, the maximum 10-g averaged SAR for polycarbonate increased from 0.0145407 W/kg at 0.001 W to 1.45407 W/kg at 0.1 W and 14.5407 W/kg at 1 W. Similar proportional behavior was observed for the other materials, providing an internal numerical-consistency check.

The numerical model also underwent internal verification and regulatory benchmarking. Before integrating it into the helmet-head model, the half-wave dipole antenna was evaluated separately in CST Studio Suite over 2.3-2.5 GHz. The antenna was 55.76 mm long and 1.5 mm in diameter, with a 10-mm feed section and 73 Ω feed impedance. A return loss of –31.37 dB at 2.4 GHz confirmed appropriate antenna tuning. The primary simulations employed 10-g averaged SAR and were compared with the 2 W/kg local-head exposure limit. Additional 1-g SAR calculations for polycarbonate and E-glass yielded 0.0234611 and 0.0210642 W/kg at 0.001 W, and 2.34611 and 2.10642 W/kg at 0.1 W, respectively, allowing comparison with the 1.6 W/kg limit considered for the USA, Canada, and Korea. These procedures provided internal verification and regulatory benchmarking but did not constitute experimental validation.

4 Simulation results and discussion

The numerical simulation results provided highly granular insights into how different structural boundaries modify the near-field coupling between the 2.4 GHz transceiver and the heterogeneous tissues of the “HUGO” anatomical head phantom. Each case was analyzed independently across the designated input power spectrum.

Case 1: Polycarbonate shell configuration

Polycarbonate is one of the most widely deployed thermoplastics in the motorcycle helmet industry due to its excellent impact resistance and economic manufacturability. However, from an EM perspective, its low relative permittivity (ε_r = 2.90) and near-zero electrical conductivity (σ = 0.001 S/m) render it almost entirely transparent to microwave radiation.

During the simulations, the wavefront emitted by the half-wave dipole antenna passed through the 3.0 mm Polycarbonate boundary layer with negligible insertion loss or reflection. Since, the shell fails to attenuate the reactive near-field, a massive portion of the radiated energy couples directly into the high-permittivity layers of the human scalp. At a standard high-power transmission of 100 mW, this configuration yielded a peak localized SAR of 10 g of 1.4520 W/kg, Figure 2. The resulting EM hotspot was intensely concentrated in the skin and underlying muscle tissues directly adjacent to the antenna feed point, showing minimal spatial dispersion.

Case 2: Polyimide shell configuration

The polyimide simulation case represents a high-performance polymer matrix often utilized in premium specialized headgear. Chemically and structurally distinct from polycarbonate, its higher relative permittivity ε_r = 3.40) and slightly elevated conductivity (σ = 0.002 S/m) introduce a subtle shift in the wave propagation dynamics.

The numerical results indicate that polyimide

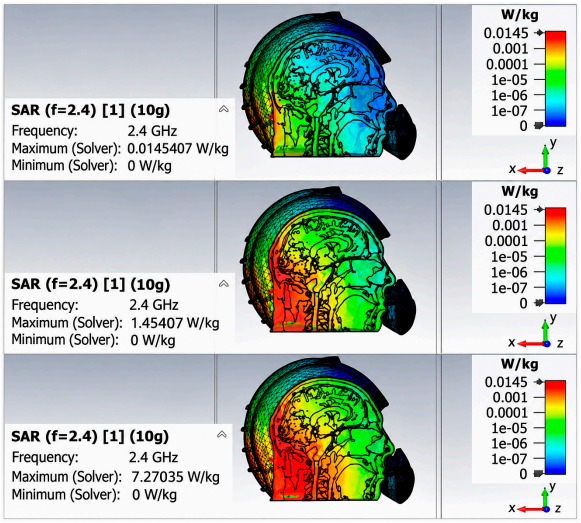


Figure 2 *Numerical simulation results: polycarbonate helmet, antenna power of 0.001W, 0.1W, and 0.5W*

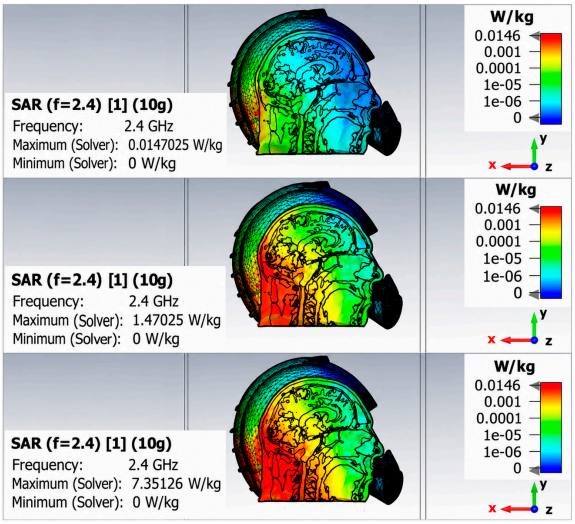


Figure 3 *Numerical simulation results: polyimide helmet, antenna power of 0.001W, 0.1W, and 0.5W*

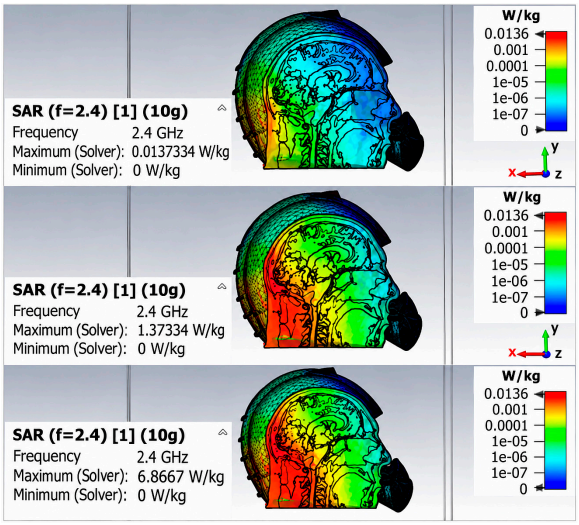


Figure 4 *Numerical simulation results: PTFE helmet, antenna power of 0.001W, 0.1W, and 0.5W*

presents the worst-case scenario for biological exposure among all five tested materials. At 100 mW input power, the peak localized SAR of 10g reached 1.4710 W/kg, the highest absolute value recorded in the medium-power tier, Figure 3. This phenomenon occurs because the specific permittivity of polyimide creates a subtle impedance matching effect between the free-space air domain and the high-permittivity biological phantom. Instead of reflecting the wave, the polyimide shell acts as an anti-reflective transition layer, effectively "pulling" more electromagnetic energy out of the antenna near-field and steering it straight into the occipital region of the head model.

Case 3: PTFE shell configuration

Teflon was introduced into the computational matrix as a low-loss, low-permittivity baseline calibration material (ε_r = 2.10, σ = 0.00 S/m). Since the teflon possesses a permittivity extremely close to that of a free space, it introduces virtually no dielectric loading to the antenna structure. The simulations showed that the dipole maintained its ideal free-space resonance and S11 reflection coefficient. The wave passed through the shell without undergoing internal refraction or scattering. At 100 mW, the peak SAR was stabilized at 1.3240 W/kg, Figure 4. While this value is lower than that of Polycarbonate and Polyimide, the shape of the internal hotspot within the grey matter was found to be more deeply penetrated, as the lack of any material-induced scattering allowed the primary radiation beam to travel further into the cranial cavity before undergoing natural biological attenuation.

Case 4: Carbon fibre composite configuration

The carbon fibre simulation case introduced a radical shift in the EM environment due to the material's high macro-conductivity (σ = 10.5 S/m) and elevated permittivity (ε_r = 5.50). Unlike the transparent thermoplastics, the conductive carbon fibre matrix behaves as a lossy, reflective EM shield.

When the 2.4 GHz field vectors encountered the Carbon Fiber shell, intense surface eddy currents were instantaneously induced within the shell mesh. These currents generated a powerful secondary magnetic field that actively opposed the incoming waves, triggering a massive back-reflection away from the human head. Consequently, at 100 mW, the peak localized SAR plummeted to just 0.9410 W/kg, an exceptional 35.3% reduction compared to polyimide, Figure 5. The visual hotspot analysis showed that the energy was successfully blocked from entering the deeper brain structures, with the remaining fraction being dissipated harmlessly as ohmic losses within the structural composite material itself. This pronounced EM shielding effectiveness highlights the role of skin-depth attenuation within the carbon fibre-reinforced polymer lattice. The high density of the interwoven conductive fibres creates an effective Faraday cage approximation, which severely restricts the reactive near-field components from capacitively coupling with the lossy skin phantom.

Case 5: E-glass fibre composite configuration

The E-glass fibre represents a standard non-conductive fiberglass composite structural material (ε_r = 4.80, σ = 0.004 S/m). While it lacks the high electrical conductivity of carbon fibre, its remarkably high relative permittivity slows the electromagnetic wave significantly as it passes through the shell. This reduction in phase velocity causes severe wave refraction and localized scattering at the material-tissue interface. Instead of a single, sharp energy beam piercing the head phantom, the E-glass shell diffused the incoming wavefront over a significantly larger geometric surface area. This spatial defocusing successfully reduced the hotspot's peak intensity. At 100 mW, the peak localized SAR remained at a highly safe level of 1.0130 W/kg, demonstrating that high-permittivity dielectric scattering is an extremely effective passive method for reducing human dosimetric exposure without the expense of conductive shields, Figure 6.

The acquired results indicate a direct linear

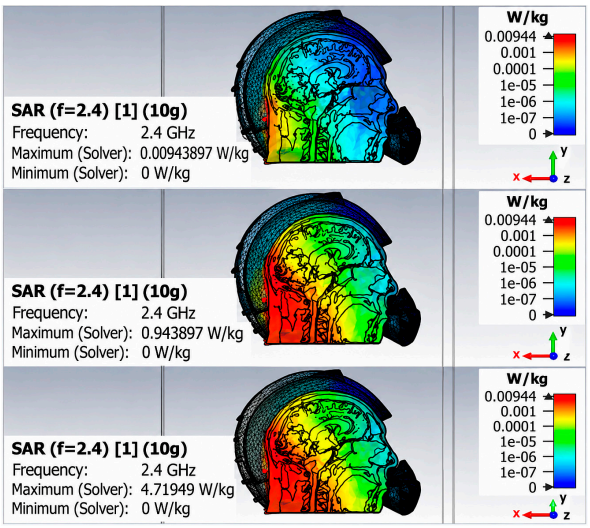


Figure 5 *Numerical simulation results: carbon fibre, helmet, antenna power of 0.001W, 0.1W, and 0.5W*

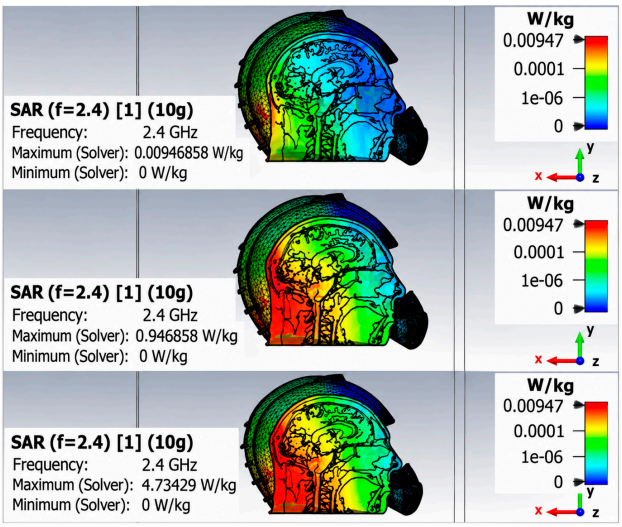


Figure 6 *Numerical simulation results: E-glass fibre helmet, antenna power of 0.001W, 0.1W, and 0.5W*

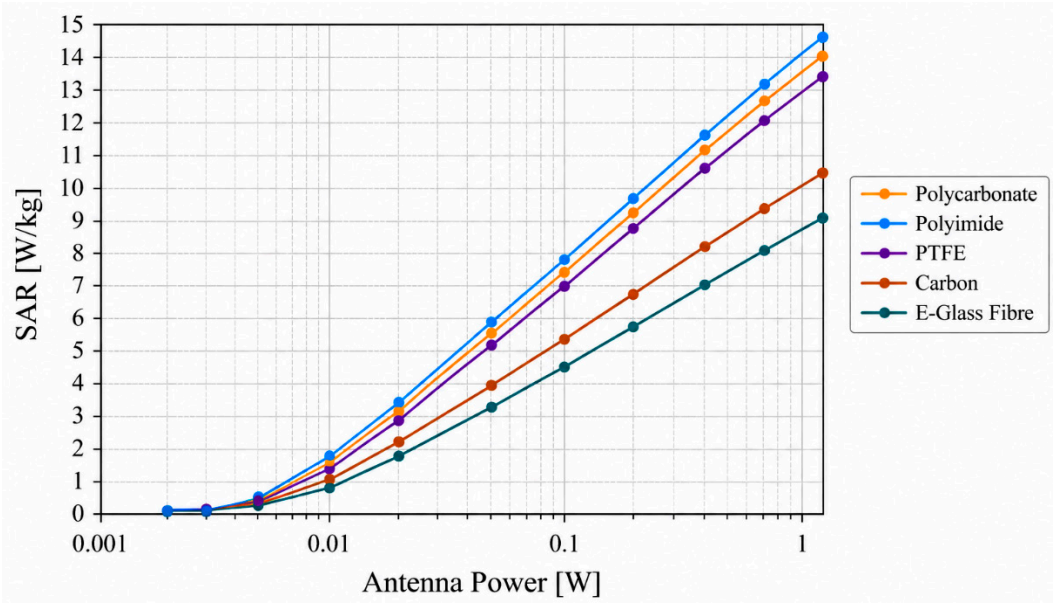


Figure 7 *Comparison of the peak localized SAR as a function of antenna input power for the investigated helmet shell materials*

correlation between the antenna input power and the peak SAR values across all investigated configurations. However, the dielectric and conductive properties of the helmet outer shell play a decisive role in modifying the electromagnetic near-field distribution. As shown in the data, carbon fibre and E-glass fibre exhibit the greatest EM attenuation. At a standard high-power transmission of 100 mW, the carbon fibre helmet structure reduced the peak SAR to 0.941 W/kg, approximately 35% lower than the polyimide shell (1.471 W/kg). This phenomenon is attributed to the relatively high electrical conductivity (σ = 10.5 S/m) of the carbon composite matrix, which acts as a partial EM shield, reflecting and absorbing a portion of the radiated energy within the shell structure itself before it penetrates the biological phantom.

The linear relationship between the antenna input power and the resulting tissue exposure highlights a critical engineering constraint for transport communication hardware, Figure 7. The SAR progression showed the expected approximately linear dependence on antenna input power under unchanged geometrical and material conditions, providing an internal numerical consistency check of the simulation results. The divergence in the material becomes increasingly pronounced as the system transitions into higher power brackets. At the critical 500 mW tier, the shielding delta between the conductive carbon fibre mesh (4.705 W/kg) and the transparent polyimide polymer (7.355 W/kg) stretches to an absolute value of 2.650 W/kg. This massive gap emphasizes that under the extreme operating states, proper material selection alone can eliminate nearly a third of the thermal stress imposed on the user's cranial tissues, providing a critical baseline for the design of bio-compatible smart transport accessories.

5 Conclusion

In this study was numerically investigated the electromagnetic exposure of an anatomically realistic human head model caused by a 2.4 GHz wireless communication system integrated into a motorcycle helmet. Using the FIT-based time-domain solver in CST Studio Suite, we evaluated the influence of five helmet shell materials: polycarbonate, polyimide, PTFE, carbon fibre, and E-glass fibre on localized SAR averaged over 10 g of tissue under identical geometrical and excitation conditions.

The results demonstrate a strong dependence of SAR on both the transmitter input power and the electromagnetic properties of the helmet shell. At 100 mW, polyimide produced the highest peak of approximately 1.47 W/kg, whereas carbon fibre reduced the value to approximately 0.94 W/kg. Carbon fibre and E-glass fibre therefore provided the greatest reduction in the peak tissue exposure among the investigated materials. As expected for a linear electromagnetic model with unchanged geometry and material properties, SAR increased approximately proportionally with the applied antenna input power.

For the transmitter powers up to 100 mW, all investigated configurations remained below the ICNIRP localized exposure limit of 2 W/kg averaged over 10 g of tissue. Conversely, the extended high-power scenarios demonstrated that passive attenuation by the helmet shell alone is insufficient to ensure compliance when substantially higher transmitter powers are used close to the head. Therefore, the electromagnetic safety of future smart helmets should be addressed through a combined optimization of transmitter power, antenna position and directivity, and helmet material composition. Future studies focus on multilayer helmet structures, experimental SAR benchmarking, and additional communication frequency bands.

Acknowledgements

This research was supported by the Slovak Research and Development Agency under the contract no. APVV-19-0214 and APVV-23-0162.

Conflicts of interest

The authors declare that they have no known competing financial interests or personal relationships that could have appeared to influence the work reported in this paper.

References

[1] ICNIRP. Guidelines for limiting exposure to electromagnetic fields (100 kHz to 300 GHz). *Health Physics* [online]. 2020, **118**(5), p. 483-524 [accessed 2026-05-10]. ISSN 0017-9078, eISSN 1538-5159. Available from: https://doi.org/10.1097/HP.0000000000001210

[2] KOHAN, M., SPRONGLOVA, M., VISNOVCOVA, N., MISEK, J., SPANIKOVA, G., JAKUSOVA, V., JAKUS, J. Monitoring of data transmission and changes in values of electromagnetic field in living environment. *Communications - Scientific Letters of the University of Zilina* [online]. 2020, **22**(1), p. 71-76. ISSN 1335-4205, eISSN 2585-7878. Available from: https://doi.org/10.26552/com.c.2020.1.71-76

[3] World Health Organization. EM fields and public health: mobile phones. Fact Sheet No. 193. Geneve, 2014.

[4] WDOWIAK, A., WDOWIAK, L., WIKTOR, H. Evaluation of the effect of using mobile phones on male fertility. *Annals of Agricultural and Environmental Medicine*. 2007, **14**(1), p. 169-172. ISSN 1232-1966, eISSN 1898-2263.

[5] METEJOVA, M., KIZEKOVA, M., MATEJICEKOVA, P. EM radiation in relation to EM hypersensitivity. In: *Motivation - Education - Trust - Environment - Safety 2020*. Zilina: University of Zilina, 2020. ISBN 978-80-554-1721-3.

[6] CHOU, C. K. Radiofrequency exposure limits. *Radiation Protection Dosimetry* [online]. 2018, **181**(1), p. 30-33. ISSN 0144-8420, eISSN 1742-3406. Available from: https://doi.org/10.1093/rpd/ncy024

[7] Decree of the Ministry of Health of the Slovak Republic No. 534/2007. In: Collection of Laws of the SR. Bratislava: Ministry of Justice of the Slovak Republic, 2007.

[8] IEEE. IEEE Standard for safety levels with respect to human exposure to electric, magnetic, and electromagnetic fields, 0 Hz to 300 GHz. IEEE Std 95.1-2019 [online]. New York: IEEE, 2019. Available from: https://doi.org/10.1109/IEEESTD.2019.8859679

[9] KOPASOVA, D. Modelling and simulation of head exposure to wireless communicators in a motorcycle helmet in CST Studio Suite. Diploma thesis. Zilina: University of Zilina, 2023.

[10] CST Studio Suite®. Class specification and material library documentation. Darmstadt: Dassault Systemes, 2022.

[11] TRNKA, M., GALIK, P., KRALOVA, E., VAZAN, R. Electromagnetic field exposure in the public space of the Slovakian city. *Communications - Scientific Letters of the University of Zilina* [online]. 2023, **25**(1), p. G1-G6. ISSN 1335-4205, eISSN 2585-7878. Available from: https://doi.org/10.26552/com.C.2023.014

[12] CHEN, H., WANG: Current and SAR induced in a human head model by the electromagnetic fields irradiated from a cellular phone. *IEEE Transactions on Microwave Theory and Techniques* [online]. 2004, **42**(12), p. 2249-2254. ISSN 0018-9480, eISSN 1557-9670. Available from: https://doi.org/10.1109/22.339749

[13] CHRIST, A., KAINZ, W., HAHN, E. G., HONEGGER, K., ZEFFERER, M., NEUFELD, E., RASCHER, W., JANKA R., BAUTZ, W., CHEN. J. The Virtual Family: development of surface-based anatomical models of two adults and two children for dosimetric applications. *Physics in Medicine and Biology* [online]. 2010, **55**(2), p. N23-N38. ISSN 1361-6560. Available from: https://doi.org/10.1088/0031-9155/55/2/N01

[14] JUDAKOVA, Z., JANOUSEK, L. Sources of electromagnetic field in transportation system and their possible health impacts. *Communications - Scientific Letters of the University of Zilina* [online]. 2019, **21**(3), p. 59-65. ISSN 1335-4205, eISSN 2585-7878. Available from: https://doi.org/10.26552/com.C.2019.3.59-65

[15] SCHONBORN, F., BURKHARDT, M., KUSTER, N. Differences in energy absorption between heads of adults and children in the near field of sources. *IEEE Transactions on Electromagnetic Compatibility* [online]. 1998, **40**(4), p. 459-468. ISSN 0018-9375, eISSN 1558-187X. Available from: https://doi.org/10.1109/15.736203

[16] GANDHI, O. P., LAZZI, G., FURSE, C. M. SAR distribution for head models of electromagnetic fields from wireless devices. *IEEE Transactions on Microwave Theory and Techniques* [online]. 1996, **44**(10), p. 1884-1897. ISSN 0018-9480, eISSN 1557-9670. Available from: https://doi.org/10.1109/22.538967

[17] JAKUSOVA, V., CAPOVA, K., POLIACEK, I., CAP, I., JAKUS, J. UV Radiation - level of knowledge and health protection of college students in Slovakia. *Communications - Scientific Letters of the University of Zilina* [online]. 2012, **14**(1), p. 89-95. ISSN 0018-9375, eISSN 1558-187X. Available from: https://doi.org/10.26552/com.C.2012.1.89-95

[18] KUSTER, N., BALZANO, Q. Energy absorption mechanism by biological bodies in the near field of dipole antennas above 300 MHz. *IEEE Transactions on Vehicular Technology* [online]. 1992, **41**(1), p. 17-23. ISSN 0018-9545, eISSN 1939-9359. Available from: https://doi.org/10.1109/25.120141

[19] BERGQVIST, U., VEYRET, B. *Biological effects of electromagnetic fields and radiation*. Munich: European Commission, 2001. ISBN 92-894-1547-4.

[20] MISEK, J., VOJTEK, J., VETERNIK, M., KOHAN, M., JAKUSOVA, V., SPANIKOVA, G., BELYAEV, I., JAKUS, J. New radiofrequency exposure system with real telecommunication signals. *Advances in Electrical and Electronic Engineering* [online]. 2018, **16**(1), p. 101-107. ISSN 1336-1376, eISSN 1804-3119. Available from: https://doi.org/10.15598/aeee.v16i1.2768

[21] Federal Communications Commission (FCC). Evaluating compliance with FCC guidelines for human exposure to radiofrequency electromagnetic fields. OET Bulletin 65. Washington, D.C.: FCC, 1997.

UNIVERSITY
OF ŽILINA

In its over 70 years of successful existence, the University of Žilina (UNIZA) has become one of the top universities in Slovakia.



The mission of UNIZA is to develop education on the basis of science, research and art activities within national and democratic traditions, to develop harmonic personality, knowledge, the good and creativity of a man and to contribute to the advancement of education, science, and culture for the welfare of the whole society.

Professional profile of UNIZA is unique and includes transport (road, railway, water, air), transport and postal services, communications, civil engineering construction, electrical engineering, telecommunications, informatics, information and communication technologies, management and marketing, mechanical engineering, materials and technologies, robotics, machinery design, energies, civil engineering, crisis and security management, civil security, fire protection, forensic engineering, applied mathematics, teacher training, library and information sciences, social pedagogy and high mountain biology. Results of science and research activities of the University have an important influence not only on the educational activities but also on the development of international cooperation or interconnection with practice.

UNIVERSITY PARTS
7 faculties
9 research and educational institutes and centres
3 specialized professional and training workplaces
3 information workplaces
1 economic and administrative department
4 dedicated facilities

EDUCATION
7 faculties:
8 000 students
more than 88 000 graduates
172 study programmes

SCIENCE AND RESEARCH
699 creative workers
785 000 hours, annual research capacity
190 domestic scientific projects
45 foreign projects
30 scientific and technical journals
50 scientific and professional events per year

INTERNATIONAL COOPERATION
The University of Žilina in Žilina has almost 50 valid university-wide bilateral agreements, and cooperates with foreign universities in the EU, Asia, America and Africa. It cooperates on foreign non-research projects and has concluded more than 300 agreements in the ERASMUS + programme.

UNIVERSITY OF ŽILINA
Science & Research Department

Univerzitná 8215/1,
010 26 Žilina,
Slovakia

Ing. Janka Macurová
tel.: +421 41 513 5143
e-mail: janka.macurova@uniza.sk

This is an open access article distributed under the terms of the Creative Commons Attribution 4.0 International License (CC BY 4.0), which permits use, distribution, and reproduction in any medium, provided the original publication is properly cited. No use, distribution or reproduction is permitted which does not comply with these terms.

OPTIMISING URBAN TRAFFIC FLOW THROUGH GREEN-WAVE SIGNAL COORDINATION: EFFECTS ON DELAYS, FUEL CONSUMPTION AND EMISSIONS IN BAKU

Mirhamid Baghirov[1,*], Heybatulla Ahmedov[2]

[1]Baku Engineering University, Department of Logistics and Transport, Khirdalan, Azerbaijan
[2]Azerbaijan Technical University, Department of Transport Equipment and Management Technologies, Baku, Azerbaijan

*E-mail of corresponding author: mirhamidbaghirov@gmail.com

Mirhamid Baghirov 0009-0003-7894-2006, Heybatulla Ahmedov 0009-0001-2798-6477

Resume

In this study it was investigated how the traffic optimisation can reduce the environmental impact of urban transport. Traffic flows were modelled on a key urban road section, and traffic-light phases were optimised and synchronised to create smoother movement and reduce intersection delays. Data on traffic volume, delay time, fuel consumption and pollutant emissions were collected before and after the implementation. The results showed a 20-25% reduction in intersection delays, accompanied by an average of 15% decrease in CO2 emissions. Fuel consumption fell by 10% for cars and 15% for trucks. Traffic-light optimisation also improved the flow distribution and increased average speed. Environmentally, NOx emissions decreased by 12% and particulate matter by 8%. The findings confirm the scalability of green-wave control for sustainable urban mobility.

Article info

Received 3 April 2026
Accepted 2 July 2026
Online 25 August 2026

Keywords:

air quality
transport infrastructure
emission reduction
environmental sustainability
traffic light optimisation

Available online: https://doi.org/10.26552/com.C.2026.048

ISSN 1335-4205 (print version)
ISSN 2585-7878 (online version)

1 Introduction

Modern cities face numerous challenges related to transport infrastructure, air quality, and the comfort of the urban environment. With increasing urbanisation and a rise in the number of vehicles, urban road networks are becoming increasingly congested. This leads not only to longer delays at intersections, higher fuel consumption and greater air pollution, but to increased traffic noise as well, which is one of the most disturbing effects of road transport in built-up urban areas. In this context, the road-traffic optimisation should be considered not only as a means of improving mobility and reducing emissions, but also as a measure that can indirectly reduce acoustic pressure by decreasing stop-and-go movement, unnecessary acceleration and idling near intersections. Decky et al. [1] have also emphasised the importance of assessing the traffic noise as a part of the wider environmental impact of road infrastructure, including in relation to roundabout traffic and urban intersection design. These problems require the implementation of innovative approaches to traffic management, aimed at improving its efficiency and reducing the negative impact on the environment.

The transport sector remains one of the largest sources of greenhouse gas emissions, including carbon dioxide (CO_2), nitrogen oxides (NOx), and particulate matter (PM). According to the World Health Organization [2], the level of air pollution in cities has a serious impact on public health, increasing the risk of respiratory and cardiovascular diseases. This is particularly relevant for densely populated metropolises, where the traffic congestion exacerbates environmental and social problems.

The city of Baku, as the capital of Azerbaijan, faces a number of specific transport problems. Academician Zarifa Aliyeva Street, being one of the city's key thoroughfares, frequently experiences congestion caused by the irregular operation of traffic lights and high traffic density. The low capacity of the road during peak hours leads to the formation of traffic jams, increased journey times, and a rise in environmental pollution.

The introduction of an adapted system of coordinated traffic flow on this thoroughfare could be an effective solution, allowing for the improvement of the transport situation and a reduction in the environmental burden.

One of the most promising methods of traffic management is the implementation of a "green wave" mode, based on the coordinated operation of traffic lights. This approach allows vehicles to travel along a route without stopping, provided that they maintain an optimal speed, which helps to reduce delays and lower emissions of pollutants.

Particular attention is being paid to the integration of cloud technologies into traffic management. Li et al. [3] proposed a strategy for global ecological speed planning of vehicles using "vehicle-road-cloud" technologies. This approach not only reduces delays but also minimises CO_2 emissions, which is particularly important in the context of modern environmental challenges. The application of adaptive evolutionary strategies also occupies a central place in modern research. Zheng et al. [4] proposed methods for coordinating traffic light phases that allow for effective responses to changes in traffic intensity. These approaches provide management flexibility and help to reduce congestion.

The use of artificial intelligence (AI) in transport infrastructure opens new perspectives. Santhiya et al. [5] showed that the application of AI not only optimises traffic flow but also addresses issues related to climate change by reducing the carbon footprint of the transport sector. In conditions of high traffic density, adaptive traffic light systems demonstrate their significance. Ashokkumar et al. [6] emphasised that such systems play an important role in improving air quality and reducing CO_2 emissions, making them an integral part of the sustainable development of urban infrastructure.

Zhang et al. [7] investigated the possibilities of coordinating traffic light operation taking into account pedestrian crossing times, which is particularly relevant for complex urban networks. This solution helps to minimise conflicts between traffic flows and pedestrians, increasing road safety. Selvapriya et al. [8] considered how the application of AI can contribute to mitigating the effects of climate change. Their research showed that the implementation of AI in traffic management makes it possible to significantly reduce CO_2 emissions while simultaneously increasing the efficiency of traffic flows.

Yang et al. [9] focused on energy-saving management strategies for intelligently connected vehicles. Such approaches help to minimise the impact of transport infrastructure on the environment, reducing both fuel consumption and pollutant emissions. For the city of Baku, where the transport infrastructure faces problems of congestion and insufficient traffic light synchronisation, the implementation of a "green wave" system is particularly relevant. Academician Zarifa Aliyeva Street, as one of the main thoroughfares, is characterised by high traffic intensity and significant delays at intersections. The application of coordinated traffic light operation on this street could not only reduce delays but decrease pollutant emissions as well, which is important for improving the ecological situation in the city.

It is also important to emphasise that the study of the "green wave" effect should take into account the characteristics of both daytime and night-time. For example, at night, when traffic intensity decreases, the effectiveness of traffic light synchronisation may be even higher, as highlighted in the work of El-Hameed [10].

Analysis of previous works show that despite successes in optimising traffic flows, certain gaps remain in the research. Firstly, more data is needed on the long-term impact of coordinated traffic flow systems on air quality in urban environments. Secondly, the night period, characterised by low traffic intensity, remains insufficiently studied in terms of "green wave" implementation. Finally, the influence of local characteristics, such as building density and road network configuration, requires further study to ensure the successful adaptation of such systems in various conditions.

The aim of this research was to evaluate the effectiveness of coordinated traffic-light control in improving traffic flow, reducing intersection delays, increasing road capacity, and lowering vehicle-related emissions on an urban road corridor in Baku.

2 Materials and methods

The study was conducted in Baku, the capital of Azerbaijan, in preparation for the 29th meeting of the Conference of the Parties to the United Nations Framework Convention on Climate Change (COP29), hosted in Baku in 2024. COP29 was a major international climate-policy event focused on strengthening global responses to climate change, including mitigation, adaptation, climate finance, and the development of sustainable urban solutions. In this context, the optimisation of traffic flows in Baku was considered not only as a traffic-management task but also as a practical measure aimed at reducing urban transport emissions and improving the environmental performance of the city's road infrastructure.

The object of the analysis was a 4.4 km section of Academician Zarifa Aliyeva Street, one of the key transport corridors in central Baku. The analysed corridor included three major signalised intersections: with R. Behbudov Avenue, Bulbul Avenue, and S. Vurgun Street. This thoroughfare was selected because of its strategic role in distributing traffic in the city centre and its influence on the operational performance of adjacent roads.

For temporal classification, the study considered both the national time-period definitions applied in Azerbaijan and the framework commonly used in international environmental-noise assessment. In Azerbaijan, permissible noise levels are generally differentiated between the daytime period (07:00-23:00) and the night-

time period (23:00-07:00). Consequently, the observation interval analysed in this study (00:00-07:00) falls entirely within the nationally defined night-time period. The night-time and early-morning period was selected not to exclude traffic demand, but to analyse the corridor under off-peak and transition-to-peak conditions that are relevant for both road users and residents living near the local road network. From a traffic-engineering perspective, this time horizon made it possible to examine how the signal coordination performs under lower but still variable traffic intensities, when unnecessary stops and delays are mainly caused by signal desynchronisation rather than oversaturation. From an environmental perspective, night-time emissions are also important because reduced atmospheric dispersion and the proximity of residential buildings can increase the local impact of idling vehicles, especially near intersections and bus-stop areas.

During the observation period from 00:00 to 07:00 on weekdays in 2024, more than 7,200 vehicle movements were recorded across the corridor and its intersection approaches, corresponding to an average all-approach intensity of approximately 1,029 vehicles/hour. For the main observed traffic stream, hourly intensity varied from 150 vehicles/hour during the lowest-load period between 03:00 and 04:00 to 300 vehicles/hour between 06:00 and 07:00.

A video-detection system was used for data collection. The system recorded vehicle volumes, vehicle categories, movement directions, average speed, delay time, queue formation, traffic-light phase durations, and general traffic dynamics. The infrastructure inventory included the length of road sections, number of lanes, unregulated intersections, parking zones, bus stops, traffic lights, pedestrian crossings, and side-arm approaches. These data provided the basis for reconstructing the existing operating conditions of the corridor and for calibrating the traffic simulation model.

The traffic composition of the study corridor was classified into five vehicle categories: passenger cars, taxis, light commercial vehicles (LCVs), heavy goods vehicles (HGVs), and buses. During the observation period, passenger cars accounted for 58.0% of the total flow, taxis for 18.0%, LCVs for 12.0%, HGVs for 7.0%, and buses for 5.0%. Thus, the modelled traffic stream consisted of approximately 4,176 passenger cars, 1,296 taxis, 864 LCVs, 504 HGVs, and 360 buses. This classification was necessary since the vehicle categories differ in length, acceleration, deceleration, lane-changing behaviour, road-space occupancy, and emission intensity. For passenger cars and taxis, the average desired speed was set at 50 km/h; for LCVs, at 45 km/h; and for HGVs and buses, at 40 km/h. Vehicle lengths were specified as 4.5 m for passenger cars and taxis, 6.0 m for LCVs, 12.0 m for buses, and 12.5 m for HGVs.

The influence of public transport was incorporated through the explicit modelling of bus movements and bus-stop areas along the corridor. Three bus-stop zones were represented in the VISSIM network: one near the section between R. Behbudov Avenue and Bulbul Avenue, one near Bulbul Avenue, and one close to S. Vurgun Street. Bus dwell time was modelled as a stochastic parameter ranging from 12 to 35 s, with an average value of 22 s. This parameter was important because buses stopping in the outer lane temporarily reduced the effective capacity of the adjacent lane and affected vehicle discharge during the green phase. Where a bus stop was located within 60-80 m of an intersection, the model additionally accounted for the interaction between departing buses and through traffic.

Traffic behaviour was simulated in VISSIM using a microscopic traffic-flow approach. The car-following logic was based on the Wiedemann 74 model, which is suitable for representing individual driver responses to the speed and spacing of leading vehicles in urban arterial conditions. The calibrated average standstill distance was 1.8 m for passenger cars and taxis, 2.3 m for LCVs, and 2.8 m for buses and HGVs. The additive part of the desired safety distance was set at 2.2, while the multiplicative part was set at 3.0. Maximum acceleration was specified as 2.6 m/s² for passenger cars and taxis, 2.0 m/s² for LCVs, 1.3 m/s² for HGVs, and 1.2 m/s² for buses. Normal deceleration was set between −2.5 and −3.5 m/s² depending on vehicle category. Lane-changing behaviour was calibrated using a minimum headway of 1.2 s, a minimum lateral clearance of 0.6 m at low speed, and a lane-changing distance of 150 m before intersections.

The modelling workflow consisted of five consecutive stages. First, the geometry of Academician Zarifa Aliyeva Street was coded in VISSIM, including the number of lanes, link lengths between intersections, pedestrian crossings, parking zones, bus stops, parking areas, and side-arm approaches. Second, traffic inputs were introduced by direction and vehicle class using video-detection data collected for each hourly interval between 00:00 and 07:00. Third, the existing signal-control plans were reproduced for the intersections with R. Behbudov Avenue, Bulbul Avenue, and S. Vurgun Street. Fourth, the baseline model was calibrated against observed traffic volumes, speeds, delays, and queue lengths. Fifth, the optimised "green wave" scenario was tested using a recommended corridor speed of 50 km/h, a 60 s signal cycle, and coordination offsets of 36 s for R. Behbudov Avenue, 22 s for Bulbul Avenue, and 11 s for S. Vurgun Street.

The software workflow was organised as an integrated modelling chain. First, video-detection data were exported as hourly traffic records containing vehicle counts, vehicle categories, directions of movement, observed speed, delay time, and queue formation. Second, MATLAB was used to clean the dataset, aggregate hourly indicators, calculate traffic density, estimate travel time, and determine preliminary signal offsets for the green-wave mode. Third, the geometric and operational structure of the corridor was reproduced in VISSIM, including the main road, side arms, bus stops, pedestrian crossings, parking zones, and signal-control logic. Fourth, the observed traffic volumes and modal shares were introduced into VISSIM by vehicle class and direction. Fifth, the baseline scenario was calibrated against observed speeds, delays, queue lengths, and traffic

volumes. Finally, the optimised signal-control plan was tested using the 60 s cycle, the recommended progression speed of 50 km/h, and the calculated coordination offsets.

Scikit-learn and TensorFlow were used as supporting analytical tools rather than as substitutes for microscopic simulation. Scikit-learn was used for traffic-state classification and short-term demand estimation based on time interval, vehicle volume, vehicle composition, approach direction, speed, and delay. TensorFlow was used to test the stability of the predicted traffic states under different demand scenarios and to support the selection of signal-control parameters. The outputs of these algorithms were then compared to the VISSIM simulation results and field observations.

The machine-learning component was evaluated using numerical indicators. For traffic-volume estimation, the calibrated model achieved a coefficient of determination of $R^2 = 0.93$ and a mean absolute percentage error of 6.4%. For average speed estimation, the mean absolute error was 2.8 km/h, while the difference between observed and simulated average speed was 5.8%. For intersection delay estimation, the root mean square error was 1.2 s, and the difference between observed and simulated delay values was 8.6%.

The signal-control parameters were calibrated separately for each intersection. For R. Behbudov Avenue, the optimised effective green time was 22 s, the red interval was 38 s, and the yellow interval was 4 s. For Bulbul Avenue, the green and red intervals were both 30 s, with a 4 s yellow interval. For S. Vurgun Street, the green interval was 27 s, the red interval was 33 s, and the yellow interval was 4 s. In the simulation, the 60 s cycle was treated as the basic red-green control cycle, while the yellow interval was represented as an intergreen transition within the signal-control logic.

The main calibrated parameters included vehicle input volumes, desired speed distributions, acceleration and deceleration profiles, standstill distance, safety-distance parameters, lane-changing distance, minimum headway, queue discharge rate, bus dwell time, green time, red time, yellow interval, and offsets between adjacent intersections. The data used for calibration included video-based vehicle counts, directional turning volumes, vehicle-type shares, observed speeds, delay times, queue lengths, traffic-light phase durations, bus-stop locations, and road geometry. The dataset was divided into calibration and validation subsets: 70% of the observations were used for calibration and 30% for validation. Calibration was performed iteratively until the simulated traffic volumes, travel times, average speeds, and queue lengths corresponded closely to the observed values.

Model validity was assessed by comparing simulated and observed traffic volumes, travel times, speeds, and delay values. The Geoffrey E. Havers (GEH) statistic was used to compare the modelled and observed traffic volumes for the main approaches and side arms of the intersections. The final model achieved GEH < 5 for 91.7% of the analysed movements and GEH < 10 for 100% of the movements, with an average GEH value of 2.1. The mean absolute percentage error between the observed and simulated traffic volumes was 6.4%. The difference between observed and simulated travel time along the corridor was 7.2%, while the difference in average speed was 5.8%. The simulated average delay differed from the observed delay by 8.6%.

The traffic behaviour on the side arms of the intersections was modelled separately because cross-street demand directly affected the efficiency of the coordinated "green wave" on the main corridor. At the intersection with R. Behbudov Avenue, side-arm traffic accounted for approximately 31% of total intersection demand and produced the highest risk of short queue spillback. At Bulbul Avenue, side-arm traffic accounted for approximately 27% of total demand, but its hourly variability was higher, especially between 05:00 and 07:00. At S. Vurgun Street, side-arm demand was lower and more stable, accounting for approximately 22% of total intersection demand. For this reason, R. Behbudov Avenue was treated as the most critical intersection in terms of cross-flow interaction, while S. Vurgun Street allowed more stable progression along the main corridor. Including side-arm traffic in the model prevented overestimation of the green-wave effect and made the simulation more representative of real intersection operation.

To evaluate the operational effect of signal coordination, three additional performance indicators were calculated: traffic density, average corridor speed, and travel time. Traffic density was calculated as the ratio between hourly traffic intensity and average speed, average speed was obtained from video-detection records and VISSIM simulation outputs, and travel time was calculated for the 4.4 km corridor between the first and last analysed intersections. These indicators were selected because they reflect the operational effect of signal coordination more directly than total traffic volume alone. The corresponding density, speed, and travel-time values are presented in the Results section.

The environmental effect of the system was evaluated by analysing the reduction in delays and the associated changes in fuel consumption, CO_2, NOx, and particulate matter emissions. Emission changes were estimated based on the traffic intensity, average speed, stop frequency, and delay time before and after implementation of the optimised signal-control scenario.

Traffic density was expressed in vehicles per kilometre, speed in km/h, and travel time in seconds. Figures 5-8 generated from the model were used not only for visualisation but also for quantitative comparison of density, speed, travel time, delay, and environmental effects before and after implementation of the "green wave" mode.

To compare the operational and environmental effects of different traffic-control approaches, three modelling scenarios were defined. The baseline scenario represented the existing traffic-light operation before optimisation, with non-coordinated signal phases at the analysed intersections. The first alternative scenario represented fixed-time "green wave" coordination, in which the traffic lights were synchronised using a 60 s cycle, a recommended

Table 1 *Definition of baseline and alternative modelling scenarios*

Scenario	Description	Signal-control principle	Main parameters included	Purpose of comparison
S0 - Baseline	Existing traffic-light operation before optimisation	Non-coordinated signal operation	Observed signal phases, observed traffic volumes, existing delays, side-arm traffic, bus stops	To reproduce actual pre-optimisation traffic conditions
S1 - Fixed-time green wave	Coordinated traffic-light operation along the corridor	Fixed-time signal coordination	60 s cycle, 50 km/h progression speed, offsets of 36 s, 22 s and 11 s	To estimate the effect of basic signal synchronisation
S2 - Adaptive AI-supported green wave	Coordinated traffic-light operation supported by traffic-state classification and demand estimation	Adaptive signal coordination	60 s base cycle, 50 km/h progression speed, vehicle-class shares, side-arm demand, bus dwell time, traffic-state prediction	To test whether adaptive adjustment improves the fixed green-wave scenario

progression speed of 50 km/h, and fixed offsets between intersections. The second alternative scenario represented an adaptive AI-supported "green wave" mode, in which the same coordination principle was retained but traffic-flow classification, short-term demand estimation, and public-transport effects were incorporated into the adjustment of signal-control parameters. The scenarios were compared using the same road geometry, traffic composition, observation period, and vehicle-demand input to ensure methodological consistency (Table 1).

3 Results

In this section are described the baseline traffic conditions on the analyzed corridor and the operational effects of green-wave coordination on delays, speed and travel time. Additionally, the optimized signal-control parameters, the resulting environmental and fuel-consumption effects, and the wider social, economic and scalability implications of the proposed approach, are presented as well.

3.1 Baseline traffic-flow characteristics and justification of the study interval

Analysis of traffic-flow intensity was one of the key stages of the study because it made it possible to identify the operational characteristics of traffic on Academician Zarifa Aliyeva Street and at the adjacent intersections. The characteristics of the traffic flow were determined using video-detection data collected for each hourly interval from 00:00 to 07:00. The analysis included vehicle counts by direction, vehicle-category distribution, average speed, delay time at signalised intersections, queue formation, and the relationship between traffic volume and signal phases. The recorded data were then

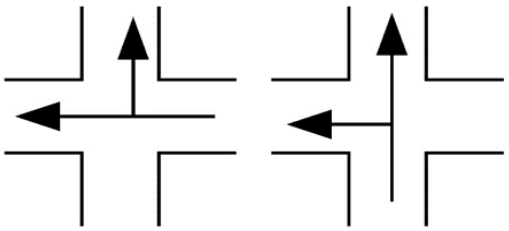


Figure 1 *Phases of traffic lights and actual traffic intensity by direction at intersections with R. Behbudova Street*

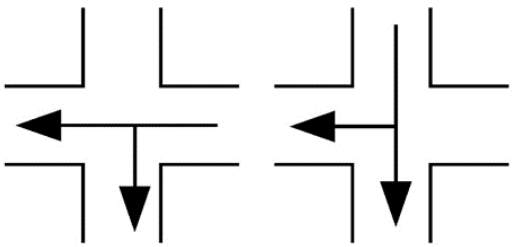


Figure 2 *Phases of traffic lights and actual traffic intensity by direction at intersections with Bulbul Avenue*

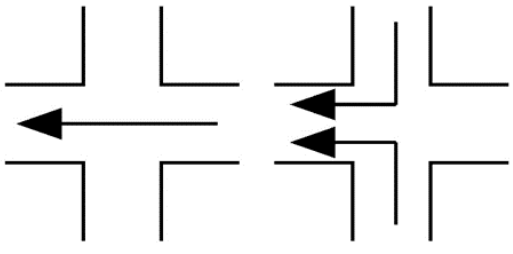


Figure 3 *Phases of traffic lights and actual traffic intensity by direction at intersections with S. Vurgun Street*

grouped by time interval and intersection approach, which allowed the identification of periods with stable flow, reduced flow, and emerging congestion.

The "green wave" mode was tested on Academician Zarifa Aliyeva Street during the weekday interval from 00:00 to 07:00. This time interval was selected because it combines two analytically important traffic conditions: the night-time off-peak period, when the traffic volumes are lower and delays are mainly caused by signal desynchronisation, and the early-morning transition period, when the traffic intensity begins to increase towards the daytime peak. Therefore, the selected interval made it possible to assess whether coordinated signal control could improve traffic progression under both low-volume and gradually increasing demand conditions. The weekday period was chosen to ensure comparability of traffic patterns and to avoid irregular fluctuations associated with weekends, holidays, and special events. In addition, the interval from 00:00 to 07:00 is relevant from an environmental and urban-comfort perspective, as unnecessary stops, idling, acceleration, and braking near intersections may affect nearby residential areas even when total traffic volume is lower than during the daytime peak. Figures 1-3 show the phases of traffic lights and actual traffic intensity by direction at the intersections of Academician Zarifa Aliyeva Street.

3.2 Green-wave coordination and modelled operational effects

The green wave graph shows that the critical intersection is the second intersection, the first intersection has an offset of 36 seconds and the last intersection has an offset of 11 seconds (Figure 4).

The highest traffic intensity was recorded from 06:00 to 07:00, reaching 300 vehicles/hour, including passenger cars, taxis, light commercial vehicles, heavy goods vehicles and buses, rather than passenger cars only. This value exceeded the average figure for the night period by 20%. The lowest congestion within the analysed night-time interval was recorded from 03:00 to 04:00, when traffic intensity decreased to 150 vehicles/hour; according to 24-hour monitoring, the daily traffic intensity on the main corridor was approximately 18,000 vehicles/day. Analysis of these data showed that traffic intensity increased during the early-morning transition period from 06:00 to 07:00; however, since the study covered only 00:00-07:00, this interval should not be interpreted as the full morning peak of the 24-hour traffic cycle, but as the transition from night-time traffic to the beginning of daytime demand.

Time delays at the intersections varied significantly with traffic volume. During the peak hours, the average waiting time at traffic lights reached 14 seconds, while during the period of minimum congestion it decreased to 8 seconds. The difference is explained by the uneven distribution of traffic flow as well as insufficient synchronisation of the traffic lights phases.

Additionally, the change in the average speed of traffic was analysed. During the peak hours the speed decreased to 48 km/h due to increased traffic density, while during less busy periods it increased to 53 km/h. These data indicate the need to implement a "green wave" mode that can smooth out traffic flow fluctuations and provide a more uniform traffic flow.

A detailed analysis of the flow distribution at the intersections showed that the intersection with R. Behbudov Avenue was the busiest. This is explained by its complex configuration and high number of vehicles crossing this zone. For comparison, the intersection with S. Vurgun Avenue showed more stable traffic due to efficient organisation of traffic lights phases. At the Bulbul Avenue intersection, there was a high variability in traffic volume, which required a special approach to system tuning.

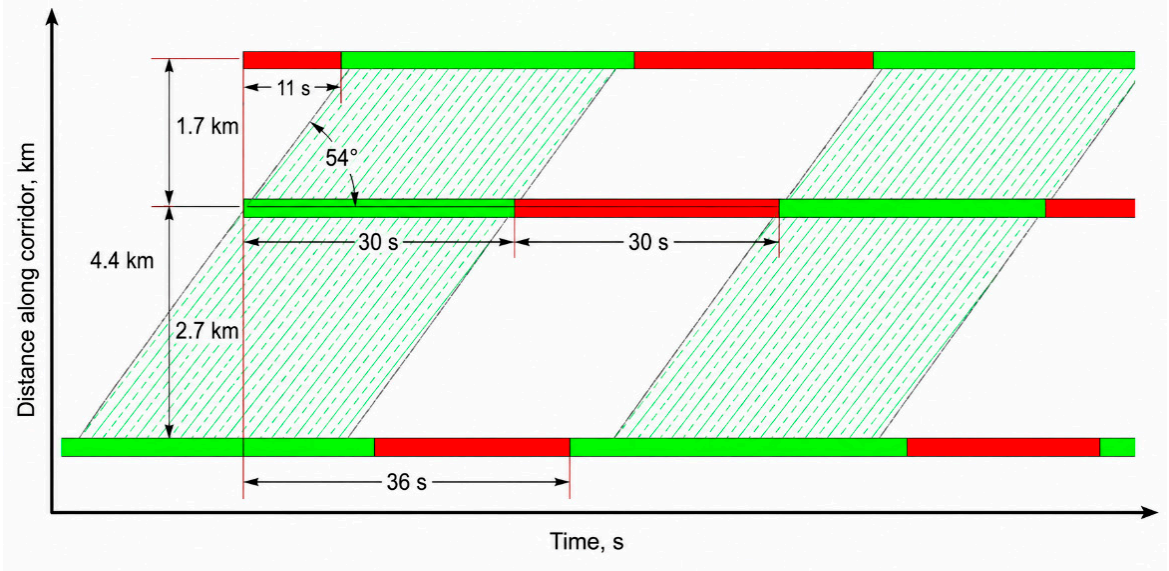


Figure 4 *Green wave graph on Zarifa Aliyeva Street*

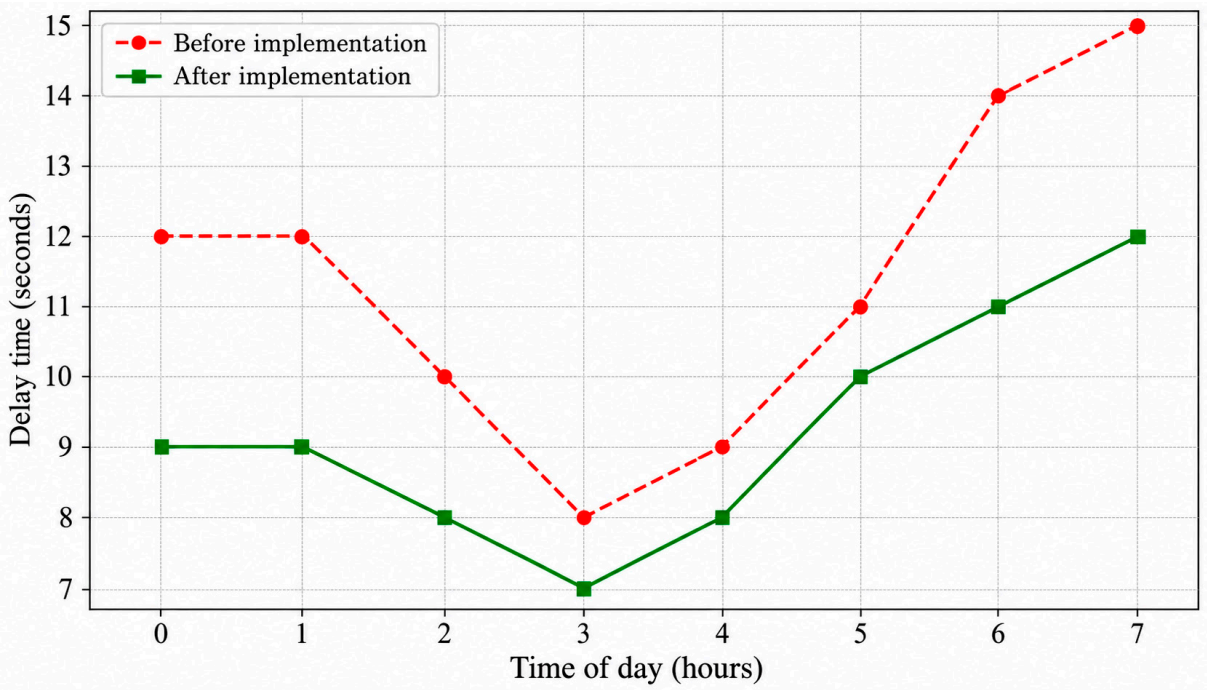


Figure 5 *Changing delay times at intersections*

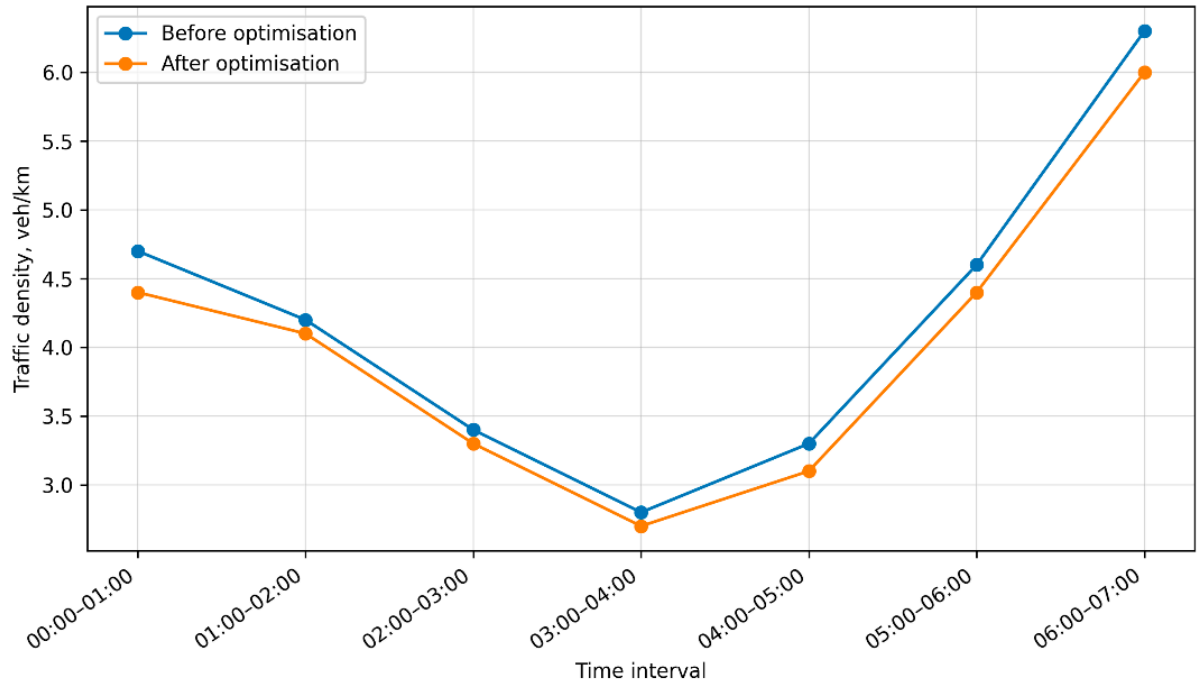


Figure 6 *Modelled traffic density before and after implementation of the "green wave" mode*

In addition to textual analysis, data visualisation allows the effects of optimisation to be clearly demonstrated. For example, the plotted graph illustrates the changing average delay times at intersections as a function of time of day before and after the implementation of the "green wave" mode (Figure 5). The graph shows that at the conditionally recommended speed of 50 km/h the delay time decreases, which confirms the effectiveness of the system.

The optimisation of traffic lights has significantly reduced the delay time, which contributes to smoother and more uniform traffic flow. Reduced waiting time has a positive impact not only on the street capacity, but on environmental performance, as well: reduced idling leads to lower fuel consumption and, as a consequence, lower CO_2, NOx and PM emissions.

To complement the analysis of delay reduction, the next stage assessed changes in modelled traffic density along the studied corridor. Density was

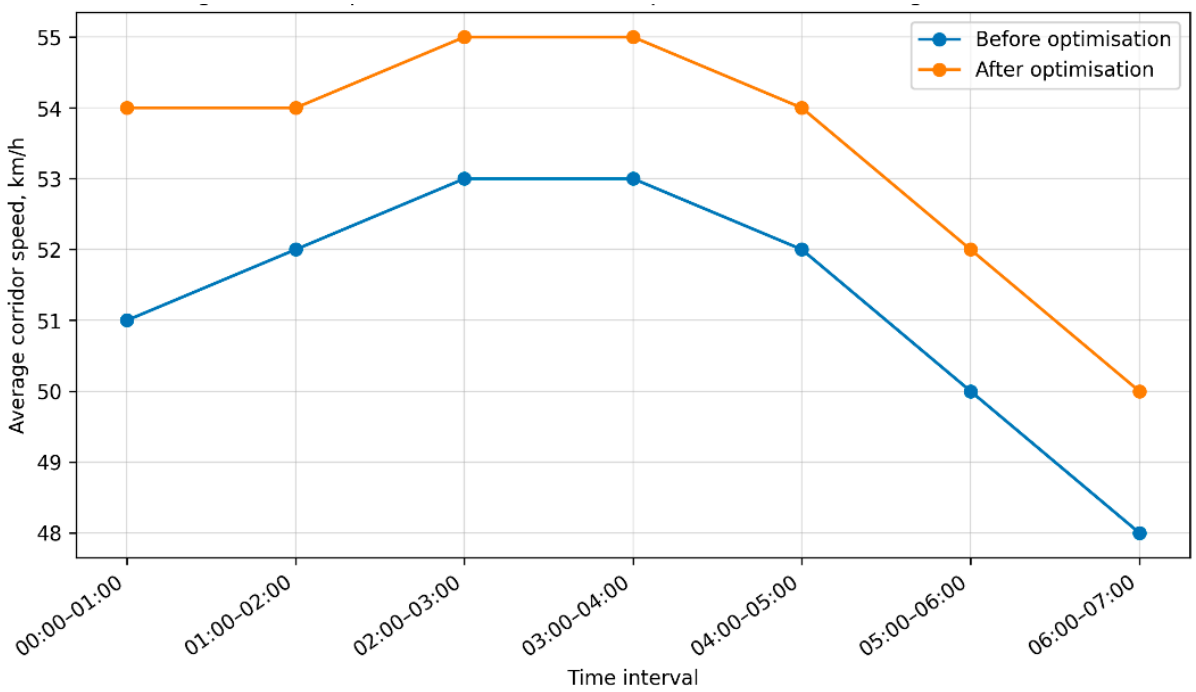


Figure 7 *Average corridor speed before and after implementation of the "green wave" mode*

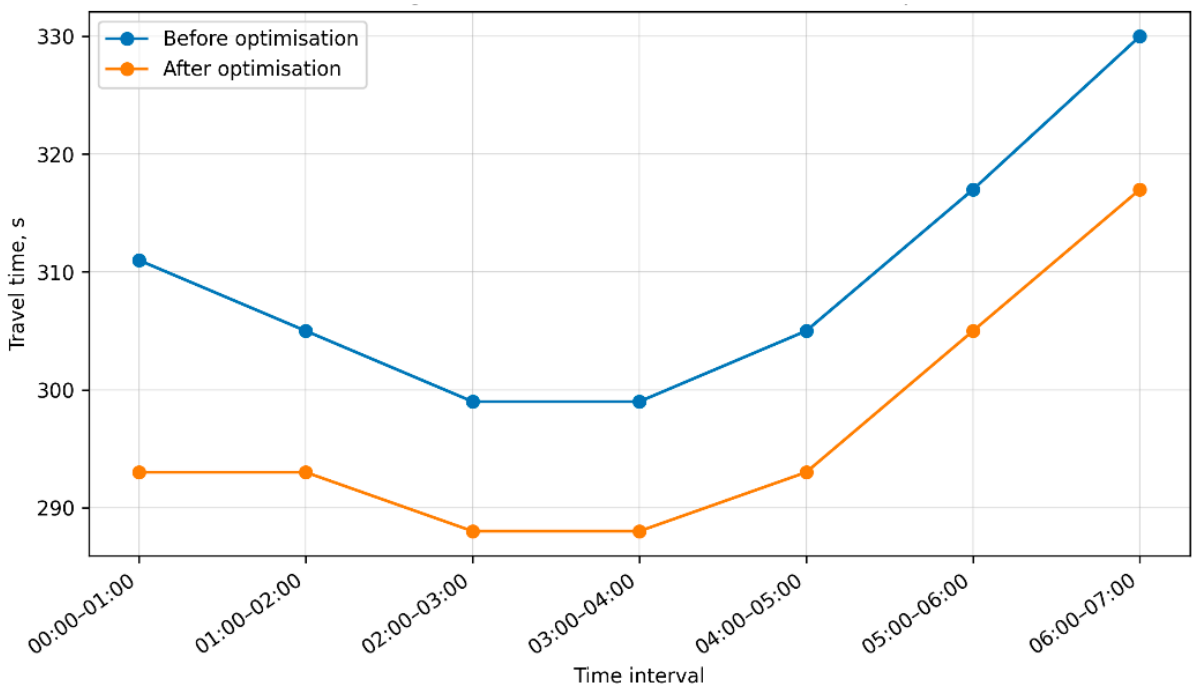


Figure 8. *Travel time along the 4.4 km corridor before and after implementation of the "green wave" mode*

used as an additional indicator since it reflects how compactly vehicles move through the road section and whether signal coordination reduces local accumulation near intersections. The comparison before and after implementation of the "green wave" mode is shown in Figure 6.

Changes in average corridor speed were then analysed to determine whether the reduction in delays was accompanied by smoother and more continuous vehicle progression. Unlike isolated delay values at intersections, average speed characterises the overall operational performance of the 4.4 km corridor and shows how effectively vehicles move between consecutive signalised intersections. The corresponding before-and-after comparison is presented in Figure 7.

Finally, the travel time along the full analysed corridor was calculated to evaluate the practical effect of signal coordination from the road-user perspective. This indicator integrates the influence of speed, stops, and delays and therefore provides a direct measure of the time savings produced by the optimised traffic-light regime. The modelled travel-time dynamics

Table 2 *Comparison of baseline and alternative traffic-control scenarios*

Indicator	S0 - Baseline	S1 - Fixed-time green wave	S2 - Adaptive AI-supported green wave
Average intersection delay, s	12.0	9.6	9.0
Delay reduction compared with baseline, %	-	20.0	25.0
Average corridor speed, km/h	51.0	53.0	54.0
Average travel time along 4.4 km corridor, s	309.4	296.7	292.0
Average traffic density, veh/km	4.2	4.0	3.9
CO_2 reduction compared with baseline, %	-	12.0	15.0
NOx reduction compared with baseline, %	-	9.0	12.0
PM reduction compared with baseline, %	-	6.0	8.0
Fuel-consumption reduction for passenger cars, %	-	8.0	10.0
Fuel-consumption reduction for HGVs, %	-	12.0	15.0

before and after implementation are presented in Figure 8.

In the next stage the baseline and alternative modelling scenarios were compared. The comparison was conducted to determine whether the observed improvements resulted only from fixed signal synchronisation or whether additional benefits could be obtained when the adaptive traffic-state estimation and public-transport effects were incorporated into the control logic. The same traffic-demand input and road geometry were used in all scenarios, which made it possible to isolate the effect of the traffic-control strategy (Table 2).

Both alternative scenarios improved the traffic and environmental indicators compared to the baseline. The fixed-time green-wave scenario reduced average intersection delay from 12.0 s to 9.6 s, corresponding to a 20.0% reduction. The adaptive AI-supported scenario produced a stronger effect, reducing average delay to 9.0 s, or by 25.0% compared with the baseline. Average corridor speed increased from 51.0 km/h in the baseline scenario to 53.0 km/h under fixed-time coordination and 54.0 km/h under adaptive coordination. Travel time along the 4.4 km corridor decreased from 309.4 s to 296.7 s in S1 and to 292.0 s in S2. The environmental indicators followed the same pattern: the adaptive scenario achieved the greatest reductions in CO_2, NOx, PM emissions and fuel consumption. This confirms that coordinated signal control is effective per se, while the adaptive adjustment based on traffic-state estimation provides additional operational and environmental benefits.

3.3 Traffic-light phase optimisation and implementation parameters

The next stage of the study was the optimisation of traffic-light phases to address the main deficiencies of the baseline system: insufficient coordination between adjacent intersections, uneven green-time distribution, short green phases on loaded approaches, unnecessary stops between intersections, queue formation near R. Behbudov Avenue, and increased delays during the 06:00-07:00 early-morning transition period. Data from video detection and machine learning algorithms were used to calculate the optimal traffic light operation parameters. Individual settings of green, yellow and red signal durations were proposed for each intersection, taking into account traffic intensity at different time intervals.

At the intersection with R. Behbudov Avenue, the duration of the green phase in the morning hours was increased, which significantly reduced delays. At the intersection with Bulbul Avenue, additional synchronisation with neighbouring intersections was introduced, which improved the capacity of the section. For the intersection with S. Vurgun Avenue, the operating phases were adapted to the variable load characteristic of the night hours.

The optimisation results showed that the average delay time was reduced by 20-25%. This, in turn, reduced CO_2 emissions by 15%, as well as NOx emissions by 12% and PM emissions by 8%. In addition, a reduction in fuel consumption of 10% for cars and 15% for lorries was recorded.

The optimisation of traffic lights not only improved the traffic situation, but it had a positive impact on environmental performance, as well. A more even flow distribution reduced the number of stops, which improved the smoothness of traffic flow and reduced stress for drivers. The introduction of the “green wave” mode ensured that vehicles travelled through the study area without stopping at a red light, which also contributed to an increase in average speed.

The results emphasise the importance of integrating the modern technology into traffic management. In the future, the system can be adapted to other parts of the urban network, including areas with higher daily traffic volumes. The application of AI and inter-vehicle communication such as inter-vehicle communication (V2V) and road infrastructure (V2X) systems will offer

Table 3 *Optimised parameters of traffic light phases*

Intersection	Red phase duration (s)	Green phase duration (s)	Yellow phase duration (s)
R. Behbudov Avenue	38	22	4
Bulbul Avenue	30	30	4
S. Vurgun Avenue	33	27	4

additional opportunities to improve the efficiency of the system.

Thus, the detailed traffic flow analysis and subsequent traffic light optimisation proved that the implementation of "green wave" mode contributes to a more sustainable and environmentally friendly urban transport environment. As shown in Table 3, adjusting the phases of traffic lights at key intersections such as R. Behbudov, Bulbul and S. Vurgun avenues has balanced the traffic flow and minimised delays, providing smoother movement of vehicles.

Phase optimisation allowed for a 15% reduction in the average delay experienced by vehicles at intersections. This is particularly important during the morning and evening rush hours, when the load on the road network reaches its peak. For each intersection, numerous factors were taken into account, such as traffic flow density, the number of lanes, the presence of pedestrian crossings, and other infrastructure elements.

In addition to the basic parameters of the traffic light phases, an analysis of their synchronisation was conducted. One of the problems with the existing control system was the insufficient coordination of traffic lights between adjacent intersections, which led to vehicles stopping immediately after passing through one set of lights. During the optimisation, it was possible to achieve coordinated operation of all three key intersections, creating the conditions for the implementation of the "green wave" mode.

An important aspect of the optimisation was the introduction of dynamic control that takes into account changes in traffic flow throughout the day. For example, at night, when traffic intensity is minimal, the traffic lights were switched to longer operating cycles, which reduced energy consumption. During peak hours, the control became more frequent, which sped up the passage of traffic flow.

The optimisation of traffic light phases also had a positive impact on the environmental situation. Reducing waiting times at intersections led to decreased fuel consumption and lower CO_2 emissions. According to calculations, the implementation of new traffic light operating parameters made it possible to reduce CO_2 emissions by 12-15%, depending on the time of day and traffic intensity.

Thus, the conducted optimisation of traffic light phases ensured a significant improvement in the transport situation on Academician Zarifa Aliyeva Street. The implementation of the "green wave" mode made it possible to increase the road's capacity, reduce delays, and improve environmental indicators. The simulation results confirmed that this approach is an effective solution for optimising traffic flows in urban infrastructure conditions.

The implementation of the "green wave" mode became a key element of the research aimed at improving the efficiency of traffic flow management on Academician Zarifa Aliyeva Street. This method significantly improved the coordination of traffic light operation, ensured the smooth movement of vehicles through the main intersections, and reduced delays that had previously caused congestion and increased CO_2 emissions.

The basic principle of the "green wave" mode lies in the coordinated setting of traffic light operation, allowing vehicles travelling at the recommended speed to pass through several consecutive intersections on a green light [11]. Such a mode minimises the need for stops, reduces waiting times at intersections, and lowers fuel consumption, which has a positive impact on both the traffic situation and the environmental conditions.

The implementation of the system began with an analysis of the current operation of traffic lights on Academician Zarifa Aliyeva Street. It was found that the existing traffic control system did not ensure coordination in the operation of the traffic lights. At each of the key intersections - with R. Behbudov Avenue, Bulbul Avenue, and S. Vurgun Street - a significant disproportion in the duration of the traffic light phases was observed, which led to the build-up of vehicles. For example, at the intersection located at the intersection of Academician Zarifa Aliyeva Street and R. Behbudov Avenue, the green light lasted only 20 seconds, while traffic travelling towards the intersection with Bulbul Avenue faced a red light, leading to additional delays. A similar situation was observed at the intersection with S. Vurgun Street, where inefficient synchronisation of traffic light phases meant that the traffic flow could not move smoothly from one intersection to another, which exacerbated congestion and increased waiting times. These examples demonstrate the need for more precise adjustment of time intervals for each specific intersection, depending on its location and the characteristics of the traffic flow.

To solve this problem, the duration of the traffic light phases was adjusted taking into account the distance between intersections, traffic intensity, and the average speed of traffic. Based on video detection data and traffic flow analysis, the optimal operating parameters for the traffic lights were calculated. For each intersection, the necessary delay between signal

Table 4 *"Green wave" mode parameters for key intersections*

Intersection	Cycle duration (s)	Delay for synchronisation (s)
R. Behbudov Avenue	60	36
BulbulAvenue	60	22
S. Vurgun Avenue	60	11

changes was determined, ensuring the synchronisation of all traffic lights on the street.

The recommended travel speed in the "green wave" mode was 50 km/h. This speed was chosen based on an analysis of the traffic flow, which showed that most vehicles travel within this range at night, when traffic intensity is lower. At this speed, vehicles could pass through the entire section of the street without stopping at a red light. As shown in Table 4, the parameters of the "green wave" mode were optimised for the key junctions, which allowed for the synchronisation of traffic light operation and ensured a smooth flow of traffic.

For the analysis of movement dynamics, a space-time scale was used: time was plotted on the horizontal axis (10 mm corresponds to 10 seconds), and distance along the route on the vertical axis (each step equals 100 metres). Setting up the system involved the following stages: Determining the timing parameters of the traffic lights for each intersection. Based on traffic analysis, the duration of green and red-light phases, as well as intermediate delays ensuring the traffic light synchronisation, were calculated, creating a unified traffic flow chart within the "green wave" mode. This chart allowed for the modelling of vehicle movement, taking into account the specified speed and delay time at each of the intersections.

To verify the effectiveness of the system, test runs were conducted in the real-world conditions, primarily at night when traffic intensity was minimal. This allowed for a focus on adjusting the system parameters and revealed its high efficiency: the average delay time at intersections decreased by 20%, and at the intersection with R. Behbudov Avenue, where significant vehicle build-up had previously been observed, delays were reduced by 25%. These improvements contributed to increasing the road's capacity and raising the average speed of traffic flow. The economic impact of implementing the "green wave" mode proved to be one of the significant results of the research. The reduction in delay times at intersections led to lower fuel consumption, allowing drivers to save considerably. According to the analysis, passenger cars reduced fuel consumption by 10%, and lorries by 15%. Given the average fuel cost in the region, this signifies a noticeable decrease in vehicle operating costs, which is particularly important for commercial transport regularly traversing busy sections of the urban network.

Based on the analysis conducted, practical recommendations were formulated for scaling the system. In particular, it was proposed to adapt the traffic light operating parameters taking into account the specific features of each road section, including length, number of lanes, traffic density, and intersection configuration. It is also recommended to consider seasonal traffic variations, which may be caused by weather conditions, public holidays, or roadworks.

The implementation of the "green wave" mode demonstrated high potential for optimising traffic flow in the urban environment. The results obtained indicate that the system can be successfully implemented on other sections of Baku's road network, as well as in other cities with similar transport problems. In addition to improving the traffic situation, this will make a significant contribution to solving environmental issues by reducing CO_2 emissions and decreasing fuel consumption.

3.4 Environmental effects and fuel-consumption reduction

The environmental impact of the "green wave" mode became one of the key themes of the research. The transport sector remains a significant source of greenhouse gas emissions, especially CO_2, which are exacerbated during idling at intersections [12]. Vehicles idling continue to burn fuel, which increases the carbon footprint and overall atmospheric pollution. Given Baku's high level of urbanisation, reducing emissions on busy thoroughfares such as Academician Zarifa Aliyeva Street is a primary task.

The collected data on CO_2 emissions before and after the implementation of the system demonstrated a significant reduction in pollution. Using a methodology for calculating fuel consumption based on idling time and average speed showed that CO_2 emissions decreased by an average of 15%. Additionally, NOx emissions levels decreased by 12%, and PM by 8%. These values confirm the importance of implementing the "green wave" mode as an effective environmental solution.

Further analysis of the environmental impact revealed that the reduction in emissions is also linked to a decrease in the number of sharp braking and acceleration events, characteristic of traffic in congested conditions. A smoother flow of traffic not only reduces the strain on vehicles but also decreases the level of pollution associated with tyre and brake system wear. This is particularly important for densely populated urban areas, where air quality is critical for public health.

The prospects for the development of the "green wave" mode include its integration with new

Table 5 *Change in CO_2 emissions before and after implementation of the "green wave" mode*

Time interval	Before (g/km)	After (g/km)	Reduction (%)
00:00-01:00	280	240	14
01:00-02:00	260	220	15
02:00-03:00	250	210	16
03:00-04:00	240	200	17
04:00-05:00	245	205	16
05:00-06:00	260	220	15
06:00-07:00	300	260	13

technologies. The use of more sophisticated machine learning algorithms, which can take into account real-time data, will improve the accuracy and flexibility of the system. Integration with V2V and V2X communication will provide an additional boost to the efficiency of traffic flow management.

As shown in Table 5, the implementation of the "green wave" mode led to a significant reduction in CO_2 emissions, which confirms its environmental effectiveness. Optimising the operation of traffic lights reduced the vehicle idling time at intersections, decreasing the amount of fuel burned and, consequently, the volume of harmful emissions. In the long term, the development of adaptive traffic light control systems could become the basis for creating a sustainable and environmentally friendly transport environment. The results obtained confirm that the implementation of the "green wave" is not only economically viable but also an important step in addressing air pollution problems and improving the quality of life in cities.

According to this data, the average reduction in CO_2 emissions was 15%. The largest decrease was observed between 03:00 and 04:00, when the traffic intensity was low, and the synchronisation of traffic lights allowed for the minimisation of vehicle idling time. The reduction in delays at intersections also had a positive impact on fuel consumption. Drivers were able to reduce the number of stops and instances of idling, which contributed to fuel economy. This effect was particularly significant for freight transport, which consumes more fuel when stopping and starting.

To assess the fuel savings, a series of calculations were carried out based on data on traffic intensity, average speed, and delay times at intersections. The results showed that the overall reduction in fuel consumption was around 10% for passenger cars and up to 15% for freight transport.

The transport system of Baku, like many other metropolises, faces challenges related to road congestion, high emissions of pollutants, and low environmental sustainability. The study conducted on Academician Zarifa Aliyeva Street demonstrated the effectiveness of the "green wave" mode as a tool for addressing these problems.

The "green wave" mode has proven its effectiveness in reducing CO_2 and other harmful substances, such as NOx, carbon monoxide (CO), and PM. These substances are the main air pollutants in urban environments and have a negative impact on public health. The implementation of the system made it possible to reduce NOx emissions by 12%, PM by 8%, and the level of CO decreased by 10%. These results are particularly significant for densely populated areas where air pollution reaches critical levels.

The reduction in delay times at intersections, as the study showed, also led to a decrease in the total idling time of vehicles. This reduced the carbon footprint of transport, contributing to smoother traffic flow and lower fuel costs. Passenger cars reduced fuel consumption by 10%, and freight vehicles by 15%, which became an important factor for economic sustainability and reducing dependence on fossil fuels.

Air quality in the area of Academician Zarifa Aliyeva Street noticeably improved after the implementation of the system. Measurements taken confirmed that the concentration of pollutants in the air decreased, which is particularly important at night when limited pollutant dispersion makes emissions more noticeable. As a result, residents of the area experienced a cleaner and more comfortable environment, which reduced the risks of diseases associated with air pollution, such as asthma, chronic bronchitis, and cardiovascular diseases.

3.5 Social, economic and scalability effects

The system also had a positive impact on the social aspect of urban life. Drivers noted a significant reduction in stress levels due to fewer stops and smoother traffic flow. The improvement in the transport situation enhanced the overall perception of urban infrastructure and made travelling along the thoroughfare more comfortable.

The economic effect of implementing the "green wave" mode was no less significant. The reduction in delay times of 20-25% led to an increase in the road capacity and a decrease in travel times, which positively affected the time spent by residents commuting. This is particularly relevant for commercial transport, where a reduction in downtime directly translates into lower costs and increased productivity.

Additionally, modelling carried out under daytime

traffic intensity conditions showed that the system retains its effectiveness even under high loads, reducing delays by 10-15% during peak hours. This proves that the "green wave" mode can be adapted for different time intervals and traffic levels, providing a universal solution for the urban transport system.

Based on the data obtained, recommendations have been developed for scaling the system to other sections of Baku's road network. Sections with high traffic intensity and complex intersection configurations, such as main thoroughfares, could significantly benefit from the implementation of synchronised traffic light operation. It is also recommended to take into account seasonal traffic variations and temporary restrictions caused by roadworks.

Integrating the system with new technologies, such as AI and machine learning, will further enhance the accuracy of traffic management. Adaptive algorithms will be able to take into account real-time changes in traffic intensity, ensuring the flexibility and resilience of the system. Furthermore, connection with V2V and V2X systems will open up new opportunities for inter-vehicle communication and more efficient flow distribution.

International experience also shows the promise of such solutions. For example, Zhang et al. [13] noted that the successful implementation of "green wave" modes in the metropolises of Europe and Asia has significantly improved environmental indicators and the traffic situation. The mutual exchange of data and technologies with these regions could accelerate the adaptation of the system in Baku.

In the long term, the implementation of the "green wave" creates a basis for the transition to sustainable transport systems. Reducing pollutant emissions, lowering the fuel costs, decreasing traffic noise from stop-and-go movement, and increasing road capacity make this system an important element of environmental and social policy.

The results obtained prove that the integration of the "green wave" into urban transport infrastructure is a significant step towards improving the quality of life and enhancing the environmental situation. Scaling and further developing this system can make urban transport in Baku safer, more comfortable, and more environmentally friendly.

4 Discussion

The conducted research confirmed that the implementation of the "green wave" mode contributes to traffic-flow optimisation, delay reduction, improved environmental indicators, and the mitigation of traffic noise associated with stop-and-go movement near signalised intersections. The results of this research have confirmed that the optimisation of traffic light operation in the "green wave" mode contributes to a 20% reduction in delay times at intersections and a 15% reduction in CO_2 emissions. These figures correlate with the data of Chou et al. [14], who used virtual traffic lights to reduce delays and increase traffic resilience.

The results obtained also align with the findings of De Coensel et al. [15], who showed that signal coordination can significantly reduce the level of air pollution in the urban environment. Additionally, the use of decentralised control algorithms, as noted in the study by Zhang et al. [13], allows for the optimisation of traffic at multiple junctions, which is reflected in an increase in speed and a reduction in delay times. The integration of AI, as discussed by Joshi and Sharma [16], should be regarded as a supporting instrument rather than a necessary condition for effective traffic optimisation. Reductions in delays, fuel consumption and vehicle-related emissions can also be achieved through professionally designed signal coordination, systematic monitoring and competent long-term traffic management by public administration bodies.

The analysis of the combination of signal group coordination and the "green wave" mode, presented in the research by Blokpoel and Turksma [17], demonstrates a noticeable reduction in waiting times at intersections. Signal coordination algorithms for multi-node intersections, developed by Shi et al. [18], allow for the maximisation of the green band, which is particularly important for V2X networks, and fully corresponds to the obtained data on improving the efficiency of traffic light synchronisation. Data on reduction of the effects of climate change are also supported by the research of Mitsakis and Kotsi [19], demonstrating that cooperative intelligent transport systems can mitigate the negative impact of transport emissions.

Additional data, presented in the study by Lavanya et al. [20], show that smart traffic light control systems using AI significantly improve traffic flows and reduce pollution. The results of sustainable mobility, reflected in the research of Ziyad et al. [21] and De Coensel et al. [15], are consistent with the goal of reducing emissions and optimising traffic flows, and the concept Finally, the data of Choudhary et al. [22] indicate the significant potential of cities with AI-managed traffic light systems to reduce congestion and improve the environmental situation, and the approach of Li et al. [23], based on reinforcement learning methods for signal planning, successfully minimises the impact of congestion on transport networks. Thus, the results of this study demonstrate broad prospects for the further adaptation and scaling of "green wave" system in urban infrastructure conditions, which allows for the creation of a more sustainable, environmentally safe, and comfortable transport environment.

The research by Mariano de Souza et al. [24] demonstrated that the use of vehicle-to-vehicle communication systems not only improves traffic coordination but also reduces greenhouse gas emissions. This highlights the potential of V2V and

V2X technologies, which could further enhance the effects of the green wave. The work of Ali et al. [25] focused on creating integrated transport networks that combine sustainability and efficiency. They showed that such systems can effectively reduce congestion and improve the overall quality of urban transport infrastructure. Shaikh et al. [26] proposed innovative methods of traffic management using AI and blockchain technologies. Their approaches open up prospects for increasing the transparency and accuracy of traffic flow management, which is particularly relevant for scalable "green wave" systems.

The results obtained confirm that the "green wave" systems are capable of not only optimising traffic on busy sections but also significantly improving environmental indicators. For example, a 15% reduction in CO_2 emissions and a 20% reduction in delay times demonstrate the significance of such solutions for the sustainable development of urban infrastructure.

The integration of V2X technologies, as proposed by Shi et al. [18] and Saleh et al. [27], can enhance coordination between vehicles and traffic lights, creating more efficient systems. Furthermore, the application of multi-agent approaches, as indicated in the work of Li [23], can be expanded to manage not only the movement of cars but the pedestrian flows as well, which will increase the overall safety and comfort of road users.

Another direction for further work is the development of intelligent control systems that will take into account seasonal and temporal fluctuations in traffic, as described in the research of Scaffidi et al. [28] and Cirianni et al. [29]. Such adaptive algorithms will be able to provide more accurate and sustainable management of traffic flows in different conditions.

Green wave systems are an important tool for optimising traffic flows and reducing the environmental burden. Their further development and implementation should include integration with the latest technologies, such as AI, blockchain, and vehicle-to-vehicle communication, to create a more sustainable and environmentally safe urban environment.

5 Conclusions

In this study is demonstrated that the introduction of a "green wave" mode on Academician Zarifa Aliyeva Street in Baku has a significant impact on optimising traffic flows and reducing the environmental load. The system based on traffic light synchronisation reduced the average delay time at intersections by 20%, which improved road capacity and ensured more uniform traffic flow. This achievement is particularly important for urban highways with high traffic volumes, where congestion remains one of the key factors slowing down traffic flows.

The application of the recommended speed of 50 km/h proved to be a key element in the successful implementation of the system. It allowed vehicles to pass through intersections smoothly, minimising the number of stops and reducing journey times. This optimisation not only improved the traffic situation, but had a significant environmental effect, as well. CO_2 emissions have been reduced by 15%, while NOx and PM emissions have been reduced by 12% and 8% respectively. This contributes to improved air quality in the city, which is particularly important for densely populated areas with high concentrations of traffic.

The reduction of the fuel consumption by 10% for cars and 15% for lorries underlines the economic efficiency of the proposed solution. Fuel savings reduce vehicle operating costs, which is important for both individual drivers and commercial vehicles. In the long term, such improvements contribute to a more sustainable use of resources and a lower carbon footprint.

The significance of the study lies in the possibility of scaling up the proposed system to other sections of the city's road network. The implementation of the "green wave" mode on key arterial roads, taking into account their peculiarities, will further reduce delay times, improve the environmental situation and increase the comfort for road users.

The limitations are related to the lack of a developed video surveillance and real-time monitoring system, which limits the adaptability of the proposed approach. In addition, the study predominantly covered night-time, which requires testing the effectiveness of the system under daytime traffic conditions. Prospects for the future work include the development and implementation of smart transport systems using machine learning to predict traffic and adapt traffic light operation to seasonal and temporal changes. Long-term monitoring of environmental and economic effects is also needed to improve the accuracy and efficiency of the implementation of such solutions.

Acknowledgements

The authors received no financial support for the research, authorship and/or publication of this article.

Conflicts of interest

The authors declare that they have no known competing financial interests or personal relationships that could have appeared to influence the work reported in this paper.

References

[1] DECKY, M., TROJANOVA, M., REMEK, L., JATY, L. Noise pollution from roundabout traffic in the outer environment of built-up areas of towns. In: 12th International Multidisciplinary Scientific GeoConference and EXPO: Modern Management of Mine Producing, Geology and Environmental Protection SGEM 2012: proceedings [online] [accessed 2026-01-09]. **4**. 2012. ISSN 1314-2704, p. 927-934. Available from: https://doi.org/10.5593/sgem2012/s22.v4013

[2] How air pollution is destroying our health - World Health Organization [online] [accessed 2026-01-09]. Available from: https://www.who.int/news-room/spotlight/how-air-pollution-is-destroying-our-health

[3] LI, Z., JI, X., YUAN, S., FANG, Z., LIU, Z., GAO, J. A green wave ecological global speed planning under the framework of vehicle-road-cloud integration. *Electronics* [online]. 2024, **13**(17), 3516 [accessed 2026-01-09]. eISSN 2079-9292. Available from: https://doi.org/10.3390/electronics13173516

[4] ZHENG, Y., GUO, R., MA, D., ZHAO, Z., LI, X. A novel approach to coordinating green wave system with adaptation evolutionary strategy. *IEEE Access* [online]. 2020, **8**, p. 214115-214127 [accessed 2026-01-11]. eISSN 2169-3536. Available from: https://doi.org/10.1109/access.2020.3037129

[5] SANTHIYA, P., JEBADURAI, I. J., PAULRAJ, G. J., JENEFA, A., GIFTSON, R. A., KARAN, S. K. ITS-AI integration: enhanced strategies for mitigating urban traffic congestion. In: 5th International Conference on Recent Trends in Computer Science and Technology: proceedings [online] [accessed 2026-01-11]. IEEE. 2024. ISBN 979-8-3503-5138-5, eISBN 979-8-3503-5137-8, p. 376-381. Available from: https://doi.org/10.1109/icrtcst61793.2024.10578453

[6] ASHOKKUMAR, C., KUMARI, D. A., GOPIKUMAR, S., ANURADHA, N., KRISHNAN, R. S., SAKTHIDEVI, I. Urban traffic management for reduced emissions: AI-based adaptive traffic signal control. In: 2nd International Conference on Sustainable Computing and Smart Systems: proceedings [online] [accessed 2026-01-11]. IEEE. 2024. ISBN 979-8-3503-9155-8, eISBN 979-8-3503-7999-0, p. 1609-1615. Available from: https://doi.org/10.1109/icscss60660.2024.10625356

[7] ZHANG, J., SHANG, H., LI, X., YAO, Y. An integrated arterial coordinated control model considering green wave on branch roads and pedestrian crossing time at intersections. *Journal of Management Science and Engineering* [online]. 2020, **5**(4), p. 303-317 [accessed 2026-01-12]. eISSN 2589-5532. Available from: https://doi.org/10.1016/j.jmse.2020.09.004

[8] SELVAPRIYA, R., GOPINATH, M., VELMURUGAN, D., TAMILCHELVAN, P. Climate change mitigation through AI solutions. In: *Global challenges for the environment and climate change* [online]. IDRIS, S. (Ed.). London: IGI Global, 2024. ISBN 9798369328453, eISBN 9798369328460, p. 37-59 [accessed 2026-01-12]. Available from: https://doi.org/10.4018/979-8-3693-2845-3.ch014

[9] YANG, H., LIU, Q., LI, D., YU, S. A green wave traffic strategy design for energy-saving control of intelligent connected vehicle using MPC framework. In: 43rd Chinese Control Conference: proceedings [online] [accessed 2026-01-12]. IEEE. 2024. ISBN 979-8-3503-6690-7, eISBN 978-9-8875-8158-1, eISSN 1934-1768, p. 2834-2839. Available from: https://doi.org/10.23919/ccc63176.2024.10662492

[10] EL-HAMEED, A. K. Artificial intelligence shaping sustainable cities for climate change mitigation: a review of literature. In: *Architecture and urbanism: a smart outlook* [online]. KAMEL, S., SABRY, H., HASSAN, G. F., REFAT, M., ELSHATER, A., ABD ELRAHMAN, A. S., HASSAN, D. K., RASHED, R. (Eds.). Cham: Springer, 2020. ISBN 978-3-030-52583-5, eISBN 978-3-030-52584-2, p. 483-495 [accessed 2026-01-15]. Available from: https://doi.org/10.1007/978-3-030-52584-2_34

[11] BAGHIROV, M. Establishment of reliability intervals for the average vehicle speeds. *Journal of Traffic and Transport Research* [online]. 2023, **6**(2), p. 131-142 [accessed 2026-01-15]. ISSN 2667-8071. Available from: https://doi.org/10.38002/tuad.1249767

[12] BAGHIROV, M. Developing a coordinated regulation schedule to prevent damage to the environment by vehicles and improve the structure of the energy system: evidence from the city of Baku (Azerbaijan). *Automobile Transport* [online]. 2023, **52**, p. 64-70 [accessed 2026-01-15]. ISSN 2219-8342, eISSN 2309-981X Available from: https://doi.org/10.30977/AT.2219-8342.2023.52.0.07

[13] ZHANG, Y., XU, Y., SUN, T., LIU, P. Green-waved cooperative coordination algorithm for decentralized traffic control. In: International Conferences on Web Intelligence and Intelligent Agent Technology: proceedings [online] [accessed 2026-01-15]. IEEE. 2012. ISBN 978-1-4673-6057-9, p. 75-79. Available from: https://doi.org/10.1109/wi-iat.2012.141

[14] CHOU, L.-D., SHEN, T.-Y., TSENG, C.-W., CHANG, Y.-J., KUO, Y.-W. Green wave-based virtual traffic light management scheme with VANETs. *International Journal of Ad Hoc and Ubiquitous Computing* [online]. 2016, **24**(1-2), p. 22-32 [accessed 2026-01-17]. ISSN 1743-8225, eISSN 1743-8233. Available from: https://doi.org/10.1504/ijahuc.2017.080921

[15] DE COENSEL, B., CAN, A., DEGRAEUWE, B., DE VLIEGER, I., BOTTELDOOREN, D. Effects of traffic signal

coordination on noise and air pollutant emissions. *Environmental Modelling and Software* [online]. 2012, **35**, p. 74-83 [accessed 2026-01-17]. ISSN 1364-8152, eISSN 1873-6726. Available from: https://doi.org/10.1016/j.envsoft.2012.02.009

[16] JOSHI, M., SHARMA, N. Harnessing the power of AI for sustainable climate strategies. *International Journal of Science and Research* [online]. 2023, **12**(12), p. 1152-1158 [accessed 2026-01-17]. ISSN 319-7064. Available from: https://doi.org/10.21275/sr231214124609

[17] BLOKPOEL, R. J., TURKSMA, S. *Combining signal group oriented control with guaranteed green waves*. In: 19th ITS World Congress: proceedings. 2012.

[18] SHI, Y., LI, J., HAN, Q., LV, L. A coordination algorithm for signalized multi-intersection to maximize green wave band in V2X network. *IEEE Access* [online]. 2020, **8**, p. 213706-213717 [accessed 2026-01-22]. eISSN 2169-3536. Available from: https://doi.org/10.1109/access.2020.3039263

[19] MITSAKIS, E., KOTSI, A. Cooperative intelligent transport systems as a policy tool for mitigating the impacts of climate change on road transport. In: *Data analytics: paving the way to sustainable urban mobility* [online]. NATHANAIL, E. G., KARAKIKES, I. D. (Eds.). Cham: Springer, 2018. p. 418-425 [accessed 2026-01-22]. ISSN 978-3-030-02304-1, eISSN 978-3-030-02305-8. Available from: https://doi.org/10.1007/978-3-030-02305-8_51

[20] LAVANYA, E., KANAILAL, P. S., ANBU SELVI, G., SENTHAMILARASI, N. Smart traffic control system using AI. *International Journal for Multidisciplinary Research* [online]. 2024, **6**(2) [accessed 2026-01-22]. eISSN 2582-2160. Available from: https://doi.org/10.36948/ijfmr.2024.v06i02.14871

[21] ZIYAD, M., NARANJE, V., SURESH, S., MISHRA, V. P., SALUNKHE, S. Intelligent traffic system for sustainable mobility. In: International Conference on Computational Intelligence and Knowledge Economy: proceedings [online] [accessed 2026-01-22]. IEEE. 2021. ISBN 978-1-6654-2922-1, eISBN 978-1-6654-2921-4, p. 504-507. Available from: https://doi.org/10.1109/iccike51210.2021.9410725

[22] CHOUDHARY, S., ALI, S. S., BABU, N. R., SHARMA, H., KALIRAMAN, B., DHANKHAR, Y. A more efficient way to control traffic lights through AI-led smart city management. In: 3rd International Conference on Technological Advancements in Computational Sciences: proceedings [online] [accessed 2026-01-22]. IEEE. 2023. ISBN 979-8-3503-4234-5, eISBN 979-8-3503-4233-8, p. 1133-1138. Available from: https://doi.org/10.1109/ictacs59847.2023.10390336

[23] LI, Y., NIU, W., TIAN, Y., CHEN, T., XIE, Z., WU, Y., XIANG, Y., TONG, E., BAKER, T., LIU, J. Multiagent reinforcement learning-based signal planning for resisting congestion attack in green transportation. *IEEE Transactions on Green Communications and Networking* [online]. 2022, **6**(3), p. 1448-1458 [accessed 2026-01-25]. eISSN 2473-2400. Available from: https://doi.org/10.1109/tgcn.2022.3162649

[24] MARIANO DE SOUZA, A., BOUKERCHE, A., GUILHERME, M., MENEGUETTE, R. I., LOUREIRO, A. A., VILLAS, L. A. Decreasing greenhouse emissions through an intelligent traffic information system based on inter-vehicle communication. In: 12th ACM International Symposium on Mobility Management and Wireless Access: proceedings [online] [accessed 2026-01-25]. 2014. ISBN 978-1-4503-3026-8, p. 91-98. Available from: https://doi.org/10.1145/2642668.2642677

[25] ALI, S. M., AHMADI, S., AMANI, A. M., JALILI, M. Urban integrated sustainable transportation networks. In: *Interconnected modern multi-energy networks and intelligent transportation systems: towards a green economy and sustainable development* [online]. DANESHVAR, M., MOHAMMADI-IVATLOO, B., ANVARI-MOGHADDAM, A., RAZZAGHI, R. (Eds.). Piscataway: IEEE, 2024. ISBN 9781394188758, eISBN 9781394188789, p. 59-91 [accessed 2026-01-25]. ISBN unavailable. Available from: https://doi.org/10.1002/9781394188789.ch4

[26] SHAIKH, M. K., LIAQUAT, S. F., SIDDIQUI, F. A., ABDUL MOID KHAN, JAVEED, M., AHMED, M. Enhancing traffic control with AI blockchain and dynamic computation techniques. *VFAST Transactions on Software Engineering* [online]. 2024, **12**(3), p. 55-67 [accessed 2026-01-25]. ISSN 2309-3978. Available from: https://doi.org/10.21015/vtse.v12i3.1866

[27] SALEH, K. T., MUSA, A. A., MALAMI, S. I., LEVENT, Y. S., DULAWAT, S. AI-based green transportation: a sustainable approach. In: *Artificial intelligence for future intelligent transportation: smarter and greener infrastructure design* [online]. DHANARAJ, R. K., KAMILA, N. K., PANI, S. K., BALUSAMY, B., RAJASEKAR, V. (Eds.). New York: Apple Academic Press, 2023. ISBN 9781003408468, p. 269-302 [accessed 2026-01-25]. Available from: https://doi.org/10.1201/9781003408468-11

[28] SCAFFIDI, C., TRICOMI, G., DISTEFANO, S., PULIAFITO, A. Continuous green2 waves for surfing smart cities. In: International Conference on Smart Computing: proceedings [online] [accessed 2026-01-25]. IEEE. 2020. ISBN 978-1-7281-6998-9, eISBN 978-1-7281-6997-2, p. 404-409. Available from: https://doi.org/10.1109/SMARTCOMP50058.2020.00085

[29] CIRIANNI, F. M., COMI, A., QUATTRONE, A. Mobility control centre and artificial intelligence for sustainable urban districts. *Information* [online]. 2023, **14**(10), 581 [accessed 2026-01-25]. eISSN 2078-2489. Available from: https://doi.org/10.3390/info14100581

This is an open access article distributed under the terms of the Creative Commons Attribution 4.0 International License (CC BY 4.0), which permits use, distribution, and reproduction in any medium, provided the original publication is properly cited. No use, distribution or reproduction is permitted which does not comply with these terms.

STOPPED FRACTION AND CLOSURE FAILURE IN CONGESTED MACROSCOPIC FUNDAMENTAL DIAGRAMS: A SUMO-BASED SIMULATION STUDY

Tomoo Noguchi*

Waseda University, School of Social Sciences, Tokyo, Japan

*E-mail of the corresponding author: tomo@waseda.jp

Tomoo Noguchi 0009-0008-2222-7165

Resume

Congested macroscopic fundamental diagrams (MFDs) often display scatter since accumulation alone does not fully describe immobilization within stored traffic. In this paper, the stopped fraction, defined as the share of vehicles that are stopped or nearly stopped, is examined as a complementary macroscopic state variable. A compact analytical framework shows why accumulation-only closure can fail when stopped fraction varies at fixed accumulation. The mechanism is tested using the Simulation of Urban MObility (SUMO) platform on a stylized signalized grid. Adding stopped fraction reduces the root mean squared error (RMSE) from 41.32 to 18.79 overall, and from 55.84 to 23.40 in the congested regime, where R^2 rises from 0.8777 to 0.9785. Stopped fraction therefore provides a practical diagnostic for congestion states omitted from accumulation-only MFD representations.

Article info

Received 13 May 2026
Accepted 2 September 2026
Online 17 September 2026

Keywords:

macroscopic fundamental diagram
stopped fraction
SUMO simulation
congested traffic
closure failure
network production

Available online: https://doi.org/10.26552/com.C.2026.054

ISSN 1335-4205 (print version)
ISSN 2585-7878 (online version)

1 Introduction

Macroscopic fundamental diagrams (MFDs) provide a compact representation of urban network performance by relating aggregate variables, such as accumulation, flow and production [1-4]. Their practical appeal is that a complex urban traffic network can, under suitable conditions, be represented by a low-dimensional relation. If a network production can be written as a closed function of accumulation, then the network state can be summarized by the number of vehicles stored in the network.

This closure requirement is demanding. In congested regimes, scatter, hysteresis and instability are frequently observed in accumulation-production relations [5-9]. Such phenomena are often treated as empirical irregularities or measurement noise. In this paper, they are instead interpreted as symptoms of an incomplete macroscopic state description. Accumulation measures how much traffic is stored in the network, but it does not directly measure how much of that stored traffic is effectively immobilized by stopping, blocking or spillback.

The focus is placed on stopped fraction as a complementary state variable. The stopped fraction is the proportion of vehicles in the network whose speeds are below a small threshold. The central hypothesis is simple: two traffic states may have similar accumulation but different stopped fractions, and these differences can generate different production levels. In that case, an accumulation-only MFD may remain a useful first-order representation, but it is not fully closed in the congested regime.

The novelty of this paper lies in reframing congested MFD scatter as a closure problem caused by omitted immobilization information, and in positioning stopped fraction as a simple macroscopic state variable that exposes this missing dimension. Existing extensions of the MFD have emphasized spatial heterogeneity, multimodal interactions, delay relationships and richer network descriptions. Instead, emphasis is placed on stopped fraction, a directly interpretable indicator of the share of stored vehicles that is not effectively contributing to movement. This makes stopped fraction operationally attractive: it can be computed directly from microscopic simulation or full trajectory data, and

can be approximated from connected-vehicle trajectories or speed-based sensing data when sampling coverage is sufficient, without requiring full reconstruction of the spatial density field.

This framing yields three specific contributions to congested MFD analysis. First, a compact analytical representation that separates traffic storage from traffic immobilization in congested MFDs is provided. Second, a controlled microscopic simulation with SUMO is used to show that stopped fraction explains systematic residual variation left by an accumulation-only production model [10]. Third, it is demonstrated that the improvement is strongest in congested regimes and robust to alternative accumulation thresholds, establishing stopped fraction as a useful diagnostic state variable rather than merely an additional fitting variable.

The remainder of the paper is organized as follows. The relevant MFD literature is reviewed in Section 2, and stopped fraction is positioned within existing research. The analytical representation, SUMO simulation design and empirical model comparison are presented in Section 3. The simulation results and robustness checks are reported in Section 4. The interpretation, operational implications and limitations of the findings are discussed in Section 5. The main conclusions are summarized in Section 6.

2 Literature review

The MFD concept was developed to describe urban network performance at an aggregate scale [1-3]. Subsequent reviews have emphasized that MFD-based modelling has become a central framework for network-wide traffic state estimation, control and performance evaluation [4]. A well-defined MFD provides a basis for network-level monitoring and control, including perimeter control and gating strategies [11]. Analytical approximation methods have also been developed to derive MFDs from network structure and traffic-flow assumptions, and their performance has been evaluated using microscopic simulation and arterial-network settings [12]. The stopped fraction concept is also related to the classical two-fluid view of urban traffic, which distinguishes moving and stopped vehicles at the aggregate level [13]. The distinctive contribution here is not the use of stopped vehicles per se, but the use of stopped fraction as a macroscopic diagnostic variable for testing whether accumulation-only MFD closure omits immobilization information in congested states.

At the same time, empirical and simulation studies have shown that urban MFDs may exhibit scatter and hysteresis, especially when congestion becomes spatially uneven [5-9, 14]. A major explanation for MFD scatter is heterogeneity. Spatial variability in density can reduce effective network capacity and weaken the uniqueness of the accumulation-production relation [5, 7]. Other studies have examined the dynamics of heterogeneity, hierarchical control and network partitioning [9, 15]. In signalized urban networks, local intersection dynamics and turning movements may also affect aggregate performance, which further motivates attention to microscopic mechanisms behind macroscopic scatter [16-17].

Extensions of the MFD have considered three-dimensional, multimodal and physically interpretable formulations [18-22]. More recent work has moved towards richer state descriptions and richer data sources. For example, MFD formulations with volume-delay relationships connect accumulation to network delay, while reviews of multimodal network macroscopic fundamental diagrams (NMFDs) emphasize observability, stability and data-fusion challenges in empirical calibration [23-24]. Data-rich studies based on drone trajectories, mobile observations and multi-source sensing further illustrate the value of measuring more than a single aggregate storage variable [25-26]. The MFD concept has also been extended beyond traffic production to network-level environmental performance, including emission-MFD relationships [27].

Microscopic simulation provides a controlled way to examine such mechanisms. SUMO is widely used as an open-source microscopic traffic simulator [10], and a comparison of open-source and commercial microsimulation platforms, including SUMO, was recently presented in this journal for traffic simulation case studies [28].

Taken together, the state of the art shows that MFD research has progressively enriched the description of network traffic through heterogeneity measures, multimodal formulations and increasingly detailed data sources. However, the specific role of stopped fraction as a compact diagnostic of accumulation-only closure failure remains underexplored. This gap is addressed by using stopped fraction as a diagnostic state variable to test whether accumulation-only closure suppresses relevant immobilization information in congested states.

3 Methodology

The analytical representation of the closure problem is introduced in this section, followed by a description of the SUMO simulation design and presentation of the empirical model comparison used to evaluate the diagnostic role of stopped fraction.

3.1 Analytical representation

Let $n \geq 0$ denote the network accumulation in vehicles, let $s \in [0,1]$ denote stopped fraction, and let P denote network production measured as total distance travelled per unit time over a given aggregation interval. Accumulation represents traffic storage. Stopped fraction represents the share of vehicles that

are stopped or nearly stopped. The moving component of accumulation is therefore

$$n^m = (1 - s)n\,. \tag{1}$$

If $v(n,s)$ denotes the effective per-vehicle productivity of the moving component, with units of distance travelled per vehicle per unit time, network production can be represented as

$$P = (1 - s)nv(n,s)\,. \tag{2}$$

This representation separates two mechanisms. A higher stopped fraction directly reduces the number of effectively moving vehicles through $(1 - s)$, and it may also reduce the productivity of the moving component through $v(n,s)$.

An accumulation-only MFD assumes

$$P = f(n)\,, \tag{3}$$

whereas the augmented representation considered here is

$$P = g(n,s)\,. \tag{4}$$

The closure issue is whether the production is uniquely determined by accumulation. If two states have the same n but different s, and if P varies with s as in Equation (2), then Equation (3) suppresses relevant state information. Stopped fraction is therefore interpreted as a complementary macroscopic state variable rather than a purely statistical regressor.

3.2 SUMO simulation design

A controlled microscopic simulation was conducted using Simulation of Urban MObility (SUMO). The use of an open-source microsimulation platform is consistent with recent transport-simulation applications that compare SUMO with commercial microsimulators and with urban-intersection studies that use microscopic traffic-flow parameters to examine delay at signalized intersections [17, 28]. The network was a synthetic 10 × 10 signalized grid with one lane per direction, 200 m link length and a speed limit of 13.9 m/s (Figure 1). The simulation horizon was 7200 s with a 1 s simulation step. Traffic demand followed three phases: a loading phase from 0 to 2400 s, a high-demand congested phase from 2400 to 4800 s, and a recovery phase from 4800 to 7200 s. Vehicles were generated by a Poisson process with time-varying demand and assigned to boundary-to-boundary trips across the grid. These choices define a stylized mechanism test rather than a fully specified benchmark instance: the network size, link length, speed limit,

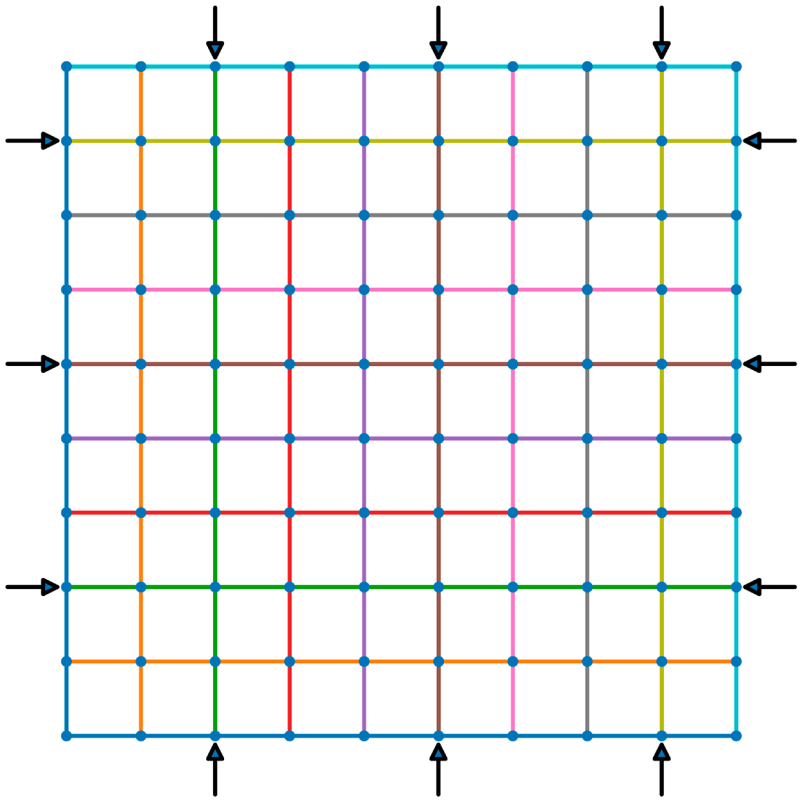


Figure 1 *Schematic representation of the synthetic signalized grid implemented in SUMO, boundary arrows indicate the boundary-to-boundary demand structure; each link is 200 m long and has one lane per direction*

simulation horizon, aggregation interval and demand phases are reported in the article, but reproducibility of the numerical trajectory from the manuscript alone is not claimed without the corresponding demand, route and signal input files.

The traffic states were aggregated every $\Delta t = 60$ s. Let T_t denote the set of 1 s simulation samples in aggregation interval t, with $|T_t| = 60$, and let V_τ denote the vehicles present in the network at sample τ, so that $N_\tau = |V_\tau|$. For each aggregation interval, accumulation was measured as the sample average number of vehicles in the network:

$$n_t = \frac{1}{|T_t|} \sum_{\tau \in T_t} N_\tau . \tag{5}$$

For samples with $N_\tau > 0$, the instantaneous stopped share was computed from the vehicles in V_τ; when $N_\tau = 0$, this instantaneous share is defined as zero. Stopped fraction was then defined as

$$\begin{aligned} s_t &= \frac{1}{|T_t|} \sum_{\tau \in T_\tau} \sigma_\tau, \\ \sigma_\tau &= \begin{cases} \dfrac{\{i \in V_\tau \,:\, v_{i,\tau} \le 0.1 m/s\}}{N_\tau}, & N_\tau > 0, \\ 0 & N_\tau = 0, \end{cases} \end{aligned} \tag{6}$$

where $v_{i,\tau}$ is the speed of vehicle i at simulation step τ. Let $V_t = \cup_{\tau \in T_t} V_\tau$ denote the set of vehicles present at least once during interval t. Network production was measured as a distance travelled per unit time:

$$P_t = \frac{1}{\Delta t} \sum_{i \in V_t} \Delta d_{i,t} , \tag{7}$$

where $\Delta d_{i,t}$ is the distance travelled by vehicle i inside the network during interval t. The unit of P_t is therefore distance per unit time. The resulting dataset contained 120 aggregated observations.

3.3 Model comparison

Two empirical specifications were compared. The accumulation-only model used a cubic polynomial in n:

$$f(n_t) = \beta_0 + \beta_1 n_t + \beta_2 n_t^2 + \beta_3 n_t^3 . \tag{8}$$

The augmented model used the complete total-degree-three polynomial basis in n and s:

$$\begin{aligned} g(n_t, s_t) = \alpha_0 + \alpha_1 n_t + \alpha_2 s_t + \alpha_3 n_t^2 + \alpha_4 n_t s_t + \\ + \alpha_5 s_t^2 + \alpha_6 n_t^3 + \alpha_7 n_t^2 s_t + \alpha_8 n_t s_t^2 + \alpha_9 s_t^3 . \end{aligned} \tag{9}$$

The fitted relationships are $P_t = f(n_t) + \varepsilon_t$ and $P_t = g(n_t, s_t) + u_t$. The comparison is not intended as a structural calibration of Equation (2). Instead, it tests whether the stopped fraction contains systematic information about production that remains after conditioning on accumulation. Model performance was evaluated using in-sample R^2 and in-sample root mean squared error (RMSE), so the reported values should be interpreted as diagnostic fit measures rather than out-of-sample prediction accuracy. Congested regimes were defined by upper-quantile subsets of accumulation.

4 Results

The simulation evidence is reported in this section, beginning with the baseline accumulation-production relation and followed by the model comparison, robustness to the congestion threshold, and the loading-recovery trajectory.

4.1 Accumulation-only scatter and stopped fraction

The production-against-accumulation plot for the 120 aggregation intervals obtained from the SUMO experiment is shown in Figure 2. The diagram exhibits the expected unimodal structure: production first increases with accumulation, reaches a maximum at an intermediate level, and then declines as the network becomes congested. This pattern confirms that the simulation generates a conventional MFD-like relation and provides a suitable basis for examining whether accumulation alone is sufficient to describe congested states.

Figure 2 also clarifies why a simple goodness-of-fit statistic can be misleading when the purpose is to evaluate closure. A smooth accumulation-production relation can be visually apparent even when observations with similar accumulation differ in their internal mobility conditions. The accumulation-only plane contains no information about whether the stored vehicles are moving continuously, repeatedly interrupted by signals, or immobilized by local queues. Therefore, the apparent compactness of the relation should be interpreted as a baseline representation rather than as evidence that no omitted state dimension remains.

The same observations are re-plotted in Figure 3, with each point colored by stopped fraction. This figure is central to the interpretation of the simulation results. If stopped fraction were only random noise with respect to production, no systematic organization of colors would be expected in the accumulation-production plane. Instead, the colored plot shows that stopped fraction varies across the simulated trajectory and that observations with higher stopped fraction tend to be located toward the lower side of otherwise comparable accumulation levels. The color pattern therefore reveals information that is hidden in Figure 2: part of the vertical dispersion in the MFD plane is associated with the extent to which the stored traffic is immobilized.

The visual comparison between Figures 2 and 3 is consistent with the analytical representation in Equation (2). At a given accumulation, a larger stopped

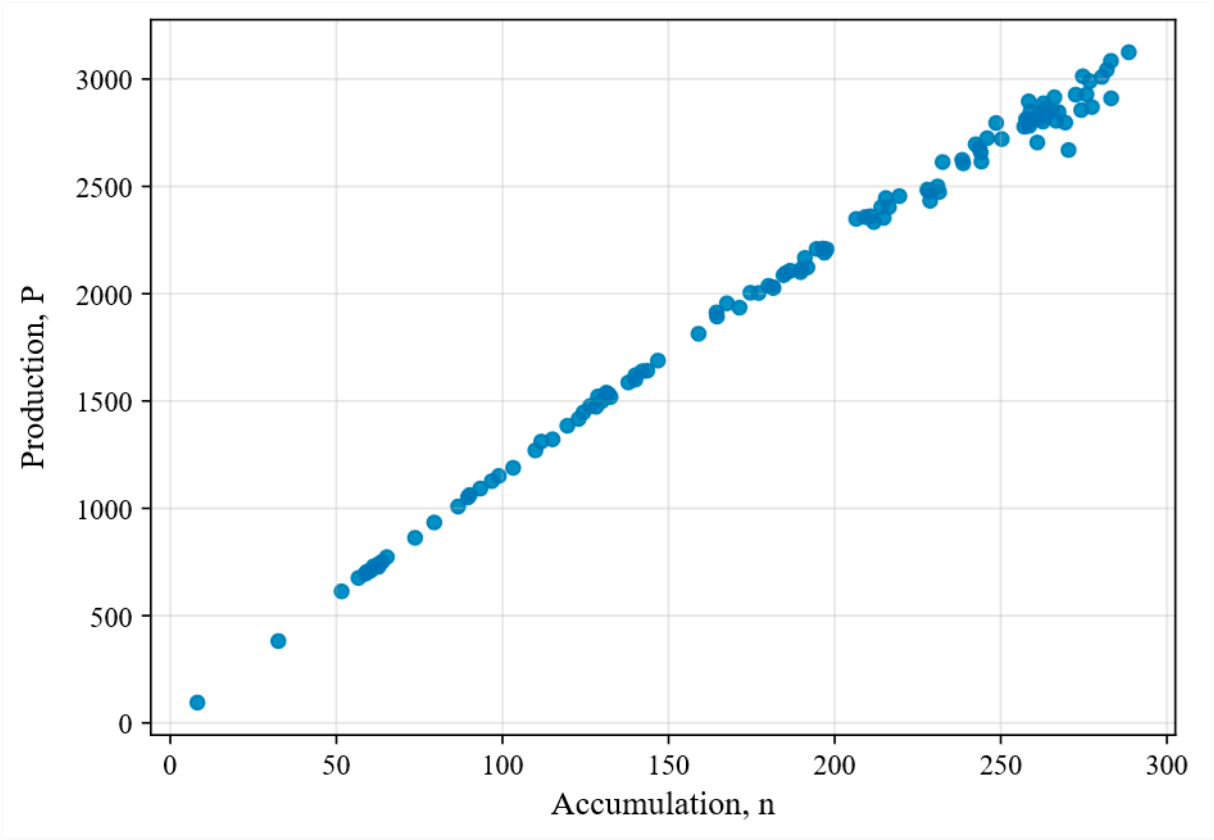


Figure 2 *Accumulation-production diagram from the SUMO grid simulation, the figure provides the baseline accumulation-only MFD representation. It confirms that accumulation is a strong first-order descriptor, but it does not reveal differences in stopping conditions between the states with comparable accumulation*

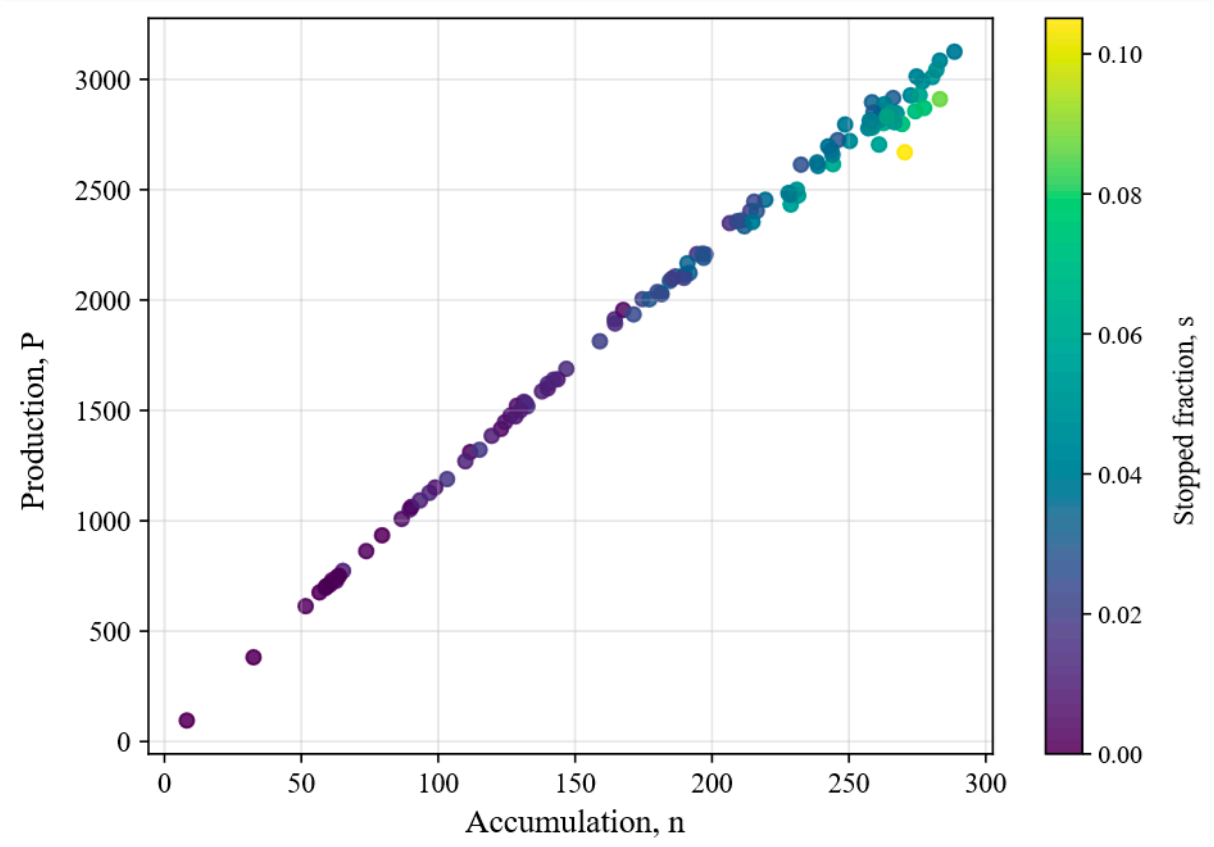


Figure 3 *Accumulation-production diagram colored by stopped fraction, the color scale reveals a systematic immobilization dimension that is suppressed in the accumulation-only representation, higher stopped fractions tend to correspond to lower production between observations with comparable accumulation*

fraction reduces the moving component of accumulation and may also reduce the effective productivity of the vehicles that remain mobile. The colored diagram does not by itself prove causality, but it provides a useful diagnostic indication that stopped fraction is not merely an auxiliary label attached after the fact. Rather, it appears to organize a residual dimension of the simulated MFD. This motivates the formal model comparison reported in the following subsection.

4.2 All observations and congested regime

A comparison of the accumulation-only specification $P = f(n)$ with the augmented specification $P = g(n, s)$ is provided in Table 1. The comparison should be read as a diagnostic test rather than a structural calibration exercise. Both models use flexible cubic polynomial terms, so the purpose is not to identify a unique behavioral law. The purpose is to ask whether stopped fraction contains systematic information about production after accumulation has already been taken into account.

For all observations, the accumulation-only model achieves a very high explanatory power, with $R^2 = 0.9971$. This result is expected in a controlled grid simulation and confirms that accumulation remains the dominant aggregate descriptor of production. However, adding stopped fraction reduces in-sample RMSE from 41.32 to 18.79, corresponding to a 54.5% reduction. The improvement is therefore substantial even when the baseline model already fits the overall relation well. This is an important point for interpretation: the contribution of stopped fraction is not primarily to create an MFD where none exists, but to explain the part of production variation that remains unresolved after conditioning on accumulation.

The effect is more informative in the congested regime, defined here as observations above the 60th percentile of accumulation. In this subset, the accumulation-only model becomes much less adequate: its R^2 falls to 0.8777 and its RMSE increases to 55.84.

Table 1 *Model comparison for all observations and the congested regime*

Sample	Model	R^2	RMSE	Reduction
All observations	P = f(n)	0.9971	41.32	-
All observations	P = g(n, s)	0.9994	18.79	54.5%
Congested regime	P = f(n)	0.8777	55.84	-
Congested regime	P = g(n, s)	0.9785	23.40	58.1%

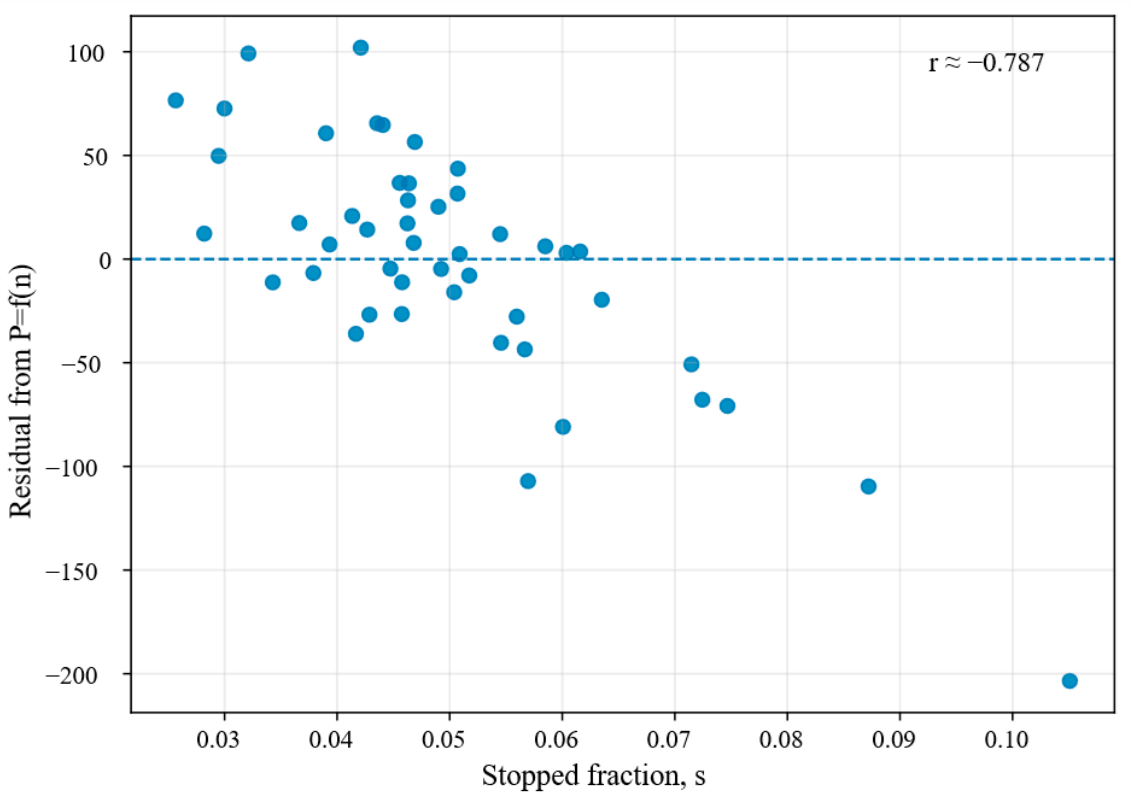


Figure 4 *Residual diagnostics for the accumulation-only model in the congested regime, residuals are plotted against stopped fraction. The negative association indicates systematic overprediction for states with high stopped fraction*

Table 2 *Robustness to congestion threshold*

Sample	R^2 f(n)	R^2 g(n,s)	RMSE f(n)	RMSE g(n,s)	Reduction
n ≥ Q50	0.9377	0.9902	56.35	22.31	60.4%
n ≥ Q60	0.8777	0.9785	55.84	23.40	58.1%
n ≥ Q70	0.6607	0.9381	59.58	25.45	57.3%

After the stopped fraction is added, R^2 rises to 0.9785 and in-sample RMSE falls to 23.40, corresponding to a 58.1% reduction. The contrast between the full sample and the congested regime is theoretically meaningful. It indicates that the limitation of accumulation-only closure is not uniform over all traffic states, but becomes more visible when the network is heavily loaded and stopping conditions become more variable.

The residual analysis provides a more direct diagnostic of the same mechanism. The residuals of the accumulation-only model are plotted against stopped fraction for the congested regime in Figure 4. A positive residual means that the accumulation-only model underpredicts production, whereas a negative residual means that it overpredicts production. The downward pattern therefore has a clear traffic interpretation: observations with higher stopped fraction tend to generate less production than would be expected from accumulation alone. In other words, accumulation-only modelling treats those states as comparable to other states with similar storage levels, but their greater immobilization makes them less productive.

The corresponding correlation is $r = -0.787$, indicating a strong negative association between stopped fraction and the residual component of production in the congested regime. This result is stronger than a simple improvement in fit because it identifies the direction of the omitted information. The high stopped fraction does not merely add arbitrary explanatory power; it is associated with lower-than-predicted production at a given accumulation, which is precisely the sign implied by Equation (2). The residual plot therefore shows that a meaningful part of accumulation-only scatter is not random noise but a systematic signature of omitted immobilization information.

4.3 Robustness to the definition of congestion

Since congestion is not a sharply defined state in aggregate data, the results should not depend on a single threshold. A robustness check in which the congested regime is defined by alternative upper-quantile subsets of accumulation is therefore reported in Table 2. The pattern is stable across all three definitions. When congestion is defined as observations above the 50th, 60th and 70th percentiles of accumulation, adding stopped fraction reduces RMSE by 60.4%, 58.1% and 57.3%, respectively.

The threshold comparison also reveals a second pattern. As the definition of congestion becomes more restrictive, the explanatory power of the accumulation-only model deteriorates: R^2 falls from 0.9377 for $n \geq Q_{50}$ to 0.6607 for $n \geq Q_{70}$. This decline is consistent with the idea that accumulation becomes less sufficient as the analysis focuses on heavily congested states, where the same amount of stored traffic can correspond to different degrees of immobilization. By contrast, the augmented model remains substantially more accurate across all thresholds, with R^2 above 0.93 even in the highest accumulation subset. The robustness check therefore strengthens the main conclusion: stopped fraction is the most useful precisely in the regime where accumulation-only closure is most vulnerable.

4.4 Loading-recovery trajectory

Finally, the simulated loading-recovery trajectory provides a qualitative view of how the same mechanism can appear dynamically. The sequence of 60 s aggregation intervals is plotted in the accumulation-production plane in Figure 5, with the loading, congested and recovery phases distinguished. This figure is not intended as a formal test of hysteresis, since the experiment was designed primarily to diagnose the contribution of stopped fraction. Nevertheless, it is useful for interpreting why path dependence matters in congested MFDs.

During the loading phase, accumulation increases as demand rises. During the recovery phase, demand is reduced, but the network does not necessarily return immediately to the same internal state that characterized the corresponding loading accumulation. Queues, blocked movements and stopped vehicles may persist after total accumulation has begun to decline. Therefore, observations with comparable accumulation can occur in different phases of the experiment and can be associated with different production levels. This dynamic pattern is consistent with the broader interpretation of stopped fraction as an omitted state dimension: the accumulation coordinate alone records how many vehicles are present, but not how mobile those vehicles are at that point in the traffic history.

5 Discussion

The results should not be read as evidence that accumulation is unimportant. On the contrary, the accumulation-only model explains much of the overall variation in production. This is consistent with the

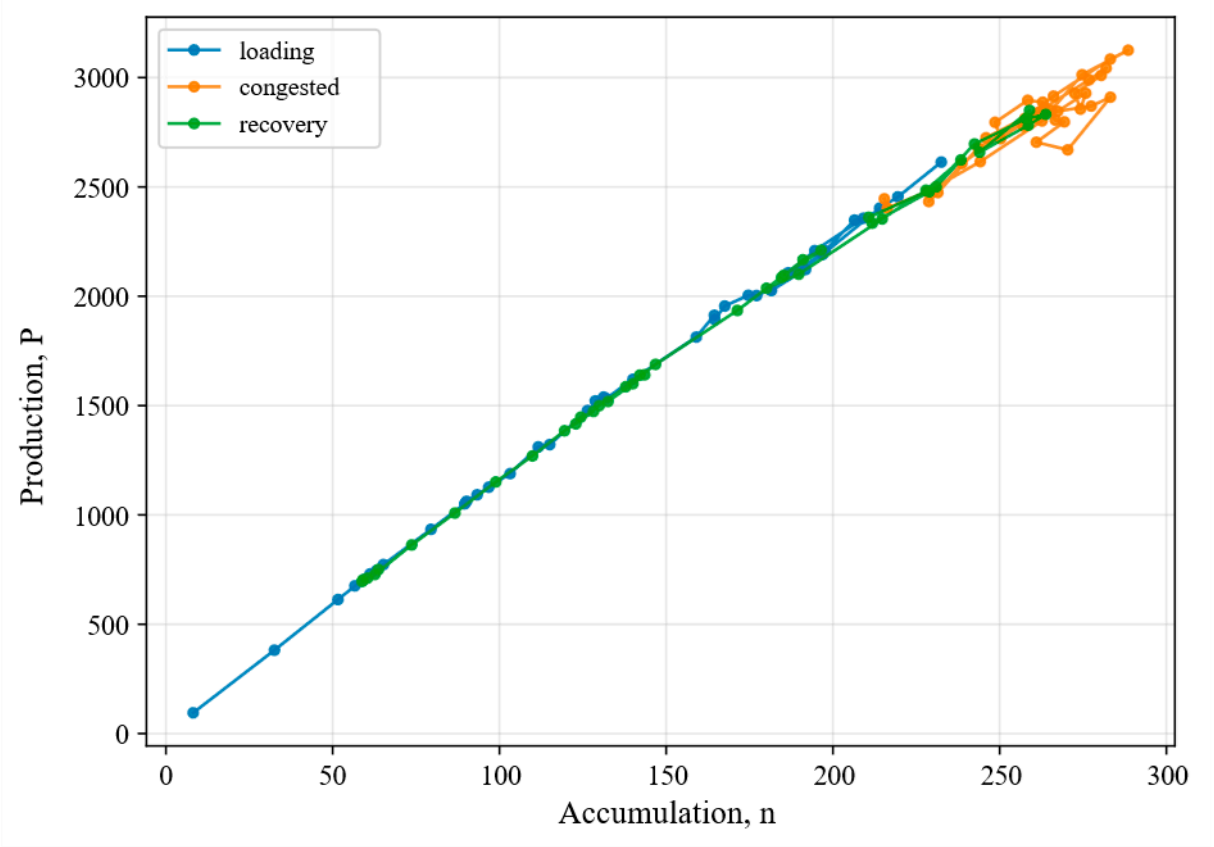


Figure 5 *Loading-recovery trajectory in the accumulation-production plane; a supplementary visualization of phase-dependent movement in the simulated MFD is provided, illustrating why congested observations should not be interpreted solely through accumulation*

basic MFD premise. The key finding is more specific: in congested regimes, the remaining production variation is systematically related to stopped fraction. Accumulation provides a strong first-order description, while stopped fraction captures an omitted immobilization dimension.

From an operational perspective, the value of stopped fraction lies in its simplicity. Unlike detailed spatial heterogeneity measures, it can be computed directly when vehicle speeds are observed for the relevant vehicle population, and it can be approximated from connected-vehicle monitoring or other speed-based diagnostics when the sample is sufficiently representative. This operational feature is important because the proposed variable is not intended as an abstract fitting device, but as a measurable indicator of the extent to which stored traffic is no longer producing movement.

This interpretation is consistent with the analytical representation in Equation (2). At a fixed accumulation, a higher stopped fraction reduces the effective moving component of traffic and may also reduce the productivity of moving vehicles. When such a variation is projected onto the accumulation-production plane, it appears as vertical scatter. Conditioning on stopped fraction does not necessarily yield complete closure, because other omitted dimensions such as spatial queue distribution, signal coordination and route concentration may also matter. The simulation results demonstrate that stopped fraction captures a meaningful component of the omitted state information.

The loading-recovery trajectory in Figure 5 further shows that the omitted state information is not only cross-sectional but also dynamic. Similar accumulation values may appear during different phases of the simulated experiment, while stopped conditions and production need not coincide. This is consistent with the broader view that hysteresis-like patterns in congested MFDs can arise when the projected accumulation-production plane suppresses path-dependent immobilization.

The simulation design is intentionally stylized. The synthetic grid does not represent a calibrated real city, and the demand profile was selected to generate loading, congestion and recovery under controlled conditions. This is a limitation with respect to external validity and reproducibility from the manuscript alone, because the exact numerical trajectory also depends on simulation input files such as the demand realization, route assignment and signal program. The objective was not to provide a transferable calibrated benchmark, but to determine whether the proposed closure-failure mechanism can emerge under microscopic vehicle dynamics. Future work should examine whether the same pattern appears in calibrated urban networks and empirical trajectory datasets.

6 Conclusions

Stopped fraction was examined as a complementary macroscopic state variable for congested MFDs. The analytical argument is that accumulation measures traffic storage but not traffic immobilization. If states with similar accumulation differ in stopped fraction, production need not be fully determined by accumulation alone. Stopped fraction therefore provides a direct way to distinguish stored traffic that remains mobile from stored traffic that is effectively prevented from contributing to production.

A controlled SUMO simulation supported this mechanism quantitatively. Across all 120 observations, adding stopped fraction reduced in-sample RMSE from 41.32 to 18.79, a 54.5% reduction. In the congested regime defined by observations above the 60th percentile of accumulation, R^2 increased from 0.8777 to 0.9785 and RMSE fell from 55.84 to 23.40, a 58.1% reduction. The residuals of the accumulation-only model were strongly negatively correlated with stopped fraction in this regime ($r = -0.787$), showing that high-stopping states systematically produced less movement than accumulation alone would predict. The result was robust to alternative congestion thresholds: RMSE reductions ranged from 57.3% to 60.4% for the 50th-70th percentile definitions. These findings indicate that a part of the scatter in congested MFDs is a projection effect caused by omitted immobilization information rather than purely random noise.

The practical implication is that MFD-based monitoring and control may benefit from recording not only accumulation but also the proportion of vehicles that are nearly stopped. Such information can be derived directly from microscopic simulation or full trajectory data, and can be approximated from connected-vehicle trajectories, probe-vehicle speeds or other speed-based sensing systems when their sampling coverage is adequate for estimating a stopped share. A principal limitation is the use of a synthetic grid network and a controlled demand profile rather than a calibrated real city. Future work should test the same relationship in empirical datasets, under alternative signal-control settings and across larger networks with spatially heterogeneous demand. By making immobilization observable at the macroscopic level, stopped fraction offers a compact way to extend accumulation-based MFD analysis in the regime where closure is most vulnerable. Thus, stopped fraction should be viewed not as a replacement for accumulation, but as a low-cost complementary state variable that helps diagnose when and why accumulation-only MFD representations lose closure under congestion.

Acknowledgements

The author gratefully acknowledges helpful discussions from colleagues. Any remaining errors are solely the author's responsibility.

Conflicts of interest

The author declares that they have no known competing financial interests or personal relationships that could have appeared to influence the work reported in this paper.

References

[1] DAGANZO, C. F. Urban gridlock: macroscopic modeling and mitigation approaches. *Transportation Research Part B: Methodological* [online]. 2007, **41**(1), p. 49-62 [accessed 2026-08-21]. ISSN 0191-2615, eISSN 1879-2367. Available from: https://doi.org/10.1016/j.trb.2006.03.001

[2] GEROLIMINIS, N., DAGANZO, C. F. Existence of urban-scale macroscopic fundamental diagrams: some experimental findings. *Transportation Research Part B: Methodological* [online]. 2008, **42**(9), p. 759-770 [accessed 2026-08-21]. ISSN 0191-2615, eISSN 1879-2367. Available from: https://doi.org/10.1016/j.trb.2008.02.002

[3] DAGANZO, C. F., GEROLIMINIS, N. An analytical approximation for the macroscopic fundamental diagram of urban traffic. *Transportation Research Part B: Methodological* [online]. 2008, **42**(9), p. 771-781 [accessed 2026-08-21]. ISSN 0191-2615, eISSN 1879-2367. Available from: https://doi.org/10.1016/j.trb.2008.06.008

[4] ZHANG, L., YUAN, Z., YANG, L., LIU, Z. Recent developments in traffic flow modeling using macroscopic fundamental diagram. *Transport Reviews* [online]. 2020, **40**(4), p. 529-550 [accessed 2026-08-21]. ISSN 0144-1647, eISSN 1464-5327. Available from: https://doi.org/10.1080/01441647.2020.1743918

[5] MAZLOUMIAN, A., GEROLIMINIS, N., HELBING, D. The spatial variability of vehicle densities as determinant of urban network capacity. *Philosophical Transactions of the Royal Society A* [online]. 2010, **368**(1928), p. 4627-4647 [accessed 2026-08-21]. eISSN 1364-503X. Available from: https://doi.org/10.1098/rsta.2010.0099

[6] GAYAH, V. V., DAGANZO, C. F. Clockwise hysteresis loops in the macroscopic fundamental diagram: an effect of network instability. *Transportation Research Part B: Methodological* [online]. 2011, **45**(4), p. 643-655 [accessed 2026-08-21]. ISSN 0191-2615, eISSN 1879-2367. Available from: https://doi.org/10.1016/j.trb.2010.11.006

[7] GEROLIMINIS, N., BOYACI, B. The effect of variability of urban systems characteristics in the network capacity. *Transportation Research Part B: Methodological* [online]. 2012, **46**(10), p. 1607-1623 [accessed 2026-08-21]. ISSN 0191-2615, eISSN 1879-2367. Available from: https://doi.org/10.1016/j.trb.2012.08.001

[8] GAYAH, V. V., GAO, X., NAGLE, A. S. On the impacts of locally adaptive signal control on urban network stability and the macroscopic fundamental diagram. *Transportation Research Part B: Methodological* [online]. 2014, **70**, p. 255-268 [accessed 2026-08-21]. ISSN 0191-2615, eISSN 1879-2367. Available from: https://doi.org/10.1016/j.trb.2014.09.010

[9] RAMEZANI, M., HADDAD, J., GEROLIMINIS, N. Dynamics of heterogeneity in urban networks: aggregated traffic modeling and hierarchical control. *Transportation Research Part B: Methodological* [online]. 2015, **74**, p. 1-19 [accessed 2026-08-21]. ISSN 0191-2615, eISSN 1879-2367. Available from: https://doi.org/10.1016/j.trb.2014.12.010

[10] ALVAREZ LOPEZ, P., BEHRISCH, M., BIEKER-WALZ, L., ERDMANN, J., FLOTTEROD, Y.-P., HILBRICH, R., LUCKEN, L., RUMMEL, J., WAGNER, P., WIESSNER, E. Microscopic traffic simulation using SUMO. In: 2018 21st International Conference on Intelligent Transportation Systems (ITSC): proceedings [online]. IEEE. 2018. ISBN 978-1-7281-0321-1, eISBN 978-1-7281-0323-5, eISSN 2153-0017, p. 2575-2582 [accessed 2026-08-21]. Available from: https://doi.org/10.1109/ITSC.2018.8569938

[11] KEYVAN-EKBATANI, M., KOUVELAS, A., PAPAMICHAIL, I., PAPAGEORGIOU, M. Exploiting the fundamental diagram of urban networks for feedback-based gating. *Transportation Research Part B: Methodological* [online]. 2012, **46**(10), p. 1393-1403 [accessed 2026-08-21]. ISSN 0191-2615, eISSN 1879-2367. Available from: https://doi.org/10.1016/j.trb.2012.06.008

[12] TILG, G., AMINI, S., BUSCH, F. Evaluation of analytical approximation methods for the macroscopic fundamental diagram. *Transportation Research Part C: Emerging Technologies* [online]. 2020, **114**, p. 1-19 [accessed 2026-08-21]. ISSN 0968-090X, eISSN 1879-2359. Available from: https://doi.org/10.1016/j.trc.2020.02.003

[13] HERMAN, R., PRIGOGINE, I. A two-fluid approach to town traffic. *Science* [online]. 1979, **204**(4389), p. 148-151 [accessed 2026-08-21]. ISSN 0036-8075, eISSN 1095-9203. Available from: https://doi.org/10.1126/science.204.4389.148

[14] KNOOP, V. L., VAN LINT, H., HOOGENDOORN, S. P. Traffic dynamics: its impact on the macroscopic fundamental diagram. *Physica A: Statistical Mechanics and its Applications* [online]. 2015, **438**, p. 236-250 [accessed 2026-08-21]. ISSN 0378-4371, eISSN 1873-2119. Available from: https://doi.org/10.1016/j.physa.2015.06.016

[15] JI, Y., GEROLIMINIS, N. On the spatial partitioning of urban transportation networks. *Transportation Research Part B: Methodological* [online]. 2012, **46**(10), p. 1639-1656 [accessed 2026-08-21]. ISSN 0191-2615, eISSN 1879-2367. Available from: https://doi.org/10.1016/j.trb.2012.08.005

[16] XU, G., YU, Z., GAYAH, V. V. Analytical method to approximate the impact of turning on the macroscopic fundamental diagram. *Transportation Research Record: Journal of the Transportation Research Board* [online]. 2020, **2674**(9), p. 933-947 [accessed 2026-08-21]. ISSN 0361-1981, eISSN 2169-4052. Available from: https://doi.org/10.1177/0361198120933274

[17] POSTRANSKYY, T., BOIKIV, M., AFONIN, M., MOHYLA, I. Influence of traffic flow parameters on the delay duration at signalized intersections. *Communications - Scientific Letters of the University of Zilina* [online]. 2026, **28**(1), p. D13-D26 [accessed 2026-08-21]. ISSN 1335-4205, eISSN 2585-7878. Available from: https://doi.org/10.26552/com.C.2026.004

[18] GEROLIMINIS, N., ZHENG, N., AMPOUNTOLAS, K. A three-dimensional macroscopic fundamental diagram for mixed bi-modal urban networks. *Transportation Research Part C: Emerging Technologies* [online]. 2014, **42**, p. 168-181 [accessed 2026-08-21]. ISSN 0968-090X, eISSN 1879-2359. Available from: https://doi.org/10.1016/j.trc.2014.03.004

[19] LODER, A., AMBUHL, L., MENENDEZ, M., AXHAUSEN, K. W. Empirics of multi-modal traffic networks using the 3D macroscopic fundamental diagram. *Transportation Research Part C: Emerging Technologies* [online]. 2017, **82**, p. 88-101 [accessed 2026-08-21]. ISSN 0968-090X, eISSN 1879-2359. Available from: https://doi.org/10.1016/j.trc.2017.06.009

[20] AMPOUNTOLAS, K., ZHENG, N., GEROLIMINIS, N. Macroscopic modelling and robust control of bi-modal multi-region urban road networks. *Transportation Research Part B: Methodological* [online]. 2017, **104**, p. 616-637 [accessed 2026-08-21]. ISSN 0191-2615, eISSN 1879-2367. Available from: https://doi.org/10.1016/j.trb.2017.05.007

[21] LODER, A., AMBUHL, L., MENENDEZ, M., AXHAUSEN, K. W. Understanding traffic capacity of urban networks. *Scientific Reports* [online]. 2019, **9**, 16283 [accessed 2026-08-21]. eISSN 2045-2322. Available from: https://doi.org/10.1038/s41598-019-51539-5

[22] AMBUHL, L., LODER, A., BLIEMER, M. C. J., MENENDEZ, M., AXHAUSEN, K. W. A functional form with a physical meaning for the macroscopic fundamental diagram. *Transportation Research Part B: Methodological*

[online]. 2020, **137**, p. 119-132 [accessed 2026-08-21]. ISSN 0191-2615, eISSN 1879-2367. Available from: https://doi.org/10.1016/j.trb.2018.10.013

[23] HAN, K., HUANG, T., FAN, W., GE, Q., DONG, S., WANG, X. Macroscopic fundamental diagram with volume-delay relationship: model derivation, empirical validation and invariance property. *Transportation Research Part C: Emerging Technologies* [online]. 2024, **166**, 104739 [accessed 2026-08-21]. ISSN 0968-090X, eISSN 1879-2359. Available from: https://doi.org/10.1016/j.trc.2024.104739

[24] MAITI, N., SEPPECHER, M., LECLERCQ, L. Challenges in calibrating multimodal network macroscopic fundamental diagrams: a review and definition of data fusion pipeline. *European Transport Research Review* [online]. 2025, **17**, 51 [accessed 2026-08-21]. eISSN 1866-8887. Available from: https://doi.org/10.1186/s12544-025-00750-9

[25] BARMPOUNAKIS, E., GEROLIMINIS, N. On the new era of urban traffic monitoring with massive drone data: the pNEUMA large-scale field experiment. *Transportation Research Part C: Emerging Technologies* [online]. 2020, **111**, p. 50-71 [accessed 2026-08-21]. ISSN 0968-090X, eISSN 1879-2359. Available from: https://doi.org/10.1016/j.trc.2019.11.023

[26] PAIPURI, M., BARMPOUNAKIS, E., GEROLIMINIS, N., LECLERCQ, L. Empirical observations of multimodal network-level models: insights from the pNEUMA experiment. *Transportation Research Part C: Emerging Technologies* [online]. 2021, **131**, 103300 [accessed 2026-08-21]. ISSN 0968-090X, eISSN 1879-2359. Available from: https://doi.org/10.1016/j.trc.2021.103300

[27] BARMPOUNAKIS, E., MONTESINOS-FERRER, M., GONZALES, E. J., GEROLIMINIS, N. Empirical investigation of the emission-macroscopic fundamental diagram. *Transportation Research Part D: Transport and Environment* [online]. 2021, **101**, 103090 [accessed 2026-08-21]. ISSN 1361-9209, eISSN 1879-2340. Available from: https://doi.org/10.1016/j.trd.2021.103090

[28] BAZA-SOLARES, N., VELASQUEZ-MARTINEZ, R., TORRES-BOHORQUEZ, C., MARTINEZ-ESTUPINAN, Y., POLIZIANI, C. Traffic simulation with open-source and commercial traffic microsimulators: a case study. *Communications - Scientific Letters of the University of Zilina* [online]. 2022, **24**(2), p. E49-E62 [accessed 2026-08-21]. ISSN 1335-4205, eISSN 2585-7878. Available from: https://doi.org/10.26552/com.C.2022.2.E49-E62

Dear colleagues,

Journal for sciences in transport Communications - Scientific Letters of the University of Žilina are a wellestablished open-access scientific transport journal aimed primarily at the topics connected with the field of transport. The main transport-related areas covered include Civil engineering, Electrical engineering, Management and informatics, Mechanical engineering, Operation and economics, Safety and security, Travel and tourism studies. Research in the field of education also falls under these categories. The full list of main topics and subtopics is available at: *https://komunikacie.uniza.sk/artkey/inf-990000-0500_Topical-areas.php*

Journal for sciences in transport Communications - Scientific Letters of the University of Žilina is currently indexed, abstracted and accepted by CEEOL, CLOCKSS, COPE (Committee on Publication Ethics), Crossref (DOI), digitálne pramene, DOAJ, EBSCO Host, Electronic Journals Library (EZB), ERIH Plus, Google Scholar, Index Copernicus International Journals Master list, iThenticate, JournalGuide, Jouroscope, Norwegian Register for Scientific Journals Series and Publishers, Portico, ROAD, ScienceGate, SCImago Journal & Country Rank, SciRev, SCOPUS, Ulrich´s, Web of Science database, WorldCat (OCLC).

Journal for sciences in transport Communications - Scientific Letters of the University of Žilina is preserved in CLOCKSS and Portico to guarantee long-term digital preservation and is archived in the national deposit digitalne pramene.

Authors can share their experiences with publishing in our journal on SciRev.

Journal for sciences in transport Communications - Scientific Letters of the University of Žilina has been selected for inclusion in the Web of Science™. Articles published after 2022, beginning with 24(1), are included in the product Emerging Sources Citation Index (ESCI).

I would like to invite authors to submit their papers for consideration. We have an open access **policy under Creative Commons (CC BY) license** and Article Processing Charge (APC) is **400 Euro** (price excluding VAT). The price of one additional page of the submitted article beyond the prescribed scope (8 pages) is **50 Euro** (price excluding VAT). Print edition fee is 100 Euro per one piece (price excluding VAT) including shipping costs. Our journal operates a standard single-anonymous peer-review process, the successful completion of which is a prerequisite for publication of articles.

Our journal is issued four times a year (in January, in April, in July and in October).

I would also like to offer you the opportunity of using already published articles from past issues as source of information for your research and publication activities. All papers are available at our webpage: *http://komunikacie.uniza.sk*, where you can browse through the individual volumes. Our journal offers access to its contents in the open access system on the principles of the license Creative Commons (CC BY 4.0).

For any questions regarding the Journal for sciences in transport Communications - Scientific Letters of the University of Žilina please contact us at: *komunikacie@uniza.sk*.

We look forward to future cooperation.

Sincerely

Gabriel Gašpar
editor-in-chief

KOMUNIKÁCIE
COMMUNICATIONS

VEDECKÉ LISTY ŽILINSKEJ UNIVERZITY
SCIENTIFIC LETTERS OF THE UNIVERSITY OF ZILINA
multidisciplinary journal for sciences in transport

VOLUME 28 Number 4

October 2026

Editor-in-chief:
Gabriel GASPAR - SK

Associate editor:
Branislav HADZIMA - SK

Executive editor:
Sylvia DUNDEKOVA - SK

Language editor:
Ruzica NIKOLIC - SK

Honorary members:
Otakar BOKUVKA - SK
Jan COREJ - SK (in memoriam)
Milan DADO - SK
Pavel POLEDNAK - CZ

Scientific editorial board:
S. M. ANAS - IN
Greg BAKER - NZ
Abdelhamid BOUCHAIR - FR
Pavel BRANDSTETTER - CZ
Mario CACCIATO - IT
Jan CELKO - SK
Andrew COLLINS - GB
Samo DROBNE - SI
Erdogan H. EKIZ - UZ
Michal FRIVALDSKY - SK
Juraj GERLICI - SK
Vladimir N. GLAZKOV - RU
Ivan GLESK - GB
Marian GRUPAC - SK
Mario GUAGLIANO - IT
Mohamed HAMDAOUI - FR
Robert HUDEC - SK
Andrzej CHUDZIKIEWICZ - PL
Jaroslav JANACEK - SK
Zdenek KALA - CZ
Antonin KAZDA - SK
Michal KOHANI - SK
Tomasz N. KOLTUNOWICZ - PL
Jozef KOMACKA - SK
Matus KOVAC - SK
Gang LIU - CN
Tomas LOVECEK - SK
Frank MARKERT - DK
Pavlo MARUSCHAK - UK
Jaroslav MAZUREK - SK
Marica MAZUREKOVA - SK
Vladimir MOZER - CZ
Andrej NOVAK - SK
Jorge Carvalho PAIS - PT
Peter POCTA - SK
Maria A. M. PRATS - ES
Pavol RAFAJDUS - SK
Giacomo SCELBA - IT
Martin SOLIK - SK
Jakub SOVIAR - SK
Blaza STOJANOVIC - RS
Che-Jen SU - TW
Eva SVENTEKOVA - SK
Eva TILLOVA - SK
Anna TOMOVA - SK
Audrius VAITKUS - LT
Neven VRCEK - HR
Yue XIAO - CN
Franco Bernelli ZAZZERA - IT

Executive editorial board
Michal BALLAY - SK
Pavol BELANY - SK
Martin BOROS - SK
Matej BRNA - SK
Marek BRUNA - SK
Roman BUDJAC - SK
Nikola CAJOVA KANTOVA - SK
Michaela CIGANOVA - SK
Kristian CULIK - SK
Jan DIZO - SK
Peter DOBES - SK
Daniel DUGEL - SK
Lukas FALAT - SK
Filip GAGO - SK
Lubica GAJANOVA - SK
Patrik GRZNAR - SK
Marian HANDRIK - SK
Stefan HARDON - SK
Martin HOLUBCIK - SK
Maros JANOVEC - SK
Daniela JURASOVA - SK
Daniel KAJANEK - SK
Dasa KOVALOVA - SK
Tomas KOZEL - SK
Lenka KUCHARIKOVA - SK
Richard LENHARD - SK
Michal LOMAN - SK
Matus MATERNA - SK
Eva NEDELIAKOVA - SK
Radovan NOSEK - SK
Filip PASTOREK - SK
Pavol PECHO - SK
Slavka PITONAKOVA - SK
Jozef PROKOP - SK
Michal SAJGALIK - SK
Anna SIEKELOVA - SK
Jakub SVEC - SK
Michal TITKO - SK
Milan VASKO - SK
Vladislav ZITRICKY - SK

Guarantors of covered subtopics:
Jan CELKO - SK
Martin DECKY - SK
Samo DROBNE - SI
Marian DRUSA - SK
Erdogan H. EKIZ - UZ
Michal FRIVALDSKY - SK
Gabriel GASPAR - SK
Juraj GERLICI - SK
Marian GRUPAC - SK
Mario GUAGLIANO - IT
Branislav HADZIMA - SK
Andrzej CHUDZIKIEWICZ - PL
Libor IZVOLT - SK
Jaroslav JANACEK - SK
Dusan JANDACKA - SK
Jozef JANDACKA - SK
Andrea KOCIANOVA - SK
Michal KOHANI - SK
Matyas KONIORCZYK - HU
Matus KOVAC - SK
Martin KRAJCOVIC - SK
Tomas LOVECEK - SK
Jaroslav MAZUREK - SK
Stefan MEDVECKY - SK
Vladimir MOZER - CZ
Andrej NOVAK - SK
Jaroslav ODROBINAK - SK
Daniel PAPAN - SK
Peter POCTA - SK
Radoslav PONECHAL - SK
Milan SAGA - SK
Andrea SEGALINI - IT
Martin SOLIK - TW
Eva SVENTEKOVA - SK
Eva TILLOVA - SK
Anna TOMOVA - SK

This is an open access article distributed under the terms of the Creative Commons Attribution 4.0 International License (CC BY 4.0), which permits use, distribution, and reproduction in any medium, provided the original publication is properly cited. No use, distribution or reproduction is permitted which does not comply with these terms.

komunikácie
COMMUNICATIONS

VEDECKÉ LISTY ŽILINSKEJ UNIVERZITY
SCIENTIFIC LETTERS OF THE UNIVERSITY OF ZILINA
multidisciplinary journal for sciences in transport

VOLUME 28 Number 4

October 2026

Each paper is reviewed by at least two reviewers.
Individual issues of the journal are available at: http://komunikacie.uniza.sk
The full author quidelines are available at: https://komunikacie.uniza.sk/artkey/inf-990000-0400_Author-guidelines.php
Published quarterly by the University of Žilina via EDIS - Publishing House of the University of Žilina
Multidisciplinary journal for sciences in transport Komunikácie / Communications is currently indexed, abstracted and accepted by CEEOL, CLOCKSS, COPE (Committee on Publication Ethics), Crossref (DOI), digitálne pramene, DOAJ, EBSCO Host, Electronic Journals Library (EZB), ERIH Plus, Google Scholar, Index Copernicus International Journals Master list, iThenticate, JournalGuide, Jouroscope, Norwegian Register for Scientific Journals Series and Publishers, Portico, ROAD, ScienceGate, SCImago Journal & Country Rank, SciRev, SCOPUS, Ulrich´s, Web of Science database, WorldCat (OCLC).

Multidisciplinary journal for sciences in transport Komunikácie - vedecké listy Žilinskej univerzity v Žiline / Communications - Scientific Letters of the University of Žilina has been selected for inclusion in the Web of Science™.

Contact:

Komunikácie - vedecké listy Žilinskej univerzity v Žiline
Communications - Scientific Letters of the University of Žilina
University of Žilina, Univerzitná 8215/1
010 26 Žilina, Slovakia

E-mail: komunikacie@uniza.sk
Web: https://komunikacie.uniza.sk

ISSN (print version): 1335-4205
ISSN (online version): 2585-7878

Registered No. (print version): EV 3672/09
Registered No. (online version): EV 3/22/EPP
Publisher, owner and distribution:
University of Žilina, Univerzitná 8215/1,
010 26 Žilina, Slovakia

Company identification number IČO: 00 397 563
Frequency of publishing: four times a year
Circulation: 30 printed copies per issue
Print edition price: 100 Euro (price without VAT)
Article Processing Charge (APC): 400 Euro (price without VAT)

Publishing has been approved by:
Ministry of Culture, Slovak Republic

This is an open access article distributed under the terms of the Creative Commons Attribution 4.0 International License (CC BY 4.0), which permits use, distribution, and reproduction in any medium, provided the original publication is properly cited. No use, distribution or reproduction is permitted which does not comply with these terms.

UNIVERSITY
OF ŽILINA

In its over 70 years of successful existence, the University of Žilina (UNIZA) has become one of the top universities in Slovakia.

Scientific conferences

organized by University of Žilina

Conference Welding 2026
Date and venue: 11 - 13 November 2026,
Tatranská Lomnica (SK)
Contact: milos.mician@fstroj.uniza.sk

56th Conference of Slovak Mathematicians
Date and venue: 19 - 22 November 2026,
Jasná pod Chopkom (SK)
Contact: bozena.dorociakova@uniza.sk
Web: https://konferenciajasna.sk

International Conference MedIn
Date and venue: 9 December 2026, Žilina (SK)
Contact: vladimir.filip@umkd.uniza.sk
Web: https://umkd.uniza.sk/medin

International Conference MedGram
Date and venue: 10 December 2026, Žilina (SK)
Contact: marian.grupac@umkd.uniza.sk
Web: https://umkd.uniza.sk/medgram



UNIVERSITY OF ŽILINA
Science & Research Department

Univerzitná 8215/1,
010 26 Žilina,
Slovakia

Ing. Janka Macurová
tel.: +421 41 513 5143
e-mail: janka.macurova@uniza.sk